Dissertation

submitted to the

Combined Faculty of Natural Sciences and Mathematics

of the Ruperto Carola University Heidelberg, Germany

for the degree of

Doctor of Natural Sciences

Presented by

Simon Frank (M.Sc.)

born in Frankfurt/Main

Oral examination: 07.12.2020

Long Acting Injectable Formulations of Biologicals: Examination of an innovative polymer family for the controlled release of peptides and proteins

Referees: Prof. Dr. Gert Fricker

Prof. Dr. Walter Mier

Danksagung

Die vorliegende Arbeit wurde im Rahmen einer Kooperation zwischen dem Steinbeis-Transferzentrum für Biopharmazie und Analytik (Heidelberg, Deutschland), der Merck KGaA (Darmstadt, Deutschland) sowie InnoCore Pharmaceuticals (Groningen, Niederlande) erarbeitet.

Mein Dank gilt insbesondere meinem Doktorvater Herrn **Prof. Dr. Gert Fricker** für seine allzeitige unkomplizierte, ungezwungene und humorvolle Unterstützung bei fachlichen Fragen und Problemen. Dabei ist vor allem auch die tatkräftige und gleichzeitig besonnene Mithilfe bei diversen Tierstudien hervorzuheben.

Herrn **Prof. Dr. Walter Mier** danke ich für die Anfertigung des Zweitgutachtens.

Der Merck KGaA danke ich für die Bereitstellung des finanziellen Rahmens meiner Forschungstätigkeit.

Mein besonderer Dank gilt Frau **Dr. Tanja Henzler** für die Ermöglichung dieser Arbeit und meiner Teilnahme an der oben genannten Kooperation, sowie für vielzählige praktische Tipps und Einblicke in die industrielle Forschung. In diesem Zusammenhang möchte ich auch Frau **Dr. Melanie Ott** für ihre stete Unterstützung bei den verschiedensten Fragestellungen sowie viele hilfreiche Vorschläge zu praktischer Durchführung von Versuchen und wissenschaftlichen Recherchen danken. Beiden danke ich für die stets angenehme, entspannte und vertrauensvolle Arbeitsatmosphäre bei unzähligen Besprechungen.

Allen derzeitigen und ehemaligen Kollegen des Arbeitskreises Fricker in der Abteilung Pharmazeutische Technologie und Biopharmazie des Instituts für Pharmazie und Molekulare Biotechnologie (IPMB) der Ruprecht-Karls-Universität Heidelberg sowie der Abteilung Liquid Formulation R&D der Merck KGaA danke ich für die allzeit angenehme Arbeitsatmosphäre, Hilfsbereitschaft und die wertvolle Zusammenarbeit.

Ich danke Frau **Carolin Wagner** für ihre tatkräftige, praktische Unterstützung in ihrer Funktion als Werkstudentin, Praktikantin und Masterandin. Carolin hat mit ihren schönen Ergebnissen wesentlich zum Gelingen dieser Arbeit beigetragen und nicht zuletzt mit ihrer positiven Art jederzeit Zuversicht verbreitet.

Silvio Krasemann und **Klaus Hillesheim** aus der Interfakultären Biomedizinischen Forschungseinrichtung (IBF), Heidelberg danke ich für die kompetente und geduldige Mithilfe bei meinen zeitintensiven Tierstudien im klinisch-experimentellen Bereich der Einrichtung.

Mein besonders herzlicher Dank richtet sich an meine Familie, die mir auf dem Weg und bis hin zum Abschluss dieser Arbeit immerwährende Unterstützung entgegengebracht hat. Mit unermüdlicher Geduld und Ermunterung haben **meine Eltern** dabei wesentlich dazu beigetragen, dass ich die nötigen Fähigkeiten zur Vollendung meiner Dissertation erwerben konnte.

Meiner Lebensgefährtin **Tanja** und unseren beiden Töchtern **Lotta und Loni** verdanke ich unzählige freudige und einzigartige Momente, die den zu einem erfolgreichen Abschluss dieser Arbeit so wichtigen Ausgleich gebildet haben.

Zusammenfassung

Depotformulierungen therapeutischer Wirkstoffe ermöglichen pharmakologische Vorteile sowie verbesserte Patienten-Compliance und Verträglichkeit im Vergleich mit konventionellen Darreichungsformen. Mit der zunehmenden Bedeutung biologischer Wirkstoffe gewinnen auch Formulierungen zur kontrollierten Freisetzung für diese Wirkstoffklasse an Relevanz. Die innovative Polymerplattform SynBiosys® verspricht typische Schwächen herkömmlicher Polymere für Mikropartikel-Depots zu überwinden. Ziel der vorliegenden Arbeit war deshalb die Evaluierung von Polymeren der SynBiosys®-Familie für die kontrollierte Freisetzung biologischer Wirkstoffe mithilfe von Integritätsanalysen repräsentativer Modelltherapeutika nach *in vitro* und *in vivo* Freisetzung aus SynBiosys®-basierten Mikropartikeln.

Im Rahmen dieser Arbeit wurden Mikropartikel-Formulierungen des anti-diabetischen Peptidwirkstoffs Exenatid *in vitro* und *in vivo* mit Bydureon® verglichen, der kommerziellen Depotformulierung von Exenatid. Das Peptid wurde *in vitro* gleichmäßig über zwei bis vier Wochen freigesetzt und die Integrität des freigesetzten Peptids wurde in ersten Experimenten mittels zellbasierten Funktionalitätstests bestätigt. Auch *in vivo* wurde Exenatid gleichmäßiger freigesetzt als aus Bydureon®-Mikropartikeln und einmalige, subkutane Injektion der SynBiosys®-Formulierungen reduzierte sowohl den Blutglukosespiegel zwischen 25-50% über vier Wochen als auch glykiertes Hämoglobin um 3.4 - 4.6% signifikant in einem Diabetes Typ II Ratten-Modell (Hochfettdiät/Streptozotozin induziert).

Die Verkapselung des monoklonalen Modellantikörpers mAbB mit verschiedenen SynBiosys®-Kompositionen erlaubte die Auswahl einer passenden Polymerzusammensetzung für die Freisetzung von Proteinen mit hohem Molekulargewicht. Die strukturelle Integrität von *in vitro* freigesetztem mAbB wurde mittels Circulardichroismus (CD) sowie Fluoreszenzspektroskopie (FS) bestätigt. Basierend auf diesen Ergebnissen wurde mAbX als onkologischer Modellantikörper in SynBiosys®-Mikropartikeln formuliert und *in vitro* über 10-14 Tage linear freigesetzt. Dabei wurde die Integrität des Antikörpers mittels SE-HPLC, CD, FS, ELISA und einem zellbasierten Funktions-Assay intensiv getestet und bestätigt. Die *in vivo* Freisetzung von mAbX resultierte in dosisabhängigen Plasmaspiegeln während reproduzierbare Werte für die absolute Bioverfügbarkeit von 25.7-30.6% in einem Xenograft Mausmodell beobachtet wurden. Signifikante Wachstumsinhibition von A-431 Tumoren zwischen 50 und 100% mit kontrolliert-freigesetztem Antikörper bestätigte dessen pharmakodynamische Effizienz im Mausmodell.

Die Kompatibilität von SynBiosys® Polymeren mit Biotherapeutika konnte anhand der hohen Integrität *in vitro* und *in vivo* freigesetzter Modellwirkstoffe demonstriert werden. Im Fall von

Exenatid konnten Vorteile in Form eines beschleunigten Wirkungseintritts und Reduktionen der nötigen Gesamtdosis sowie Injektionsanzahl erreicht werden. SynBiosys®-Polymere sind eine vielversprechende Technologie für die kontrollierte Freisetzung biologischer Wirkstoffe.

Abstract

The controlled release of therapeutic agents offers certain benefits in pharmacology, patient compliance and tolerability compared to conventional dosage forms. Nowadays, long acting injectables for peptide and protein therapeutics gain in importance as increasing numbers of biotherapeutics receive approval and subcutaneous self-administration attracts attention due to cost reductions and improved patient acceptance. The innovative polymer platform SynBiosys® claims to overcome weaknesses of conventional polymers for microparticle-based controlled release. As objective of this work, the suitability of these polymers for controlled release of biotherapeutics was evaluated based on various integrity analyses of representative models after *in vitro* and *in vivo* release from SynBiosys®-based microparticles.

Microparticle formulations of the anti-diabetic peptide drug exenatide were examined *in vitro* and *in vivo* in comparison with the marketed benchmark formulation Bydureon®. Exenatide was released *in vitro* with high linearity over two to four weeks and integrity of liberated peptide was preliminarily confirmed with a cell-based functional assay. Likewise, SynBiosys® formulations exhibited a more continuous release behavior *in vivo* compared to the benchmark Bydureon®. Single subcutaneous injection of SynBiosys®-based microparticles significantly reduced non-fasting blood glucose between 25-50% over approximately four weeks and decreased glycated hemoglobin significantly by 3.4 - 4.6% in a rat model of type II diabetes (high fat diet/streptozotocin induced).

Formulation of the monoclonal antibody mAbB in differently composed SynBiosys® polymer matrices allowed the choice of a suitable polymer composition for the controlled release of proteins with high molecular weight. The structural integrity of *in vitro* released mAbB was confirmed by circular dichroism and fluorescence spectroscopy. Based on these results, mAbX as oncological model drug was encapsulated and its integrity after linear *in vitro* release over 10-14 days was confirmed by a powerful combination of SE-HPLC, circular dichroism and fluorescence spectroscopy, ELISA as well as a cell-based functional assay. The *in vivo* liberation of mAbX resulted in highly dose-dependent antibody plasma levels as well as reproducible values for the absolute bioavailability of 25.7-30.6% in xenograft mouse models. Pharmacodynamic efficacy of mAbX released from SynBiosys® microparticles was demonstrated by significant growth reduction of A-431 epidermoid carcinoma cell tumors between 50 and 100%.

In conclusion, the compatibility of SynBiosys® polymers with sensitive peptides and large protein therapeutics was demonstrated herein by *in vitro* and *in vivo* release of model biotherapeutics in highly functional condition as confirmed by a comprehensive analytical

method composition. In the case of exenatide, the accelerated onset of therapeutic effect, the lower number of treatments and the significantly reduced total dose required were remarkable. The SynBiosys® platform is a promising tool for the improved controlled release of biologicals.

Table of contents

Abbreviations

ADA	anti-drug antibody
API	active pharmaceutical ingredient
AUC	area under the curve
BCA	bicinchoninic assay
CD	circular dichroism
C_{max}	maximum plasma concentration
CMC	carboxymethyl cellulose
DCM	dichloromethane
DMSO	dimethyl sulfoxide
e.g.	for example
EGF	epidermal growth factor
EGFR	epidermal growth factor receptor
ELISA	enzyme-linked immunosorbent assay
EXT	exenatide
FcRn	neonatal Fc receptor
F_{abs}	absolute bioavailability
F_{rel}	relative bioavailability
FBS	Fetal bovine serum
FDA	United States Food and Drug Administration
GdnHCl	Guanidine hydrochloride
GLP-1	Glucagon-like peptide-1
GLP1-R	GLP-1 receptor
HEPES	(4-(2-hydroxyethyl)-1-piperazineethanesulfonic acid)
HbA_{1c}	glycated hemoglobin
HFD	high fat diet
HPLC	high performance liquid chromatography
i.a.	inter alia
i.p.	intraperitoneal
i.v.	intravenous
IVR	*in vitro* release
kDa	kilodalton
mAb	monoclonal antibody
mg	milligram/milligrams
min	minute/minutes
mL	milliliter/milliliters

mmol	millimole/millimoles
mmol/L	millimoles per liter
µL	microliter/microliters
µmol	micromole/micromoles
MSP	microsphere
n.a.	not applicable
NaOH	sodium hydroxide
NFBG	non-fasting blood glucose
P-O	polymer-only
PBS	phosphate buffered saline
PLGA	Poly(D,L-lactide-co-glycolide)
PTFE	polytetrafluoroethylene
PVA	polyvinyl alcohol
RP-HPLC	reversed-phase HPLC
rpm	rounds per minute
RT	room temperature
s.c.	subcutaneous
SD	standard deviation
SDa	Sprague Dawley
SDS	sodium dodecyl sulfate
sEGFR	soluble EGFR
SE	standard error of the mean
SEM	scanning electron microscopy
SE-HPLC	size exclusion HPLC
STZ	streptozotocin
t_{max}	Time point of C_{max}
TMB	3,3′,5,5′-Tetramethylbenzidine
T2DM	type 2 diabetes mellitus
w/o	without

Figures

Tables

1. Introduction

Nowadays, the biopharmaceutical sector is well established in healthcare industry and underwent a remarkable development in the past decades since the approval of recombinant human insulin in 1982 as breakthrough in the field. Meanwhile, hundreds of biologicals are marketed and demands for improved patient compliance, pharmacological performances and therapeutic utility arise. Long-acting injectable systems for peptide and protein therapeutics open opportunities to serve the abovementioned performance demands.

1.1. Biologicals

1.1.1. Biologicals – a definition

Despite the success of the biopharmaceutical industry sector, definitions for the term 'Biological' still vary and many authors keep their approaches for specification relatively vague [1, 2]. Already in 2002, Gary Walsh defined biopharmaceuticals (or biological/biologic) as "protein or nucleic acid based pharmaceutical substance used for therapeutic or *in vivo* diagnostic purposes, which is produced by means other than direct extraction from a native (non-engineered) biological source" [3], and Ronald Rader stated that a biopharmaceutical is "a pharmaceutical inherently biological in nature and manufactured using biotechnology" [1]. Walsh later specified his definition: Biologicals are "recombinant proteins, including recombinant antibody-based products, and nucleic acid-based and genetically engineered cell–based products" [4]. The United States Food and Drug Administration (FDA) declared recently, that a "Biological product means any virus, therapeutic serum, toxin, antitoxin, or analogous product applicable to the prevention, treatment or cure of diseases or injuries of man" [5].

Herein, one peptide as well as two monoclonal antibodies were used as model active pharmaceutical ingredients (APIs), representative for sensitive biologicals of various molecular size and complexity.

1.1.2. Biopharmaceutical history and future trends

Reproducible production of biologicals was challenging before genetic engineering and hybridoma technologies were established in the 1970s enabling the production of large amounts of recombinant proteins under increased safety aspects [6]. Biosynthetic human insulin as first biological was developed thereafter, achieving approval by U.S. and European regulatory authorities in 1982 under the trade name Humulin® [7-9]. Muromonab-CD3 as first ever monoclonal antibody received FDA approval in 1986 and was used to prevent rejection of organs after kidney transplantations [10]. The biopharmaceutical industry gained momentum

and, amongst others, commercially produced human growth hormone (1985) [11, 12], α-interferon (1986) [13, 14], erythropoietin (1989) [15, 16], granulocyte-stimulating factor (1991) [17, 18] and rituximab (1997) [19] were introduced. In 2017, rituximab was still among the most successful biopharmaceutical products, together with adalimumab, etanercept, infliximab and trastuzumab as measured by annual sales [4]. Fields of application for biologicals are broadly based including common diseases like cancer, diabetes, inflammation-related indications or hemophilia as well as less frequent indications like asthma and HIV [4].

Monoclonal antibodies still drive the enormous growth of the biopharmaceutical branch while nucleic acid-based as well as cell therapies are of increasing relevance as demonstrated by the approval of the first RNAi-based therapy in 2018 [20, 21].

1.2. Long-acting formulations of biologicals

In comparison to conventional small molecule drugs, biopharmaceuticals are commonly characterized by a higher target specificity leading to increased potency in combination with lowered potential for adverse effects as well as improved tolerability and safety [22, 23]. However, molecular structures of biologicals are complex and prone to physical as well as chemical degradation [24]. Furthermore, short *in vivo* half-life and fast elimination rates are typical drawbacks of peptide and protein therapeutics [23]. As a result, frequent dosing is required which significantly lowers patient compliance [25]. Strategies to overcome frequent dosing of biologicals include the induction of chemical changes leading to prolonged circulation times as well as controlled release systems liberating biological APIs over extended time periods. Both strategies as well as general challenges associated with the formulation of peptide and protein therapeutics are elucidated in the following sections.

1.2.1. Challenges in peptide and protein formulation

Irrespective of the type or strategy to realize a modified and prolonged duration of action, peptide and protein APIs can be exposed to physical and chemical hazards during manufacturing and also later *in vivo*. These stress factors include but are not limited to extreme pH, shaking, ultrasonication, water/organic solvent interfaces or temperature during manufacturing processes, storage or *in vivo* at the site of action. The structural integrity of biomacromolecules is essential to therapeutic functionality. Primary to quaternary structures are indispensable to unrestricted efficacy of the respective drug and structural modifications can result in enhanced immunogenicity or other undesired adverse effects.

Table 1 shows degradation pathways of peptides and proteins occurring after hazardous influences, according to Yang and Frokjaer, 2009 [26]. Induction of physical and chemical modifications during manufacturing, storage and release/handling are undesirable as structural

Table 1: Physical and chemical instabilities of peptide and protein therapeutics, according to Yang and Frokjaer (2009) [26].

Physical instabilities	Chemical instabilities
Denaturation	Hydrolysis
Adsorption	Deamidation
Aggregation	Oxidation
Precipitation	Racemization
	Isomerization
	Disulfide exchange
	B-elimination

integrity may be influenced. Consequently, peptide and protein therapeutics liberated from modified release formulations require extensive analyses to exclude instabilities.

As mentioned in the previous section, protein therapeutics often suffer from a short *in vivo* half-life. Proteins and peptides with molecular weights below approximately 65 kDa are most commonly cleared by glomerular filtration [27, 28]. Larger proteins usually undergo enzymatic degradation and subsequently are as well cleared by ultrafiltration in the kidneys. However, also endocytosis, phagocytosis and immune responses like the formation of anti-drug antibodies (ADAs) contribute to rapid clearance and short *in vivo* half-life of biopharmaceuticals.

1.2.2. Induction of chemical changes

An opportunity to modify plasma half-life and elimination as well as drug efficacy is the induction of chemical changes. Examples for chemical modifications are PEGylation, glycoengineering and amino acid exchanges which are described along with other technologies subsequently.

PEGylation

Pharmacokinetic performances of biologicals can be modified by coupling of the peptide or protein to one or more polyethylene glycol (PEG) molecules referred to as PEGylation. Abuchowski et al. first described PEGylation [29, 30] and a pegylated form of adenosine deaminase was marketed in 1990 after FDA approval [31]. Several pegylated drugs entered the markets since then. Prominent examples are pegylated granulocyte-colony stimulating factor (Pegfilgrastim), pegylated asparaginase (pegaspargase) and certolizumab pegol which is a humanized monoclonal antibody fragment conjugated to PEG.

PEGs can vary in size and are generally recognized as safe according to the FDA. Different coupling reactions and mechanism are used for conjugation of biological and PEG molecules. Activation of PEG with chemically active groups enables linkage to specific amino acid residues like lysine or other n-terminal moieties. The conjugation of PEG to peptides or proteins offers various advantages. PEGylation increases the actual size of the modified biological lowering the probability of renal clearance which increases circulation time and plasma half-life [37, 38].

Typical examples are listed in Table 2 and considerable half-life prolongations were achieved by PEGylation compared to the native forms of the biologicals, respectively. The half-life of certolizumab pegol is comparable to that of regular monoclonal antibodies which is remarkable as it is only a Fab fragment that would undergo significantly faster clearance without

Table 2: Examples of biologicals and the corresponding plasma half-life of native and PEGylated forms.

Active pharmaceutical ingredient	Plasma half-life [hours]		References
	Native Form	PEGylated Form	
Asparaginase	~ 20.0	114.0 - 600.0	Ho et al., 1986 [32]
Granulocyte-stimulating factor	2.0 - 4.7	42.0	Molineux et al., 2004 [33] and Kearns et al., 1993 [34]
Human Growth Hormone	15.0 - 30.0	~ 100.0	Muller et al., 2004 [35]
Certolizumab pegol	n.d.	14.0	Choy et al., 2002 [36]

PEGylation [36]. Furthermore, PEG as hydrophilic component can enhance the biologics' solubility and prevent peptides or proteins from chemical modifications by external stimuli [39]. Additionally, steric shielding after conjugation of PEG changes degradation pathways as well as immunogenicity because pegylated peptides or proteins are protected from recognition by the immune system [40].

Glycoengineering

Carbohydrates are linked to proteins during naturally occurring post-translational glycosylation processes forming glycoconjugates. Glycoengineering aims at the artificial introduction of additional polysaccharides or exchange of protein-bound carbohydrates. Indigestible PEGs are excreted without degradation or accumulate in the body depending on the molecular weight while carbohydrates are biodegradable using material excretion pathways which is commonly seen as advantage of hyperglycosylation over PEGylation [41, 42]. Inherent characteristics of protein therapeutics like structure, function, biological activity, immunogenic potential or the pharmacokinetic behavior can be modified by glycoengineering. Elliot et al. (2003) demonstrated prolonged circulation as well as enhanced activity of glycoengineered proteins of different subclasses which shows the versatile applicability of the technology [43]. Furthermore, glycosylation patterns substantially contribute to protein stability and structural integrity. For example, the activity of human interferon-β was compared between a native and a glycosylated variant and advantages of the modified protein were found in form of enhanced stability in response to stress factors [44]. Solubility of glycosylated proteins is improved in comparison with non-glycosylated forms which was demonstrated for Fibrinogen and *Plasmodium falciparum* merozoite surface protein 1 [45, 46].

Darbepoietin-alfa as glycoengineered form of erythropoietin received approval by the FDA in 2001 for the treatment of anemia in patients with chronic renal failure [47]. However, stable reproducibility of correct glycosylation patterns remains a major challenge in production of glycoengineered drug products as undesired modifications can also induce adverse effects.

Amino acid exchanges and further techniques

Pharmacological characteristics of peptides and proteins can be modified by substitution of amino acids in the primary structure. Exchange of single amino acid residues can lead to increased stability and altered solubility as well as prolonged plasma circulation or enhanced receptor binding resulting in improved therapeutic efficacy.

Prominent examples are modified insulin variants. Insulin glargine is a recombinant protein based on an *Escherichia coli* expression system which differs from native human insulin in three amino acid positions causing lowered solubility at physiological pH [48]. Altered solubility allows reduction of administration frequency as the amino acid substitutions of insulin glargine lead to prolonged plasma half-life. Another example is insulin lispro in which the position of two adjacent amino acids is inverted resulting in shortened duration of action compared to native human insulin [49]. This is beneficial in blood glucose level management directly following ingestion.

Acylation is a further method to modify plasma half-life and stability of therapeutic peptides and proteins. Carboxylic groups are added to N-terminal amine groups by amine bonds of peptides or proteins causing increased hydrophobicity and altered therapeutic behavior. Typically, the impact of an acylation decreases with increasing peptide or protein size [26].

Finally, genetically engineered fused genes of different proteins are used to express fusion proteins combining characteristic properties of contributing peptides or proteins. Thereby, the increased size improves circulation time of fusion proteins compared to half-life of single protein components. Etanercept is a fusion protein combining the TNF-alpha receptor and the Fc part of immunoglobulin G1 (IgG1) representing the first of its class to receive FDA approval in 1998 [50]. On the one hand inhibition of TNF as inflammation-inducing cytokine allows the treatment of autoimmune diseases like rheumatoid arthritis while on the other hand the plasma half-life of etanercept is enhanced by inclusion of the IgG1 Fc part.

1.2.3. Controlled release of biologicals

The controlled release of drugs offers certain benefits over conventional dosage forms. The most obvious advantage is the extended duration of action which is illustrated in Figure 1. Immediate release formulations typically result in plasma peak concentrations followed by strongly decreasing drug levels and concentrations mainly either exceed the therapeutic window or fall below the threshold for an effective therapy. On the one hand, this can lead to undesirable adverse effects resulting from toxic drug levels and on the other hand phases of adequate efficiency and inadequate efficiency alternate as the therapeutic window is reached or missed.

In contrast to that, long acting release formulations result in constant and intermediate drug concentrations within the therapeutic window over a certain period of time. Obviously, unintended side-effects are avoided while therapeutic efficacy is improved as result of constant drug concentrations within the target concentration. Additional to the improved pharmacological performance, sustained liberation formulations potentially enhance patient compliance by the decreased number of injections required which is, in sum, less painful and time consuming as well as more comfortable. Hence, the burden for healthcare systems is lowered as less therapies are discontinued due to compliance reasons. More precisely, nonadherence to therapies is attributed to 3-10% of total annual US health care costs demonstrating enormous savings potential for societies [51].

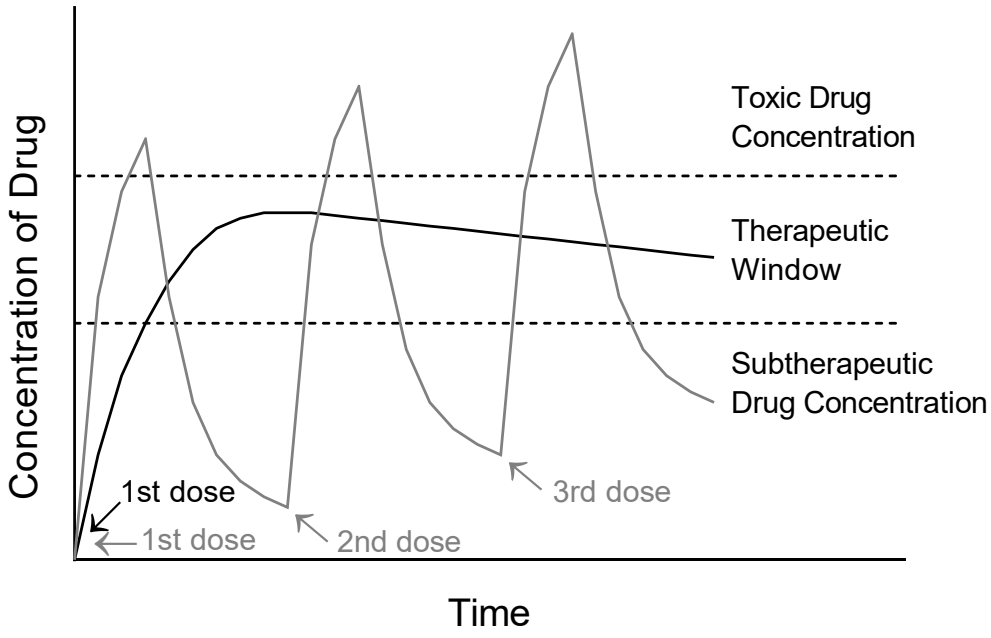

Figure 1: Schematic illustration of drug plasma levels after consecutive administration of a conventional dosage form (—) or after single injection of a controlled release formulation (▬). Arrows indicate the dose regimen of conventional (doses 1-3) and controlled release formulations (dose 1). The therapeutic window is marked by dashed lines, with toxic or subtherapeutic drug concentrations above or below these limits.

Finally, the total amount of drug administered can be reduced using extended release therapies as a result of the improved release profile (Figure 1). As sustained release formulations contain relatively large amounts of drug to provide sufficient API for extended time periods, dose dumping is a typical risk describing the sudden liberation of large drug quantities which could lead to severe adverse effects [52].

As described earlier, biotherapeutics often suffer from short *in vivo* half-life and high elimination rates resulting in the need for frequent dosing to maintain therapeutic plasma levels. In contrast to that, half-life of antibodies is often prolonged due to the large protein size avoiding renal clearance and neonatal FC receptor recycling additionally increases circulation time [53, 54]. Nevertheless, the most common route of administration for monoclonal antibodies are intravenous injections representing a less favorable route when compared to subcutaneous administration [55, 56]. Intravenous injections require hospitalization and additional working hours of medical personnel increasing the pressure on healthcare systems while patients can self-administer subcutaneous injections at home. Oral administration of biologicals would represent a promising but challenging approach due to molecule complexity and stability under harsh environmental conditions in the gastrointestinal tract.

Hence, subcutaneously administered controlled release formulations of biologicals pose an opportunity to reduce the administration frequency, expenses and efforts for administration as well as injection pain while overall patient compliance, safety and efficacy are potentially increased. Different technologies for the realization of extended release formulations for biologicals are described in the following sections.

1.2.4. *In situ* depot-forming systems

One approach for sustained release of biologicals are *in situ* depot-forming systems composed of biodegradable matrix substances in solution with the biopharmaceutical [26]. Typically, the mixture forms a depot system after parenteral injection out of which the drug is released over a prolonged time period. Mechanisms inducing formation of depots are versatile. An example is the *in situ* deport-forming product Eligard® consisting of the luteinizing-hormone releasing hormone agonist leuprolide acetate in combination with biodegradable poly (DL-lactide-co-glycolide) (PLGA) polymers and a liquid carrier [57]. Following subcutaneous injection, the water-miscible liquid carrier diffuses into neighboring tissues allowing water influx in the injection area which results in polymer precipitation, and hence entrapment of leuprolide acetate. The drug is subsequently released in a controlled manner from the polymer depot over variable periods of one, three or six months.

A different technology is the ReGel® platform of biodegradable and biocompatible polymers for the controlled release of proteins and other molecules. ReGel® polymers remain water-soluble

at temperatures below body temperature and form a thermally-induced gel depot after injection as the polymers become water-insoluble in the body [58]. Entrapped drugs are hindered physically from further distribution which accounts for the controlled release effect.

Manufacturing of *in situ* depot-forming controlled release systems is characterized by simplicity as drug and polymer solution are only mixed forming a ready-to-inject solution. However, dependence of release behavior on depot morphology on the specific injection site represents a serious challenge of sustained release approaches based on these technologies [59].

1.2.5. Implant systems

Implantable depot systems are administered via minor operative surgery and a second procedure is required if the implant system is non-biodegradable. Obviously, patient compliance is lowered in consequence of surgical procedures. However, even non-biodegradable systems still offer benefits like reduced peak plasma levels and injection frequency.

A prominent example is the implant system Zoladex® which is a long-acting cylindrical implant based on biodegradable PLGA polymers releasing goserelin acetate, a luteinizing hormone-releasing hormone agonist used for treatment of prostate and breast cancer [60]. After first approval of Zoladex® 3.6 mg in 1989, further indications entered the market.

Viadur® is a non-biodegradable controlled release system based on the DUROS® technology, a titanium osmotic implant. Leuprolide acetate is used in advanced prostate cancer treatment and liberation of the peptide from Viadur® implants occurs over 12 months [61]. Histrelin acetate is a gonadotropin hormone-releasing hormone agonist and is released over 12 months from Vantas®, a subcutaneous implant composed of non-biodegradable copolymers of hydroxypropyl methacrylate and 2-hydroxyl methacrylate [62].

1.2.6. Microparticulate systems

Microparticle-based controlled release systems are commonly known as drug delivery technology. Microparticles are spherical solid objects in the range between 1 to 1000 µm [63]. In the following section, focus will be placed on polymer-based microparticle systems. APIs are encapsulated within polymeric matrices which can be of natural or synthetic origin. They are typically stored in a freeze-dried, stable state and are resuspended in an aqueous vehicle solution for parenteral administration. Different microparticulate species are known ranging from microcapsules with polymeric wall and drug core to classical microparticles with homogenous drug distribution within the polymer matrix. Microparticles are often also referred to as microspheres and both terms are used synonymously in this work.

Types of polymers

A large variety of materials is typically utilized in microsphere production. As stated above, this work will focus on polymeric materials for microparticle manufacturing which can be divided into polymers of natural or synthetic origin referring to the respective resource substances. Particle characteristics are tunable with respect to release behavior, immunogenicity or durability by usage of different polymer types, sizes and chemical variants.

Natural polymers. The group of natural polymers can be clustered into proteins and polysaccharides which are obtained from plants or animals. Therefore, they are relatively easily accessible constituting a major advantage. However, reproducible quality of materials is a challenge for substances derived from natural sources. Furthermore, natural polymers are usually enzymatically degradable which strongly influences the degradation rate in dependence to the area of injection making the release behavior difficult to control. Additionally, the high hydrophilicity of natural polymers complicates control over preservation of shape and stability *in vivo*.

One of the most commonly used proteins for controlled release is the plasma protein albumin which is widely known for its ability to prolong the plasma half-life of coupled drugs by enhancing stability as well as reducing clearance rates by increased size. An exemplary field of application for albumin-based microparticles is the local treatment of arthritic joints and the controlled release of antiarthritic drugs [64, 65]. Drug concentration at the site of inflammation is increased by injection in close vicinity to the affected tissue enabling both prolonged duration of treatment and increased efficacy as systemic exposure is lowered [65].

The extracellular matrix component collagen has also been used for microparticle-based controlled release approaches. For example, vascular endothelial growth factor, a 40-kDa protein, was released *in vitro* over approximately four weeks from collagen-based

microparticles [66]. Gelatin as hydrolyzed degradation product of collagen is also used as material for microparticle manufacturing [67]. Examples include gelatin-based and genipin-stabilized microspheres for the locally directed sustained release of bone morphogenetic protein 2 [68].

Poly (amino acids) are composed of one type of amino acid solely giving them similar characteristics like protein-based polymers. Poly (amino acids) were used for particle-based controlled release approaches for gene and protein delivery [69, 70].

Besides proteins, a further group of natural polymers are polysaccharides consisting of monosaccharides which are linked by glycosidic bonds. A first example for a polysaccharide polymer is chitosan, a chemical derivative of chitin. Chitosan is created by alkaline deacetylation of chitin leading to random arrangements of D-glucosamine and N-acetylglucosamine. Chitosan-based microparticles were used as controlled release systems in protein as well as DNA delivery [71, 72]. Especially delivery of gene products is well feasible as chitosan as polycationic agent effectively binds DNA and related molecules [72]. Amidi et al. used a combinational approach of chitosan and dextran materials to produce inhalable insulin-loaded microspheres [73]. Dextran as complex polysaccharide was further used in different experimental setups for the microparticle-based controlled release of various proteins and protein therapeutics [74, 75].

Synthetic polymers. In contrast to natural polymers, this group of polymers is produced synthetically attributing a higher reproducibility. However, biocompatibility and toxicity are recurrently discussed by the virtue of the non-natural source of synthetic polymers. The chemical composition of synthetic polymers is tunable affecting degradation rate and release behavior of the delivery device. Synthetic polymers are degraded hydrolytically which represents an advantage over the enzymatic degradation of natural polymers. The most intensively studied group of synthetic polymers are poly(esters). In most cases they are synthetized by ring-opening polymerization of corresponding cyclic monomers [76].

Among the most prominent examples for poly(esters) are poly(glycolic acid) (PGA), poly(L-lactic acid) (PLA) and the copolymer of both, poly(DL-lactic-*co*-glycolic acid) (PLGA)

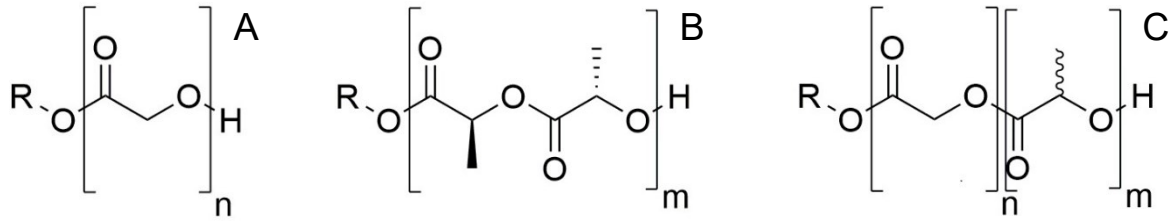

Figure 2: Molecular structures of poly(glycolic acid) (PGA, A), poly(L-lactic acid) (PLA, B), and the copolymer poly(DL-lactic-co-glycolic acid) (PLGA, C). The number of lactic and glycolic acid repeating units is represented by n and m, respectively.

which received approval of regulatory authorities for use in humans and formed the basis of several microparticle drug products. The first patent describing PLA-based microparticles for controlled drug delivery was granted in 1973 [77]. The molecular structures of PGA, PLA and PLGA are depicted in Figure 2. Generally, PLA is the most hydrophobic species among the abovementioned polymers as a consequence of the additional methyl group which is missing in PGA. Accordingly, the hydrolytic degradation rate usually increases from PLA over PLGA to PGA depending on hydrophobicity, but also on molecular weight and functionalization of the polymer end groups with either ester or carboxylic end caps [78, 79]. Moreover, increasing molecular weight results in more rapid biodegradation while ester end groups prolong the survival rate of polymers [80]. Furthermore, the composition and especially pH value of release media or *in vivo* environment strongly influence the degradation and release behavior of PGA, PLA and PLGA with higher pH values decelerating degradation of polymers [78]. In particular the rate of hydrolysis of PLGA is flexible depending on the proportion of lactic and glycolic acid moieties as well as the distribution of the monomers in the final copolymer [80]. However, a 50:50 lactide to glycolide ratio represents a special case and generally results in the fastest degradation [81] while pure PGA or PLA polymers show slower hydrolysis rates. Although the release rate of PLGA-based microspheres is adaptable according to the drug specific requirements, the liberation pattern is typically characterized by a pronounced multiphasic release including periods of initial burst, lag periods with reduced liberation and bulk release.

Owing to the high hydrophilicity and resulting fast degradation rates of PGA, it is not used in sustained release applications until today. In contrast to that, the three-month sustained release formulation of leuprolide acetate, Lupron Depot®, was patented in 1987 and profited from hydrophobicity and slow degradation rates of PLA [82]. The faster release rate of PLGA in comparison to PLA is exploited by the one-month Lupron Depot® formulation which is based on PLGA [79].

Degradation of PLGA is typically characterized by three phases, starting with random chain scission of polymers by hydrolysis leading to significant reduction in molecular weight while particle weight reduction and amounts of escaping monomers are negligible. The second phase is characterized by further hydrolysis and mass loss of particles [83]. Soluble oligomers and monomers diffuse in neighboring regions. Polymers are eliminated in the third phase by ongoing degradation and diffusion of monomers. PLGA is usually considered biocompatible as its monomers glycolide and lactide are naturally occurring in the body. Both monomers can enter the tricarboxylic acid cycle followed by metabolization and excretion as carbon dioxide and water [83]. However, glycolide is also commonly excreted unchanged by the kidneys.

A further biodegradable polymer is poly(ε-caprolactone) (PCL) which also belongs to the most commonly used polyesters in drug delivery and particle manufacturing [84]. With high organic

solvent solubility and a pronounced hydrophobicity together with crystallinity, its degradation rate is generally low when compared to PLGA [85]. PCL is typically degraded *in vivo* over two to three years, and hence usage for long-term release products is reasonable. A prominent example is Capronor, a biodegradable PCL-based contraceptive which releases the synthetic progestogen levonorgestrel over a very long period of 12 to 18 months after subdermal administration [86]. The slow hydrolysis rate of PCL over several years complicates FDA approval of pure PCL-based products. Consequently, polymer blends composed of PCL in combination with PLGA or other faster degrading biodegradable polymers are of increasing interest [87, 88]. Hydrolytic degradation of PCL produces ω-hydroxy hexanoic acid which is excreted unchanged by the kidney route and urine.

Another representative of synthetic polymers is the poly(ester ether) polydioxanone (PDX). It is obtained by ring-opening polymerization of *p*-dioxanone. The polymer degrades over approximately 60 days and complete mass loss occurs after a period of 9 to 12 months [89]. Therefore, PDX is still considered a rather slowly degrading polymer. Conventionally, PDX has been used as suture material since several decades [90]. Degradation is hydrolytically driven and similar to PGA, PDX is either excreted as 2-hydroxy ethoxy acetic acid by the kidneys together with urine or metabolized to carbon dioxide and water in the citric acid cycle. PDX already gained attention for usage in protein-loaded microparticle manufacturing [91].

The synthetic polyether polymer polyethylene glycol (PEG) is hydrophilic and biocompatible. Incorporation of or blending with PEG can modify the inherent characteristics of biodegradable polymers as well as the release behavior of resulting drug delivery carriers [92]. Typically, the introduction of PEG increases release rates from microparticles due to enhanced formation of pores as well as higher water influx [93]. PEGs are neither hydrolytically nor enzymatically degraded *in vivo* and undergo unchanged excretion. Therefore, concerns about *in vivo* accumulation especially for higher molecular weight species of PEG aroused recently and recommendations for usage of lower molecular weight polyethers in biomedical applications appeared [94].

Manufacturing methods for polymeric microparticles

Numerous production processes for protein-loaded microparticle formulation were established with growing interest in microsphere-based drug delivery. The most promising approaches are presented hereafter.

Single emulsion manufacturing methods. Polymer as well as drug molecules are dissolved in an organic solvent and the organic phase is emulsified in an aqueous phase forming an oil in water (O/W) single emulsion [95]. Microparticle droplets are subsequently hardened during evaporation of the organic solvent. The single emulsion technique is especially suitable for hydrophobic drug molecules which are soluble in the organic phase. Hydrophilic drugs have the tendency to escape to the external water phase during particle manufacturing resulting in low entrapment efficiency.

Double emulsion manufacturing methods. Water-in-oil-in-water (W/O/W) based microparticle preparation processes are commonly used for encapsulation of therapeutic peptides and proteins [96, 97]. As presented in Figure 3 according to Lee and Pokorski [98], an aqueous protein solution is added to an organic phase containing the polymer of choice which forms the primary emulsion or dispersed phase. Typical solvents for PLGA in the organic phase are dichloromethane and ethyl acetate. Formation of microparticulate droplets is supported by stirring of the primary emulsion. Thereafter, the mixture is added to a large volume of a second aqueous phase, also called external water phase or continuous phase. The external water phase typically contains polyvinyl alcohol (PVA) which stabilizes microparticulate droplets preventing agglomeration. Subsequently, the organic solvent is removed by evaporation leading to particle hardening. Microparticles are washed and freeze-dried in the next steps. The lyophilized product is generally stable and ready-to-use for reconstitution and administration for drug delivery purposes.

Effective protein loading and high encapsulation efficiency are crucial to serve high dosing requirements occurring for subcutaneously administered controlled release delivery devices of

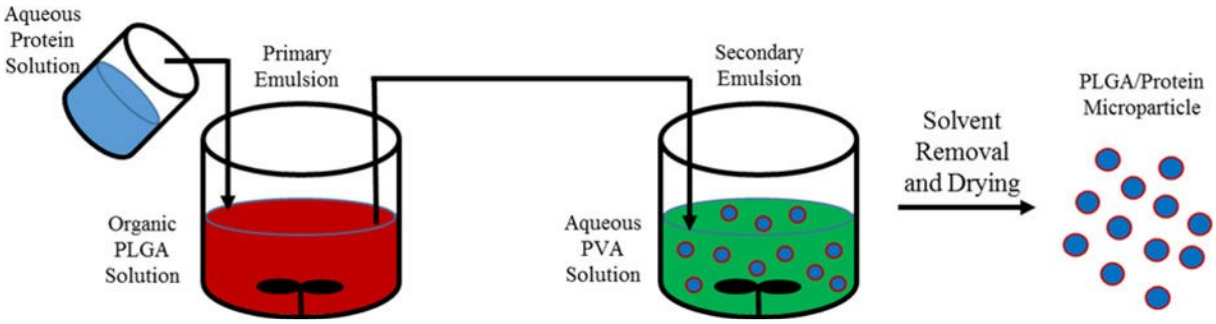

Figure 3: Schematic illustration of a typical water-in-oil-in-water emulsification process for microparticle encapsulation of a protein drug according to Lee and Pokorski [98].

biologicals. Particle characteristics (e.g. loading and encapsulation efficiency) are tunable by various factors like ratio of different phases, addition of stabilizing agents like salts and surfactants, modification of stirring rates and periods, viscosity especially of the primary emulsion or concentration of polymer as well as drug in the respective phases [99-101].

An important technique to gain control over the particle size distribution of microparticle formulations is membrane emulsification [102, 103]. Homogenously distributed particle sizes are beneficial as the drug release pattern is more reproducible and injectability is enhanced allowing the usage of smaller needle sizes which reduces the injection pain of patients. A typical membrane emulsification process is depicted in Figure 4 according to Joscelyne and Träghårdh [104]. The primary emulsion or dispersed phase containing water droplets with API in polymers dissolved in organic solvent is pressed through the pores of a membrane. The continuous aqueous phase circulates over the membrane leading to the formation of uniformly sized microdroplets. Factors affecting the microdroplet size and thereby the size of the final microparticle product are for example the ratio between continuous and dispersed phases, membrane pore size, circulation speed of the continuous phase and pressure applied to the dispersed phase.

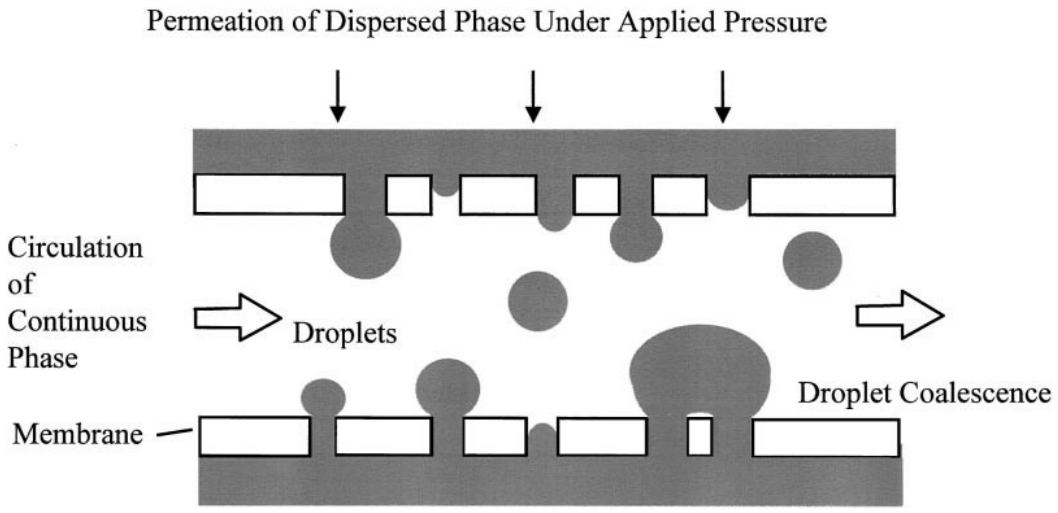

Figure 4: Schematic figure of a membrane emulsification during a W/O/W microparticle manufacturing process according to Joscelyne and Träghårdh [104].

Coacervation-based manufacturing processes. An alternative technique to encapsulate protein therapeutics within polymeric microparticles is the coacervation or phase separation representing a water in oil in oil (W/O/O) process. The coacervation approach is depicted in Figure 5 according to Lee and Pokorski [98]. Typically, the polymer of interest is dissolved in a primary solvent like dichloromethane or ethyl acetate [105]. An aqueous protein solution is thereafter added to the polymer solution and a primary emulsion is prepared thereby. In the next step, a primary, organic polymer non-solvent is added which extracts the primary polymer

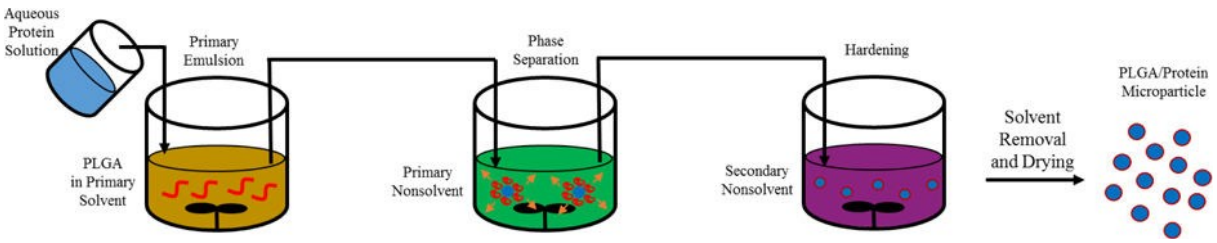

Figure 5: Schematic illustration of a coacervation (W/O/O) process for encapsulation of a protein in PLGA microparticles according to Lee and Pokorski [98].

solvent resulting in phase separation of the polymer [105]. Commonly used non-solvents are silicone oils or paraffins [106]. Premature microparticles are obtained at this stage. Subsequently, microparticles are hardened by addition of a secondary polymer non-solvent, typically hexanes or heptanes [106]. Finally, solvents are removed and microparticles are dried for storage.

Encapsulation of hydrophilic compounds can be achieved with higher efficiency using coacervation processes when compared the conventional single or double emulsions as described herein previously [107, 108]. Especially in the case of W/O/W manufacturing processes, the external aqueous phase poses an attractive environment for hydrophilic compounds resulting in lowered encapsulation efficiencies due to escaped API.

During solvent extraction in coacervation, premature microparticles tend to agglomerate if stirring speeds, temperature and volumetric ratios of polymeric and protein phases are chosen unfavorably [105, 109, 110]. This demonstrates a relatively low control over particle size in phase separation processes which is a common drawback of the technique. Nevertheless, W/O/O particle manufacturing allows fast screening for suitable formulation candidates and rapid development progression which can be beneficial during microparticle formulation studies.

Further manufacturing approaches. Several additional methods are used for microparticle manufacturing and will be mentioned shortly in this work. During spray drying, a primary emulsion consisting of a polymer-containing oil phase and an API-containing aqueous phase is led through the inner channel of a spray drying nozzle while a hot gas stream flows through an outer channel. This leads to the formation of small droplets when both streams are forced through a narrow opening. The droplets are directed into a drying chamber where the residual solvents are removed. Different types of nozzles exist offering certain advantages and disadvantages.

Electrohydrodynamic methods like electrospinning or electrospraying use electric potentials to overcome the surface tension of a W/O emulsion containing both, polymer and drug molecules. The emulsion is leaving a tip in response to the electrical charge either in form of a jet or as droplets. Polymeric items are collected on grounded plates or rotating drums.

Melting solid polymers like PLGA together with proteins during hot melt extrusion processes using high temperatures in a heated barrel is another technique for the preparation of polymeric drug delivery devices. However, as a result of the high temperatures that are necessary during this process its use for incorporation of sensitive biotherapeutics is limited.

Protein instabilities and conventional PLGA-based microparticle release systems

As described previously, PLGA is among the most commonly used copolymers for microparticle-based drug delivery solutions. Despite its success and application in numerous controlled release products, also serious drawbacks of PLGA in combination with peptide and protein release are known. Protein degradation leading to incomplete release is a major issue that can on one side reduce the therapeutic efficacy and on the other side enhance the immunogenic potential as degraded proteins may contribute to toxic side effects. Degradation of biotherapeutics can occur during different stages of particle manufacturing as well as during drug release. Stress factors during manufacturing include amongst others exposure to organic solvent interfaces, stirring and shear stress as well as challenging temperatures. These stressors are obviously not limited to PLGA-based manufacturing processes. Release-related instabilities as well as PLGA-protein interactions influencing protein stability are outlined hereafter.

Protein instability during release. Protein degradation in PLGA microparticles can be mainly attributed to microacidification as well as protein-PLGA interactions. Acidification of the microclimate within PLGA-based microparticles is a commonly observed phenomenon which is caused by accumulation of acidic degradation products of polymers following hydrolytic splitting. Numerous studies reported influences of a pH drop within microspheres on protein stability resulting in protein hydrolysis and structural changes [111-113]. The microclimate within PLGA microparticles has been demonstrated to drop to pH values as low as 1.5 clearly representing a challenging environment for sensitive peptide and protein therapeutics [114-116]. Referring to this, Ding and Schwendeman demonstrated influences of polymer molecular weight, monomer ratio, manufacturing technique as well as PEG incorporation in particles on the pH drop within microspheres which is especially diminished by inclusion of PEG [116]. Amide bond hydrolysis and resulting peptide chain cleavage depends on the extent of the pH drop and is especially observed after asparagine residues [117, 118], as for example observed following PLGA-based encapsulation of carbonic anhydrase [119]. Furthermore, the acidic climate not only resulted in protein degradation but also induced deamidation and covalent dimerization of encapsulated insulin [115].

Interactions between PLGA and proteins. Polyesters of lactide and glycolide as well as copolymers thereof are hydrophobic in varying degrees and hydrophobic interactions between

the polymer matrix and embedded protein cargo can occur potentially leading to irreversible formation of insoluble aggregates [120, 121]. Furthermore, electrostatic interactions between protein and polymer influence the release behavior while the degree of the release modification depends on the polymer characteristics [122, 123]. In both studies, the release rate from polymers with free carboxylic end groups was decreased compared to the rates observed for polymers with capped end groups. Additionally, release from PLGA with free carboxylic end groups proved to be beneficial regarding protein integrity while capped end groups impaired protein stability significantly [122]. Park et al. demonstrated that non-covalent aggregation as well as hydrophobic protein-PLGA interactions were responsible for incomplete release of the model protein lysozyme from microparticles [124]. The acidic microclimate within PLGA-based microparticles supports acid catalyzed chemical modification of proteins like deamidation meaning removal or modification of amide groups in side chains of asparagine or glutamine. This was stated by different groups and for different model proteins, for instance bovine insulin [125, 126]. The degree of deamidation correlates with the PLGA hydrolysis rate which is obviously related to the microclimate pH [127].

A further chemical degradation pathway are acylation reactions between peptides or proteins and ester bonds of PLGA. Na and DeLuca demonstrated that the N-terminus of octreotide is predominantly involved in the acylation reaction with PLGA polymers leading to significant protein degradation [39]. Up to 45% of the total amount of different PLGA-encapsulated peptides were acylated during *in vitro* release studies [128, 129]. Higher molecular weight of PLGA and increased content of glycolide monomers favor acylation reactions with peptides and proteins [130].

Approaches to prevent protein degradation. The most promising tactic to prevent peptide and protein aggregation in PLGA microspheres is the co-encapsulation of basic pH modifiers within particles. Common examples are basic salts like calcium carbonate [131], magnesium hydroxide [120] or zinc carbonate [132] buffering the microenvironment within microparticles after accumulation of acidic PLGA degradation products. Basic stabilizers as well as their concentration within the polymer matrix require careful choice as influences on polymer degradation rate were observed [120, 131]. Furthermore, an initially basic microenvironment within microparticles resulting from incorporation of high basic salt concentrations can induce, similar to acidic polymer degradation products, peptide break down [120, 132].

PEGylation of encapsulated peptides or proteins is a further approach to reduce protein degradation by either shielding potential cleavage sites at the drug molecule or leading to increased water influx which reduces the pH drop. The peptide drug octreotide in a PEGylated form was successfully prevented from acylation while the biological efficacy remained unaffected [39, 133].

As a consequence of the instabilities described in the preceding section, currently, no PLA or PLGA based drug delivery product for protein therapeutics has FDA approval exhibiting a clear need for alternative polymers which show a higher compatibility with sensitive cargos like large proteins or susceptible peptides.

1.2.7. SynBiosys® polymer platform

The release of peptides and proteins from conventional PLGA-based drug delivery systems exhibits several serious drawbacks as described in the previous section. Simultaneously, a clear need for alternative release systems for biotherapeutics arises driven by their increasing relevance in the pharmaceutical sector. A promising approach for microparticle based long acting injectable formulations for peptide and protein therapeutics is the SynBiosys® polymer platform which was developed by InnoCore Pharmaceuticals (The Netherlands). The suitability of SynBiosys® polymers for controlled release of biologicals is the research object of the present work.

The SynBiosys® platform is a family of biodegradable poly (ether ester) multi-block copolymers composed of variable amounts of clinically proven safe monomers which are shown in Figure 6. Inherent characteristics of glycolide, lactide, ε-caprolactone and *p*-dioxanone were described earlier. Starting from variable amounts of these monomers, prepolymers comprised of different quantities of DL-lactide, glycolide, ε-caprolactone, dioxanone and/or polyethylene glycol are linked with the chain extender 1,4-butanediol by ring-opening polymerization thereby forming prepolymeric species which are tunable regarding their hydrophilicity and crystallinity (Figure 7) [134]. The prepolymers are chain-extended to form multi-block copolymers by using 1,4-butanediisocyanate in the next step. In this way, a phase-separated polymer matrix is obtained which combines hydrophilic amorphous and hydrophobic crystalline domains. While hydrophobic regions add stability and rigidity to the polymer matrix, hydrophilic parts allow water-influx thereby introducing swellability and protein-friendly environments inside microparticles. Water-influx induces swelling regions in microparticles which allows a diffusion-controlled release. As described earlier, conventional PLGA-based microparticles for

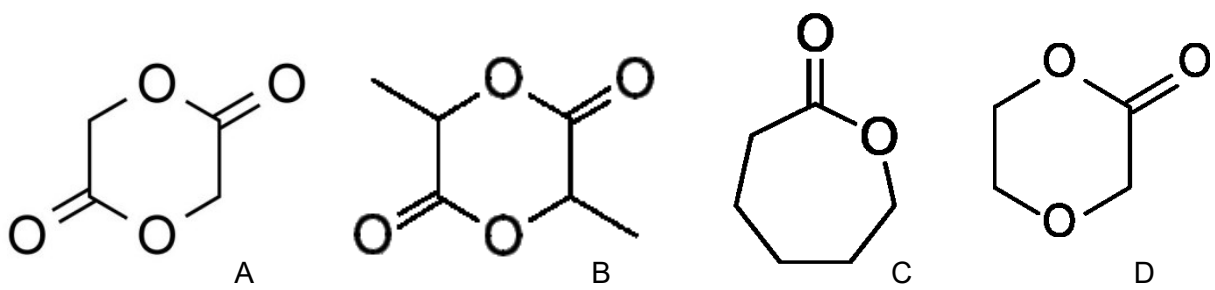

Figure 6: Monomers of the SynBiosys® platform include glycolide (A), lactide (B), ε-caprolactone (C) and p*-dioxanone (D). This figure was customized and originated from internal cooperation documents.*

controlled release often exhibit multiphasic release patterns resulting from degradation-based release following polymer hydrolysis. In contrast to that, hydrophilic, swellable domains within SynBiosys® microparticles with diffusion-controlled release characteristics allow a more continuous release of the encapsulated API.

Variables to tune the release behavior and inherent characteristics of multi-block copolymers are the type of monomer as well as monomer ratio, block length and the amount and molecular weight of PEG incorporated. Furthermore, the manufacturing process plays an important role as polymer concentration, stirring speeds and times, phase ratios as well as the addition of surfactants or other additives influence the release behavior of resulting SynBiosys® microspheres. SynBiosys®-based microparticles examined as part of this work were prepared by water-in-oil-in-water (W/O/W) membrane emulsification or water-in-oil-in-oil (W/O/O) manufacturing processes as described earlier herein. Details on manufacturing processes and exact polymer compositions of microparticles investigated herein are described in section 2.7.

SynBiosys® polymers are degraded hydrolytically and similar to classical polymeric controlled delivery systems degradation products are acidic which is obvious as conventional monomers are incorporated in multi-block copolymers. However, the water-influx in hydrophilic, swellable regions within SynBiosys® microparticles potentially avoids the accumulation of acidic degradation products creating protein-friendly microenvironments. The beneficial effects of PEG on encapsulated peptides and proteins has been described earlier by different groups [135-137]. The degradation products of lactide, glycolide, ε-caprolactone and *p*-dioxanone were already described in the previous section. Additionally, 1,4-butanediol and 1,4-butanediisocyanate are used within SynBiosys® multi-block copolymers which are excreted unchanged (1,4-butanediol) or as 1,4-butanediamine (1,4-butanediisocyanate) via the urinary route.

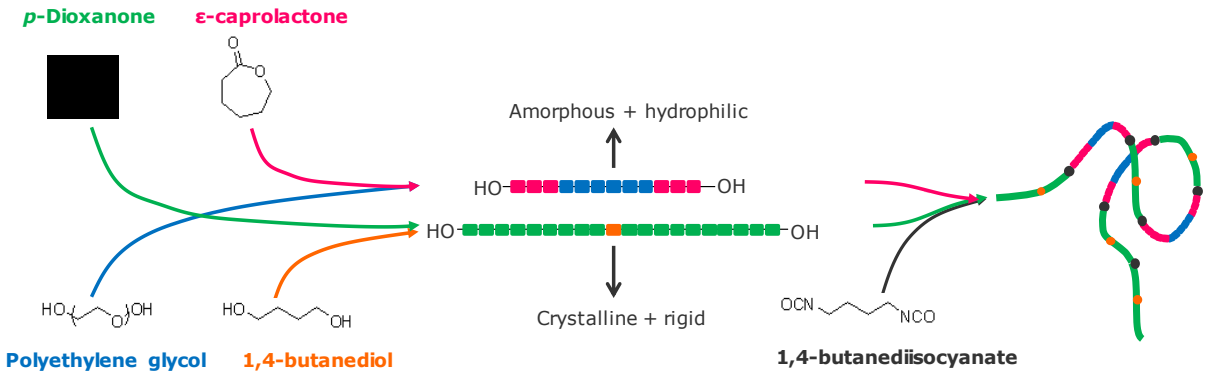

Figure 7: Schematic representation of the synthesis process for SynBiosys® multi-block copolymers. Monomers of choice are combined with initiators like polyethylene glycol or 1,4-butanediol to form prepolymers with tunable characteristics. Prepolymers are assembled by chain extension using 1,4-butanediisocyanate. The monomers ε-caprolactone and p-dioxanone are shown here representatively and could also be replaced by lactide and glycolide or combinations of all four monomers. This figure was customized and originated from internal cooperation documents.

The SynBiosys® polymer platform already attracted attention for various applications like microparticles, extruded implants and microspheres tailored for local delivery, for example intravitreally [138-143] for sustained delivery of different molecules. Furthermore, SynBiosys® polymers are used for coating of the COMBO™ Dual Therapy drug-eluting stent by OrbusNeich® (People's Republic of China) which already received market approval [144].

However, the beneficial properties of polymers of the SynBiosys® platform for controlled release of sensitive peptides and proteins require confirmation and demonstration on the basis of diverse case studies which is targeted in the present work.

1.3. Model drugs

The SynBiosys® polymer platform was evaluated herein regarding the suitability for controlled release of biotherapeutics. For that purpose, model drugs with different properties were encapsulated to demonstrate the versatility of the polymers. As described earlier, biologicals cover a large variety of molecular sizes and types of molecules. Herein, the controlled release properties of SynBiosys® were examined using a sensitive peptide and two monoclonal antibodies to implement a comprehensive overview of the polymers' flexibility.

1.3.1. Exenatide

Diabetes is among the most widespread diseases and the number of people with diabetes is estimated to increase from approximately 463 million in 2019 to 578 million people in 2030 and further to 700 million in 2045 [145]. Remarkably, 10% of global health expenditure is spent on diabetes [146]. Thereby, approximately 90% of diabetes cases account for type 2 diabetes mellitus (T2DM) demonstrating the relevance of this disease nowadays [145]. T2DM is mainly defined by a dysregulated glucose metabolism which is basically resulting from impaired insulin secretion of pancreatic β-cells and insulin resistance in muscles and liver [147]. According to DeFronzo et al. (2015), T2DM is additionally characterized by several factors outlined hereafter [148]. Enhanced glucose production in the liver, increased renal glucose reabsorption, vascular insulin resistance and inflammation contribute to T2DM pathology [148]. Furthermore, adipocyte insulin resistance leads to lipolysis as well as enhanced plasma free fatty acids, and insulin resistance is further exacerbated [148]. Finally, neurotransmitter dysfunctions in the brain lead to further weight gain aggravating the disease [147]. Numerous complications result from T2DM, for instance renal failure, blindness, damages of the nervous system as well as accelerated progression of cardiovascular disease [149].

Common therapies for glycemic control include administration of insulin (lowering blood glucose), metformin (lowering hepatic glucose production), sulfonylureas (improved insulin secretion), thiazolidinediones (improved β-cell function and insulin sensitivity),

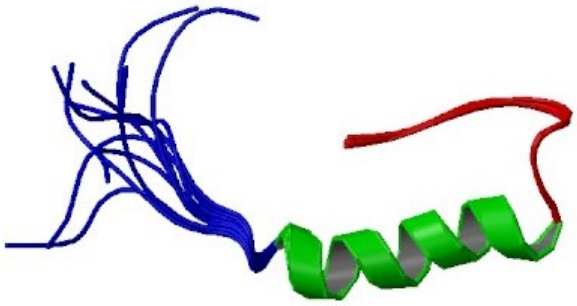

Figure 8: Peptide structure of exenatide, as presented by drugbank.ca [152]. The secondary structure is dominated by α-helices.

dipeptidylpeptidase 4 inhibitors (lowering glucagon secretion and improving insulin secretion), sodium/glucose co-transporter 2 inhibitors (lowered glucosuria and glucotoxicity), α-glucosidase inhibitors (lowering carbohydrate uptake) and glucagon-like peptide 1 receptor (GLP1-R) agonists (lowering glucagon and improving insulin secretion) [148].

A well-known representative of GLP1-R agonists is exendin-4, a GLP-1 analogue which was first isolated in the early 1990's from *Heloderma suspectum* venom [150]. Exenatide is a synthetic peptide with the same amino acid sequence as exendin-4 and shares approximately 53% sequence homology with mammalian GLP-1 [151]. It is composed of 39 amino acids and has a total molecular weight of 4.187 kDa. The peptide structure of exenatide is presented in Figure 8, according to drugbank.ca [152]. The secondary structure of the peptide is dominated by α-helices [153].

Exenatide bears a multi-facetted mechanism of action. The most prominent effect of exenatide is its glucose-lowering role in consequence of GLP1-R stimulation on pancreatic β-cells leading to glucose-dependent insulin secretion [154, 155]. Additionally, exenatides leads to reduced rates of gastric emptying and glucagon secretion as well as improved β-cell proliferation which can affect the clinical picture positively [156-158]. Food intake was reduced and body weight was lost following exenatide therapy in a rodent diabetes model [159].

Exenatide received approval for treatment of T2DM by the FDA in 2005. Bydureon® is a one-week extended release formulation of exenatide based on PLGA microparticles and received FDA approval in 2012 [160, 161]. Bydureon® therapy consists of weekly administrations of encapsulated exenatide (2 mg/week). The immediate release exenatide formulation Byetta® was introduced in 2005 and is typically administered twice daily at doses between 5 to 10 µg per injection. Representing a PLGA-based microparticle formulation, Bydureon® served as benchmark to showcase common limitations of these release systems and to demonstrate benefits of the SynBiosys® polymer platform. Additionally, the marketed, immediate release formulation of exenatide, Byetta®, was used as a reference.

1.3.2. Monoclonal antibodies

Monoclonal antibodies (mAbs) cover the upper molecular weight range of protein-based biotherapeutics. The molecular complexity is generally high when compared to peptides or smaller proteins which is typically accompanied by pronounced sensitivity. Monoclonal antibodies originate from identical hybrid cells produced with the hybridoma technology which was introduced in 1975 [162]. The key characteristic of this antibody class is the binding ability to monovalent epitopes which is a major difference to polyclonal antibodies binding multivalent epitopes. During the past decades, technological improvements have been achieved with the production of chimeric [163], humanized [164] and fully human monoclonal antibodies [165] leading to reduced immunogenic potentials with increasing humanization of the antibody molecule. Monoclonal antibody-based treatments cover a wide range of therapeutic areas including cancer, autoimmune, genetic, infectious and cardiovascular diseases as well as transplant rejection and many others.

Human antibodies or immunoglobulins (IG) are generally divided into 5 classes: IgM, IgD, IgA, IgE and IgG. The classes differ in effector functions and IgG represents the most commonly used class among marketed, therapeutically used mAbs. IgG antibodies are then further divided into subclasses of IgG1 to IgG4 of which IgG1 is the most frequently occurring type [166].

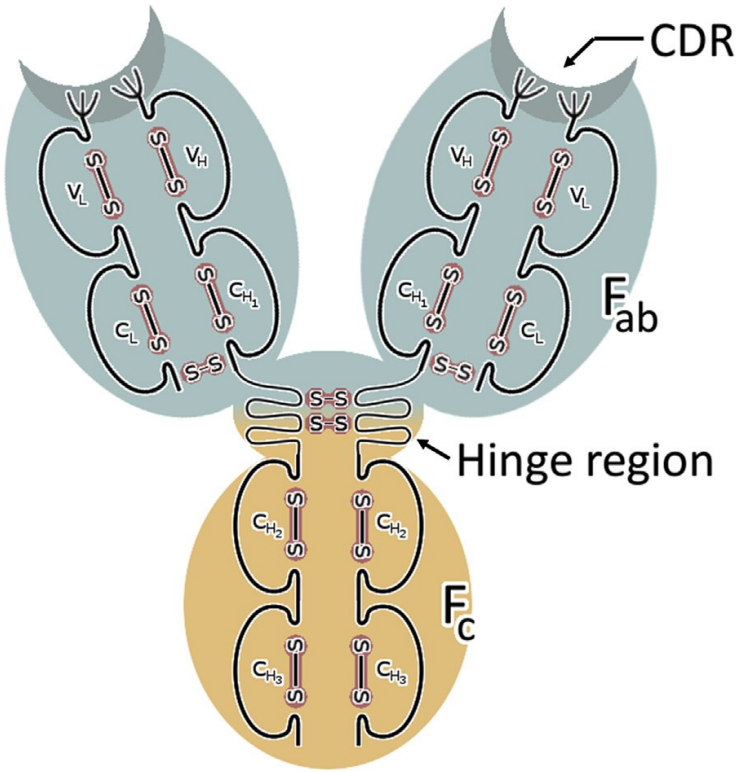

Figure 9: Typical structure of an antibody molecule. Complementary determining regions (CDR) define the antibodies' antigen specificity. Two heavy (H) and two light (L) chains are linked together by disulfide bridges (S) forming variable (V) and constant (C) regions in the antigen-binding (F_{ab}) and the crystallizable fragments (F_c). The hinge region provides flexibility. This figure was taken from Basle et al., 2020 [167].

Figure 9 was taken from Basle et al., 2020 [167], and shows the typical structure of an antibody. In total, antibodies are composed of two heavy and two light chains forming variable and constant regions. In that context, variable regions are responsible for highly specific antigen-binding, especially supported by complementary determining regions. Variable regions are found in the antigen-binding fragment (F_{ab}) which is the counterpart of the crystallizable fragment (F_c) triggering activation of the complement system. The complex structure of antibodies is stabilized by numerous disulfide bridges, especially in the flexibility-introducing hinge region. The sensitivity of antibodies to instabilities and external stress factors is comprehensible in consideration of the highly complex molecular structures. Antibodies are prone to chemical as well as physical degradation elucidating the challenge of delivering biologically active mAbs in a controlled manner. Two different mAbs were utilized as representative models herein to examine the suitability of SynBiosys® polymers for the controlled release of functionally intact proteins.

mAbB. The monoclonal model antibody B is a protein of 144.9 kDa which is directed against *S*ty1/Spc1-*in*teracting protein 1 (Sin1). This protein is an essential part of the mammalian target of rapamycin (mTOR) complex 2 and the dysregulation of mTOR complex 2 in cells is a typical feature of multiple diseases including cancer, obesity and type 2 diabetes mellitus [168-170]. Consequently, mAbB has wide-ranging potential for use in therapies of various diseases demonstrating its role as versatile developmental candidate drug.

mAbX. The model antibody mAbX also belongs to the IgG1 family and is directed against the epidermal growth factor receptor (EGFR) which was initially isolated from human A-431 epidermoid carcinoma cells by Cohen et al. in 1980 [171]. EGFR is a family member of receptor tyrosine kinases which are known to play critical roles in oncogenesis of numerous types of human cancer by supporting cell proliferation and opposing apoptosis [172-174]. Expression of the EGFR gene is upregulated in a multitude of cancer types like cancers of head and neck [175]. Hence, binding of mAbX to EGFR leads to growth inhibition of tumor cells in combination with antibody-mediated recruitment of anti-tumoral immune responses.

1.4. Objectives of this work

The overarching aim of this work was the implementation of a comprehensive portfolio of *in vitro* as well as *in vivo* methods to allow a reliable evaluation of the suitability of SynBiosys® polymers for the microparticle-based controlled release of sensitive peptide and protein therapeutics.

SynBiosys®-based microparticle formulations of different model APIs were developed by InnoCore Pharmaceuticals which represented the objects of research for the work presented herein. The peptide therapeutic exenatide was encapsulated to represent the lower end of the size range of biologicals while mAbB was utilized for the determination of suitable polymer compositions for large, complex proteins. Especially the release of therapeutically intact, large proteins is challenging, and hence a second monoclonal antibody, mAbX, was formulated in SynBiosys® microparticles based on the findings of mAbB experiments to demonstrate the versatility of the polymer platform.

A first objective was the intensive *in vitro* and *in vivo* examination of exenatide-based microparticle formulations. For that purpose, implementation of a cell-based functional assay for exenatide released from microspheres was of interest demonstrating the functional binding of the peptide to the GLP-1 receptor (GLP1-R) leading to intracellular responses of GLP1-R overexpressing CHO-K1/GLP1/Gα15 cells. However, the examination of *in vivo* release behavior of microparticles and the determination of the therapeutic efficacy of *in vivo* released exenatide were of greater relevance. Hence, implementation of a T2DM animal model and relevant analysis methods were expedient. Additionally, the immunogenic potential of microparticle formulations was targeted by introducing a cytokine release assay in combination with histochemical staining of skin samples from injection areas.

In vitro release studies of mAbB were aiming at the determination of suitable SynBiosys® polymer compositions for the controlled release of large proteins with high protein integrity over a reasonable time period. Consequently, the central objective of the mAbB work package was to establish methods for evaluation of the protein integrity after *in vitro* release. Circular dichroism and fluorescence spectroscopy are appropriate methods for the determination of secondary and tertiary structure intactness of released protein allowing statements concerning the influence of the polymer composition on the protein cargo.

Finally, an extensive *in vitro* and, in particular, *in vivo* examination of mAbX-loaded SynBiosys® microparticles was targeting to demonstrate of the polymer platforms' flexibility with regard to large proteins. Circular dichroism and fluorescence spectroscopy methods, an enzyme-linked immunosorbent receptor binding assay as well as a functional cell-based assay for mAbX were

implemented to extensively evaluate the integrity of the monoclonal antibody after *in vitro* release. Objectives during *in vivo* studies were the implementation of methods for the determination of the microparticles' immunogenic potential, for instance a cytokine release assay and histochemical staining of skin samples from injection areas. Furthermore, pharmacokinetic as well as pharmacodynamic studies of mAbX-loaded SynBiosys® microparticles required careful planning and analyses to assess *in vivo* release behavior and therapeutic efficacy of *in vivo* released antibody.

2. Materials & Methods

The following section lists materials and methods used for experiments described in this work. All other materials and chemicals were purchased from the usual commercial sources at the best grade available.

2.1. Devices and instruments

The devices and instruments used herein are described in the following Table 3.

Table 3: Devices and instruments.

Device / Instrument	Equipment-#	Manufacturer
Axiovert 40 CFL Microscope	70104900	Carl Zeiss AG
Bio-Plex MCV plate IV	171-203033	Bio-Rad Laboratories, Inc.
BioSpectrometer® kinetic	70263804	Eppendorf AG
Cary eclipse fluorescence spectrophotometer	70084100	Agilent Technologies, Inc.
Cary temperature controller	70084100	Agilent Technologies, Inc.
Centrifuge 5810 R	70266343	Eppendorf AG
Coulter Counter Multisizer III	INN/2010/004	Beckmann Coulter, Inc.
Envision 2014 multiplate reader	70160330	PerkinElmer, Inc.
Hellma cuvette 110-QS	110-1-40	Hellma GmbH & Co. KG
Hellma cuvette 114F-QS	114F-10-40	Hellma GmbH & Co. KG
HPLC Agilent 1290 Infinity	70226187	Agilent Technologies, Inc.
Incubator BBD 6220	51020241	Thermo Fisher Scientific, Inc.
JCM-5000 Neoscope	INN/2011/039A	JEOL Ltd.
J-815 circular dichroism spectrometer	70104613	Jasco, Inc.
LA-960 Laser Particle Size Analyzer	n.a.	Horiba Ltd.
LaminAir HB 2448	70024003	Heraeus GmbH
Luminex® 200	70099826	Luminex corporation
Microplate Reader Multiskan spectrum	70112939	Thermo Fisher Scientific, Inc.
Microtiter plate shaker Thermomixer comfort	n.a.	Eppendorf AG
Milli-Q advantage A10	70227286	Merck KGaA
Minitron Infos HT	70229753	Infors AG
QuixSep micro dialysis capsules	H448.1	Carl Roth GmbH & Co. KG, Germany
SevenExcellence pH meter	70230229	Mettler Toledo, Inc.
SW22 Water Bath	10097008	JULABO Labortechnik GmbH
Systec VX-150	101291150	Systec GmbH
Ultra Turrax T25 basic	INN/2014/092	IKA®-Werke GmbH & Co. KG
Ultrasonic cleaner	142-6044	VWR/Avantor, Inc.
UPLC Aquity H class	n.a.	Waters corporation
ViCellXR	70249850	Beckman Coulter corporation
Waters 2690 HPLC system	n.a.	Waters corporation

2.2. Consumables and disposables

Table 4 shows consumables and disposables used for experiments of this work.

Table 4: Consumables and disposables.

Consumable / Disposable	Catalogue-#	Manufacturer
Acquity UPLC CSH C18 column	186005296	Waters corporation
Bottle Top Filtration Units	514-0349	VWR/Avantor, Inc.
Cellstar Aspirator pipette, 2 mL	710183	Greiner-Bio One GmbH
Cellstar cell culture flask, 75cm², 250 mL	658175	Greiner-Bio One GmbH
Cellulose Acetate membrane filter 0.22 µm	11107-47-N	Sartorius AG
Complete tear off aluminium seal 13 mm	Coutw13	Adelphi Healthcare Packaging Ltd.
Deepwell protein LoBind plate	89085-654	Eppendorf AG
Dialysis tubing cellulose membrane	D9527-100FT	Merck KGaA
FluroTec® stoppers 13 mm	20180223	Disposable-Lab SAS
Glass capillary	n.a.	Carl Roth GmbH & Co. KG
CELLSTAR® serological pipette 5, 10, 25 mL	P7615, 7740, 7865	Greiner-Bio One GmbH
High-clarity polypropylene conical tube, 15 and 50 mL	352096, 352098	Corning, Inc.
HPLC vial 0.2 and 1.5 mL	548-3308, 548-0030	VWR/Avantor, Inc.
Microtiter plate Nunc Maxisorb	M5785-1CS	VWR/Avantor, Inc.
Microvette 200 K3E	20.1288	Sarstedt AG & Co.KG
Multiscreen HTS Filter plates	MSBVN1210	Merck KGaA
Nunc microtiter plate Maxisorb	735-0034	VWR/Avantor, Inc.
Nunclon™ Delta Surface 96-well plate	168055	Thermo Fisher Scientific, Inc.
Obesity-inducing diet w/ 60% energy from fat	C1090	Altromin Spezialfutter GmbH
Pasteur pipettes	612-1701	VWR/Avantor, Inc.
PCR foil	0030127820	Eppendorf AG
Protein LoBind Tube 1.5 mL	0030108.116	Eppendorf AG
Pyrofree® 2 mL clear tubular glass vials	20180265	Disposable-Lab SAS
QPath microstar III, yellow	720-2084	VWR/Avantor, Inc.
QPath Schwämmchen	720-2254	VWR/Avantor, Inc.
Reagent reservoir 25 and 50 mL	613-1176, 613-1183	VWR/Avantor, Inc.
Safe-lock tubes 1.5 mL	0030120.086	Eppendorf AG
Sealing tape (sterile)	236366	Thermo Fisher Scientific, Inc.
TSKgel Guard column	18762	Tosoh Bioscience GmbH
TSKgel SuperSW3000	18675	Tosoh Bioscience GmbH

2.3. Chemicals and reagents

Chemicals and reagents used for experiments described in this work are listed in Table 5.

Table 5: Chemicals and reagents.

Chemical/reagent	Catalogue-#	Manufacturer
Aqualon™ sodium carboxymethylcellulose	7HF-PH	Ashland, Inc.
Bio-Plex® Calibration Kit	171203060	Bio-Rad Laboratories, Inc.
Bio-Plex® Validation Kit 4.0	171203001	Bio-Rad Laboratories, Inc.
Cell viability reagent kit	2400102	Beckman Coulter, Inc.
Dulbecco's Modified Eagle's Medium/Nutrient Mixture F-12 Ham	D8437-500ml	Merck KGaA
Dulbecco's phosphate buffered saline	D8537	Sigma-Aldrich/Merck KGaA
Dulbecco's phosphate buffered saline (w/o Ca^{2+}/Mg^{2+}, low endotoxin)	L1825	Merck KGaA
Dulbecco's phosphate buffered saline, 10x, w/o Ca^{2+}/Mg^{2+}	SH30378.02	Thermo Fisher Scientific, Inc.
Exenatide acetate	4044219	Bachem Holding AG
Fetal bovine serum (FBS)	1600-044	Thermo Fisher Scientific, Inc.
Formaldehyde solution 4%, buffered, pH 6.9	1.00496.8350	Merck KGaA
Gel filtration standard	151-1901	Bio-Rad Laboratories, Inc.
Gentamycin sulfate	345815-20ML	Merck KGaA
GLP-1 (9-36)	3266	Bio-Techne Ltd.
Goat-anti human kappa light chain-HRPO	A1764-1mL	Sigma-Aldrich/Merck KGaA
Guanidine hydrochloride	G4505-500G	Merck KGaA
Ham's F12 cell culture medium	FG0815	Merck KGaA
Hellmanex III	2805939-1EA	Hellma GmbH & Co. KG
Hygromycin B	400052-20ML	Merck KGaA
mAbB	n.a.	Merck KGaA
mAbX	n.a.	Merck KGaA
mAb05 Merck-internal reference standard	mAb05-RS	Merck KGaA
Mouse plasma NMRI, female, pooled, K3EDTA	CUST-BB-NMRIPLK3-50ML-1800-2	BIOTREND Chemikalien GmbH
Mouse plasma NMRI nude, female, pooled, K3EDTA	n.a.	Provided by Charles River Laboratories, Inc. as part of animal studies
Rat plasma, Sprague Dawley, male, EDTA	RATPLEDTA	BIOTREND Chemikalien GmbH
RPMI 1640	FG 1215	Biochrom GmbH
sEGFR from mammalian cells	002291	Merck KGaA: GM-QAO-CL1
Streptozotocin	572201-1GM	Merck KGaA
TMB substrate	34021	Thermo Fisher Scientific, Inc.
Trypsin/EDTA, 0.05%	25300-096	Thermo Fisher Scientific, Inc.
TrypLE™ Express Enzyme	12604013	Thermo Fisher Scientific, Inc.
Zeocin	R25001	Thermo Fisher Scientific, Inc.

2.4. Frequently used buffers and assay solutions

Composition of frequently used buffers and assay solutions for experiments of this work are presented in Table 6.

Table 6: Frequently used buffers and solutions.

Assay buffer for mAbX functional ELISA	
Phosphate buffer	10.00 mM
Sodium chloride	140.00 mM
Potassium chloride	3.00 mM
Tween® 20	0.05 wt.%
CMC solution	
Carboxymethyl cellulose	0.60 wt.%
Phosphate buffered saline	12.50 mM
Complete growth medium CHO-K1	
Fetal bovine serum (FBS)	10.00% (v/v)
Ham's F12 cell culture medium	volume of choice
Concentrated antibody solution in PBS - mAbB	
mAbB	221.40 mg/mL
Phosphate buffer	10.00 mM
Sodium chloride	140.00 mM
Potassium chloride	3.00 mM
Tween® 80	0.02% (w/v)
Hydrochloric acid / sodium hydroxide	adjust pH to 6.0
Concentrated antibody solution in PBS - mAbX	
mAbX	225.50 mg/mL
Phosphate buffer	10.00 mM
Sodium chloride	140.00 mM
Potassium chloride	3.00 mM
Tween® 80	0.02% (w/v)
Hydrochloric acid / sodium hydroxide	adjust pH to 6.0
Culture medium CHO-K1	
Fetal bovine serum (FBS)	10.00% (v/v)
Hygromycin B	100.00 µg/mL
Zeocin	200.00 µg/mL
Ham's F12 cell culture medium	volume of choice

Culture medium A-431

Fetal bovine serum (FBS)	10.00% (v/v)
Gentamycin	0.05 mg/mL
In RPMI 1640	

Customized *in vitro* release buffer for monoclonal antibodies

Phosphate buffer	5.00 mM
Tween® 20	0.02 wt.%
Sodium azide	0.02%
Hydrochloric acid / sodium hydroxide	adjust pH to 7.4

DiFi culture medium

Fetal bovine serum (FBS)	10.00% (v/v)
Dulbecco's Modified Eagle's Medium/Nutrient Mixture F-12 Ham's	volume of choice

HEPES buffer used during exenatide particle manufacturing

HEPES sodium salt	10.00 mM
Sodium chloride	100.00 mM
Hydrochloric acid / sodium hydroxide	adjust pH to 7.4

In vitro release buffer for exenatide

HEPES sodium salt	10.00 mM
Sodium chloride	100.00 mM
Tween® 80	0.01 wt.%
Sodium azide	0.02%
Hydrochloric acid / sodium hydroxide	adjust pH to 7.4

In vitro release buffer for monoclonal antibodies

Phosphate buffer	100.00 mM
Tween® 20	0.02 wt.%
Sodium azide	0.02%
Hydrochloric acid / sodium hydroxide	adjust pH to 7.4

Mobile phase A for RP-HPLC

Trifluoroacetic acid	0.10%
in H_2O	

Mobile phase B for RP-HPLC

Trifluoroacetic acid	0.10%
in acetonitrile	

Mobile phase SE-HPLC

Phosphate buffer	50.00 mM
Perchlorate buffer	400.00 mM
Hydrochloric acid / sodium hydroxide	adjust pH to 6.3

PBS supplemented with Tween® 20

Phosphate buffer	10.00 mM
Sodium chloride	140.00 mM
Potassium chloride	3.00 mM
Tween® 20	0.02 wt.%

PVA solution for particle manufacturing

Polyvinyl alcohol 5-88	0.40 wt.%
Sodium chloride	5.00 wt.%
Water for injection	adjust volume

Stop solution for mAbX functional ELISA

Sulfuric acid	2.25 M
in H_2O	

Streptozotocin administration solution

Sodium citrate	100.00 mM
Hydrochloric acid / sodium hydroxide	adjust pH to 4.5

Wash buffer for mAbX functional ELISA

Phosphate buffer	10.00 mM
Sodium chloride	140.00 mM
Potassium chloride	3.00 mM
Tween® 20	0.15 wt.%

2.5. Assay kits, cell lines and laboratory animals

Table 7 shows assay kits, cell lines and laboratory animals used for experiments described herein.

Table 7: Assay kits and cell lines.

Assay kit / cell line	Catalogue-#	Manufacturer
A-431 epidermoid colorectal cancer cell line	n.a.	Charles River Laboratories, Inc.
cAMP Hunter Exendin-4 assay	90-0075LM-25	Eurofins Scientific SE
CellTiter 96® AQueous One Solution Cell Proliferation Assay	G3581	Promega GmbH
CHO-K1/GLP1/Gα15	M00451	GenScript Biotech Corporation
DiFi cell line	n.a.	provided by GM-QAO-CM (Merck KGaA)
Exendin-4 EIA Kit (for rat plasma samples)	S-1311	Peninsula Laboratories LLC
Mouse cytokine/chemokine magnetic bead panel	MCYTMAG-70K-PX32	Merck KGaA
NMRI mice, Crl:NMRI(Han), outbred	Strain Code: 605	Charles River Laboratories, Inc.
NMRI nu/nu mice, Crl:NMRI-Foxn1^{nu}, immunodeficient outbred	Strain Code:639	Charles River Laboratories, Inc.
Rat cytokine/chemokine magnetic bead panel	RECYMAG65K27PMX	Merck KGaA
Sprague Dawley rats, Crl:SD, outbred	Strain Code: 400	Charles River Laboratories, Inc.

2.6. Medicinal products and microparticle formulations

Medicinal products and microparticle formulations are listed in Table 8.

Table 8: Medicinal products and microparticle formulations.

Product/formulation	Catalogue-#	Manufacturer
Accu-Chek Guide mg/mL	PZN 11664921	Roche Diabetes Care Deutschland GmbH
Accu-Chek Guide Kontrolllösung	PZN 11664950	Roche Diabetes Care Deutschland GmbH
Accu-Chek Guide Teststreifen	PZN 11664909	Roche Diabetes Care Deutschland GmbH
Water for injection	PZN 6724092.00.00	B. Braun AG
Bydureon®	PZN 07749882	AstraZeneca GmbH
Byetta® injection pen	PZN 00839139	AstraZeneca GmbH
Saline, 0.9% NaCl solution	174078001	B. Braun AG
Exenatide-related materials		
Exenatide microparticle formulation ICE-2wF	AMD17001	InnoCore Pharmaceuticals
Exenatide microparticle formulation ICE-4wF	AMD17006	InnoCore Pharmaceuticals
Polymer-only microparticle formulation	AMD17030	InnoCore Pharmaceuticals
mAbB-related materials		
mAbB microparticle formulation	SR19-002.A	InnoCore Pharmaceuticals
	SR19-002.B	
	SR19-002.C	
	SR19-002.D	
	SR19-002.E	
	SR19-002.F	
mAbX-related materials		
mAbX microparticle formulation ICX-2wF	AMD18-012	InnoCore Pharmaceuticals
mAbX stock (119.4 mg/mL), diluted to 10 mg/mL	SF20180928	Merck KGaA
Polymer-only microparticle formulation	AMD18-017	InnoCore Pharmaceuticals

2.7. Particle manufacturing and characterization

Particle manufacturing and characterization was performed by InnoCore Pharmaceuticals (The Netherlands). Polymer compositions and manufacturing of exenatide and antibody loaded particles are described in the following sections. Furthermore, basic particle analyses for final particle products are explained.

2.7.1. Polymers and manufacturing process

Different particles were prepared by InnoCore Pharmaceuticals and were examined in this work. Compositions and manufacturing methods are described in the next sections. Table 9 shows the polymer compositions of SynBiosys® microsphere formulations that were analyzed herein.

Table 9: Polymer composition of different SynBiosys® microparticle formulations.

Polymer composition of formulations					
Exenatide	ICE-2wF ICE-4wF	65% amorphous block 100GL40		35% phase-separated block 20CP30C40-D25	
		100 wt.% of copolymer		20 wt.% of copolymer	80 wt.% of copolymer
		PLGA copolymer $MW_{copolymer}$: 4000 g/mol		PCL-PEG-PCL prepolymer MW_{total}: 4000 g/mol MW_{PEG}: 3000 g/mol	Polydioxanone prepolymer MW_{total}: 2500 g/mol
mAbB	SR19-002.A	100% phase-separated block 50CP30C40-LL40		0% phase-separated block 50CP10C20-LL40	
		50 wt.% of copolymer	50 wt.% of copolymer	50 wt.% of copolymer	50 wt.% of copolymer
		PCL-PEG-PCL prepolymer MW_{total}: 4000 g/mol MW_{PEG}: 3000 g/mol	Poly(L-lactide) prepolymer MW_{total}: 4000 g/mol	PCL-PEG-PCL prepolymer MW_{total}: 2000 g/mol MW_{PEG}: 1000 g/mol	Poly(L-lactide) prepolymer MW_{total}: 4000 g/mol
	SR19-002.B	90% phase-separated block 50CP30C40-LL40		10% phase-separated block 50CP10C20-LL40	
		50 wt.% of copolymer	50 wt.% of copolymer	50 wt.% of copolymer	50 wt.% of copolymer
		PCL-PEG-PCL prepolymer MW_{total}: 4000 g/mol MW_{PEG}: 3000 g/mol	Poly(L-lactide) prepolymer MW_{total}: 4000 g/mol	PCL-PEG-PCL prepolymer MW_{total}: 2000 g/mol MW_{PEG}: 1000 g/mol	Poly(L-lactide) prepolymer MW_{total}: 4000 g/mol
	SR19-0002.C	80% phase-separated block 50CP30C40-LL40		20% phase-separated block 50CP10C20-LL40	
		50 wt.% of copolymer	50 wt.% of copolymer	50 wt.% of copolymer	50 wt.% of copolymer
		PCL-PEG-PCL prepolymer MW_{total}: 4000 g/mol MW_{PEG}: 3000 g/mol	Poly(L-lactide) prepolymer MW_{total}: 4000 g/mol	PCL-PEG-PCL prepolymer MW_{total}: 2000 g/mol MW_{PEG}: 1000 g/mol	Poly(L-lactide) prepolymer MW_{total}: 4000 g/mol
	SR19-002.D	70% phase-separated block 50CP30C40-LL40		30% phase-separated block 50CP10C20-LL40	
		50 wt.% of copolymer	50 wt.% of copolymer	50 wt.% of copolymer	50 wt.% of copolymer
		PCL-PEG-PCL prepolymer MW_{total}: 4000 g/mol MW_{PEG}: 3000 g/mol	Poly(L-lactide) prepolymer MW_{total}: 4000 g/mol	PCL-PEG-PCL prepolymer MW_{total}: 2000 g/mol MW_{PEG}: 1000 g/mol	Poly(L-lactide) prepolymer MW_{total}: 4000 g/mol
	SR19-002.E	50% phase-separated block 50CP30C40-LL40		50% phase-separated block 50CP10C20-LL40	
		50 wt.% of copolymer	50 wt.% of copolymer	50 wt.% of copolymer	50 wt.% of copolymer
		PCL-PEG-PCL prepolymer MW_{total}: 4000 g/mol MW_{PEG}: 3000 g/mol	Poly(L-lactide) prepolymer MW_{total}: 4000 g/mol	PCL-PEG-PCL prepolymer MW_{total}: 2000 g/mol MW_{PEG}: 1000 g/mol	Poly(L-lactide) prepolymer MW_{total}: 4000 g/mol
	SR19-002.F	25% phase-separated block 50CP30C40-LL40		75% phase-separated block 50CP10C20-LL40	
		50 wt.% of copolymer	50 wt.% of copolymer	50 wt.% of copolymer	50 wt.% of copolymer
		PCL-PEG-PCL prepolymer MW_{total}: 4000 g/mol MW_{PEG}: 3000 g/mol	Poly(L-lactide) prepolymer MW_{total}: 4000 g/mol	PCL-PEG-PCL prepolymer MW_{total}: 2000 g/mol MW_{PEG}: 1000 g/mol	Poly(L-lactide) prepolymer MW_{total}: 4000 g/mol
mAbX	ICX-2wF	90% phase-separated block 50CP30C40-LL40		10% phase-separated block 50CP10C20-LL40	
		50 wt.% of copolymer	50 wt.% of copolymer	50 wt.% of copolymer	50 wt.% of copolymer
		PCL-PEG-PCL prepolymer MW_{total}: 4000 g/mol MW_{PEG}: 3000 g/mol	Poly(L-lactide) prepolymer MW_{total}: 4000 g/mol	PCL-PEG-PCL prepolymer MW_{total}: 2000 g/mol MW_{PEG}: 1000 g/mol	Poly(L-lactide) prepolymer MW_{total}: 4000 g/mol

Exenatide-loaded microparticles

Exenatide-loaded particles were manufactured by InnoCore Pharmaceuticals under sterile conditions using a class-B laminar flow cabinet in a class C cleanroom applying a water-in-oil-in-water (W/O/W) membrane emulsification process. Two different microparticle formulations were prepared with target release durations of two and four weeks (ICE-2wF, ICE-4wF), respectively. While equal polymers were used for preparation of formulations (see Table 9), process parameters varied as described below.

All glass and metal materials used for particle manufacturing were sterilized and de-pyrogenated at 260°C for 150 min before utilization. All other materials were steam-sterilized and transferred to the cleanroom. All solutions utilized during particle production were sterile filtered with a 0.2 µm filter except for the carboxymethyl cellulose (CMC) aqueous solution (0.6 wt.% CMC 7HF-PH in 12.5 mM PBS) which was autoclaved at 121°C for 20 minutes.

An amount of 6 g of polymer (35 wt.% 20CP30C40-D25, 65 wt.% of 100GL40) was added to 54 g of dichloromethane (DCM) to prepare a 10 wt.% polymer solution. The solution was filtered with a 0.2 µm PTFE filter prior to proceeding. An exenatide solution with a concentration of 105.3 mg/g was prepared by adding 0.4 g exenatide to 3.8 g of HEPES buffer (10 mM HEPES, 100 mM NaCl, pH 7.4). An amount of 3.3 g of aqueous exenatide solution was added to 50 g of the polymer solution. The mixture was emulsified by Ultra Turrax (ICE-2wF: T19, 21.6k rpm, 40 s; ICE-4wF: T10, 21.6k rpm, 2x40 s), collected into a syringe and placed into a syringe pump. A membrane emulsification cell equipped with a membrane containing pores of 20 µm was used to inject the primary emulsion to an aqueous PVA solution (0.4 wt.% PVA 5-88 and 5 wt.% NaCl in water for injection) forming the secondary emulsion. DCM was removed by evaporation and resulting microparticles were washed before lyophilization. Polymer-only microparticles were prepared with the same manufacturing method with the exception that no exenatide was added to the initial aqueous phase.

Lyophilized microparticles were stored at -18°C until preparation of injection suspensions. For preparation of injection suspension, microparticles were mixed with CMC solution (0.6 wt.% CMC 7HF-PH in 12.5 mM PBS). Injection suspensions were stored at -80°C until usage in animal trials.

mAb-loaded microparticles

Particles loaded with different mAbs were manufactured by InnoCore Pharmaceuticals under sterile conditions using a class-B laminar flow cabinet in a class C cleanroom applying a water-in-oil-in-oil (W/O/O) double emulsion process. Microparticle formulations of mAbB with various polymer compositions were manufactured to demonstrate the versatility of the SynBiosys®

platform *in vitro*. Additionally, a promising polymer composition was used to encapsulate mAbX to illustrate the compatibility with a further antibody as well as the *in vivo* performance of the formulation. Multi-block copolymer compositions for formulation of both mAbB and mAbX are described in Table 9.

Materials used during particle manufacturing were sterilized as described in the previous section. A polymer solution of 10 wt.% was prepared by adding 10 g of polymers (varying composition according to Table 9) to dichloromethane and polymer dissolution was completed before filtration through a 0.2 µm PTFE filter. An aqueous high concentration solution of the respective antibody (mAbB: 221.4 mg/mL, mAbX: 225.5 mg/mL, both in PBS, 0.025% (w/v) Tween® 80, pH 6.0) was added to the polymer solution with an oil to water (O/W) ratio of 9.5 creating the primary emulsion by Ultra Turrax treatment (T25, 12k rpm). The primary emulsion was added to the coacervation agent (silicone oil) using a second Ultra Turrax step (T25, 12k rpm) and a silicone oil to dichloromethane weight to weight ratio of 0.75. The resulting embryonic microparticles were transferred to 6.7 L of heptane to extract dichloromethane and silicone oil from the product followed by a further washing step with heptane. Microspheres were sifted with a 200 µm sieve to remove oversized particles after vacuum drying overnight and dried particles were stored at -18°C until preparation of injection suspensions. Polymer-only microparticles were prepared according to the same manufacturing method with the exception that no antibody was added to the initial aqueous phase.

For preparation of injection suspensions, microparticles were mixed with CMC solution (0.6 wt.% CMC 7HF-PH in 12.5 mM PBS).

2.7.2. Particle size distribution

The particle size distribution of final microparticles was determined under usage of different methods described in the next sections. Particle size was determined by InnoCore Pharmaceuticals.

Coulter counter for particle size distribution of Exenatide-loaded microspheres

The particle size distribution of exenatide-loaded microspheres was determined using a Coulter Counter Multisizer III. Electrolyte solution was added to the measuring cell and microparticles were transferred into the solution. The volume average particle size and the coefficient of variation were determined.

Laser diffraction for analysis of particle size distribution of mAb-loaded microspheres

The particle size distribution of mAb-loaded microspheres was determined using a LA-960 laser diffraction particle size analyzer. An amount of 20 mg of microparticles was resuspended in 15 mL of water followed by ultrasonication for 15 s. Suspensions were measured in a range of 10 nm to 5000 µm with a transmittance between 70 and 90%.

2.7.3. Encapsulation efficiency and particle loading

Microparticles were dissolved by different methods releasing the respective cargo to determine encapsulation efficiency and particle loading. Determination of loading and encapsulation efficiency was performed by InnoCore Pharmaceuticals.

Determination of exenatide content of particles

The exenatide content was determined in triplicate for each formulation. An amount of 20 mg of particles was dissolved in 2 mL of DMSO and samples were subsequently diluted 1:10 with 10 mM HEPES buffer containing 100 mM NaCl and 0.1% (w/v) Tween®80 (pH 7.4) before exenatide was quantified by reversed-phase high performance liquid chromatography (RP-HPLC) as described in section 2.8.5.

Determination of mAb content of particles

The mAb content of particles was determined using a bicinchoninic acid assay (BCA). An amount of 10 mg of particles was dissolved in 1 mL DMSO and 5 mL of a 0.1 N NaOH, 0.5% sodium dodecyl sulfate (SDS) solution were added. The sample was mixed overnight on a roller mixer before 100 µL were analyzed using a standard commercial BCA kit according to the manufacturers' protocol. Calibration standards were prepared by treating known amounts of the respective mAb according to the sample preparation described above in the presence of 10 mg of blank polymer. Calibration range was between 50-600 µg/10 mg microparticles and the calibration curve was fitted by first order, unweighted linear regression.

2.7.4. Scanning electron microscopy

Surface morphology of all particle formulations was evaluated by InnoCore Pharmaceuticals using scanning electron microscopy with a JCM-5000 Neoscope. Samples were placed on carbon conductive tape and coated with a thin gold layer. Coated samples were introduced in the microscope and vacuum was applied. Microsphere images were recorded using a 10 kV electron beam.

2.8. *In vitro* release and analysis of model drugs

SynBiosys®-based microparticle formulations and especially released model drugs were intensively examined *in vitro*. The *in vitro* release (IVR) behavior of the microparticles was monitored and integrity of the released biologicals was determined with orthogonal methods described in the following sections.

The experimental setup of IVR experiments slightly varied between microparticle formulations. IVR Methods are depicted hereafter. IVR of model protein therapeutics and preparation of release profiles by high performance liquid chromatography based analyses were performed by InnoCore Pharmaceuticals. Residual *in vitro* analyses were part of this work.

2.8.1. *In vitro* release of exenatide loaded microparticles

For IVR of exenatide, 20 mg of exenatide-loaded microspheres were incubated with 1.8 mL of IVR buffer (10 mM HEPES, 100 mM NaCl, 0.01% Tween® 80, 0.02% sodium azide, pH 7.4) at 37°C and a shaking speed of 236 rpm. Samples of 1.6 mL were collected at predetermined time points every 2-3 days after centrifugation at 5000 rpm for 5 minutes. An equivalent volume of 1.6 mL of fresh IVR buffer was added before returning tubes to the shaker. To avoid repeated freeze-thaw cycles, samples were stored at 4°C until completion of release. Exenatide content in IVR samples was quantified by reversed-phase high performance liquid chromatography (see section 2.8.5). Calculation of the recovery of the model drug after IVR was based on the cumulative release over all time points.

2.8.2. *In vitro* release of antibody loaded microparticles

For IVR of antibodies from microspheres, 20 mg of particles were incubated with 0.9 mL IVR buffer (100 mM phosphate buffer, 0.02% Tween® 20, 0.02% sodium azide, pH 7.4) at 37°C and a shaking speed of 236 rpm. Samples of 0.8 mL were collected at predetermined time points every 3-4 days after centrifugation at 5000 rpm for 5 minutes. An equivalent volume of 0.8 mL of fresh IVR buffer was added before returning tubes to the shaker. To avoid repeated freeze-thaw cycles, samples were stored at 4°C until completion of release. Antibody content in IVR samples was quantified by size exclusion high performance liquid chromatography (see section 2.8.5). Calculation of the recovery of the model drug after IVR was based on the cumulative release over all time points.

2.8.3. Photometric determination of the protein concentration

Protein concentration was determined spectrophotometrically as part of various experiments. Measurements were performed with a BioSpectrometer® kinetic based on the strong

absorbance of aromatic amino acids and disulfide bonds at 280 nm [176]. Blank buffer signal was determined in preparation of measurements and was automatically subtracted subsequently. The detection range of the device lays between 5 to 2000 µg/mL, according to the manufacturer. Samples with protein concentrations exceeding the measuring range were diluted accordingly. Reciprocal values of the absorption coefficient were used for determination of the concentration of exenatide (0.761), mAbB (0.714), and mAbX (0.714).

2.8.4. Stability study of mAbX

The decision for IVR buffer (100 mM phosphate buffer, 0.02% Tween® 20, 0.02% sodium azide, pH 7.4) as suitable release medium was based on fundamental stability experiments of mAbX under different conditions performed by InnoCore. However, complete IVR conditions including shaking and temperature stress over time were not part of these studies. Consequently, a deeper investigation of mAbX integrity under IVR conditions in IVR buffer and PBS supplemented with Tween® 20 (10 mM phosphate, 140 mM NaCl, 3 mM KCl, 0.02% Tween® 20, pH 7.4) was part of this work to facilitate the identification of causes for potential stability loss during *in vitro* and *in vivo* experiments.

Pyrofree® 2 mL clear tubular glass vials with 1 mL of IVR buffer supplemented with 300 µg/mL mAbX were incubated over 29 days at 37°C and shaking at 236 rpm. Vials were closed with FluroTec® stoppers and aluminum seals. Samples were taken every 4-5 days by collecting 3 vials (triplicates) at 7 time points. The content of each vial was divided in 125 µL aliquots which were stored at -20°C until further analysis. Samples were analyzed by size exclusion high performance liquid chromatography, enzyme-linked immunosorbent functional assay, circular dichroism and fluorescence spectroscopy as well as a cell-based functional assay. These methods are described hereafter.

2.8.5. High performance liquid chromatography

Model drugs were quantified in IVR samples by different high/ultra performance liquid chromatography methods described in the following sections.

Reversed-phase ultra performance liquid chromatography

Exenatide was quantified by reversed-phase ultra-performance liquid chromatography (RP-UPLC) using a Waters Acquity H-class system equipped with an Acquity UPLC CSH C18 column and a binary buffer system consisting of Mobile Phase A (0.1% TFA in water) and Mobile Phase B (0.1% TFA in acetonitrile) at a flow rate of 0.6 mL/min at 45°C. After an initial ratio of 65% Mobile Phase A and 35% Mobile Phase B, the following gradient was set: during the first 3.0 minutes, the ratio was changed to 55% Mobile Phase A and 45% Mobile Phase B;

subsequently, the initial ratio was restored between 3.0 to 3.1 minutes and maintained until complete elution after 4.5 minutes. Sample volumes of 3 µL were injected without any sample pretreatment. Exenatide signal was detected at a wavelength of 210 nm. The system was calibrated with exenatide standards ranging from 5 to 500 µg/mL and exenatide content of IVR samples was calculated by interpolation of the peak response on the calibration curve. A weighted least squares regression (weighting factor $1/x^2$) was used to fit the calibration curve.

Size exclusion high performance liquid chromatography

The content as well as aggregation and fragmentation of mAb models in IVR samples was determined by size exclusion high performance liquid chromatography (SE-HPLC) using a Waters 2690 HPLC system equipped with a TSK gel size exclusion SuperSW3000 column and an UV detector operated at 214 nm. The elution was isocratic with a mobile phase consisting of a 50 mM phosphate, 0.4 M perchlorate buffer at pH 6.3 and a flow rate of 0.35 mL/min. Gel Filtration Standard was used as reference. Samples were analyzed without specific pretreatment after injection of 10 µL of precooled (4°C) sample. The column was operated at RT and with a run time of 16 minutes/sample. The calibration curve ranged from 5 to 1000 µg/mL calculated with a first order weighted linear regression (weighting factor 1/x). Standards of mAbB or mAbX were used for calibration, respectively.

2.8.6. Circular dichroism spectroscopy of monoclonal antibody models

Circular dichroism (CD) spectra were recorded to evaluate the secondary structure stability of model antibodies in IVR samples. Optically active peptide bonds absorb left and right polarized light to certain extents resulting in polarized light of a specific ellipticity which is detectable by CD. Spectra were measured with a Jasco J 815 CD spectrometer at a scan speed of 20 nm/min between 200 and 280 nm. A Hellma absorption cell with a pathlength of 1 mm was used for measurements. Depending on protein concentration and resulting signal to noise ratio, between 5 and 10 accumulations of each spectrum were collected for analysis. The predominant secondary structure elements of mAbB and mAbX as members of the IgG1 family are β-sheets leading to a characteristic peak at 218 nm [177-183]. Hence, signal intensity at 218 nm was observed as key parameter during all measurements. Generally, measurements were corrected for buffer signals and normalized according to Kelly et al. (2005) [184]:

$$[\theta]_{MRW,\ \lambda} = \frac{MRW * \theta_\lambda}{10 * d * c} \quad (1)$$

with θ_λ as ellipticity at wavelength λ in degree, d as pathlength in cm, c as concentration in g/mL and MRW as mean residue weight in g/mol which is calculated according to the following equation (2):

$$MRW = \frac{M}{N-1} \quad (2)$$

with the molar mass of the peptide or protein of interest in g/mol (M) and the number of amino acids per molecule (N). Normalization allowed the comparison of samples with different protein concentrations.

Method development experiments revealed an interference of the high phosphate content of IVR buffer (100 mM phosphate buffer, 0.02% Tween® 20, 0.02% sodium azide, pH 7.4) with CD measurements. Consequently, IVR samples were prepared and dialyzed in QixSep micro dialysis capsules against customized IVR buffer (5 mM phosphate buffer, 0.02% Tween® 20, 0.02% sodium azide, pH 7.4) with significantly reduced phosphate content. Additionally, the detection ranges for mAbB and mAbX were determined during method development by measurement of serially diluted reference samples of the respective antibody. CD signals within the detection range were independent from saturation effects (upper concentration limit) or influences of signal noise (lower concentration limit).

Furthermore, reference samples of mAbB or mAbX were denatured stepwise by increasing concentrations of guanidine hydrochloride (GdnHCl) or increasing temperatures to determine the ellipticity range at 218 nm between native and completely unfolded antibody. Denaturation experiments were performed with antibody solutions of 330 µg/mL in customized IVR buffer. Samples were heated with a rate of 1°C/min and spectra were recorded every 5°C for thermal denaturation. GdnHCl is a well-known chaotropic agent and denaturant leading to protein unfolding without aggregation [185]. To examine chemical denaturation, sample solutions were supplemented with increasing concentrations of GdnHCl followed by overnight incubation at 4°C. Spectra were recorded between 0 and 6 M GdnHCl which was increased in 0.5 or 1 M steps.

Determination of the Fraction Folded allowed the comparison between CD results and findings obtained with other methods. The Fraction Folded was calculated according to equation (3):

$$Fraction\ Folded = \left(\frac{(\theta_{218\,nm} - \theta_{218\,nm,\ denatured})}{(\theta_{218\,nm,\ native} - \theta_{218\,nm,\ denatured})}\right) * 100 \quad (3)$$

where the ellipticity at 218 nm is represented for antibody in unknown samples ($\theta_{218\ nm}$), completely unfolded by 6 M GdnHCl or 95°C ($\theta_{218\,nm,\,denatured}$), and intact reference ($\theta_{218\,nm,\,native}$).

2.8.7. Fluorescence spectroscopy of monoclonal antibody models

The tertiary structure of mAbB and mAbX in IVR samples was evaluated by fluorescence spectroscopy using the intrinsic fluorescence of aromatic amino acids in proteins. Especially tryptophan fluorescence contributes to the spectral behavior and strongly depends on the environmental polarity around the respective residue. Conformational changes of proteins potentially lead to environmental changes of certain amino acid residues inducing shifted emission maxima of tryptophan fluorescence signals which allows insights in tertiary protein structure [186]. After a lead time of 15 minutes, tryptophan fluorescence was measured with a Cary eclipse fluorescence spectrophotometer operated at an excitation wavelength of 280 nm. Emission spectra were recorded between 290 and 450 nm with 120 nm/min and a data interval of 1 nm. Measurements were performed using quartz cells with a path length of 3x3 mm. Slit width of excitation and emission slits as well as detector voltage were adjusted to yield a signal between 200 and 1000 a.u. during measurements. Generally, background spectra with equal settings were collected and subtracted from sample measurements to correct for buffer signals. Furthermore, measurements of each sample were performed in triplicates. Results were normalized to compensate concentration dependent effects according to the following equation (4):

$$Normalized\ fluorescence\ intensity\ = \frac{x - x_{Min}}{x_{Max} - x_{Min}} \quad (4)$$

with x as the fluorescence intensity and x_{Min} and x_{Max} as minimum and maximum fluorescence intensities, respectively. The wavelength of the maximum fluorescence intensity was determined by use of Savistsky-Golay smoothing (6th order, 10 neighbors, Graphpad prism).

In preparative experiments, the measuring range was determined to avoid artifacts caused by higher or lower protein concentrations. Linear dilutions were prepared, and the lower detection limit was defined as protein concentration at which no change in spectral behavior was observed. The inner filter effect is a result of high protein concentrations leading to complete light absorption prior to illumination of the whole cell resulting in lowered fluorescence intensity [187-189]. Consequently, the upper detection limit was defined as the protein concentration which induced the highest fluorescence intensity.

Furthermore, reference samples of mAbB and mAbX were denatured stepwise by increasing concentrations of GdnHCl or increasing temperatures to determine the maximum possible wavelength shift of the fluorescence signal peak between native and denatured model protein. Reference samples of mAbB or mAbX were heated with a rate of 1°C/min and spectra were collected every 5°C for thermal denaturation. As described earlier, GdnHCl is a strong chaotropic agent and denaturant leading to protein unfolding without aggregation [185]. To

examine chemical denaturation, sample solutions were supplemented with increasing concentrations of GdnHCl followed by overnight incubation at 4°C. Spectra were recorded between 0 and 6 M GdnHCl which was increased in 0.5 or 1 M steps. Determination of the Fraction Folded allowed the comparison between fluorescence spectroscopy results and findings obtained with other methods. The Fraction Folded was calculated according to equation (5):

$$Fraction\ Folded\ = \left(\frac{(x - \lambda_{Max,\ denatured})}{(\lambda_{Max,\ native} - \lambda_{Max,\ denatured})}\right) * 100 \quad (5)$$

where the wavelength of the fluorescence signal peak is represented by x (unknown samples), $\lambda_{Max,\ denatured}$ (completely unfolded mAb), and $\lambda_{Max,\ native}$ (intact reference).

2.8.8. Enzyme-linked immunosorbent assays

Enzyme-linked immunosorbent assays (ELISA) are a commonly used tool for peptide and protein quantification characterized by high sensitivity and specifity [190]. The assay procedure for quantification of mAbX is described in the next section while the ELISA-based quantification of exenatide is described later (section 2.9.6).

Quantification of functional mAbX by ELISA

A non-commercially available ELISA was used to quantify functional mAbX binding its target epidermal growth factor receptor (EGFR). A 96-well Nunc maxisorb plate was coated with soluble EGFR (sEGFR) by preparing a 2 µg/mL solution of sEGFR in PBS. A volume of 100 µL of the sEGFR solution was added to each well and the plate was incubated for at least 12 h at 2-8°C prior to use. Coated plates were stable and ready-to-use for 10 days at 2-8°C. Plates were equilibrated to room temperature (RT) before all wells were washed 3 times by adding and discarding 250 µL/well of wash buffer (0.15% (w/v) Tween® 20 in PBS). For blocking of remaining binding sites, 200 µL/well of assay buffer (0.05% (w/v) Tween® 20 in PBS) were added and plates were incubated for 1 h at RT and 350 rpm shaking with a Thermomixer comfort.

Before proceeding with the addition of reference standards and samples, plates were washed five times by adding and discarding 250 µL/well of wash buffer. Standards and samples were generally prepared in separate dilution plates to simplify and accelerate the transfer to assay plates. For the analysis of mAbX IVR samples, a reference solution of mAbX of a concentration of 100 ng/mL (= Standard 1) was serially diluted 1:2 in mAbX IVR buffer resulting in 7 reference standards with concentrations between 1.56 and 100 ng/mL. IVR samples of mAbX were diluted to concentrations of 25, 12.5 and 6.25 ng/mL in IVR buffer based on concentration determination by SE-HPLC. Reference standards were assayed in triplicate while dilutions of

each sample (25, 12.5, 6.25 ng/mL) were examined in duplicate. Figure 10 shows a typical plate scheme for mAbX IVR sample analysis. Volumes of 100 µL/well of standards and samples were transferred from dilution to assay plates followed by 1.5 h incubation at RT and 350 rpm shaking.

Unbound antibody was removed during 5-fold washing by adding and discarding 250 µL/well of wash buffer. Subsequently, captured mAbX was bound by goat-anti human kappa light chain horse radish peroxidase (HRPO) conjugate. Suitable dilution ratios of the conjugate was determined from batch-to-batch aiming at absorption values of 2-3 for the highest concentrated mAbX standard and a substrate incubation of 5 minutes. Assay plates were incubated for 1.5 h at RT and 350 rpm shaking after addition of 100 µL of conjugate solution. Plates were again washed thereafter 5-fold by adding and discarding 250 µL/well of wash buffer.

The resulting antigen-antibody-antibody-peroxidase complex was quantified by conversion of the chromogenic substrate 3,3′,5,5′-Tetramethylbenzidine (TMB). Equal parts of TMB substrate solution A and B were united directly prior to adding 100 µL/well of the final TMB solution. Assay plates were incubated for 5 minutes after addition of substrate at RT and 350 rpm shaking. Reactions were stopped by addition of 100 µL/well of stop solution (2.25 M sulfuric acid) and the absorption at 450 nm was read within 5 minutes with a Microplate Reader

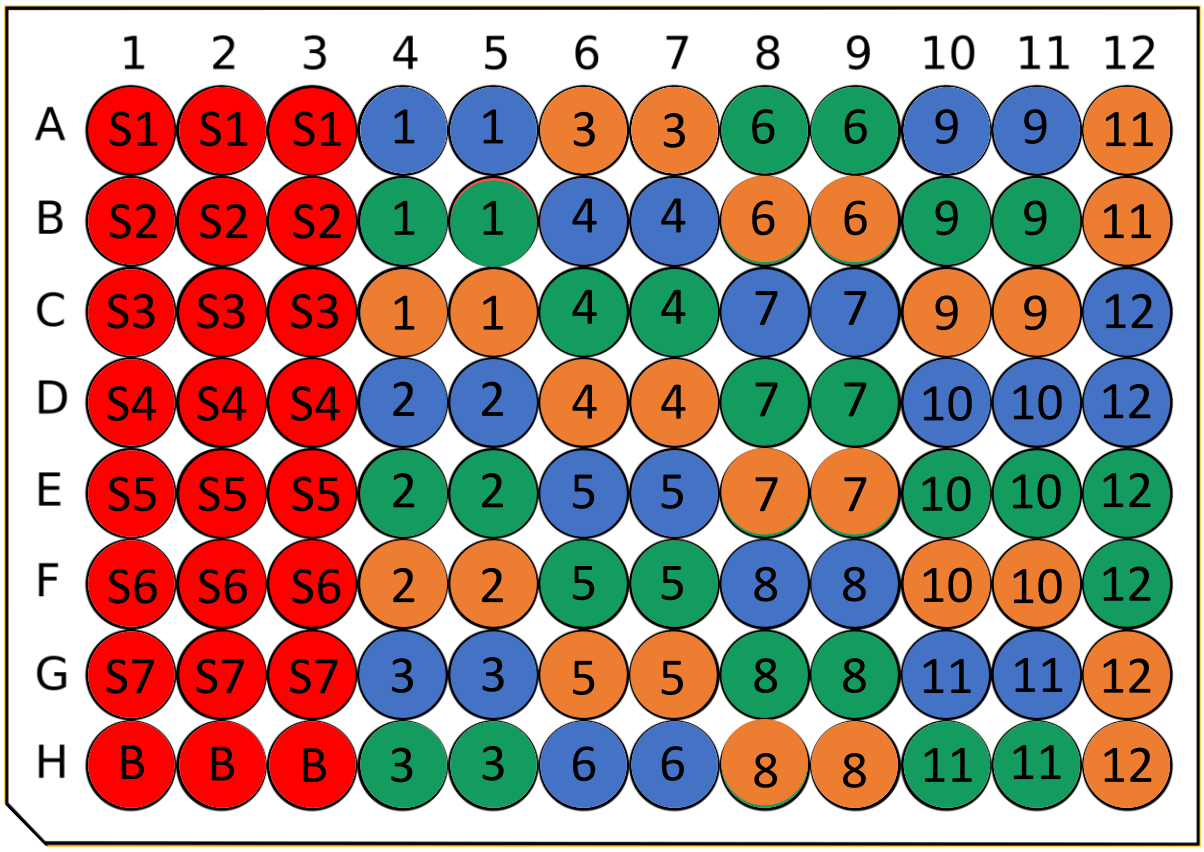

Figure 10: General plate scheme of mAbX functional ELISA for analysis of IVR samples. Standards 1-7 and blank wells (IVR buffer) are depicted in red and were assayed in triplicates. Each IVR sample was diluted to concentrations of 25 (blue), 12.5 (green) and 6.25 ng/mL (orange). A maximum of 12 samples was analyzed on each assay plate (1-12).

Multiskan spectrum (Thermo Fisher Scientific, Inc.). Results were analyzed using a 5-parametric logistic fit (Graphpad Prism) for creation of the standard curve.

As part of the method establishment described in section 5.3.1, the limit of quantitation (LOQ) was determined according to the following equation 6 [191]:

$$LOQ = X_{b1} + 10S_{b1} \quad (6)$$

where X_{b1} represents the absorption value of the respective blank and S_{b1} is the standard deviation of blank absorption values. LOQ was determined using the respective assay matrix as blank and a minimum of 10 blank wells. Values below the LOQ were excluded from results. Additional to LOQ calculation, further assay quality requirements were introduced:

- Reference standards 2-7 (1.56-50.00 ng/mL) must not exceed the theoretical concentration by ± 20% after back calculation based on 5-parametric logistic fit
- Absorption value of lowest standard reference must exceed the value of the blank wells + 3 standard deviations
- Coefficient of determination for the 5-parametric logistic fit curve must exceed 0.98

Assay plates which failed to fulfill any of the quality requirements were excluded from results and analysis of the respective samples was repeated.

2.8.9. Cell-based functional assay for exenatide

The functionality of exenatide released from microparticles was evaluated with a cell-based functional assay demonstrating the ability of the peptide to bind its target glucagon-like peptide 1 receptor (GLP1-R). Exenatide induces insulin secretion from pancreatic β-cells by binding to GLP1-R and thereby stimulating the adenylyl cyclase pathway [149, 192]. The CHO-K1/GLP1/Gα15 cell line overexpresses the GLP1-R and was used herein for determination of the functionality of *in vitro* released exenatide. Exenatide binding to GLP1-R leads to enhanced intracellular cAMP secretion. Hence, cAMP level in cells was quantitatively indicating functional binding of exenatide to GLP1-R. The commercially available HitHunter® cAMP Assay for Biologics was used to quantify intracellular cAMP after stimulation by *in vitro* released exenatide compared to reference samples. Assay procedures were implemented and adapted as described in section 3.3.1.

Cell culture routine

Cell culture works were generally performed under sterile conditions in a laminar flow hood using sterile media, reagents and materials. For seeding of cells, a vial containing a number of 5x10^6 CHO-K1/GLP1/Gα15 cells was thawed in a 37°C water bath until only sporadic ice

fragments were left. The vial was disinfected, and the cell suspension was transferred to 9 mL of prewarmed complete growth medium CHO-K1 (Ham's F12, 10% fetal bovine serum (FBS)) under laminar flow. After cells were centrifuged at 200 g for 5 minutes (Centrifuge 5810 R, rotor A-4-62), the supernatant was discarded, and cells were resuspended in 10 mL of prewarmed complete growth medium CHO-K1. A volume of 1 mL of the cell suspension was transferred to a 75 cm² cell culture flask containing 14 mL of prewarmed complete growth medium CHO-K1. Seeded cells were incubated at 37°C (95% air, 5% carbon dioxide) for 24 h before medium was exchanged and cells were cultivated with regular culture medium CHO-K1 (Ham's F12, 10% FBS, 200 µg/mL zeocin and 100 µg/mL hygromycin B) as selection medium for continuation of GLP1-R overexpression.

During ordinary cell culture routine, medium was exchanged every 2-3 days by replacing consumed medium with 15 mL of fresh and prewarmed culture medium CHO-K1. CHO-K1/GLP1/Gα15 cells were passaged every 3-4 days or as soon as confluency reached 80-90%. Medium was aspirated and cells were washed with 10 mL of phosphate buffered saline (PBS) w/o Ca^{2+} and Mg^{2+} for 1-2 minutes. PBS was aspirated and 1.5 mL of Trypsin/EDTA were added ensuring an even distribution of the enzyme solution. Cells were trypsinized for approximately 3 minutes at RT until complete detachment and the enzymatic activity was stopped by addition of 7.5 mL of prewarmed complete growth medium CHO-K1. Remaining cell-cell contacts were destroyed by vigorously resuspending the cell suspension approximately 10 times using shear forces of a 10 mL pipette. Subsequently, the suspension was centrifuged at 200 g for 5 minutes (Centrifuge 5810 R, rotor A-4-62) and the supernatant was discarded. Cells were resuspended in 9 mL of prewarmed culture medium CHO-K1. Depending on cell density in the originating flask, cells were reseeded with a ratio of approximately 1:18-1:36 using 250-500 µL of the cell suspension. Volume of prewarmed culture medium CHO-K1 in the new cell culture flask was adapted to the dilution ratio aiming at a target volume of 15 mL.

All cell culture works were performed according to "Gentechnikgesetz" (GenTG) guidelines of the local authorities as CHO-K1/GLP1/Gα15 cells are genetically modified.

Assay procedure

In preparative experiments, a suitable number of cells/well and dilution steps for standards and samples were determined as described in section 3.3.1. For seeding of cells on assay plates, a cell suspension was prepared by trypsinization of cells after cultivation for 3-4 days as described in the previous section. The suspension was centrifuged at 200 g for 5 minutes (Centrifuge 5810 R, rotor A-4-62) and the supernatant was discarded. Cells were resuspended in 9 mL of prewarmed culture medium CHO-K1. Subsequently, the cell number was

determined by measurement with the cell counter ViCellXR. A volume of 1 mL was transferred to a measuring cup and the cell suspension was analyzed applying standard settings for CHO cells. Based on the results of cell counting, a suspension of $6x10^4$ viable cells/mL was prepared and a cell number of 6000 viable cells was seeded per well of a 96 well assay plate. Cells were incubated for 48 h at 37°C (95% air, 5% carbon dioxide) before assay start.

Exenatide standards and IVR samples were prediluted prior to the start of functionality assays to a concentration of 40 ng/mL representing the starting concentration of dilution rows. Calculation of dilutions for exenatide IVR samples were based on RP-HPLC quantification. Solutions containing exenatide were generally handled with products of the Protein LoBind series of Eppendorf to minimize protein adsorption. Standards and samples were further diluted 8-fold with steps of 1:2.7 as defined during method implementation (section 3.3.1) to the lowest standard/sample concentration of 38.24 pg/mL. Dilution rows of standards and samples were prepared in LoBind dilution plates and were subsequently transferred to the assay plate for cell incubation lasting 60 minutes at 37°C (95% air, 5% carbon dioxide) according to the instructions in the manufacturers' protocol. A typical plate scheme is shown below (Figure 11). Further steps of the assay were performed according to the manufacturers' protocol. After the last step, assay plates were incubated for 5 h at RT and protected from light. Luminescence was read with an Envision 2014 multiplate reader (PerkinElmer, Inc.) using

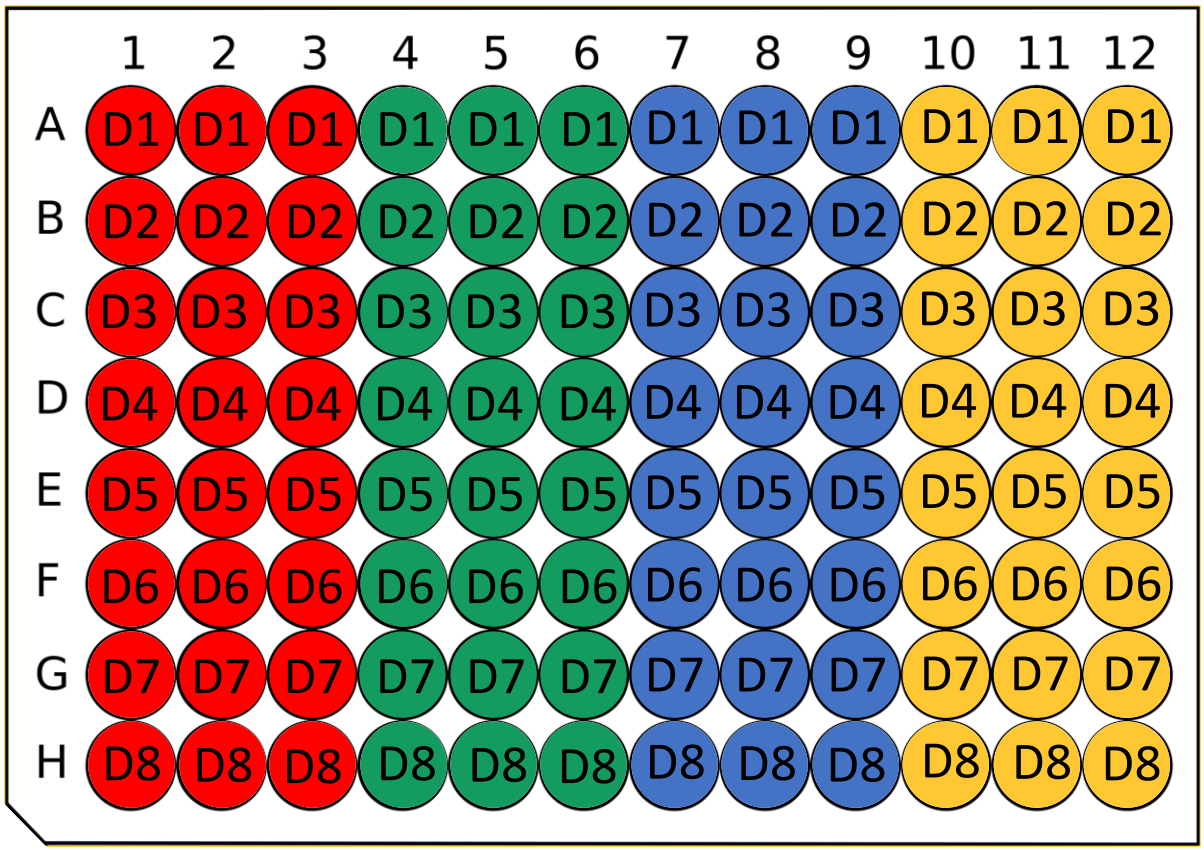

Figure 11: General plate scheme for exenatide cell-based functional assay. Exenatide reference (red), and IVR samples (green, blue, yellow) were assayed in triplicates and serial 8-fold dilutions (D1-8).

standard settings. EC_{50} values of IVR samples and references calculated by [Agonist] vs. response – Variable slope (four parameters) fitting (GraphPad Prism) were compared expressing the percentage of functional exenatide released from microspheres. Sample values were compared to the reference value on the respective plate.

2.8.10. Cell-based functional assay for mAbX

Functionality of mAbX after release from SynBiosys® microparticles was evaluated by a cell-based assay using human DiFi colorectal cancer cells. DiFi cells overexpress the epidermal growth factor receptor (EGFR) representing the target of mAbX [193]. The antibody inhibits cell proliferation by binding to EGFR. Consequently, relative growth inhibition of DiFi cells was measured after incubation with mAbX released from microspheres compared to reference samples.

Cell culture routine

Cells of a low passage number were obtained by GM-QAO-CM (Merck KGaA) in 75 cm² cell culture flasks and were generally cultured at 37°C (92.5% air, 7.5% carbon dioxide). DiFi culture medium (Dulbecco's Modified Eagle's Medium/Nutrient Mixture F-12 Ham supplemented with 10% FBS) was exchanged regularly after 3-4 days and cells were passaged every 7 days. Medium was exchanged by aspiration of used medium and subsequent addition of 25 mL of fresh, prewarmed DiFi culture medium.

For passaging of cells, medium was aspirated and 10 mL of PBS w/o Ca^{2+} and Mg^{2+} were added to cell culture flasks. After incubation of cells in PBS for 1-2 minutes, PBS was aspirated and 1.5 mL of trypsin/EDTA were added to the cells ensuring an even distribution of the enzyme distribution. Trypsinization was continued for 5 minutes at 37°C until cells were completely detached, and the enzymatic activity was stopped by addition of 8.5 mL of prewarmed DiFi culture medium. Subsequently, the cell number was determined by ViCellXR measurement. A volume of 1 mL was transferred to a measuring cup and the cell suspension was analyzed applying standard settings. Simultaneously, the cell suspension was centrifuged at 200 g for 5 minutes (Centrifuge 5810 R, rotor A-4-62) and the supernatant was discarded thereafter. Based on cell number determination, cells were resuspended in a suitable volume of prewarmed DiFi culture medium to prepare a cell suspension with $1.3x10^6$ viable cells/mL. Finally, 1 mL of the resulting cell suspensions were transferred to a 75 cm² cell culture flask containing 24 mL of prewarmed DiFi culture medium and cells were incubated for 3-4 days until medium exchange.

Assay procedure

A mAbX reference solution and IVR samples were diluted in IVR buffer for monoclonal antibodies to a concentration of 30 µg/mL. Calculation of dilutions of IVR samples was based on mAbX quantification by SE-HPLC. Reference and IVR samples were further diluted 1:10 in DiFi culture medium leading to a concentration of 3 µg/mL representing the highest concentrated reference or sample solution. After transferring 100 µL of solutions to a Nunclon™ Delta Surface 96 well plate, another 50 µL of DiFi culture medium were added resulting in a mAbX concentration of 2 µg/mL. Solutions in the first wells were serially diluted 10-fold with a factor of 1:1.5 by transferring 100 µL from one well to the next of which each contained 50 µL of DiFi culture medium. The lowest mAbX concentration of each dilution row was 52 ng/mL.

At the same time, cells were separated from the continuous cell culture during trypsinization and a cell suspension containing $2x10^5$ viable cells/mL was prepared. A volume of 50 µL accounting for 10^4 viable cells was transferred to each well of the Nunclon™ Delta Surface 96 well assay plate containing 50 µL of dilution rows of mAbX reference and samples. Consequently, mAbX solutions were further diluted 1:2 by adding cell suspension. Each

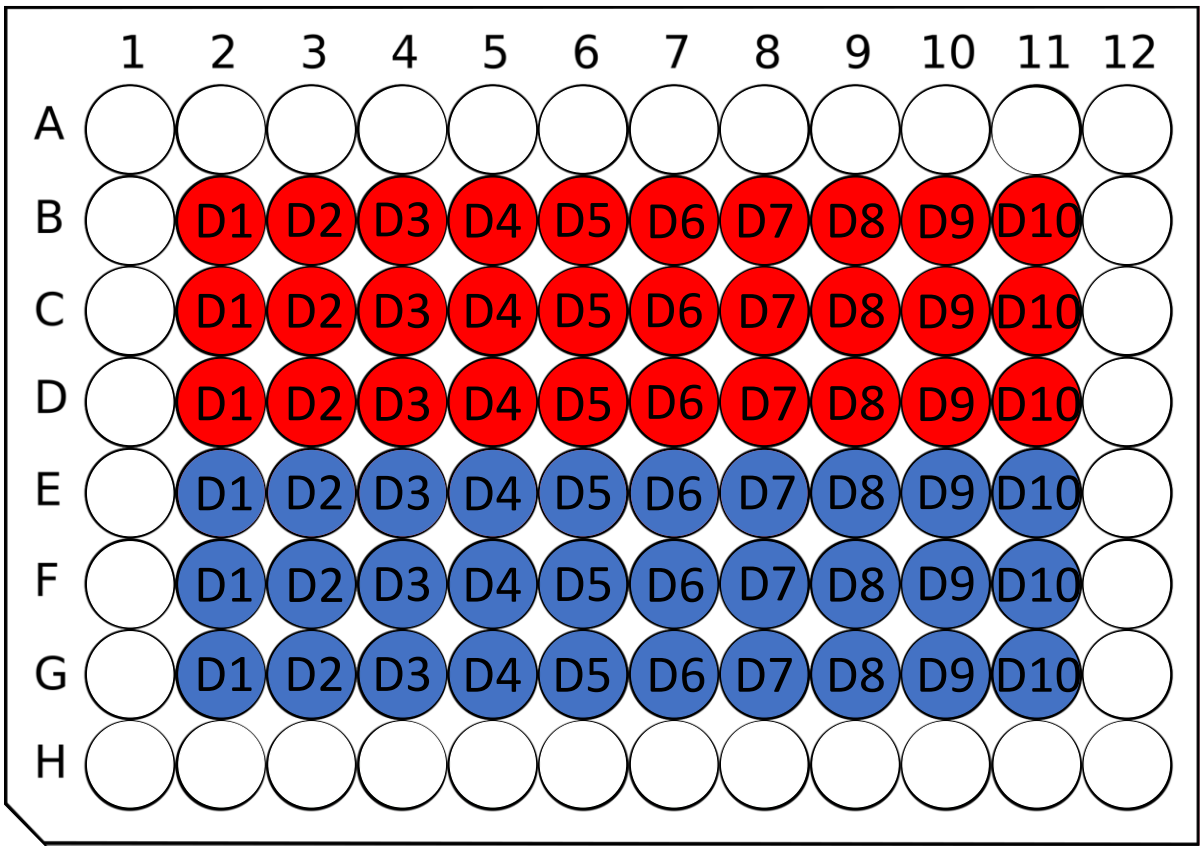

Figure 12: General plate scheme for mAbX cell-based functional assay. A reference of mAbX (red) and an IVR sample (blue) were assayed on each plate in triplicate and 10-fold dilution (D1-10). Outer wells containing cells and medium without mAbX served as blank.

dilution row was assayed in triplicate. Figure 12 shows a typical plate scheme. Cells were incubated together with the respective sample or reference for 96 h at 37°C.

Subsequently, the number of viable cells was determined with the CellTiter 96 Aqueous One Solution Cell Proliferation Assay by addition of 20 µL of detection solution per well. After 4 h, absorption at 490 nm was measured with a Microplate Reader Multiskan spectrum (Thermo Fisher Scientific, Inc.) and IC_{50} values of reference and samples were calculated by [Inhibitor] vs. response – Variable slope (four parameters) fitting (GraphPad Prism). Bioactivity of mAbX in IVR samples was determined as percentage of IC_{50} value of the reference. Sample values were compared to the reference value on the respective plate.

2.9. *In vivo* studies and sample analysis

SynBiosys®-based microparticle formulations of exenatide and mAbX were analyzed *in vivo* regarding pharmacokinetic behavior and pharmacodynamic efficacy. While exenatide formulations were examined using healthy and diabetic Sprague Dawley (SDa) rats, mAbX containing formulations were administered to healthy NMRI and immune-deficient NMRI nude (NMRI-*Foxn1*^{nu}) mice. Practical execution of mAbX animal trials was carried out by Charles River Laboratories in Freiburg, Germany. However, sample analysis was part of the present thesis. Overview tables of animal trials for *in vivo* analysis are illustrated hereafter for exenatide-based microparticles (Table 10) and mAbX-based microparticles (Table 11).

Table 10: Overview of in vivo *study design for exenatide microparticle experiments. Different treatments were administered with varying routes of administration (ROA) to healthy or diabetic SDa rats during five major experiments. A high fat diet (HFD) was followed by different streptozotocin (STZ) treatments for implementation of a type 2 diabetes mellitus (T2DM) model. Exenatide (EXT) in different dosage forms was administered as part of bioavailability, immunogenic, pharmacokinetic and pharmacodynamic studies and EXT plasma level, cytokine release, skin staining, non-fasting blood glucose (NFBG) as well as glycated hemoglobin (HbA_{1c}) were target parameters.*

	Treatment and dosing of exenatide	Number of animals	Number of treatments	ROA	Target parameter
Bioavailability study	20 µg/animal of Byetta®	2	1	s.c.	EXT plasma level
T2DM model	2 weeks HFD & 35 mg/kg STZ	3	1	i.p.	NFBG
	3 weeks HFD & 40 mg/kg STZ, 20 µg/animal of Byetta®	4	1 1	i.p. s.c.	NFBG
	3 weeks HFD & 30 mg/kg STZ, 20 µg/animal of Byetta®	4	2 1	i.p. s.c.	NFBG
Immunogenicity study	4.0 mg/kg (1.2 mg/animal) of ICE-2wF	3	1	s.c.	Cytokine release Skin staining
	4.0 mg/kg (1.2 mg/animal) of ICE-4wF	3	1	s.c.	Cytokine release Skin staining
	2.0 mg/mL (0.6 mg/animal) of Bydureon®	3	1	s.c.	Cytokine release Skin staining
	Polymer-only, amount of particles ≙ ICE-2/4wF (4.0 mg/kg)	4	1	s.c.	Cytokine release Skin staining
Pharmacokinetic study	0.4 mg/kg (0.12 mg/animal) of ICE-2wF	6	1	s.c.	EXT plasma level
	2.0 mg/kg (0.6 mg/animal) of ICE-2wF	6	1	s.c.	EXT plasma level
	4.0 mg/kg (1.2 mg/animal) of ICE-2wF	6	1	s.c.	EXT plasma level
	0.8 mg/kg (0.24 mg/animal) of ICE-4wF	6	1	s.c.	EXT plasma level
	4.0 mg/kg (1.2 mg/animal) of ICE-4wF	6	1	s.c.	EXT plasma level
	8.0 mg/kg (2.4 mg/animal) of ICE-4wF	6	1	s.c.	EXT plasma level
	2.0 mg/kg (0.6 mg/animal) of Bydureon®	6	1	s.c.	EXT plasma level
Pharmacodynamic study	0.4 mg/kg (0.12 mg/animal) of ICE-2wF	10+10	2	s.c.	NFBG, HbA_{1c}
	2.0 mg/kg (0.6 mg/animal) of ICE-2wF	10	2	s.c.	NFBG, HbA_{1c}
	4.0 mg/kg (1.2 mg/animal) of ICE-2wF	10	2	s.c.	NFBG, HbA_{1c}
	0.8 mg/kg (0.24 mg/animal) of ICE-4wF	10	1	s.c.	NFBG, HbA_{1c}
	4.0 mg/kg (1.2 mg/animal) of ICE-4wF	10	1	s.c.	NFBG, HbA_{1c}
	8.0 mg/kg (2.4 mg/animal) of ICE-4wF	10	1	s.c.	NFBG, HbA_{1c}
	2.0 mg/kg (0.6 mg/animal) of Bydureon®	10	4	s.c.	NFBG, HbA_{1c}
	Polymer-only, amount of particles ≙ ICE-2/4wF (4.0 mg/kg)	6+6	1	s.c.	NFBG, HbA_{1c}

Table 11: Overview of in vivo *study design for mAbX microparticle experiments. Different treatments were administered with varying routes of administration (ROA) to healthy NMRI and tumor-bearing NMRI nude mice during three major experiments. All animals received single injections without repetitive treatments. Different dosage forms of mAbX were injected as part of immunogenic, pharmacokinetic and pharmacodynamic studies and cytokine release, skin staining, mAbX plasma level as well as tumor volume were target parameters.*

	Treatment and dosing of mAbX	Number of animals	ROA	Target parameter
Immunogenicity study	untreated	3	n.a.	Cytokine release, skin staining
	8.0 mg/mouse of mAbX reference solution	9	i.v.	Cytokine release, skin staining
	1.0 mg/mouse of ICX-2wF	9	s.c.	Cytokine release, skin staining
	8.0 mg/mouse of ICX-2wF	9	s.c.	Cytokine release, skin staining
	Polymer-only, amount of particles ≙ ICX-2wF (8.0 mg/mouse)	9	s.c.	Cytokine release, skin staining
Pharmacokinetic study Part I	1.0 mg/mouse of mAbX reference solution	6	i.v.	mAbX plasma level
	1.0 mg/mouse of mAbX reference solution	6	s.c.	mAbX plasma level
	1.0 mg/mouse of ICX-2wF	6	s.c.	mAbX plasma level
	4.0 mg/mouse of ICX-2wF	6	s.c.	mAbX plasma level
	8.0 mg/mouse of ICX-2wF	6	s.c.	mAbX plasma level
Pharmacokinetic studiy Part II & Pharmacodynamic study	1.0 mg/mouse of mAbX reference solution	7	i.v.	mAbX plasma level, tumor volume
	1.0 mg/mouse of mAbX reference solution	7	s.c.	mAbX plasma level, tumor volume
	1.0 mg/mouse of ICX-2wF	7	s.c.	mAbX plasma level, tumor volume
	2.0 mg/mouse of ICX-2wF	7	s.c.	mAbX plasma level, tumor volume
	4.0 mg/mouse of ICX-2wF	7	s.c.	mAbX plasma level, tumor volume
	8.0 mg/mouse of ICX-2wF	7	s.c.	mAbX plasma level, tumor volume
	Polymer-only, amount of particles ≙ ICX-2wF (8.0 mg/kg)	7	s.c.	mAbX plasma level, tumor volume

2.9.1. Animal housing and general circumstances

Sprague Dawley rats

Animal trials with Sprague Dawley rats (SDa rats) were executed in rooms of the Interfaculty Biomedical Facility of the Heidelberg University. Male SDa rats were acclimatized for 7 days prior to the start of experiments. Animals were housed under standard conditions and a 12-hour dark/light cycle. Standard diet and water were provided *ad libitum* throughout the pharmacokinetic studies. Free access to a high fat diet (HFD) and water was allowed during the pharmacodynamic studies apart from certain fasting periods (see section 2.9.2). Animal studies were executed according to regulations of the local authorities and in compliance with approval number 35-9185.81/G-293/16 (Regierungspräsidium Karlsruhe, Germany).

NMRI and NMRI nu/nu mice

Animal studies using NMRI and NMRI nu/nu mice were executed at the Freiburg site of Charles River Laboratories. Female NMRI and NMRI nu/nu (NMRI-*Foxn1*^{nu}) were acclimatized for 7 days prior to the start of experiments. Animals were housed in individually ventilated cages under a 14L:10D artificial light circle at 22 ± 1°C with relative humidity of 40-70% and 60-65 air changes per hour. Standard rodent diet and acidified as well as sterile filtered water were provided *ad libitum* throughout animal studies. Animal studies were executed according to regulations of the local authorities and in compliance with approval numbers G-16-97 and G-18-12 (Regierungspräsidium Karlsruhe, Germany).

2.9.2. Type 2 diabetes mellitus model implementation

A type 2 diabetes mellitus (T2DM) model was implemented to evaluate the pharmacodynamic efficacy of exenatide released from SynBiosys®-based microspheres. For that purpose, a combination of a high fat diet (HFD) inducing insulin resistance and treatment with streptozotocin (STZ) selectively destructing pancreatic islet β-cells was chosen to induce a state closely resembling the human pathogenesis [194-196]. The suitability and performance of three different treatment protocols based on the descriptions of Brian Furman [197] were examined.

General instructions. Animals were fed with an obesity-inducing high fat diet (HFD) with 60% energy from fat (Altromin Spezialfutter GmbH) throughout implementation experiments for the T2DM model and pharmacodynamic studies. For administration of STZ, a 100 mM sodium citrate buffer, pH 4.5 was prepared and filtrated with a 0.22 µm filter unit. Animals were fasted for 12 h before STZ treatments by removal of HFD chow. Directly prior to injections, STZ was dissolved in sterile sodium citrate buffer to a final concentration of 20 mg/mL. Subsequently, different doses were administered intraperitoneally according to the respective protocol.

Protocol 1. Animals were treated with a single dose of 35 mg/kg of STZ after an initial HFD phase of 2 weeks. Non-fasting blood glucose (NFBG) was monitored over 7 days as described in section 2.9.5 and animals with NFBG levels ≥200 mg/dL after this period were considered diabetic.

Protocol 2. Male SDa rats were fed with HFD over 3 weeks before a single dose of 40 mg/kg of STZ was administered. Non-fasting blood glucose (NFBG) was monitored over 7 days as described in section 2.9.5 and animals with NFBG levels ≥200 mg/dL after this period were considered diabetic.

Protocol 3. An initial phase of 3 weeks of HFD was followed by a first administration of 30 mg/kg of STZ to animals. After 72h, a second dose of 30 mg/kg of STZ was injected. Non-

fasting blood glucose (NFBG) was monitored over 7 days after the first injection as described in section 2.9.5 and animals with NFBG levels ≥200 mg/dL after this period were considered diabetic.

NFBG levels of animals were monitored over a maximum of 55 days after the first STZ treatment to ensure a stable T2DM model for the duration of pharmacodynamic studies. To confirm the suitability of the model for evaluation of the therapeutic efficacy, animals were treated with a single exenatide dose of 20 µg (in the form of Byetta®) at the second last day of the respective study. NFBG levels were measured in a close monitoring 0 h, 2 h, 4 h and 24 h after administration of Byetta® and animals were sacrificed thereafter.

Stably elevated NFBG values over 7 weeks and a clear glucose-lowering effect of exenatide treatment indicating the presence of functionally active pancreatic β-cells were determined as parameters confirming a suitable T2DM model.

2.9.3. Induction of A-431 cell-based tumors in NMRI nu/nu mice

Prior to the start of the pharmacodynamic evaluation of mAbX-containing SynBiosys® microparticles, A-431 cell line based tumors were induced in NMRI nu/nu mice to monitor growth inhibition as result of functionally intact released mAbX. The commercially available epidermoid carcinoma A-431 cell line is well-established as model system for studies on EGF-related effects due to high expression levels of EGFR [198, 199].

Cells were cultured in RPMI 1640 medium supplemented with 10% fetal bovine serum and 0.05 mg/mL gentamycin. Animals received an injection of 1 x 10^7 cells (200 µL of a suspension in PBS) by injection into the left flank region. As soon as implants reached a volume of 80-200 mm³ in a sufficient number of animals, mice were assigned to groups aiming at comparable group mean tumor volumes. The day of randomization was designated as day 0 of the study. A total number of 49 tumor-bearing mice with a mean body weight of 25.3 ± 1.9 g was part of the experiment.

2.9.4. Administration of formulations

Exenatide-loaded microparticles

As described earlier, lyophilized microparticles were stored at -18°C until preparation of injection suspensions. For preparation of injection suspensions, microparticles were mixed with CMC solution (0.6 wt.% CMC 7HF-PH in 12.5 mM PBS). Appropriate amounts of microspheres were suspended to obtain final injection volumes of 1 mL/animal. Injection suspensions were stored at -80°C until usage in animal trials. Before usage, suspensions were thawed at RT over approximately 2 h. Bydureon® was prepared according to the

manufacturers' protocol with a subsequent dilution step using 0.9% sterile saline resulting in similar injection volumes of 1 mL/animal. Suspensions were vortexed for 30 seconds directly prior to administration and inverted regularly during treatments to ensure a homogenous distribution of microparticles. At day 0, 1 mL of the respective suspension was injected subcutaneously to the right flank region of the animals using 21G needles. The injection area was shaved prior to administration of formulations to simplify precise dosing.

mAbX-loaded microparticles and reference solutions

Lyophilized microparticles were thawed for 30 minutes at RT. A CMC solution (0.6 wt.% CMC 7HF-PH in 12.5 mM PBS) was thawed overnight at 2-8°C and inverted four times before transferring appropriate volumes to microsphere vials. Reconstituted microparticles were vortexed for 30 seconds and inverted regularly during administration to ensure a homogenous distribution of particles. Fixed volumes of 250 µL/animal of microsphere solutions were injected subcutaneously in the right flank region.

Additionally, mAbX was diluted in PBS under sterile conditions to obtain reference formulations with immediate release for intravenous and subcutaneous injections. Fixed volumes of 100 µL/animal of reference solution were administered to tail veins (i.v.) or in the right flank region (s.c.).

2.9.5. Collection of *in vivo* samples and direct readouts

Blood collection, determination of NFBG and skin sampling in Sprague Dawley rats

Blood collection. After fixation of animals, tails were prewarmed in heated water for 1-2 minutes to increase the blood flow. Approximately 200-300 µL of blood were sampled from tail veins using 20G needles and K3EDTA blood collection tubes. Coagulation of blood was prevented by inversion of tubes ensuring a comprehensive distribution of EDTA. Collection tubes were placed on ice until sampling of all animals was completed. Plasma was separated after centrifugation of blood collection tubes at 5000 rpm for 10 minutes. Plasma samples were stored at -80°C.

Determination of NFBG levels. The level of NFBG was determined by fixation of animals and subsequent punctuation of a tail vein. The first drops of blood were discarded to avoid imprecise measurements. Determination of NFBG was then performed with an Accu-Chek® Guide meter (Roche Diabetes Care GmbH, Germany) according to the manufacturers' instructions.

Skin sampling. Samples of the skin around the injection area were collected after sacrifice of SDa rats at the end of the experiments. The area of interest was shaved at the beginning and

during animal studies to ensure sampling at the correct site. Biopsies of approximately 1x1 cm were collected and stored in QPath microstar III biopsy cassettes. Skin was fixed and stored in 4% formaldehyde solution for at least 24h with subsequent incubation in 50%, 70%, 80% and 96% ethanol for 1.5 hours, respectively. Samples were then further dehydrated by incubation in 100% isopropanol and 100% xylene. Finally, samples were embedded in paraffin.

Blood microsampling, determination of tumor growth and skin sampling in NMRI and NMRI nu/nu mice

Blood collection. Blood samples were collected from tail veins during pharmacokinetic and pharmacodynamic studies or by retrobulbar sinus puncture for the immunogenicity study. Samples collected by sinus puncture were transferred directly to K3EDTA powder containing vials. Vials were stored on ice until all samples were collected. Microsamples of 20 µL were taken from tail veins directly into K3EDTA coated capillaries. Samples were transferred from capillaries to larger tubes on ice containing K3EDTA and 40 µL of PBS (1:3 dilution). All blood samples were centrifuged at 2000 x g for 5 minutes at 4°C. Plasma was transferred to separate tubes thereafter and was stored at -80°C until further analysis.

Determination of tumor growth. During pharmacodynamic experiments, the tumor dimensions were determined by two-dimensional measurement with a digital caliper. Absolute tumor volumes were calculated according to the following formula (7):

$$Tumor\ volume\ = (l\ x\ w^2)\ x\ 0.5 \qquad (7)$$

with l and w representing length and width of the tumor in mm, respectively. Tumor volumes were measured at day 0 and subsequently twice weekly.

Skin sampling. Skin samples of the injection site were collected from euthanized animals. The area of interest was shaved prior to sample collection and skin biopsies with an approximate size of 1 cm² were transferred to small cassettes. Thereafter, samples were formalin fixed for 24h with subsequent incubation in 70% ethanol for 7 days. In the next steps, samples were dehydrated by incubation in increasing concentrations of 80-100% ethanol followed by 100% isopropanol and 100% xylene. Finally, samples were embedded in paraffin.

2.9.6. Determination of exenatide plasma level

Plasma exenatide concentrations were determined using an Exendin-4 EIA Kit (Peninsula Laboratories, Inc., USA) according to the manufacturers' instructions. Influence of plasma samples on assay performance was minimized by usage of pooled plasma from male SDa rats as standard matrix. Samples were at least diluted 1:2 with the assay buffer due to limited sample volumes and samples with higher exenatide content were diluted further. However,

sample and standard matrices were always designed similarly to equalize potential influences on assay performance. Reference standards were assayed in triplicate while samples were examined in duplicate as presented in Figure 13. Absorption values were read with a Microplate Reader Multiskan spectrum (Thermo Fisher Scientific, Inc.).

LOQ was determined with a lower statistical significance compared to calculations described before (section 2.8.8) according to the following equation 7:

$$LOQ = X_{b1} + 3S_{b1} \quad (7)$$

where X_{b1} represents the absorption value of the respective blank and S_{b1} is the standard deviation of blank absorption values. LOQ was determined at 55.86 pg/mL using the respective assay matrix as blank and a minimum of 10 blank wells (see section 3.4.1). Values below the LOQ were excluded from results. Additional to LOQ calculation, further assay quality requirements were ensured:

- Reference standards 2-5 (202.5-7500.0 pg/mL) must not exceed the theoretical concentration by ± 20% after back calculation based on 5-parametric logistic fit
- Coefficient of determination for the 5-parametric logistic fit curve must exceed 0.98

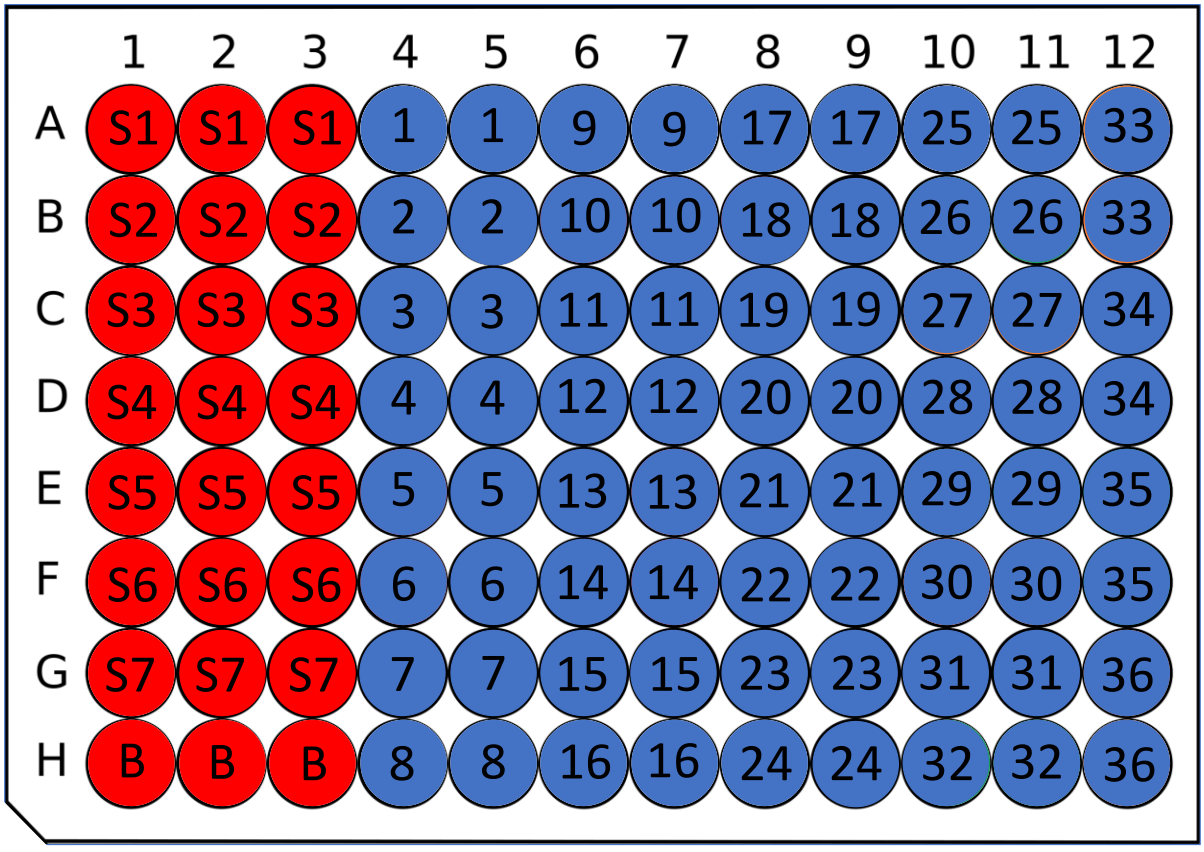

Figure 13: General plate scheme for exenatide quantification assay. A reference of exenatide (red) was examined in triplicate and a maximum number of 36 plasma samples (blue) was assayed in duplicate.

2.9.7. Determination of mAbX plasma level

Functional mAbX was quantified in plasma by ELISA. Fundamental experimental procedures were already explained in section 2.8.8. However, for *in vivo* sample analysis assay procedures were slightly adapted. First, mAbX content in plasma samples was predetermined during preparative ELISA experiments by examination of different dilutions of each sample. Final determination of mAbX content in animal samples was then performed by individual dilutions for all samples ensuring measuring values within the measuring range. Furthermore, samples of individual animals were only analyzed on single assay plates without splitting to different plates to avoid inter-plate variances. Additionally, samples and reference standards were diluted in 1:40 NMRI:Assay buffer matrix ensuring equal performance of standards and *in vivo* samples. Standards and samples were analyzed in triplicates as illustrated in Figure 14.

LOQ in plasma matrix was determined as described before (see section 2.8.8) and was found to be at 0.17 ng/mL. Assay quality requirements were applied as described above.

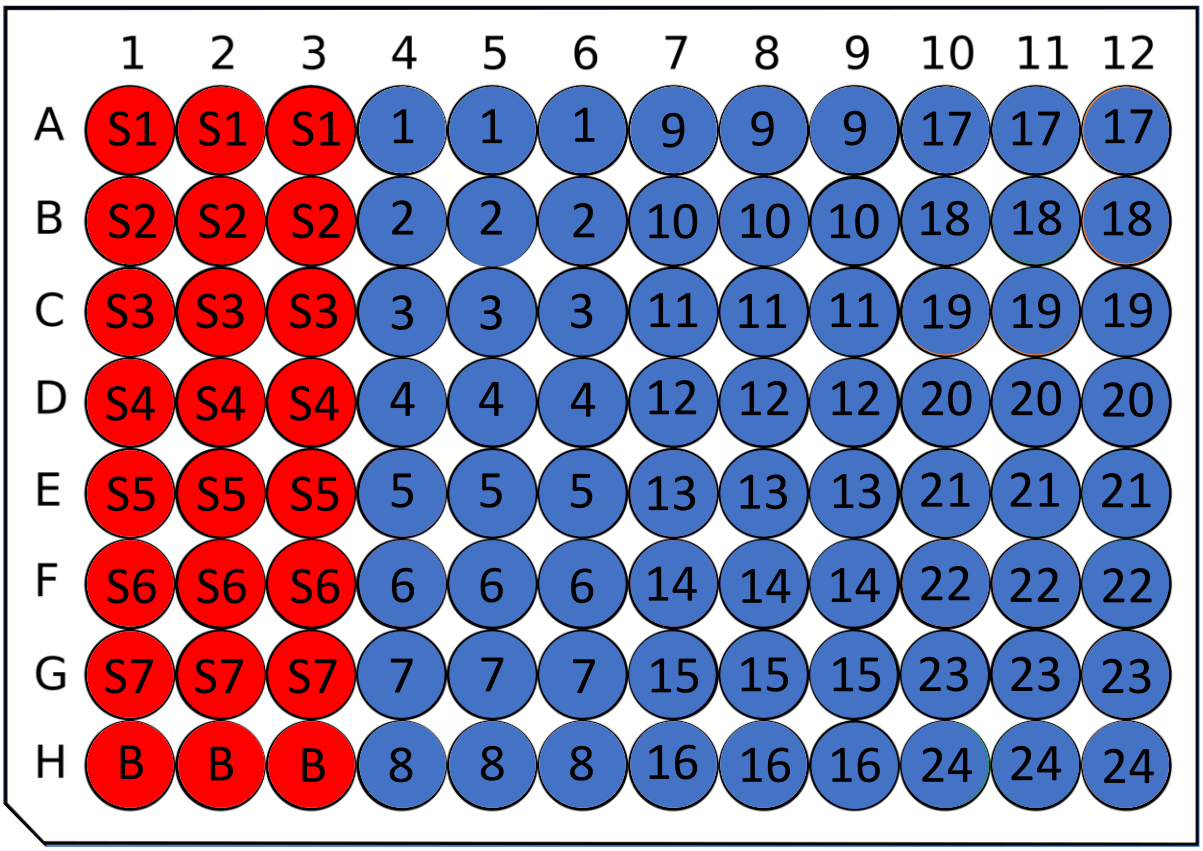

Figure 14: General plate scheme for quantification of functional mAbX in in vivo *samples. A reference of mAbX (red) and a maximum number of 24 plasma samples (blue) was assayed in triplicate.*

2.9.8. Quantification of glycated hemoglobin

The total hemoglobin contains different minor glycated hemoglobins of which HbA_{1c} constitutes the main portion [200]. Nowadays, determination of the percentage of HbA_{1c} in total hemoglobin represents a reliable marker for long-term glycemic levels over the preceding 8-12 weeks [200-202]. Consequently, this marker is less error-prone when compared to daily measurements of the non-fasting blood glucose level.

The percentage of HbA_{1c} in total hemoglobin was determined by HPLC from blood samples taken before STZ treatment in SDa rats and at the end of the pharmacodynamic studies. Blood was sampled as described previously (section 2.9.5). Experiments were executed by the central laboratories of the Heidelberg University Hospital. The method for hemoglobin species separation has been described elsewhere [203]. Briefly, samples were analyzed with a PolyCAT A cation exchange column using a binary solvent gradient consisting of buffer A (35 mM BisTris, 16.85 mM ammonium acetate, 90 mM sodium acetate, 1.5 mM potassium cyanide, pH 6.8) and B (35 mM BisTris, 3 mM ammonium acetate, 1.5 mM potassium cyanide, pH 6.5). Hemoglobin elution was monitored by absorbance at 415 nm.

2.9.9. Determination of cytokine release

Cytokine release during *in vivo* immunogenicity studies was examined with fluorescent bead-based Luminex technology which enables the simultaneous measurements of various analytes in a single sample significantly saving on sample volume and time [204, 205]. Samples of exenatide and mAbX based microparticle evaluation were measured as depicted in the overview (Table 10 and Table 11) using the Luminex® 200 system. General technological procedures as well as sample specific handling are described in this section.

General instructions. In preparation of measurements, the sample needle was cleaned and sonicated for 30 seconds with an Ultrasonic cleaner (VWR/Avantor, Inc.). After rinsing with ddH_2O, the sample needle was remounted and the needle height was adjusted according to the instructions of the Bio-Plex Manager 6.0. Subsequently, the start-up procedure was initiated in the software.

The device was calibrated on each working day after completion of the start-up procedure. For this purpose, the calibration beads (Bio-Plex Calibration Kit) were vortexed for 30 seconds followed by addition of each calibrator to the appropriate wells on the Bio-Plex MCV plate IV, and subsequently the calibration process was initiated.

If calibration was passed, the device was validated once monthly with the Bio-Plex Validation Kit 4.0. Validation beads were vortexed for 30 seconds and added to the appropriate wells on

the Bio-Plex MCV plate IV. The validation was initiated and the Luminex® 200 device was ready-to-use if validation was passed successfully.

HTS Filter plates were used for the assay procedure enabling vacuum supported washing procedures. Plates were generally incubated at RT and at a shaking speed of 550 rpm using a Thermomixer.

Exenatide-loaded microparticles. The immunogenic potential of exenatide-loaded microparticles was evaluated in healthy SDa rats after subcutaneous injection of formulations. Blood was sampled as described previously (section 2.9.5) and 27 different cytokines were quantified in plasma samples using a Milliplex® Rat Cytokine/Chemokine magnetic bead panel according to the manufacturers' protocol. Plasma influence was evaluated during method implementation described in section 3.4.1. Consequently, all plasma samples were diluted 1:2 in assay buffer and reference standards as well as quality controls were reconstituted in a similar matrix using blank SDa plasma to compensate plasma influence on assay performance. Samples were assayed in duplicate due to limited samples volumes. Results were considered as reliable if quality controls were recovered in the target range and if standards 2-7 of the references were found within ± 20% of theoretical concentrations after back calculation based on 5-parametric logistic fit.

mAbX-loaded microparticles. The immunogenic potential of mAbX-loaded microparticles was evaluated in healthy NMRI mice after subcutaneous injection of formulations. Blood was sampled as described previously (section 2.9.5) and 32 different cytokines were quantified in plasma samples using a Milliplex Mouse Cytokine/Chemokine magnetic bead panel according to the manufacturers' protocol. Plasma influence was evaluated during method implementation described in section 5.4.1. Consequently, all plasma samples were diluted 1:10 in assay buffer and reference standards as well as quality controls were reconstituted in a similar matrix using blank NMRI plasma to compensate plasma influence on assay performance. Samples were assayed in triplicate. Results were considered as reliable if quality controls were recovered in the target range and if standards 2-7 were found within ± 20% of theoretical concentrations after back calculation based on 5-parametric logistic fit.

2.9.10. Histological staining of skin samples of injection area

Skin biopsies were embedded in paraffin by RD-XND-PA (Merck KGaA) or Charles River Freiburg site (Charles River Laboratories, Inc.) as described above in section 2.9.5. Further analysis was performed by RD-XND-PA (Merck KGaA). Paraffin blocks were incubated at -20°C for one hour prior to preparation of tissue sections with a thickness between 3-5 µm using a sliding microtome. Fresh tissue sections were stretched in cooled ddH_2O to remove potential folding. Sections were transferred to microscope slides and were incubated in ddH_2O at 40°C to remove residual irregularities or uneven surfaces. Tissue sections were surface dried for at least 1 hour at 38-45°C in a heating cabinet. Subsequently, hematoxylin-eosin (H&E) stains of tissue sections were prepared with standard protocols of a Symphony H&E system (Ventana Medical Systems, Inc.). The basic H&E stain is the well-known standard to allow fundamental differentiation between the most important cell and tissue structures [206]. Tissue sections were completely dried, deparaffinized as well as stained and coverslips were added automatically by the Symphony System. In the following analysis of tissue stains using an Axioplan microscope (Carl Zeiss AG), cell nuclei, cartilage and calcium oxide appeared blue while all residual tissue structures were stained in different shades of red. Biopsies of animals treated with exenatide as well as mAbX-loaded microparticles were processed equally as described above.

2.10. Statistical methods

Resulting values of *in vitro* and *in vivo* studies were reported as means ± standard deviation (SD) or means ± standard error of the mean (SE) of at least three individual experiments unless otherwise stated calculated by the Excel software (Microsoft Office 365 ProPlus) or GraphPad Prism (Version 8.2.0). The determination of the wavelength of maximum fluorescence intensity in fluorescence spectroscopy measurements was simplified by Savistsky-Golay smoothing of spectra (6^{th} order, 10 neighbors) using GraphPad Prism. As indicated previously in the respective sections, 4-parametric logistic fits ([Agonist]/[Inhibitor] vs. response) or 5-parametric logistic fits (GraphPad Prism) were used for determination of EC_{50}/IC_{50} values or fitting of standard curves. Statistical analyses were performed with GraphPad Prism and Gaussian distribution of pharmacodynamic data was confirmed by Shapiro-Wilk testing. Statistical significance of pharmacodynamic data was determined using unpaired t-tests with Welch's correction and confidence levels of 95% ($p < 0.05$) or less in the case of exenatide *in vivo* studies while regular unpaired t-tests with similar confidence levels were used to test for statistical significance in mAbX-based experiments.

3. Controlled release of the sensitive model peptide exenatide by SynBiosys®-based microparticles

3.1. Objective

The overarching aim of this work was the evaluation of the suitability of the SynBiosys® polymer platform for the controlled release of biologicals as drug class of increasing relevance. For that purpose, model drugs ranging from peptides to monoclonal antibodies were encapsulated in SynBiosys®-based microparticles to demonstrate the versatility of the platform.

In vitro and *in vivo* performances of SynBiosys® microparticle formulations of exenatide as sensitive model peptide are presented in this chapter.

Exenatide is a synthetic 39 amino acid (AA) peptide with a molecular weight of 4.1 kDa which is used in type 2 *Diabetes Mellitus* therapy as it enhances the glucose-dependent insulin secretion from pancreatic β-cells [149, 192]. Bydureon® is a PLGA-based one-week extended release formulation of exenatide and served as benchmark to showcase common limitations of PLGA in comparison with SynBiosys®-based microparticles. Additionally, the marketed, immediate release formulation of exenatide, Byetta®, was used as a reference.

A two-week (ICE-2wF) and a four-week (ICE-4wF) SynBiosys®-based long acting release formulation of exenatide was implemented by InnoCore Pharmaceuticals. Part of the development process was *in vitro* release and reversed-phase HPLC analysis of liberated peptide. A cell-based functional assay for confirmation of exenatide integrity after release from microparticles was developed as part of this work. As described in 2.8.9, the CHO-K1/GLP1/Gα15 cell line overexpresses the GLP1-R and was consequently used to confirm the ability of *in vitro* released exenatide to bind its target receptor. Binding of exenatide to GLP1-R caused intracellular cAMP secretion which was quantitatively indicating functionality of exenatide. The cAMP level after stimulation by *in vitro* released exenatide was quantified by the commercially available HitHunter® cAMP Assay for Biologics.

Furthermore, pharmacokinetic and pharmacodynamic performances of SynBiosys® microparticle formulations ICE-2wF and ICE-4wF were determined in comparison with Bydureon®. For pharmacokinetic analyses, exenatide plasma levels of Sprague Dawley rats (SDa rats) were monitored after single subcutaneous injection of formulations in different doses and pharmacokinetic parameters were compared.

Pharmacodynamic studies were executed in a type 2 diabetes mellitus rat model which was implemented as described in sections 2.9.2 and 3.4.4. Diabetic SDa rats were treated with ICE-2wF, ICE-4wF and polymer-only microparticles without exenatide in comparison to

Bydureon® over four weeks and non-fasting blood glucose (NFBG) levels as well as glycated hemoglobin were monitored over six weeks. Pharmacodynamic efficacy of formulations was compared.

3.2. Particle manufacturing and final products

Exenatide-loaded microparticles based on SynBiosys® polymers were developed and manufactured by InnoCore Pharmaceuticals. Optimized formulations are described in this section. Microparticles were manufactured with a water-in-oil-in-water (W/O/W) membrane emulsification process. The primary emulsion was mixed by Ultra Turrax (UT) treatment for 40 (ICE-2wF) or 80 seconds (ICE-4wF) while the polymer composition of both microparticle types was identical as shown in Table 12. Polymer 20CP40C40-D25 consisted of 20 wt.% of a hydrophilic poly(ε-caprolactone)-PEG_{3000}- poly(ε-caprolactone) (PCL-PEG_{3000}-PCL) block with a molecular weight of 4000 g/mol and 80 wt.% of a semi crystalline poly(*p*-dioxanone) (D) block with a molecular weight of 2500 g/mol. Additionally, polymer 100GL40 is a classical PLGA copolymer with a molecular weight of 4000 g/mol. A PEG content of 5.3 wt.% was incorporated in the polymer matrix of ICE-2wF and ICE-4wF.

Table 12: Polymer composition and manufacturing process parameters of exenatide-loaded microparticles.

Formulation	Composition of polymer matrix						Manufacturing parameters	
	Polymer 1		Polymer 2		PEG			
	Grade	wt.%	Grade	wt.%	g/mol	wt.%	Polymer concentration	UT
ICE-2wF	100GL40	65	20CP30C40-D25	35	3000	5.3	10%	40 seconds
ICE-4wF	100GL40	65	20CP30C40-D25	35	3000	5.3	10%	80 seconds

As illustrated in Table 13, particle sizes were highly consistent between ICE-2wF, ICE-4wF and the polymer-only microparticles with average particle diameters between 49.0 and 51.1 µm. Additionally, a high similarity of exenatide loading (5.5 to 5.6 wt.%) and encapsulation efficiency (84.8 to 86.2%) was observed, respectively.

Table 13: Characteristics of exenatide-loaded SynBiosys® microparticles. Particle size as well as exenatide loading and encapsulation efficiency are presented.

	Particle size [µm]	Exenatide load [wt.%]	Exenatide encapsulation efficiency [%]
ICE-2wF	49.2 ± 14.2	5.5	84.8
ICE-4wF	49.0 ± 12.1	5.6	86.2
Polymer-only (w/o exenatide)	51.1 ± 9.9	-	-

Furthermore, particles were examined in scanning electron microscopy (SEM) and the particle surface morphology was evaluated (Figure 15). Surfaces of ICE-2wF and ICE-4wF microparticles (Figure 15A, B) were smooth and particles were homogenously distributed while the surface morphology of polymer-only microparticles (Figure 15C) was porous as a result of the absence of exenatide during manufacturing.

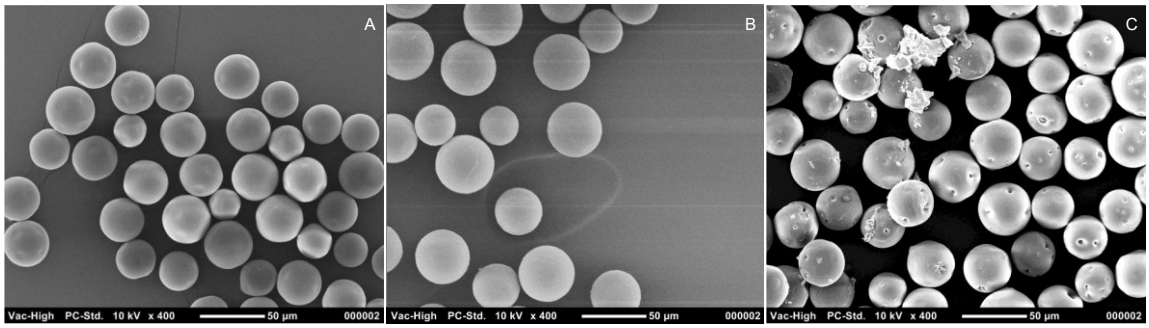

Figure 15: SEM images of ICE-2wF (A), ICE-4wF (B) and polymer-only microparticles (C).

3.3. *In vitro* results

Method implementation as well as results of *in vitro* release (IVR) and analysis of *in vitro* released exenatide are presented in the following section. Solely method implementation of a cell-based functional assay for exenatide was part of this work while other methods used for *in vitro* analysis were developed elsewhere and are consequently not further described herein.

3.3.1. Method implementation

Cell-based functional assay for exenatide

Numerous preparative experiments were performed to establish a cell-based assay to quantify functional exenatide which was released *in vitro*. A suitable number of cells seeded into wells of the assay plate was determined at 6000 cells/well and exenatide incubation time was increased from 30 (protocol recommendation) to 60 minutes as this period turned out to be beneficial regarding signal yield. Furthermore, luminescence signals were measured after 5 hours of incubation as values reached the maximum at this time point. Results of these studies are not shown herein. Thermally degraded exenatide reference samples were examined to gain an impression of exenatide signals after degradation of various severity. However, exenatide retained its native structure after thermal degradation, no effects were observed and results are not shown. Therefore, a commercially available n-terminally truncated metabolite of GLP-1 was used as negative control, referred to as GLP-1 (9-36) [207, 208]. Usage of GLP-1 (9-36) in experiments demonstrated that cells were solely stimulated by functional exenatide.

According to the manufacturers' protocol, reference standards and samples should be diluted 11-fold to ensure proper fitting and calculation of EC_{50} values. However, a reduction of dilution steps was desirable to reduce the total number of plates needed for analysis of *in vitro* release (IVR) sample sets as well as inter-plate variability. Amongst others, a reduction from 11 to 8 dilution steps was examined and results are shown in Figure 16. Curve shapes were comparable between 8-fold and 11-fold diluted reference peptide while stimulation with GLP-1 (9-36) was without effect on CHO-K1/GLP1/Gα15 cells. As indicated by Figure 16B, EC_{50} values decreased clearly with reduced dilution steps. However, also reduced values were reproducible and reference standards as well as IVR samples were diluted 8-fold during cell-based functional analysis of released exenatide.

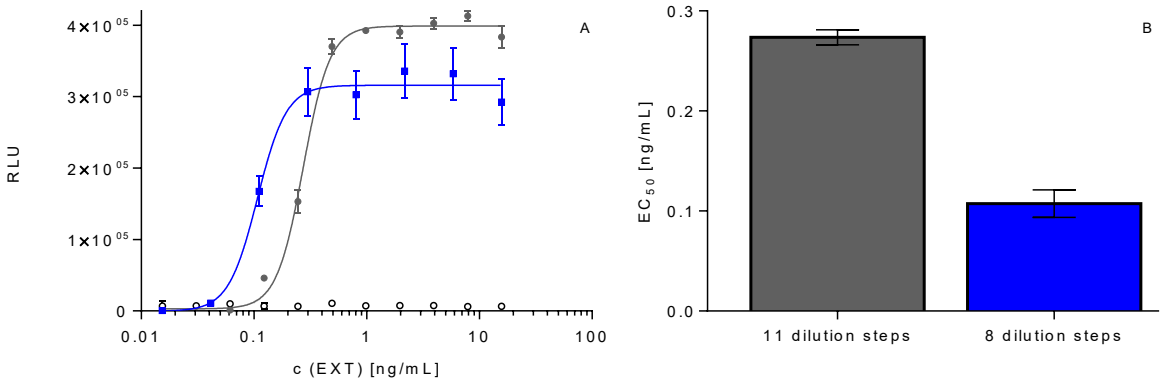

Figure 16: Comparison of relative luminescence unit (RLU) signals (A) and EC_{50} values (B) after cellular stimulation with 11- and 8-fold dilution rows of exenatide. Four parametric fits of 11-fold diluted exenatide (●) and 8-fold diluted exenatide (■) were used to calculate EC_{50} values. Calculation of the EC_{50} value of 11-fold diluted GLP-1 (9-36) (○) was not possible as RLU values remained at low levels. Data represent mean values ± SE (A) or SD (B) of n = 3 (11-fold dilutions) and n = 6 (8-fold dilutions).

3.3.2. *In vitro* release and functionality of exenatide

As described earlier herein, Bydureon® is a marketed, one-week extended release formulation of exenatide which is based on classical PLGA. Therefore, Bydureon® served as a reference formulation to demonstrate limitations of PLGA-based controlled release approaches. Figure 17 demonstrates the *in vitro* release behavior of Bydureon® in comparison with SynBiosys® microparticle formulations of exenatide, ICE-2wF and ICE-4wF. An initial lag phase over approximately three weeks was characteristic for Bydureon®-based exenatide release (Figure 17A) and a bulk release was observed thereafter between days 25 and 35. Only small amounts of exenatide were released during the final phase after day 35 and later.

In contrast to that, exenatide was released more continuously by SynBiosys®-based ICE-2wF and ICE-4wF (Figure 17B, C). While most exenatide was released during the first 20 days with ICE-2wF, the release duration was extended to 35 days with ICE-4wF. Thereby, the proportion of exenatide released as burst during the initial 24 hours after beginning of the respective study was limited to 8.9% (ICE-4wF) or 15.2% (ICE-2wF). Additionally, the integrity of exenatide released from ICE-4wF (69.3%) and ICE-2wF (80.5%) was higher compared to Bydureon® (65.0%) based on HPLC analysis.

Furthermore, IVR samples were analyzed with a cell-based functional assay to evaluate the ability of the released peptide to bind GLP1-R as presented in Figure 17D-F. Analysis of Bydureon® IVR samples was highly variable (Figure 17D). However, most values were obtained between 100 and 200% functionality compared to an exenatide reference sample. Lower values were found especially at later time points. In comparison to that, functionality of

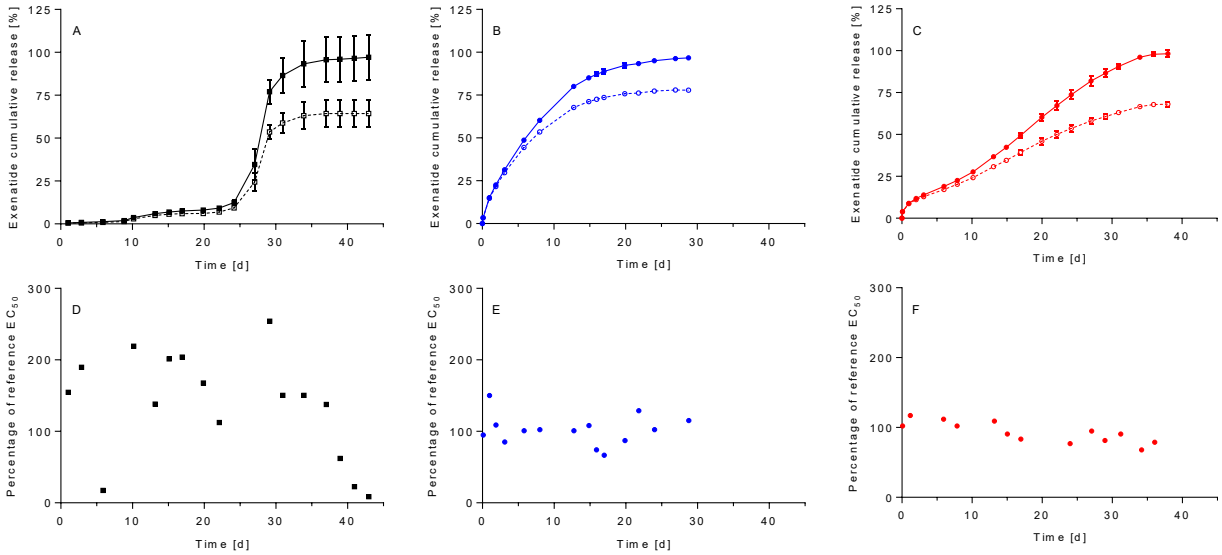

Figure 17: Exenatide IVR from Bydureon® (A), ICE-2wF (B) or ICE-4wF (C) and corresponding cell-based functionality determination (D-F), respectively. Exenatide release behavior of Bydureon® (Total: ■, intact: □), ICE-2wF (Total: ●, intact: ○) and ICE-4wF (Total: ●, intact: ○) formulations was compared as well as the functionality of exenatide release expressed as percentage of EC_{50} of reference standard. Mean values of n = 3 samples are shown in A-C ± SD while data in D-F represents n = 1 without errors.

exenatide released from ICE-2wF was narrowly distributed around 100% and the majority of values exceeded 85%. No loss in function was observed over time (Figure 17E). Similarly, exenatide released from ICE-4wF was highly functional with values around 100% and most measurements indicating a functionality over 80%. A tendency to slightly decreasing functionality over time was observed (Figure 17F).

3.4. *In vivo* results

As a next step, exenatide-loaded microparticle formulations ICE-2wF and ICE-4wF were analyzed *in vivo* regarding their immunogenic, pharmacokinetic as well as pharmacodynamic potential. Results of method implementation and *in vivo* studies are shown in the following section. Solely methods that were established or adapted as part of this work are presented during method implementation.

3.4.1. Method implementation

Cytokine magnetic bead panel for Luminex analysis

A 27-plex cytokine/chemokine magnetic bead panel for the simultaneous quantification of 27 different cytokines in plasma samples was adapted to experimental requirements for *in vivo* studies. Blank, pooled Sprague Dawley (SDa) rat plasma was used as assay matrix to reduce potential matrix effects of the *in vivo* samples. In preparative experiments, the influence of 1:2 diluted SDa plasma on standard curve performances was tested and Figure 18 presents standard curves for epidermal growth factor (EGF) in different matrices as representative example for the whole cytokine panel. Median fluorescent intensities of the standard curve diluted in 1:2 plasma matrix were generally lower compared to assay buffer dilution matrix.

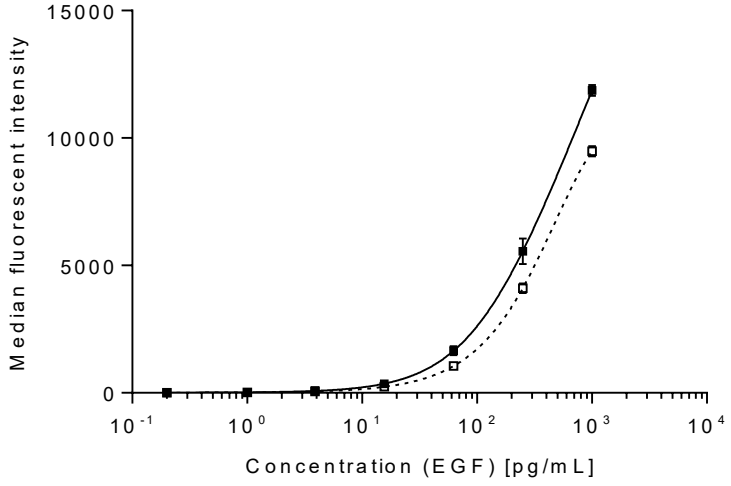

Figure 18: Median fluorescent intensity of EGF standard curves in different assay matrices. EGF was diluted in assay buffer (■) or 1:2 SDa rat plasma in assay buffer matrix (□) and curves were fitted with a 5 parametric logistic fit. Data represent mean values of n = 3 ± SD.

However, differences were relatively small and the influence on assay performance was expected to be negligible. Furthermore, assay quality requirements were fulfilled using the adapted plasma matrix. Dilution of plasma samples with a ratio of 1:2 and usage of 1:2 plasma matrix was found to be suitable for *in vivo* sample analysis.

Quantification of exenatide in plasma samples

Exenatide was quantified using a commercially available ELISA kit. However, to correct for matrix related influences on the assay performance, the effect of SDa rat plasma was examined during preparative method development experiments. Figure 19 presents exenatide standard curves diluted in assay buffer or 1:2 SDa rat plasma in assay buffer. Absorption values generally decreased inverse proportionally with increasing exenatide concentrations. Additionally, exenatide diluted in plasma matrix led to reduced values especially for the lowest peptide concentrations. However, differences were negligible and assay quality requirements were fulfilled in both matrices tested. Furthermore, the limit of quantification was determined at 55 pg/mL using the rat plasma matrix.

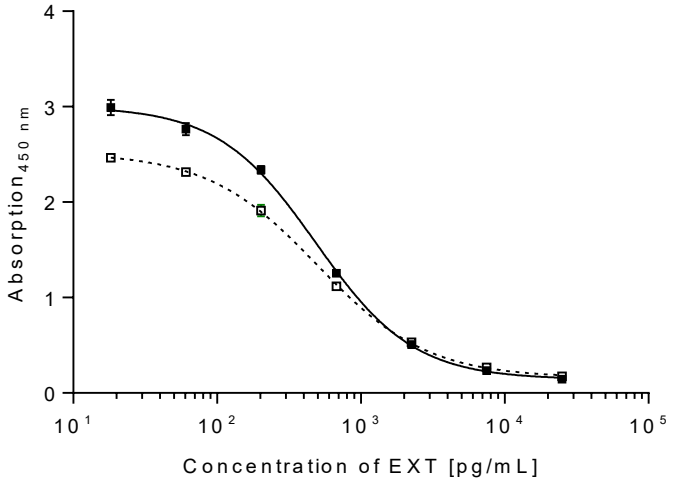

Figure 19: Influence of assay matrix on exenatide standard curves. Exenatide was diluted in assay buffer (■) or 1:2 SDa rat plasma in assay buffer matrix (□) and curves were fitted with a 5 parametric logistic fit. Data represents mean values of n = 3 ± SD.

3.4.2. Immunogenicity

As illustrated in Table 10, animals were treated with single subcutaneous injections of ICE-2wF, ICE-4wF, Bydureon® and SynBiosys® polymer-only microparticles to evaluate the immunogenic potential of the polymer platform. Systemic cytokine release as well as local inflammatory responses were examined.

Cytokine release after administration of microparticles

A number of 27 cytokines was quantified in plasma samples of animals over 48 hours after single subcutaneous treatment with ICE-2wF (4.0 mg exenatide/kg), ICE-4wF (4.0 mg exenatide/kg), Bydureon® (2.0 mg exenatide/kg) and SynBiosys® polymer-only microparticles (amount of particles equivalent to 4.0 mg exenatide/kg). While the majority of cytokines remained below the limit of detection at all time points and data is consequently not shown, epidermal growth factor (EGF) was elevated significantly as depicted in Figure 20. EGF plasma levels were elevated between 40 to 100 pg/mL approximately, one to four hours after administration of Bydureon® and polymer-only as well as ICE-4wF microparticles. Values decreased again after 24 to 48 hours post injections. EGF plasma levels remained generally low after treatment with ICE-2wF. Concerning EGF, all assay specific quality requirements were fulfilled and quality controls were recovered in the target ranges.

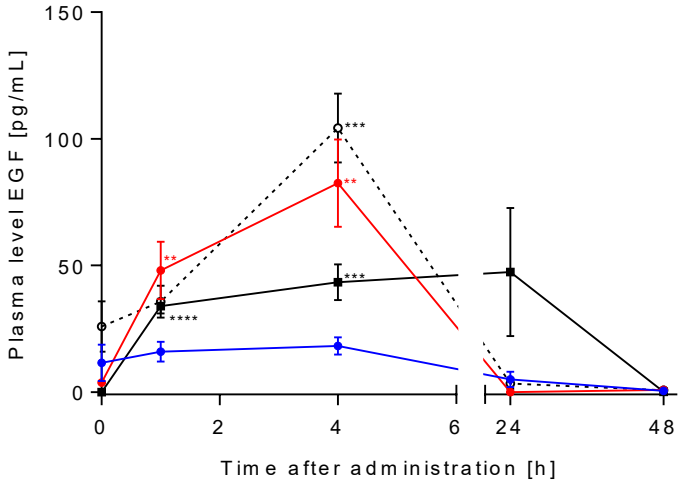

*Figure 20: Plasma levels of EGF after treatment with SynBiosys® microparticles and references. ICE-2wF (●), ICE-4wF (●), Bydureon® (■) and polymer-only microparticles (○) were administered once subcutaneously and doses of 2.0 mg/kg (Bydureon®) and 4.0 mg/kg (ICE-2wF, ICE-4wF) were injected. An equivalent amount of polymer-only microparticles to doses of ICE-2/4wF formulations was used. Data represents mean values of n = 4 (polymer-only) or n = 3 (other formulations) animals ± SE. Significant differences between EGF plasma levels at 0 hours and the following time points in the respective group are illustrated by ** (p<0.01), *** (p<0.001) and **** (p<0.0001).*

Histochemical staining of injection area

Additional to systemic cytokine release, the local immune response at the injection site was examined with hematoxylin & eosin staining which was performed by Merck internal experts (RD-XND-PA; Merck KGaA). A representative illustration for reactions on subcutaneous injections of SynBiosys® microparticles is shown in Figure 21. Various immune cells like eosinophilic granulocytes, multinucleated giant cells and macrophages migrated to the microparticle-containing injection area three days after injection. Immune responses were locally limited to the area of administration and were clearly distinguishable from neighboring areas which remained unaffected. Reactions to other formulations or at later time points were comparable to the results shown in Figure 21 and are therefore not presented in detail herein.

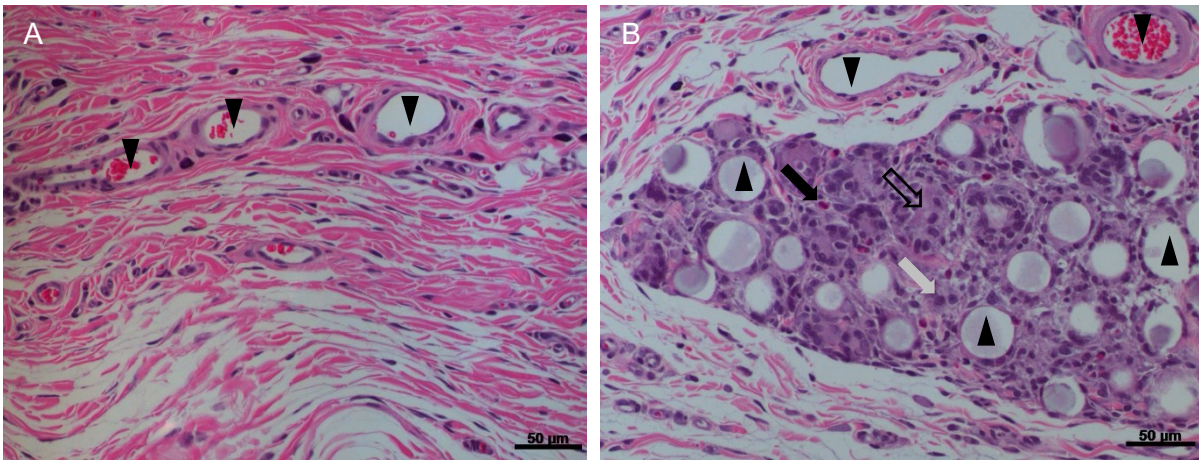

Figure 21: Hematoxylin & eosin staining of SynBiosys® microparticle injection site (B) and untreated reference biopsy (A) 3 days after s.c. injection. Blood vessels with or without erythrocytes (▼) and microparticles (▲) are shown as well as eosinophilic granulocytes (black arrow), multinucleated giant cells (blank arrow) and macrophages (grey arrow). Biopsies were collected following subcutaneous injection of ICE-2wF (4.0 mg/kg) and are representative for other formulations and time points.

3.4.3. Pharmacokinetic studies

In vivo release behavior of SynBiosys® exenatide formulations in comparison with Bydureon® was determined in pharmacokinetic experiments. In total, six groups each consisting of six animals received single subcutaneous injections of different doses of ICE-2wF, ICE-4wF and Bydureon® as illustrated in Table 10.

Exenatide plasma levels

Exenatide levels in plasma were quantified as described earlier in sections 2.9.6 and 3.4.1 and the results are presented in Figure 22. Additionally, pharmacokinetic parameters (C_{max} *(Peak1/2),* t_{max} *(Peak ½),* $AUC_{0\text{-}45d}$, F_{rel}) were determined and are listed in Table 14. Bydureon® was used as reference and was administered with an exenatide dose of 2.0 mg/kg (Figure 22A, B). The release profile was characterized by a first peak plasma concentration of 5.4 ng/mL after 24 hours and a subsequent lag phase until day 17. Comparable to *in vitro* data

(Figure 17A), the main portion of exenatide was released thereafter between days 20 to 40 following administration while exenatide peak plasma concentrations of 6.1 ng/mL were observed.

ICE-2wF was administered at exenatide doses of 0.4, 2.0 and 4.0 mg/kg leading to the plasma levels depicted in Figure 22A. Exenatide plasma concentrations remained at 2.4, 9.8 and 20.4 ng/mL, respectively, for approximately 3 to 6 days and decreased clearly thereafter. Exenatide was released over 3-14 days using ICE-2wF.

Furthermore, ICE-4wF was injected at exenatide doses of 0.8, 4.0 and 8.0 mg/kg resulting in plasma levels illustrated in Figure 22B. After an initial peak, the bulk amount of exenatide was released with peak levels of 6.6, 20.6 and 31.4 ng/mL, respectively and values decreased continuously thereafter. A release duration of 6-45 days was achieved with ICE-4wF.

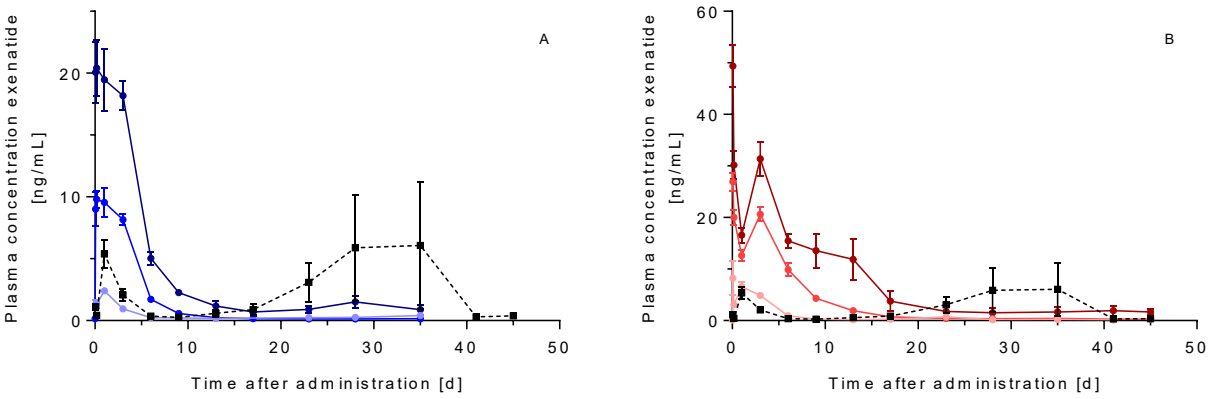

Figure 22: Exenatide plasma levels after single s.c. injection of Bydureon® (A, B), ICE-2wF (A) and ICE-4wF (B) over 35-45 days. Bydureon® was administered with an exenatide dose of 2.0 mg/kg (■) while ICE-2wF was injected at doses of 0.4 (●), 2.0 (●) and 4.0 mg/kg (●). ICE-4wF was administered at exenatide doses of 0.8 (●), 4.0 (●) and 8.0 mg/kg (●). Data represents mean values of n = 6 animals/group ± SE.Table 14: Pharmacokinetic parameters after administration of Bydureon®, Byetta®, ICE-2wF and ICE-4wF in various exenatide doses. Maximum exenatide plasma concentration (C_{max} (Peak 1/2)), time point of maximum plasma levels (t_{max} (Peak 1/2)), area under the curve (AUC_{0-45d}) and relative bioavailability (F_{rel}) are presented.

	C_{max} (Peak 1/2) [ng/mL]	t_{max} (Peak 1/2) [h or d]	AUC_{0-45d} [ng/mL*h]	F_{rel} [%]
Bydureon® (2.0 mg/kg)	5.4 / 6.1	1 d / 35 d	2784.7	32.0
ICE-2wF (0.4 mg/kg)	2.4	1 d	338.1	19.4
ICE-2wF (2.0 mg/kg)	9.8	4 h	1206.5	13.9
ICE-2wF (4.0 mg/kg)	20.4	4 h	3178.6	18.3
ICE-4wF (0.8 mg/kg)	8.2 / 6.6	2 h / 2 d	869.5	25.0
ICE-4wF (4.0 mg/kg)	26.9 / 20.6	2 h / 3 d	3511.2	20.2
ICE-4wF (8.0 mg/kg)	49.4 / 31.4	2 h / 3 d	7748.0	22.3
Byetta® (20 µg/animal)	79.4	4 h	289.8	100.0

Dose linearity and relative bioavailability

Based on the results on pharmacokinetic behavior of SynBiosys® microparticles and reference formulations presented previously, the area under the curve (AUC) between days 0 to 45 after administration was calculated as presented in Table 14. Linear relationships between exenatide plasma levels after administration of different doses of exenatide-loaded SynBiosys® microparticle formulations were found for ICE-2wF and ICE-4wF (Figure 23). The strong dose-dependency of plasma concentrations was demonstrated by determination of regression coefficients between 0.98 and 0.99. Furthermore, the relative bioavailability of ICE-2wF and ICE-4wF was calculated compared to the marketed immediate release reference formulation of exenatide, Byetta®. While ICE-2wF achieved relative bioavailability values of 19.4 (0.4 mg/kg), 13.9 (2.0 mg/kg) and 18.3% (4.0 mg/kg), ICE-4wF administration resulted in values of 25.0 (0.8 mg/kg), 20.2 (4.0 mg/kg) and 22.3% (8.0 mg/kg). In contrast to that, relative bioavailability of Bydureon® (2.0 mg/kg) was higher (32.0%).

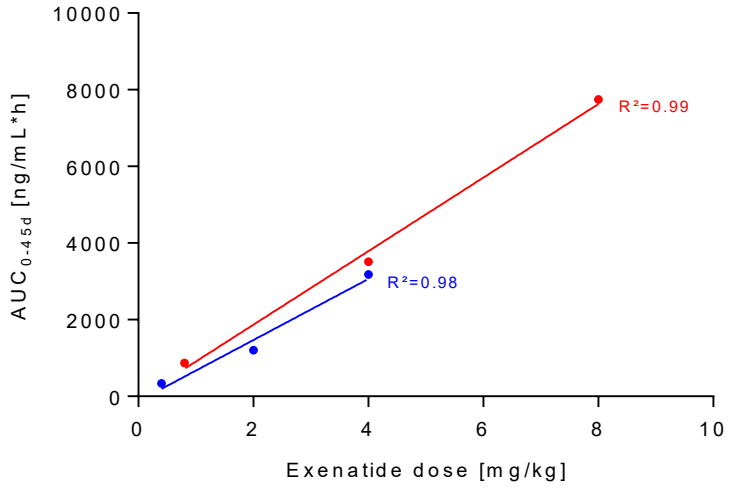

Figure 23: Area under the curve (AUC) from day 0 to 45 after single s.c. administration of different doses of ICE-2wF (●) and ICE-4wF (●) and corresponding regression lines. Dose linearity was demonstrated by determination of the regression coefficient (R^2).

3.4.4. Pharmacodynamic studies

After pharmacokinetic examination of exenatide-loaded SynBiosys® microparticles, pharmacodynamic studies were performed according to the experimental design summarized in Table 10. A type 2 diabetes mellitus rat model was established during a preparative experimental series. Subsequently, pharmacodynamic efficacy of different doses of ICE-2wF and ICE-4wF was compared to Bydureon® and polymer-only microparticles as references over approximately six weeks.

Implementation of type 2 diabetes mellitus model

A type 2 diabetes mellitus SDa rat model was established in preparation for pharmacodynamic studies as described in section 2.9.2. Initially, a group of three animals received a two weeks high fat diet (HFD) and was subsequently treated with a single intraperitoneal (i.p.) injection of 35 mg/kg streptozotocin (STZ) as part of protocol 1. The experiment was discontinued after 9 days as two out of three animals repeatedly showed non-fasting blood glucose (NFBG) values below the threshold of 200 mg/dL (Figure 24A). Protocol 2 consisted of a three weeks HFD followed by single i.p. administration of 40 mg/kg STZ. Half of the animals involved exhibited elevated NFBG levels exceeding 200 mg/mL over seven weeks and received a single subcutaneous exenatide treatment after 54 days to confirm the type 2 diabetic state (Figure 24B). NFBG values were clearly reduced over 2 and 4 hours after Byetta® treatment before rising again after 24 hours. Three out of four animals exhibited elevated NFBG levels over seven weeks after treatment according to protocol 3 which included a three weeks HFD in combination with two consecutive i.p. administrations of 30 mg/kg STZ (Figure 24C). Single s.c. injection of exenatide led to slight NFBG reductions within 4 hours followed by re-raised values 24 hours after treatment. One animal died spontaneously as consequence of protocol 2 and 3 treatments, respectively. As further elucidated in section 3.5, protocol 2 was chosen

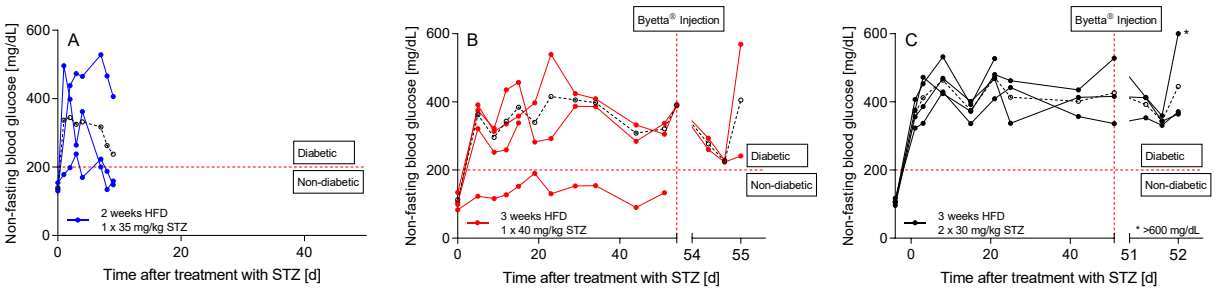

Figure 24: NFBG levels after application of three different HFD/STZ protocols over seven weeks. Protocols 1 (A, ●), 2 (B, ●) and 3 (C, ●) with varying duration of HFD and STZ dosing schemes were compared. Finally, Byetta® was administered with an exenatide dose of 20 µg/animal to confirm the type 2 diabetes mellitus resembling state of rats. Red dotted lines represent the threshold for diabetic NFBG levels (200 mg/dL) and the time point of Byetta® therapy. Data represent values of single animals. Additionally, average NFBG levels (o, dashed line) are shown to simplify comparison between protocols. Animals with NFBG values solely below the threshold of 200 mg/dL were excluded from mean value calculation.

as suitable method for induction of type 2 diabetes mellitus in pharmacodynamic studies as the reaction to exenatide treatment was pronounced most clearly.

Determination of changes in non-fasting blood glucose

NFBG levels of diabetic SDa rats were monitored over six weeks after therapies with ICE-2wF, ICE-4wF, Bydureon® and polymer-only microparticles. While Bydureon® was administered weekly over four weeks according to official dosing instructions, ICE-2wF was administered biweekly in different doses. Additionally, animals were treated once with polymer-only microparticles and variously dosed ICE-4wF in the time frame observed. NFBG levels were determined one day before start of therapies and changes were expressed by relating measuring values to the initial NFBG level of the respective animal. Results are depicted in Figure 25.

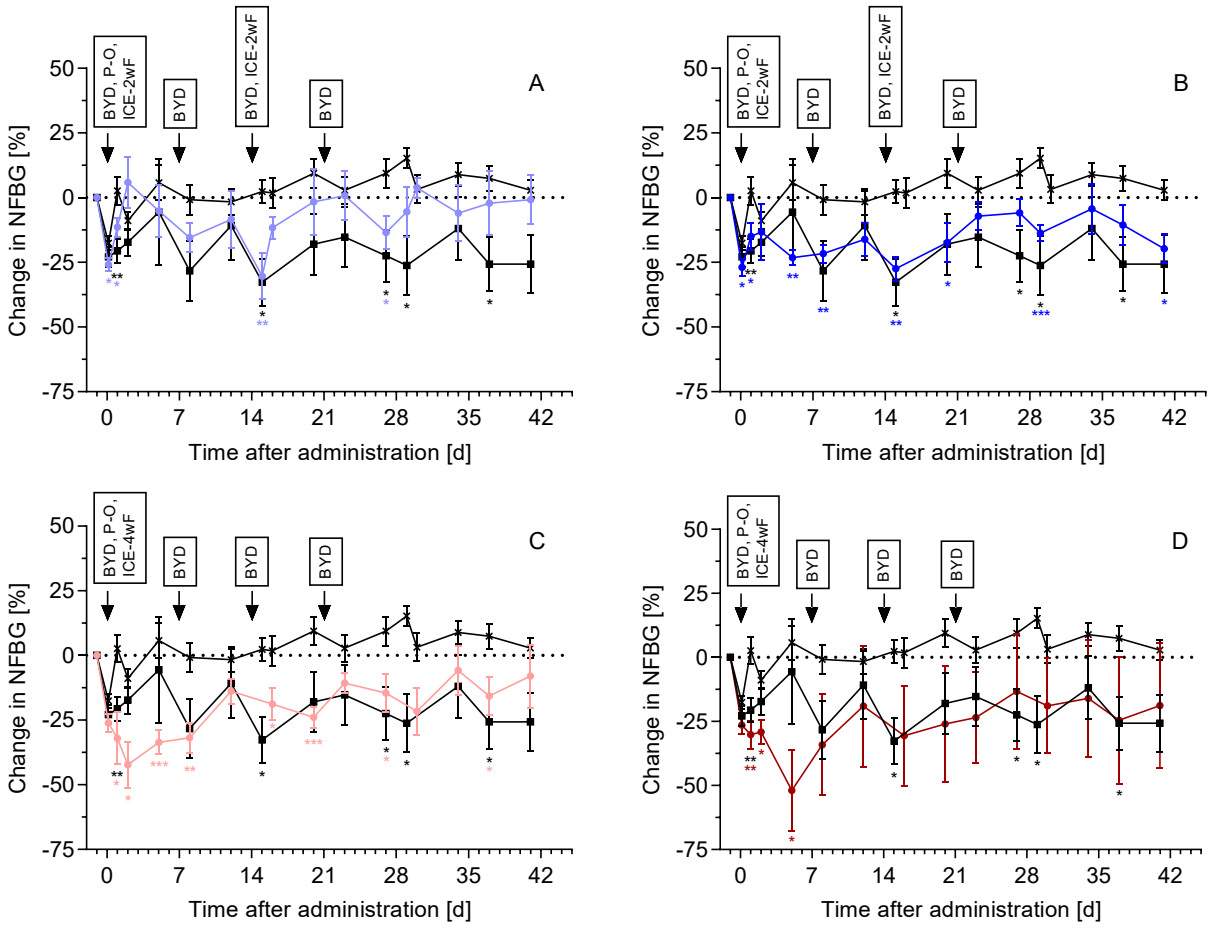

*Figure 25: Changes of NFBG levels in diabetic SDa rats over 41 days after treatment with Bydureon® (BYD) and polymer-only microspheres (P-O) in comparison with different doses of ICE-2wF (A, B) as well as ICE-4wF (C, D). Changes were related to NFBG values at day -1 prior to administration of formulations and the dotted line visualizes the baseline indicating unchanged NFBG. Arrows represent injection time points of Bydureon® (4 x 2.0 mg/kg, ■, n = 6), low-dosed ICE-2wF (2 x 0.4 mg/kg, ●, n = 8), medium-dosed ICE-2wF (2 x 2.0 mg/kg, ●, n = 4), low-dosed ICE-4wF (1 x 0.8 mg/kg, ●, n = 4), regular-dosed ICE-4wF (1 x 8.0 mg/kg, ●, n = 3) and polymer-only microparticles (no exenatide, x, n = 11). Mean values are presented ± SE. Significant differences between the P-O group and groups treated with exenatide-containing formulations are depicted by * (p<0.05), ** (p<0.01) and *** (p<0.001), colored in the group specific marking, respectively.*

Animals treated with polymer-only microparticles remained at hyperglycemic NFBG levels throughout the study serving as reference group for exenatide-containing therapies. Repeated Bydureon® treatment led to a slow decrease in NFBG with time resulting in approximately 25% reduction from day 27 on demonstrated by significant differences between Bydureon® and polymer-only microparticle groups (Figure 25A-D). NFBG levels were also punctually decreased 24 hours after the first injections of Bydureon®, respectively.

As illustrated in Figure 25A and B, therapy with ICE-2wF (2 x 0.4 mg/kg: Figure 25A, 2 x 2.0 mg/kg: Figure 25B) resulted in punctually lowered NFBG particularly 24 hours after injections represented by significant differences compared to the polymer-only reference group. However, efficacy of low-dosed ICE-2wF (2 x 0.4 mg/kg) was less pronounced while medium-dosed ICE-2wF (2 x 2.0 mg/kg) led to equally decreased NFBG values when compared to the Bydureon® reference group.

A single treatment with ICE-4wF with an exenatide dose equal to the Bydureon® total dose (8.0 mg/kg) was followed by significant NFBG reductions of approximately 25-50% during the initial 8 days and values remained at similar levels compared to the Bydureon® group until the end of the period observed (Figure 25D). Furthermore, a reduced-dose of ICE-4wF (0.8 mg/kg) was administered also resulting in significant NFBG level reductions between 25-40% during the first 8 days (Figure 25C). Blood glucose remained at lowered levels with comparable efficacy to the Bydureon® therapy until day 37 after administration with punctual, significant differences compared to the control group.

Unexpected death of animals treated with exenatide-containing formulations resulted in reduced group sizes. Therefore, ICE-2wF (2 x 4.0 mg/kg) and ICE-4wF (1 x 4.0 mg/kg) were excluded from analysis and results are not shown herein.

Determination of glycated hemoglobin

The proportion of HbA_{1c} in total hemoglobin of diabetic animals in pharmacodynamic studies was determined before and 45 days after the first treatment to support results from NFBG level measurements. Results are illustrated in Figure 26. Healthy animals without anti-diabetic therapy were found with HbA_{1c} levels around 5%. In contrast to that, diabetic animals treated with polymer-only microspheres (no exenatide) exhibited values around 10% after 45 days post diabetes induction and served as reference group.

Bydureon® therapy resulted in a reduction to 6.8% (4 x 2.0 mg/kg) while low-dosed ICE-2wF (2 x 0.4 mg/kg) led to a less pronounced reduction to 8.7%. However, medium-dosed ICE-2wF (2 x 2.0 mg/kg) achieved a decrease to 6.8% comparable to Bydureon® with a halved exenatide total dose. Moreover, an equal exenatide total dose compared to Bydureon® administered once as ICE-4wF (1 x 8.0 mg/kg) significantly reduced the percentage of HbA_{1c}

to 5.2% and single injection of a strongly lowered ICE-4wF dose (1 x 0.8 mg/kg) led to a significant HbA_{1c} reduction to 6.4%.

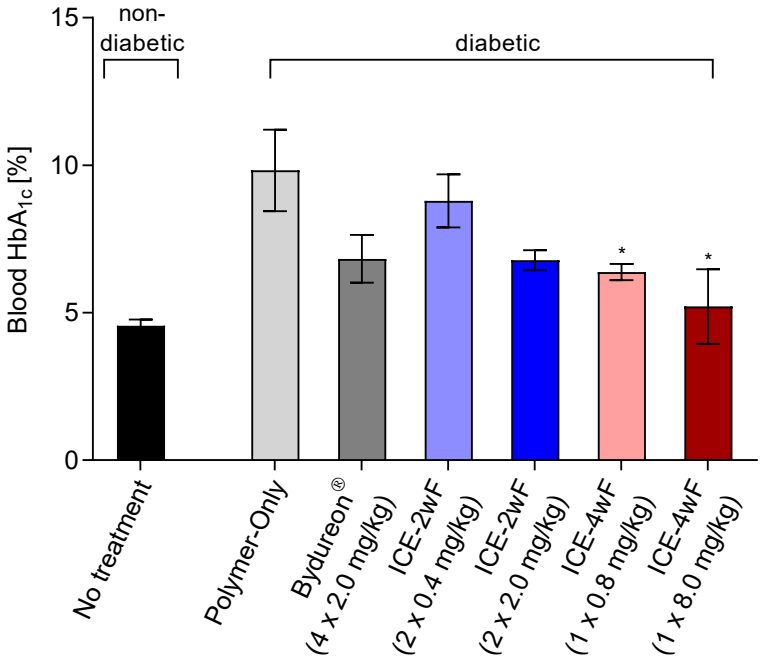

*Figure 26: Percentage of blood HbA_{1c} in non-diabetic and diabetic SDa rats after therapy with P-O microspheres (n = 11), Bydureon® (4 x 2.0 mg/kg, n = 6), low-dosed ICE-2wF (2 x 0.4 mg/kg, n = 8), medium-dosed ICE-2wF (2 x 2.0 mg/kg, n = 4), low-dosed ICE-4wF (1 x 0.8 mg/kg, n = 4) and high-dosed ICE-4wF (1 x 8.0 mg/kg, n = 3) 45 days after the initial treatment. Non-diabetic animals without therapy served as reference (n = 36). Mean values are shown ± SE. Significant differences between the P-O group and groups treated with exenatide-containing formulations are illustrated by * (p<0.05).*

3.5. Summary and discussion

Exenatide was used as model biotherapeutic to demonstrate the suitability of the SynBiosys® platform for the controlled release of a sensitive peptide drug. Together with InnoCore Pharmaceuticals, exenatide-microparticle formulations with target release durations of two (ICE-2wF) and four weeks (ICE-4wF) were developed. Intensive *in vitro* and *in vivo* performance analysis of these formulations were part of this work.

Release duration between ICE-2wF and ICE-4wF was tuned by variation of UltraTurrax configuration and duration of mixing during preparation of the primary emulsion in particle manufacturing. Variating compositions of the multi-block copolymers pose additional opportunities to further fine-tune release behavior, hydrophilicity, rigidity, permeability and degradation characteristics [134].

Bydureon® as prominent PLGA-based microparticle formulation of exenatide was used for analytical method validation and as reference formulation. The release pattern of Bydureon®

is well-known being characterized by an initial lag phase and a subsequent bulk release resulting from hydration and erosion of the polymer matrix [209-211]. This could be reproduced *in vitro* confirming a suitable experimental setup.

Microparticle formulations ICE-2wF (49.2 ± 14.2 µm) and ICE-4wF (49.0 ± 12.1 µm) were both homogenously distributed in size and encapsulation efficiencies were high varying between 84.8-86.2% resulting in exenatide particle loading of 5.5-5.6%. Most exenatide was liberated from ICE-2wF within the first 20 days *in vitro* while the release from ICE-4wF was prolonged to approximately 35 days. Release from both formulations was continuous to a great extent. Burst release within the initial 24 hours was slightly lower with ICE-4wF (8.9%) compared to ICE-2wF (15.2%) which was as expected with respect to the target release durations of the formulations. No lag phase was observed and exenatide was released with a higher integrity (69.3-80.5% monomer content) compared to Bydureon® (65.0% monomer content) based on HPLC analysis.

In the past, multiple groups started attempts on developing microparticle-based extended release formulations of exenatide to overcome common weaknesses of Bydureon®. However, achieving relevant improvements is challenging; Shi et al. for example ended up with release profiles resembling the unfavorable liberation pattern of Bydureon® [212] while microparticles of Liu et al. could not overcome the therapeutic efficacy of Byetta® [213]. Further attempts to prolong the circulation time of exenatide include the induction of structural changes like PEGylation [214] or amino acid exchange [215]. Although promising, inducing chemical changes in APIs raises safety and regulatory questions.

The functionality of exenatide released from Bydureon® and SynBiosys® formulations was determined with a cell-based functional assay which has been described by Golla and Seethala in 2002 [216]. Results confirmed the high functionality of exenatide that was released from ICE-2wF (>85% functional peptide) and ICE-4wF (>80% functional peptide) consistent with HPLC findings. Analysis of Bydureon® IVR samples was more variable with decreased values of functionality at later time points indicating lowered exenatide stability. However, these results require confirmation by further repetitions as Bydureon® analysis was variable and number of replicates should be increased to strengthen statistical interpretation. Nevertheless, these results indicated a higher *in vitro* stability of exenatide released from SynBiosys® microparticle compared to Bydureon®.

Acidic microclimate as consequence of accumulated PLGA degradation products inside particles as well as protein adsorption to polymer surfaces are factors potentially impairing the stability of exenatide liberated from Bydureon® [120, 126, 217]. Especially results on lowered exenatide functionality at later time points indicate beginning polymer hydrolysis and consequently peptide degradation due to pH drop inside PLGA microparticles. In contrast to

that, hydrophilic polyethylene glycol (PEG) is part of the polymer composition of ICE-2wF and ICE-4wF formulations allowing a higher degree of water influx, which in turn leads to a more continuous diffusion-controlled release behavior and a less pronounced pH drop inside the microspheres [135, 217]. Consequently, the microclimate in particles becomes more protein-friendly leading to a higher percentage of intact peptide released [136, 217, 218]. Hence, advantageous aspects of IVR behavior of ICE-2wF and ICE-4wF in comparison with Bydureon® can potentially be explained by positive impacts of the inclusion of PEG in the polymer matrix.

IVR of Bydureon® showed poor reproducibility compared to SynBiosys® based formulations as demonstrated by clearly higher standard deviations. As Bydureon® microparticles are manufactured with a W/O/O coacervation process resulting PLGA microspheres exhibit a polydisperse particle size distribution which can cause a highly variable release behavior. On the contrary, a W/O/W membrane emulsification process as used during manufacturing of exenatide-loaded SynBiosys® formulations leads to a narrow size distribution with beneficial IVR reproducibility representing a further advantage over the benchmark Bydureon®.

The immunogenic potential of ICE-2wF, ICE-4wF (Exenatide dose: 4.0 mg/kg, respectively) and SynBiosys® polymer-only microparticles (equivalent amount of particles to exenatide containing formulations) was compared to Bydureon® (Exenatide dose: 2.0 mg/kg) by single subcutaneous administration. A panel of 27 different cytokines was monitored quantitatively over 48 hours after injections and significantly elevated levels of EGF were observed as reaction to ICE-4wF, polymer-only microparticles and Bydureon®. EGF is secreted by local inflammatory cells and especially macrophages in association with wound healing enhancing keratinocyte and fibroblast motility and proliferation [219, 220]. These findings were consistent with hematoxylin & eosin stains of the injection area where macrophages were present at the injection site together with eosinophilic granulocytes and multinucleated giant cells. Immune reactions were locally limited to the area of administration. However, no clear differences between SynBiosys®-based microparticles and Bydureon® were observed, and moreover immune responses were limited to an expectable degree representing a typical foreign body reaction following a subcutaneous injection.

Exenatide doses of 0.4 (ICE-2wF), 0.8 (ICE-4wF), 2.0 (ICE-2wF, Bydureon®), 4.0 (ICE-2wF, ICE-4wF) and 8.0 mg/kg (ICE-4wF) were administered in pharmacokinetic studies. Plasma exenatide concentrations were measured and the inconsistent *in vitro* performance of Bydureon® was reproduced *in vivo* resulting in an initial peak followed by a lag phase and the main bulk release after 20-40 days. These results confirmed the experimental setup and were comparable to patent data and literature [160, 211]. No lag phase was observed after administration of ICE-2wF and ICE-4wF formulations in contrast to these findings.

A beneficial property of formulation candidates are linear pharmacokinetics facilitating dosing and dose adjustments [221]. A strict dose dependency of exenatide plasma levels was found after administration of ICE-2wF and ICE-4wF formulations as favorable characteristic. On the contrary, Bydureon® did not exhibit dose proportional exenatide plasma concentrations after administration of different doses as stated earlier by different groups [209, 211]. Furthermore, calculation of relative bioavailability revealed lower values of 13.9-19.4% (ICE-2wF) and 20.2-25.0% (ICE-4wF) compared to 32.0% for Bydureon®. The bioavailability of subcutaneously administered drug products is influenced by different factors such as viscosity, tonicity, pH or excipients [222-224]. Improvements in bioavailability of exenatide-based SynBiosys® formulations could be realized by integration of additional excipients and additives to the microparticle formulations [120, 225].

In preparation for pharmacodynamic studies, a type 2 diabetes mellitus SDa rat model was implemented. Three treatment protocols produced differently stable disease patterns. The high fat diet (HFD) / streptozotocin (STZ) approach is an experimentally-induced model of type 2 diabetes mellitus. In a first step, hyperinsulinemia, insulin resistance and/or glucose intolerance are induced by HFD over weeks to months depending on the protocol followed by STZ treatment leading to a severe reduction of pancreatic β-cell mass [194, 195]. Protocol 1 was excluded at an early stage as two out of three animals returned to regular NFBG levels after 9 days. Decision for protocol 2 as method of choice for generation of diabetic animals was based on results of NFBG measurements following single exenatide treatment. Protocols 2 and 3 effectively induced sufficiently elevated NFBG levels over 7 weeks. However, exenatide treatment was obviously more efficient in animals prepared according to protocol 2 as NFBG levels of these animals were clearly affected by the therapy while the effect in protocol 3 animals was limited. According to literature, at least 80% of animals treated with similar protocols develop diabetes including morbidity and inherent variability [197].

As already indicated in section 3.4.4, pharmacodynamic studies were influenced by unforeseeably high morbidity of animals after administration of exenatide-containing formulations. Literature research revealed few occasional cases of unexpectedly elevated blood glucose levels after administration of GLP-1 receptor agonists to rats [226, 227] potentially induced by central nervous system-based GLP-1 receptors mediating glucose tolerance [228, 229]. Others referred to that effect as species and medication-specific individual phenomenon requiring further research [230, 231]. However, unexpected side effects were observed in all groups treated with exenatide-containing formulations (including Bydureon®) indicating no contribution of the respective polymer matrix to the effect. Consequently, pharmacodynamic study results were focused on treatment groups with at least three unaffected animals to guarantee statistically reliable results.

Dosing of SynBiosys® microparticle formulations in pharmacodynamic experiments was based on the benchmark Bydureon®. Highest ICE-2wF and ICE-4wF total doses were equivalent to Bydureon® total exenatide doses. Diabetic SDa rats were treated once-weekly with Bydureon® (4 x 2.0 mg/kg), biweekly with ICE-2wF (2 x 0.4 / 2.0 mg/kg) or once-monthly with ICE-4wF (1 x 0.8 / 8.0 mg/kg) and polymer-only microparticles (no exenatide) over 4 weeks. Changes in NFBG were monitored over 6 weeks. However, measurements of NFBG are easily affected by spontaneous daily variabilities, and consequently the proportion of HbA_{1c} of total hemoglobin was analyzed additionally. As depicted earlier, the percentage of HbA_{1c} represents the average blood glucose level over the past 120 days and is less error prone than NFBG measurements [200-202, 232, 233].

NFBG values remained stable over six weeks in animals treated with polymer-only microparticles serving as reference for groups with various exenatide therapies. Bydureon® treatment led to punctually reduced NFBG levels after the initial three injections and values were relatively constantly lowered about 25% until the end of the experiment after the fourth administration. These findings were consistent with *in vitro* release behavior and pharmacokinetic analyses presented herein as well as patent data [160]. Significant NFBG reductions after Bydureon® therapy were expected about 20 days after the first treatment representing the period of the first exenatide bulk release. The percentage of HbA_{1c} was reduced by approximately 3% in Bydureon® treated animals supporting NFBG results. These insights confirmed the suitability of the type 2 diabetes mellitus animal model and the experimental setup of the pharmacodynamic studies.

ICE-2wF therapy resulted in punctually lowered NFBG levels especially 24 hours after respective treatments reflecting the relatively short *in vivo* release duration and demonstrating release of functionally intact exenatide from SynBiosys® microparticles. However, with respect to HbA_{1c} results the efficacy of ICE-2wF (2 x 2.0 mg/kg) was highly comparable to Bydureon® (4 x 2.0 mg/kg) although the total amount of exenatide administered was considerably reduced by 50%.

Furthermore, also the therapeutic efficacy of ICE-4wF showed improvements after single treatment with an equal total exenatide dose (1 x 8.0 mg/kg) compared to Bydureon® (4 x 2.0 mg/kg). A significant reduction of NFBG was observed during the initial eight days after administration and values remained lowered until day 41. During HbA_{1c} measurements, a reduction about 4.6% was observed after ICE-4wF (1 x 8.0 mg/kg) therapy. Surprisingly, also much lower dosed ICE-4wF (1 x 0.8 mg/kg) resulted in comparable NFBG reductions accompanied by HbA1c decrease of 3.4%.

Remarkably, pharmacodynamic efficacy of Bydureon®, ICE-2wF (2 x 2.0 mg/kg) and ICE-4wF was highly comparable in the time frame observed. Exenatide dose reductions of 50 (ICE-2wF)

to 90% (ICE-4wF) were achieved by usage of SynBiosys® formulations demonstrating advantages of the more constant release compared to the biphasic Bydureon® release pattern. Drastically reduced number of treatments from four (Bydureon®) to one (ICE-4wF) or two (ICE-2wF) as well as a dramatic acceleration in onset of effect represented further benefits of the polymer platform.

4. Evaluation of a suitable SynBiosys® polymer composition for controlled release of a monoclonal antibody based on the model protein mAbB

4.1. Objective

The aim of this work was the evaluation of the SynBiosys® polymer platform for sustained release of biologicals. After performance analysis of peptide-loaded microparticles in the previous chapter, various polymer ratios were tested in the following section to identify a suitable composition to release the monoclonal model antibody mAbB in an intact form.

The monoclonal model antibody B is a protein of 144.9 kDa which is directed against *S*ty1/Spc1-*in*teracting protein1 (Sin1), an essential part of the mammalian target of rapamycin (mTOR) complex 2. Dysregulation of this complex is a key feature of various diseases which demonstrates the crucial role of mTOR complex 2 as drug target [168-170].

A total number of six multi-block copolymer combinations composed of poly(ε-caprolactone)-PEG- poly(ε-caprolactone) (PCL-PEG-PCL) and poly(L-lactide) prepolymers with varying hydrophilicity was used to encapsulate mAbB and *in vitro* performances of the microparticle formulations were examined. The release behavior was monitored over 28 days and integrity of released antibody was analyzed utilizing size exclusion high performance liquid chromatography (SE-HPLC) as well as circular dichroism and fluorescence spectroscopy.

Methods for analysis of mAbB secondary (circular dichroism spectroscopy) and tertiary structure (fluorescence spectroscopy) integrity were implemented to support findings from aggregation and fragmentation analysis by SE-HPLC.

The integrity of mAbB was evaluated after controlled release from differently composed SynBiosys® polymer matrices and a suitable polymer composition with respect to a reasonable release duration in combination with high protein compatibility was determined as objective of this chapter. Thereby, also the variability of the polymer platform was observed.

4.2. Particle manufacturing and final formulations

SynBiosys® microparticles loaded with mAbB were manufactured with a water-in-oil-in-oil (W/O/O) double emulsion process by InnoCore Pharmaceuticals. A highly concentrated mAbB solution with a protein concentration of 221.4 mg/mL was added to a 10 wt.% polymer solution with an oil to water (O/W) ratio of 9.5 creating the primary emulsion by Ultra Turrax treatment (T25, 12k rpm). The secondary emulsion was prepared by addition of the primary emulsion to silicone oil and embryonic microparticles were hardened by transferring the secondary emulsion to a large volume of heptane. Six different multi-block copolymer compositions were utilized to demonstrate the versatility of the SynBiosys® platform *in vitro* as illustrated in Table 15. Multi-block copolymers were composed of various ratios of polymer 50CP30C40-LL40 and polymer 50CP10C20-LL40. Polymer 50CP30C40-LL40 consisted of 50 wt.% of a hydrophilic poly(ε-caprolactone)-PEG_{3000}-poly(ε-caprolactone) (PCL-PEG_{3000}-PCL) block with a molecular weight of 4000 g/mol and 50 wt.% of a hydrophobic poly(L-lactide) block with a molecular weight of 4000 g/mol. Polymer 50CP10C20-LL40 was composed of 50 wt.% of a hydrophilic poly(ε-caprolactone)-PEG_{1000}-poly(ε-caprolactone) (PCL-PEG_{1000}-PCL) block with a molecular weight of 2000 g/mol and 50 wt.% of a hydrophobic poly(L-lactide) block with a molecular weight of 4000 g/mol. The total PEG content of the multi-block copolymers of formulations SR19-002.A-F was tuned between 37.50 and 28.13 wt.% by variation of the ratio between polymers 50CP30C40-LL40 and 50CP10C20-LL40.

Table 15: Polymer composition and total PEG content of mAbB-loaded microparticles.

Formulation	Composition of polymer matrix					
	Polymer 1		Polymer 2		PEG	
	Grade	wt.%	Grade	wt.%	g/mol	wt.%
SR19-002.A	50CP30C40-LL40	100	50CP10C20-LL40	0	3000 (100%)	37.50
SR19-002.B		90		10	3000 (90%) 1000 (10%)	36.25
SR19-002.C		80		20	3000 (80%) 1000 (20%)	35.00
SR19-002.D		70		30	3000 (70%) 1000 (30%)	33.75
SR19-002.E		50		50	3000 (50%) 1000 (50%)	31.25
SR19-002.F		25		75	3000 (25%) 1000 (75%)	28.13

Table 16 shows particle size distribution, protein loading as well as encapsulation efficiency of the six microparticle formulations of mAbB. Particle size distributions were relatively broad with high size variations and mean particle sizes between 48.0 and 88.9 µm. However, the antibody was encapsulated with a high efficiency of 91.0% or more in all formulations while mAbB loading was constant between 17.5 and 18.4 wt.%.

Table 16: Characteristics of mAbB-loaded SynBiosys® microparticles. Particle size as well as mAbB loading and encapsulation efficiency are presented.

	Particle size [µm]	mAbB load [wt.%]	mAbB encapsulation efficiency [%]
SR19-002.A	68.5 ± 43.2	18.0	93.7
SR19-002.B	62.0 ± 37.2	17.5	91.0
SR19-002.C	88.9 ± 63.1	18.4	95.8
SR19-002.D	67.1 ± 51.7	17.7	92.1
SR19-002.E	57.7 ± 34.0	18.1	94.5
SR19-002.F	48.0 ± 30.2	17.8	92.5

Additionally, particles were observed in scanning electron microscopy (SEM) and the particle surface morphology was evaluated (Figure 27A-F). Surface morphology was generally smooth while particles were distributed heterogeneously.

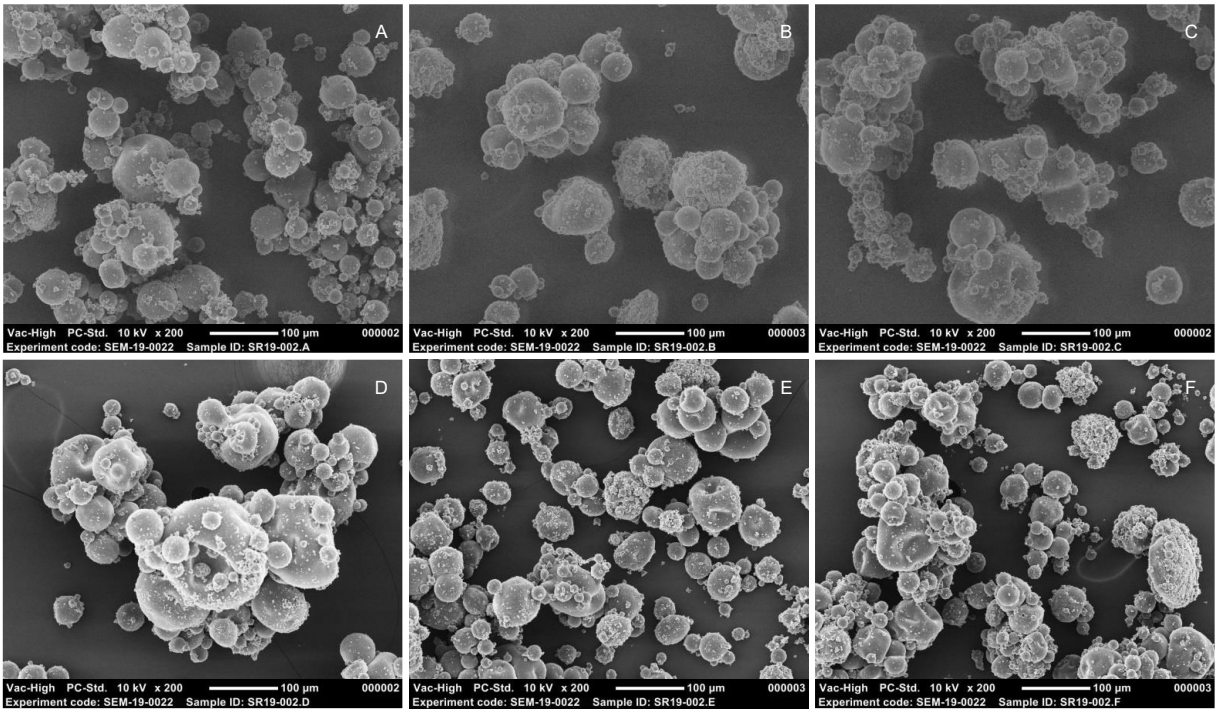

Figure 27: SEM images of mAbB-loaded microparticles formulated with different polymer compositions. Images of SR19-002.A (A), SR19-002.B (B), SR19-002.C (C), SR19-002.D (D), SR19-002.E (E) and SR19-002.F (F) are depicted.

4.3. *In vitro* results

Implementation of circular dichroism and fluorescence spectroscopy methods for analysis of *in vitro* released mAbB from SynBiosys® microparticles is described in the following section. Furthermore, *in vitro* release results and analysis of liberated protein are presented.

4.3.1. Method implementation

Circular dichroism spectroscopy

The secondary structure of mAbB was observed with circular dichroism (CD) spectra to evaluate the structural stability in IVR samples. As explained in section 2.8.6, the predominant secondary structure elements in monoclonal antibodies of the IgG1 family are β-sheets characteristically resulting in a signature peak at 218 nm [177-183]. Consequently, signal intensity at 218 nm was monitored as key parameter.

For determination of the detection limit, mAbB was serially diluted in customized IVR buffer and spectra were evaluated concerning saturation effects or signal noise influences. Recorded spectra are depicted in Figure 28. A selection of spectra is presented to simplify differentiation between curves. Noisy signals were obtained during measurements of test solutions with mAbB concentrations of 15.5 and 31.3 µg/mL indicating protein concentrations below the detection limit. A solution with 62.5 µg mAb/mL was determined as lower detection limit as no signal interferences were observed. Saturation effects resulting in variable signals below

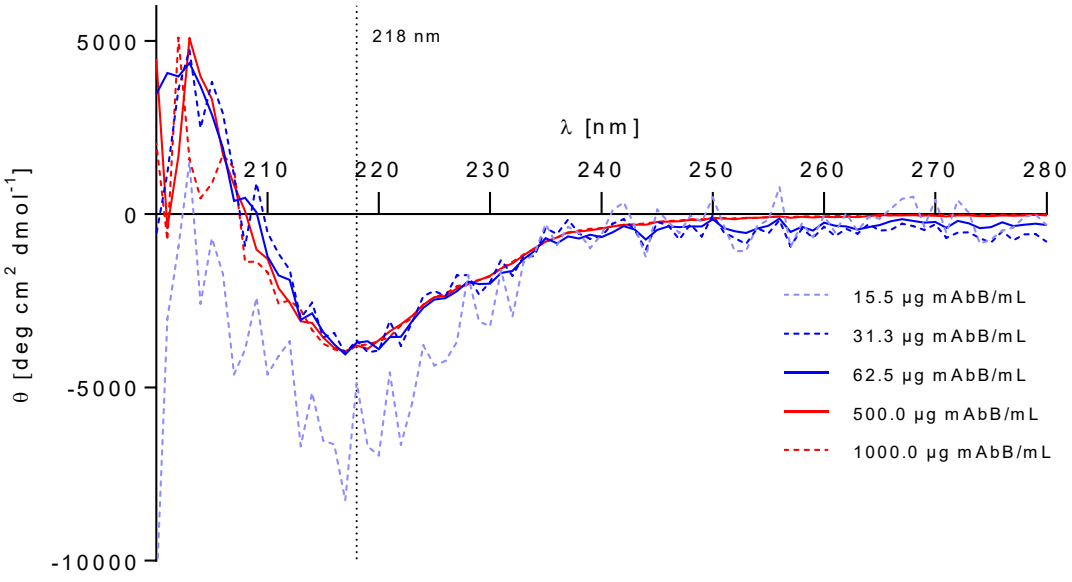

Figure 28: Determination of mAbB detection limits in CD spectroscopy. Spectra were recorded from 200 to 280 nm and solutions outside detection limits are marked by dashed lines. Concentrations of mAbB between 62.5 and 500.0 µg/mL were indicative for samples within detection limits represented by solid lines. The dotted line marks the characteristic signal of IgG1 β-sheets at 218 nm.

210 nm were detected with a 1 mg/mL solution, and hence 500 µg mAbB/mL was defined as upper detection limit. Accordingly, mAbB CD analyses were only performed with samples within the detection range while solutions with lower concentrations were excluded from analysis and higher concentrated samples were diluted appropriately.

Reference samples of mAbB were denatured thermally or chemically by treatment with increasing concentrations of guanidine hydrochloride (GdnHCl) to determine the signal range at 218 nm between native and completely unfolded antibody (Figure 29). A selection of measuring conditions is shown, respectively, to enhance clarity. The condition of *in vitro* released antibody was subsequently evaluated on the basis of the signal shift at 218 nm. While thermal denaturation led to a change in ellipticity signal from - 4751 to – 1640 deg cm² dmol^{-1}, after chemical denaturation the signal difference was smaller and the peak was shifted to smaller wavelengths and influenced by interferences. Consequently, calculation of the Fraction Folded of IVR samples was based on the signal range after thermal denaturation.

Ultimately, the influence of the dialysis procedure on mAbB integrity was determined. As no effects were observed, results are not shown herein.

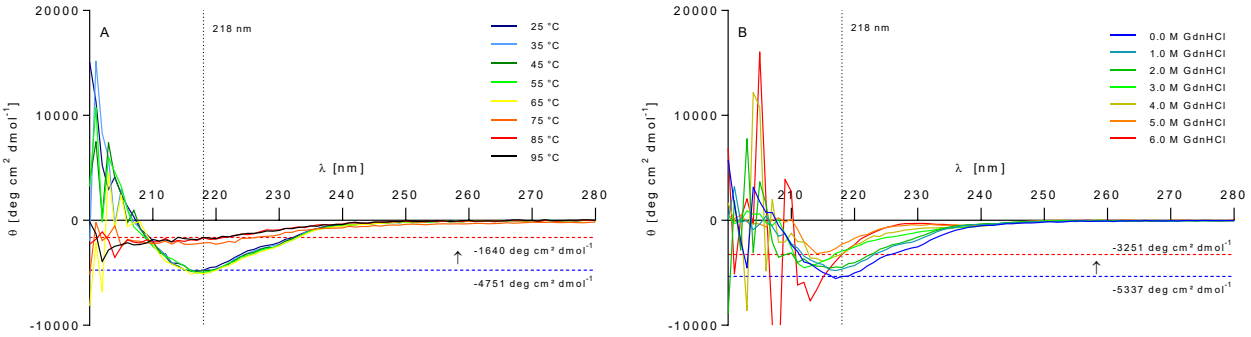

Figure 29: Thermal (A) and chemical (B) denaturation of mAbB observed by CD spectroscopy. Spectra were recorded between 200 and 280 nm. Ellipticity of native (dashed blue lines) and completely denatured (dashed red lines) mAbB indicate the signal range at 218 nm. Thermal denaturation resulted in a larger signal shift enabling a higher sensitivity and subsequent calculations of the Fraction Folded of IVR samples were based on results obtained with thermally denatured mAbB. Chemical denaturation was obtained by treatment with increasing concentrations of guanidine hydrochloride (GdnHCl). The dotted line illustrates the characteristic signal of IgG1 β-sheets at 218 nm.

Fluorescence spectroscopy

The tertiary structure of mAbB after *in vitro* release from SynBiosys®-based microparticles was observed with fluorescence spectroscopy. As described in section 2.8.7, especially tryptophan fluorescence depends on the environmental polarity allowing conclusions about the tertiary protein structure and changes thereof [186].

Linear dilution series of mAbB in IVR buffer were prepared and fluorescence spectra were recorded to determine the detection limits for the antibody. Results are shown in Figure 30. Fluorescence intensities were observed at the wavelength of the maximum to determine the upper detection limit at the concentration which resulted in the highest intensity (Figure 30A). As described in section 2.8.7, the protein concentration in fluorescence spectroscopy measurements is limited to a certain maximum due to the inner filter effect causing complete light absorption prior to illumination of the entire cell resulting in lowered fluorescence intensity [187-189]. Hence, the upper detection limit was determined at 2.5 mg mAbB/mL. Higher concentrated samples were diluted accordingly. Normalized spectra of low concentrated mAbB reference solutions were compared to evaluate the lower detection limit (Figure 30B). Spectral shifts and noisy signals were observed with mAbB concentrations of 5 µg/mL or less and the lower detection limit was determined at 10 µg/mL. Samples with concentrations below that limit were excluded from analysis.

Furthermore, reference samples of mAbB were denatured thermally and chemically by increasing concentrations of GdnHCl up to 6 M as shown in Figure 31 to evaluate the range of potential peak shifts between native and unfolded antibody. To enhance clarity of plots, a selection of denaturation conditions is shown. Thermal denaturation resulted in a small peak shift from 342 to 344 nm (Figure 31A, B) while a larger shift from 342 to 355 nm was observed

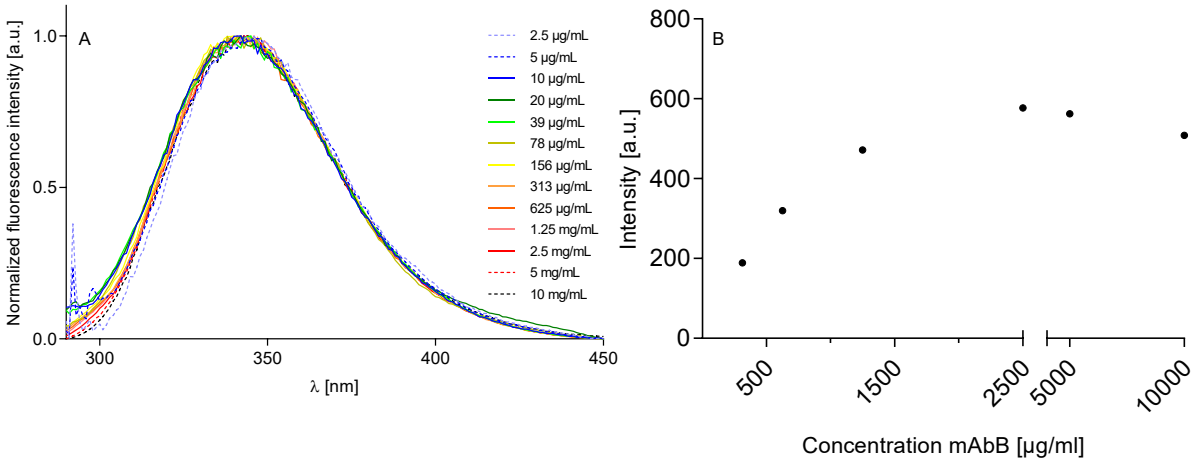

Figure 30: Determination of upper and lower detection limits of mAbB in fluorescence spectroscopy. Normalized spectrum shifts of low concentrated mAbB samples were monitored and the lower detection limit was defined at 10 µg/mL (A). Linear dilution series of mAbB were prepared in IVR buffer and fluorescence intensity values at the maximum wavelength were compared to determine the upper detection limit at 2.5 mg/mL (B). Dashed lines represent reference solutions outside the detection limits.

after chemical denaturation (Figure 31C, D). Therefore, calculation of the Fraction Folded during IVR sample analysis was based on chemical denaturation experiments.

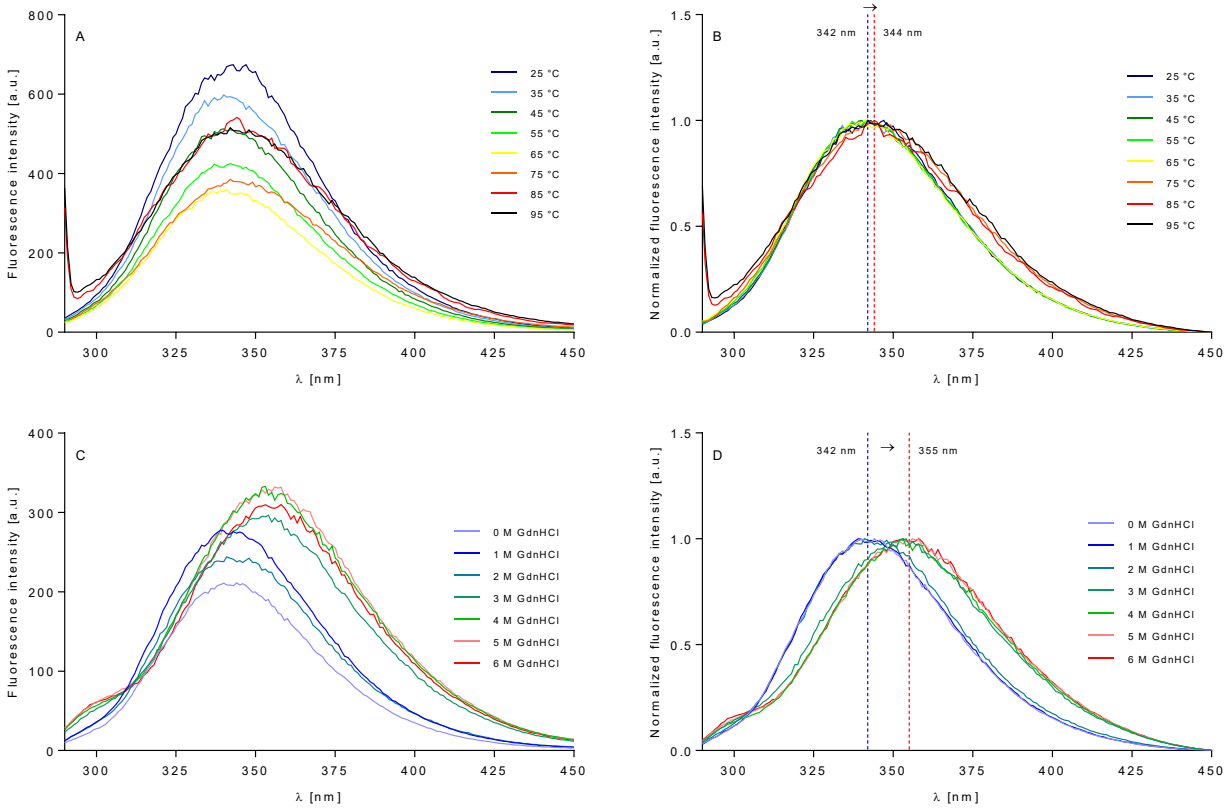

Figure 31: Thermal and chemical denaturation of mAbB reference solutions observed by fluorescence spectroscopy. Fluorescence spectra of thermally (A) and chemically (C) denatured mAbB were normalized and corresponding spectra are presented in B (thermal denaturation) and D (chemical denaturation). The shift of the maximum fluorescence intensity wavelength from native (dashed blue lines) to completely denatured (dashed red lines) is shown.

4.3.2. *In vitro* release and integrity analysis of mAbB

In vitro release behavior and the integrity of released mAbB from differently composed SynBiosys® microparticles was examined to determine a suitable polymer composition for the controlled release of intact antibody.

As illustrated in Table 15, the ratio of polymers 50CP30C40-LL40 and 50CP10C20-LL40 was varied and percentage of PEG in total polymer weight was reduced from 37.50 (SR19-002.A) over 36.25 (SR19-002.B), 35.00 (SR19-002.C), 33.75 (SR19-002.D) and 31.25 (SR19-002.E) to 28.13 wt.% (SR-19.002.F). Thereby, the relation between hydrophilic PEG and hydrophobic poly(L-lactide) or poly(ε-caprolactone) changed resulting in growing hydrophobicity from formulations SR19-002.A to F. Figure 32 presents *in vitro* release behavior of formulations SR19-002.A to C and corresponding integrity analyses of released mAbB. The release duration was prolonged from approximately 10 to 20 days by variation of the polymer

composition and mAbB was liberated consistently with relatively constant integrity considering mAbB monomer content between 87.9 and 90.6% as determined by SEC (Figure 32A, C, E). Secondary and tertiary structure integrity of mAbB were additionally examined as illustrated in Figure 32B, C, F. While tertiary structure remained unaffected with Fraction Folded values around or over 90% for all formulations, secondary structure was impaired slightly at the first

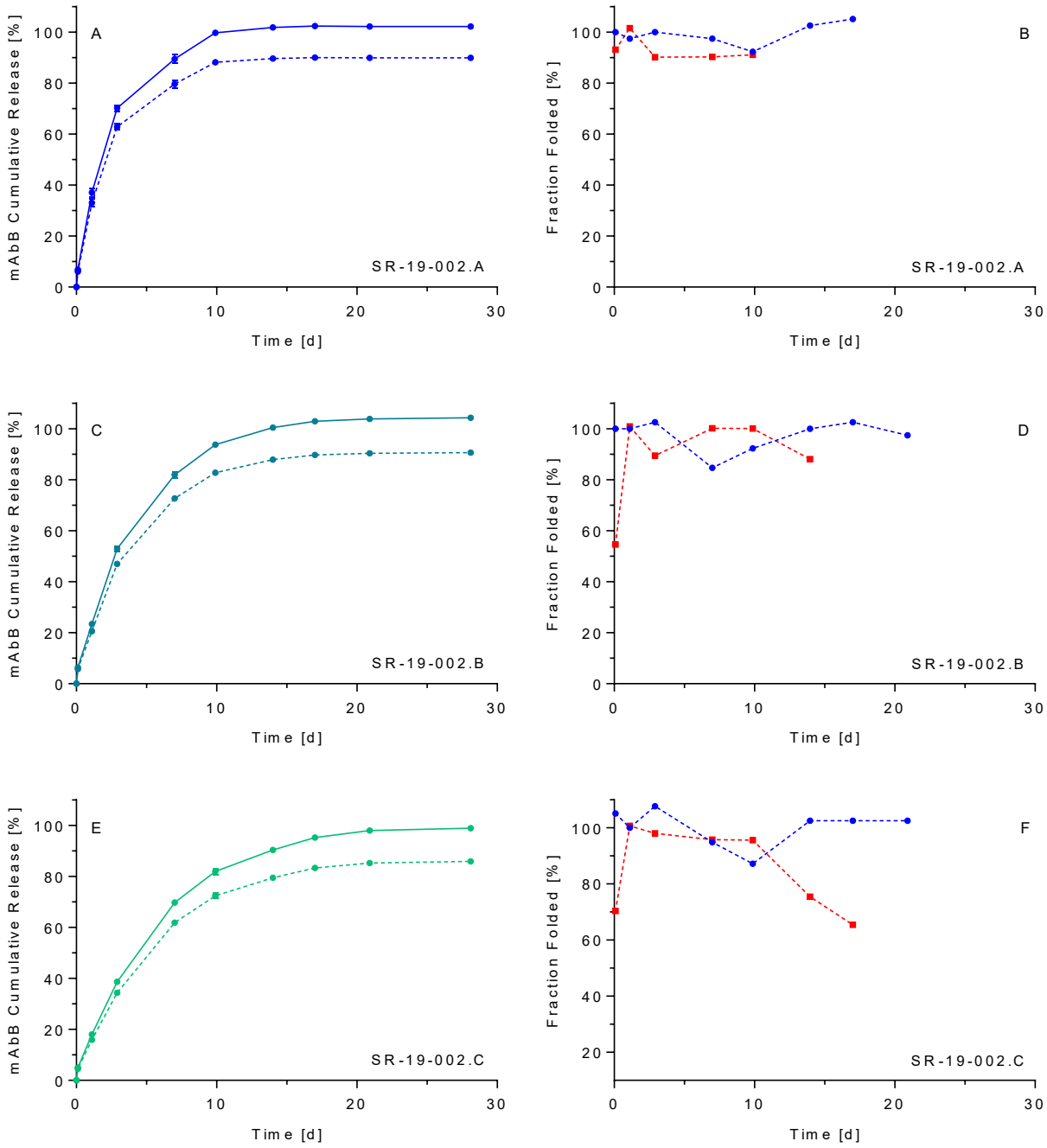

Figure 32: In vitro *release of mAbB and integrity analysis of released antibody I. Release behavior is presented in A (SR19-002.A), C (SR19-002.B) and E (SR19-002.C) while cumulative release of total (solid lines) and intact (dashed lines) protein is shown. Accordingly, circular dichroism (●) and fluorescence spectroscopy (■) Fraction Folded results of released mAbB are shown in B, D and F on the right site of the arrangement. IVR data represent mean values of n = 3 ± SD while circular dichroism and fluorescence spectroscopy data were processed as described in sections 2.8.6 and 2.8.7.*

time point after release from SR19-002.B. As indicated by Figure 32F, secondary structure stability of mAbB was further reduced also at later time points after release from SR19-002.C.

Furthermore, release behavior of SR19-002.D-F is depicted in Figure 33 in combination with secondary and tertiary structure integrity analyses of released mAbB. Compared to the results presented in Figure 32, liberation of mAbB was further decelerated resulting in the longest release duration around 30 days of SR19-002.F (Figure 33A, C, E). Release of mAbB

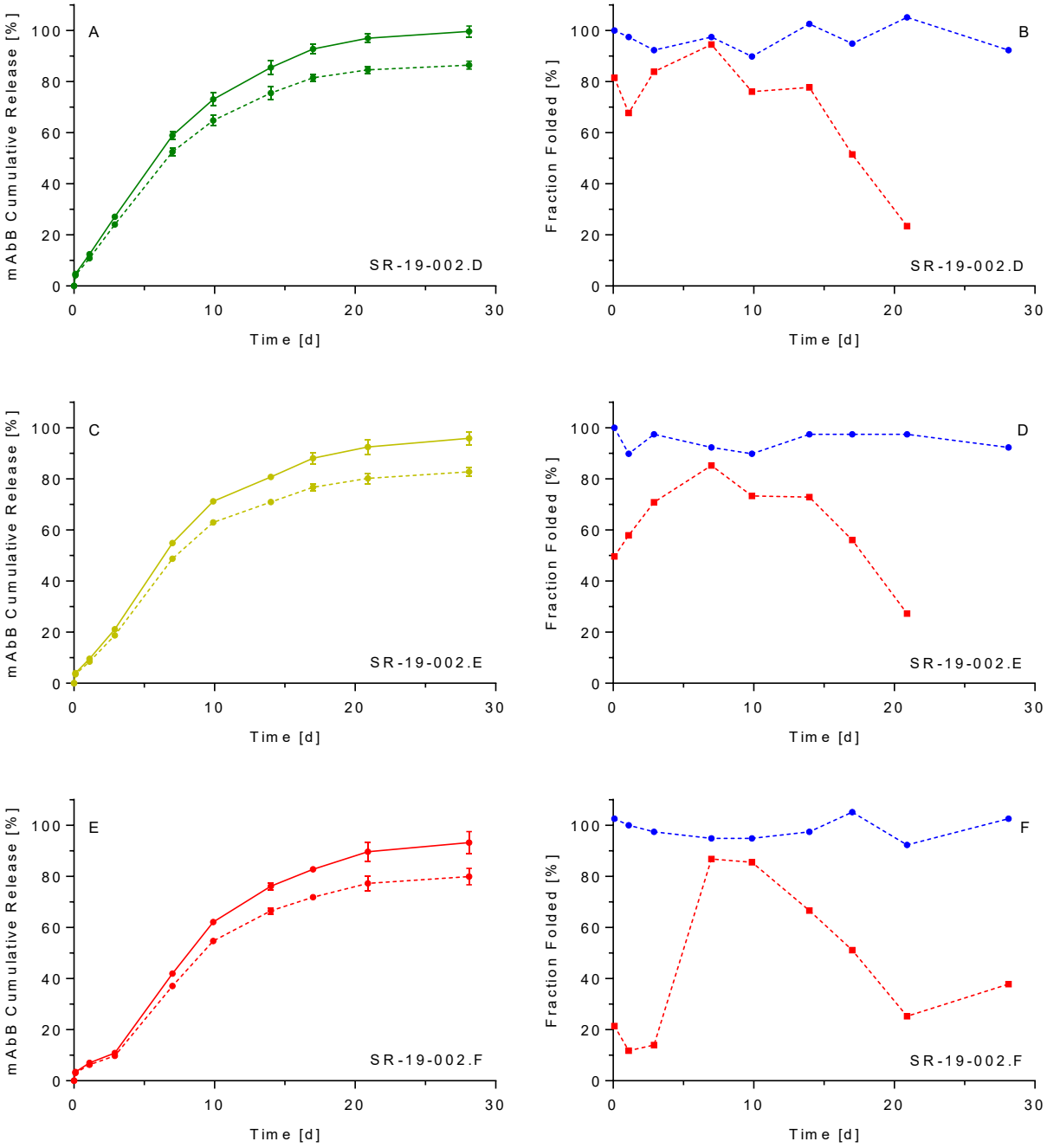

Figure 33: In vitro *release of mAbB and integrity analysis of released antibody II. Release behavior is presented in A (SR19-002.D), C (SR19-002.E) and E (SR19-002.F) while cumulative release of total (solid lines) and intact (dashed lines) protein is shown. Accordingly, circular dichroism (●) and fluorescence spectroscopy (■) Fraction Folded results of released mAbB are shown in B, D and F on the right site of the arrangement. IVR data represent mean values of n = 3 ± SD while circular dichroism and fluorescence spectroscopy data were processed as described in sections 2.8.6 and 2.8.7.*

monomer was again generally lower between 82.7 and 87.4% compared to the amount of total protein. Tertiary structure integrity remained at Fraction Folded values around or over 90% without exception. Simultaneously, secondary structure stability was increasingly impaired. While in Figure 33B (SR19-002.D) secondary structure was maintained around 80% apart from three clearly lower values, results for SR19-002.E and F indicated severe reductions of secondary structure integrity especially at early and late time points. In particular, secondary structure of mAbB was reduced to Fraction Folded values between 10 and 20% until day 3 of IVR after release from SR19-002.F.

4.4. Summary and discussion

The monoclonal model antibody mAbB was encapsulated in SynBiosys® microparticles with various polymer compositions to determine a suitable polymer matrix for the controlled release of a large protein. *In vitro* release behavior was examined to demonstrate the variability of the platform and the integrity of the released antibody was analyzed subsequently.

A W/O/O process was used as fast screening manufacturing process for microparticles. However, while this process is established in a short period of time the control over the particle size is poor resulting broad size distributions. Moreover, the process allowed high mAbB loading around 18 wt.% and encapsulation efficiencies of 91.0% or more which is a common advantage of W/O/O based manufacturing methods [234]. The hydrophobicity of polymer matrices was varied from more hydrophilic SR19-002.A to more hydrophobic SR19-002.F by reduction of the PEG proportion of total multi-block copolymer weight from 37.50 to 28.13 wt.%. *In vitro* release behavior was tuned from a total release duration around 10 days (SR19-002.A) to approximately 30 days (SR19-002.F) while the percentage of intact monomer of total protein released remained relatively constant between 83 and 90% as determined by SE-HPLC. Variation of the PEG content in polymeric controlled release systems is a well-accepted tool to tune release rates and initial burst [234-236]. These data demonstrated the high versatility of the SynBiosys® polymer platform.

In vitro release and aggregation as well as fragmentation of released mAbB was analyzed by SE-HPLC which is the most widely used system for determination of the composition of protein samples [237]. Nevertheless, the use of SEC for determination of protein integrity is limited as aggregates of certain sizes may be filtered out by precolumns, samples are highly diluted for analysis potentially affecting measurements or protein state, and non-specific interactions between protein species and resin materials may occur [238, 239]. Further analytics were required to gain information about structural changes of the model protein. Hence, circular dichroism and fluorescence spectroscopy were established to detect changes in secondary or tertiary

structures of *in vitro* released mAbB by usage of intrinsic tryptophan fluorescence or peptide bond absorption of circularly polarized light [184, 186, 240].

Circular dichroism spectra can be affected by buffer components like phosphate resulting in erroneous measurement artifacts or signal overlap [241]. As IVR buffer sample matrix caused interferences, buffer exchange as well as dialysis procedure influence were evaluated in preparative experiments and no influence on mAbB secondary structure integrity was found. Artifact-free mAbB spectra were collected between the detection limits of 62.5-500 µg/mL in circular dichroism spectroscopy while samples with concentrations between 10 µg/mL and 2.5 mg/mL were measurable in fluorescence spectroscopy.

As part of method development, reference samples of mAbB were denatured and analyzed with circular dichroism as well as fluorescence spectroscopy to determine the signal range between natively folded and unfolded protein, respectively. Among chemical denaturants, urea and guanidine hydrochloride (GdnHCl) are prominent examples leading to most complete unfolding [240, 242]. Herein, GdnHCl was used to denature proteins chemically by formation of hydrogen bonds with the protein backbone and destabilization through electrostatic interaction with charged residues [243, 244]. However, although thermally denatured proteins contain residual secondary structures thermal denaturation represents an alternative if chemical denaturants cause interferences with measuring signals [245]. Therefore, thermal as well as chemical denaturation of mAbB was analyzed with circular dichroism and fluorescence spectroscopy, respectively, to determine the method leading to the largest possible signal shift between native and unfolded protein and minimized measurement interferences.

During preparative experiments for circular dichroism spectroscopy method development, chemical unfolding using GdnHCl led to a spectral shift of the signature peak wavelength as well as signal interferences and the signal range between native and completely unfolded mAbB was small compared to thermal denaturation. This indicated variable stabilities of different secondary structure elements during chemical denaturation. Therefore, calculations of the Fraction Folded of IVR samples analyzed with circular dichroism spectroscopy were based on results obtained by thermal denaturation.

Contrary to this, chemical denaturation was beneficial in fluorescence spectroscopic determination of the tertiary structure as the signal range between native and unfolded protein was large compared to thermal denaturation effects. Consequently, calculations of the Fraction Folded of IVR samples examined with fluorescence spectroscopy were based on the results obtained after chemical denaturation of mAbB.

Analyses of secondary and tertiary structure integrity of *in vitro* released mAbB are presented in this work. Generally, tertiary structure of mAbB appeared to remain intact (Fraction Folded

> 85%) over time after release from all formulations tested. However, impairments of the secondary structure were detected in different formulations. While mAbB released from SR19-002.A remained completely unaffected, secondary structure integrity of mAbB initially liberated during the first hours after experiment start from SR19-002.B was reduced to 55%. Nevertheless, values strongly increased thereafter and remained over 90% for the residual IVR accounting for the bulk amount of total mAbB. This trend continued until secondary structure stability of mAbB released during the first three days of IVR was clearly lowered to 10-20%. Additionally, secondary structure integrity of mAbB released from SR-19-002.C-F after 14 days or later was increasingly impaired.

Interfaces between water and organic solvents typically pose a challenge for proteins being a common destabilizing factor [246-248]. As these interfaces are obviously part of the W/O/O manufacturing process, this could potentially explain loss of secondary structure. Van de Weert and colleagues stated that degraded proteins are likely to be formed during preparation process or storage if the protein fraction released during the first day is partly degraded [248]. However, impairment of the secondary structure stability of mAbB was especially observed after release from formulations SR19-002.C-F while the W/O/O process was utilized for manufacturing of all formulations. Consequently, a combined effect of W/O/O process induced changes in protein structure and influences caused by the polymer composition seems likely. Lactic acid and ε-caprolactone as rather lipophilic polymers add hydrophobicity to the polymer matrix while a higher PEG content influences the encapsulation process and creates hydrophilic domains stabilizing proteins [98, 135-137, 249, 250]. Figure 34 illustrates the PEG-induced stabilization of water droplets during W/O/O microparticle manufacturing. Amphiphilic SynBiosys® polymers are dissolved in the oil phase and PEG chains accumulate at W/O interfaces minimizing interaction of proteins with organic solvent interfaces which contributes to improved protein integrity during particle manufacturing. Therefore, exposure of mAbB to organic solvent interfaces during the W/O/O process and simultaneously fewer stabilizing effects due to lower PEG content in SR19-002.C-F polymer matrices are a potential explanation for lowered secondary structure integrity during the initial part of the release of these formulations.

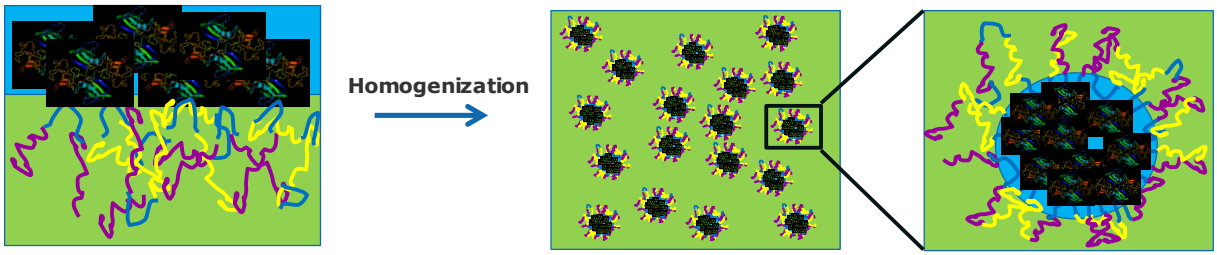

Figure 34: Accumulation of PEG on organic solvent interfaces during microparticle processing. Amphiphilic SynBiosys® polymers are dissolved in dichloromethane (DCM, green) while PEG chains enter and stabilize water droplets which are obtained after homogenization during W/O/O microparticle manufacturing. Proteins dissolved in the water phase or droplets (blue) are shielded from the W/O interface by accumulated PEG chains. This figure was customized and originated from internal cooperation documents.

Additionally, decreased secondary structure stability of *in vitro* released mAbB of certain formulations after two weeks or more is plausible and most likely a result of the increasingly reduced PEG content. As mentioned earlier herein, the integration of hydrophilic PEG chains in polymer-based sustained release systems induces an increased water-influx during *in vitro* release resulting in a swollen polymer matrix allowing a continuous diffusion-controlled release [93, 135, 140]. Furthermore, the enhanced presence of water within microparticles leads to a less pronounced degradation-induced pH drop creating a more protein-friendly microenvironment [136, 218]. Alternative approaches to obtain a less acidic microenvironment inside PLGA microparticles include different studies of Schwendeman et al. who worked on the incorporation of basic additives like magnesium hydroxide and magnesium carbonate which resulted in enhanced protein stability [120, 251, 252]. Encapsulation of pegylated biologicals also resulted in the release of a higher percentage of intact API [253]. Moreover, attempts for stabilization were made using proteins complexed with zinc or co-encapsulation of trehalose or mannitol [254, 255]. Shirangi et al. demonstrated the successful inhibition of the formation of acylated octreotide species after PLGA-based release by introducing self-immolative protective groups [256]. However, the functionality of this technology was only confirmed *in vitro* while its applicability is limited to the protection of peptides in the first instance [256].

Albeit promising, these approaches also increase complexity and additionally bear the risk of inducing protein aggregation by the excipient itself as a result of alkali-induced thiol-disulfide exchange necessitating careful formulation development [257]. Furthermore, especially PEGylation of biotherapeutics or the addition of protective groups can also provoke regulatory challenges.

The objective of the current chapter was the determination of a suitable polymer composition for the sustained release of a monoclonal antibody. Formulation SR19-002.B was chosen with an appropriate polymer composition (36.25 wt.% PEG) combining a reasonable release duration over approximately two weeks with uniform liberation of highly intact mAbB according to secondary and tertiary structure analyses.

5. Controlled release of the monoclonal antibody mAbX by SynBiosys® microparticles

5.1. Objective

The overall aim of this work was the evaluation of the suitability of the SynBiosys® polymer platform for the controlled release of protein therapeutics. After demonstration of promising *in vitro* and *in vivo* performances of SynBiosys®-based peptide formulations in chapter 3, an appropriate polymer composition for the controlled release of a larger biotherapeutic was determined in the previous chapter. Hence, an optimized microparticle formulation of the monoclonal model antibody mAbX (ICX-2wF) was extensively studied *in vitro* and *in vivo* in the following chapter to confirm the compatibility of SynBiosys® with large proteins.

The marketed model antibody mAbX is directed against the epidermal growth factor receptor (EGFR) which is a receptor tyrosine kinase playing a crucial role in the development of several human cancer types by promoting cell proliferation and inhibiting apoptosis [172-174]. The expression of EGFR is typically upregulated in certain forms of cancer and binding of mAbX leads to inhibited cancer cell growth and enhances antibody-mediated recruiting of anti-tumoral immune responses [175].

Based on the results gained in the previous chapter, the SynBiosys®-based microparticle formulation ICX-2wF of mAbX was developed by InnoCore Pharmaceuticals with a target release duration of two weeks. In accordance with the mAbB formulation SR19-002.B, mAbX microparticles were manufactured with a similar process and the same multi-block copolymer composition containing a hydrophilic proportion of 36.25 wt.% PEG. *In vitro* release behavior of ICX-2wF was examined by SE-HPLC, and subsequently, liberated mAbX was analyzed extensively. Circular dichroism and fluorescence spectroscopy methods were introduced to monitor secondary and tertiary structure integrity of mAbX throughout IVR. Additionally, the functionality of mAbX after IVR was investigated intensively with an enzyme-linked immunosorbent assay (ELISA) as well as a cell-based assay. Both assays were established during preparative experiments as part of this work. Hence, the condition of *in vitro* released mAbX was examined extensively utilizing a powerful analytical repertoire.

Moreover, pharmacokinetic and pharmacodynamic performances of the SynBiosys®-based microparticle formulation ICX-2wF were determined. Initially, the immunogenic potential of ICX-2wF was examined in healthy NMRI mice by monitoring of systemic cytokine release and immune responses at injection sites. Furthermore, mAbX plasma levels were observed after administration of mAbX microparticles as well as reference solution in pharmacokinetic studies using healthy NMRI mice. The relative tumor growth of A-431 xenografts in immunodeficient

NMRI nu/nu mice was observed in a pharmacodynamic study. Plasma levels of mAbX in tumor-bearing animals were determined additionally.

5.2. Particle manufacturing and final product

SynBiosys®-based microparticles loaded with mAbX were developed and manufactured by InnoCore Pharmaceuticals. Similar to mAbB microparticles, microspheres loaded with mAbX were manufactured using a water-in-oil-in-oil (W/O/O) double emulsion process. A highly concentrated mAbX solution (225.5 mg mAbX per mL) was added to a 10 wt.% polymer solution with an oil to water (O/W) ratio of 9.5 forming the primary emulsion by Ultra Turrax treatment (T25, 12k rpm). The secondary emulsion was prepared by addition of the primary emulsion to silicone oil and embryonic microparticles were hardened by transferring the secondary emulsion to a large volume of heptane. A suitable multi-block copolymer composition for encapsulation of large proteins was determined in the previous chapter. Consequently, a ratio of 90% of polymer 50CP30C40-LL40 and 10% of polymer 50CP10C20-LL40 was used for manufacturing of mAbX-loaded microparticles as shown in Table 17. Polymer 50CP30C40-LL40 consisted of 50 wt.% of a hydrophilic poly(ε-caprolactone)-PEG_{3000}- poly(ε-caprolactone) (PCL-PEG_{3000}-PCL) block with a molecular weight of 4000 g/mol and 50 wt.% of a hydrophobic poly(L-lactide) block with a molecular weight of 4000 g/mol. Polymer 50CP10C20-LL40 was composed of 50 wt.% of a hydrophilic poly(ε-caprolactone)-PEG_{1000}- poly(ε-caprolactone) (PCL-PEG_{1000}-PCL) block with a molecular weight of 2000 g/mol and 50 wt.% of a hydrophobic poly(L-lactide) block with a molecular weight of 4000 g/mol. The total PEG content of the multi-block copolymer of formulation ICX-2wF was 36.25 wt.%. Polymer-only microparticles were manufactured with the same multi-block copolymers and without addition of mAbX-containing aqueous phase.

Table 17: Polymer composition and total PEG content of mAbX-loaded microparticles.

Formulation	Composition of polymer matrix					
	Polymer 1		Polymer 2		PEG	
	Grade	wt.%	Grade	wt.%	g/mol	wt.%
ICX-2wF	50CP30C40-LL40	90	50CP10C20-LL40	10	3000 (90%) 1000 (10%)	36.25

The candidate formulation ICX-2wF was examined in detail as part of this work and is characterized in this section together with a corresponding polymer-only microparticle formulation. As shown in Table 18, particle size distributions were broad and polymer-only microparticles were clearly smaller in average (40.0 µm) compared to mAbX-loaded ICX-2wF particles (84.0 µm). A mAbX loading of 14.9 wt.% was achieved and 80.0% of antibody used were encapsulated successfully.

Table 18: Characteristics of mAbX-loaded SynBiosys® microparticles. Particle size, mAbX loading and encapsulation efficiency are presented.

	Particle size [µm]	mAbX load [wt.%]	mAbX encapsulation efficiency [%]
ICX-2wF	84.0 ± 54.6	14.9	80.0
Polymer-only (w/o mAbX)	40.0 ± 30.8	-	-

Furthermore, particles were observed using scanning electron microscopy (SEM) and the particle surface morphology was evaluated (Figure 35). Surfaces of ICX-2wF (Figure 35A) and polymer-only microparticles (Figure 35B) were smooth without evidence of porous structures and particles were broadly distributed in size.

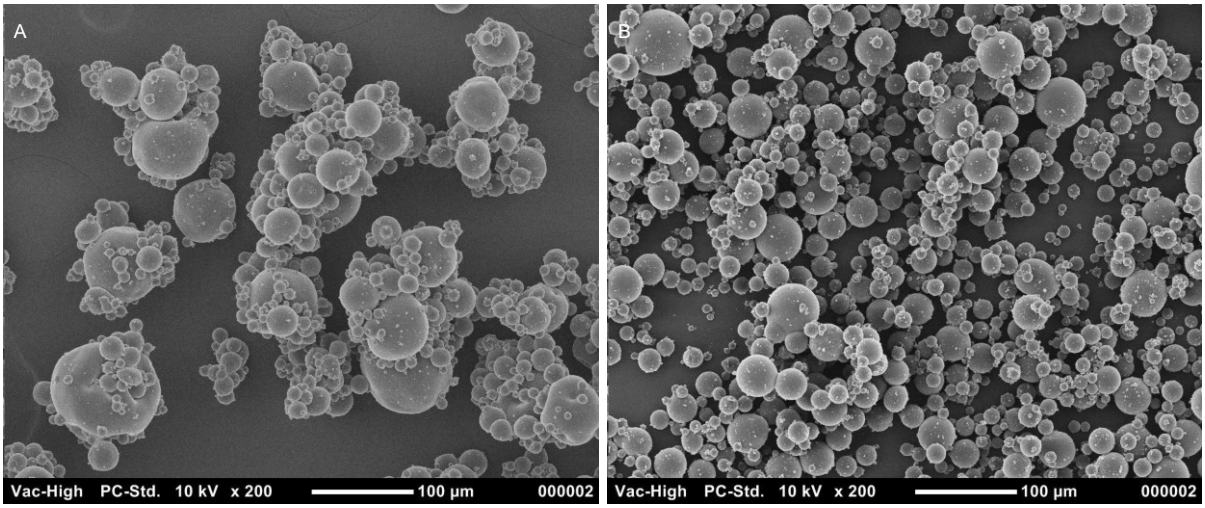

Figure 35: SEM images of ICX-2wF (A) and polymer-only microparticles (B).

5.3. *In vitro* results

In the subsequent section, preparative experiments of *in vitro* analysis methods for mAbX are described as well as *in vitro* release results of ICX-2wF and integrity investigation of released antibody.

5.3.1. Method implementation

Circular dichroism spectroscopy

The secondary structure integrity of *in vitro* released mAbX was monitored with circular dichroism spectroscopy. The dominating secondary structure element of IgG1 antibodies are β-sheets which are measured at a characteristic signature peak at 218 nm, as also explained earlier (section 2.8.6) [177-183]. Hence, the signal intensity at this peak was observed as key parameter.

A reference solution of mAbX was diluted serially to determine the detection limit of the antibody in circular dichroism measurements. Spectra were evaluated with respect to high noise contribution or shift of the signal peak to determine the detection limits. A selection of recorded spectra is presented in Figure 36 to enhance clarity. The upper detection limit was defined at 600 µg/mL representing a concentration covering the majority of IVR sample concentrations at the upper end. No interfering effects were observed with this reference solution. High noise contribution was measured with a 41.3 µg/mL mAbX reference solution

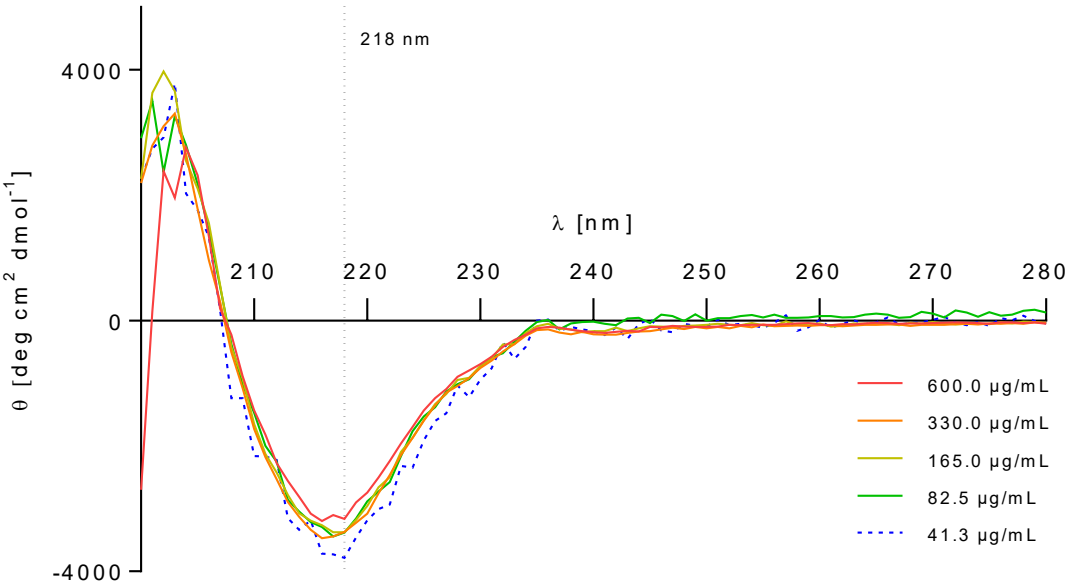

Figure 36: Determination of mAbX detection limits in CD spectroscopy. Spectra were recorded from 200 to 280 nm and concentrations outside of detection limits are marked by dashed lines. Concentrations of mAbX between 82.5 and 600 µg/mL were determined as upper and lower detection limits and spectra of mAbX concentrations within detection limits are represented by solid lines. The dotted line shows the characteristic signal of IgG1 β-sheets at 218 nm.

indicating a concentration below the detection limit. The lower detection limit was determined at 82.5 µg/mL as no impairing effects were observed at this concentration. IVR samples with mAbX concentrations beyond the detection limits were either excluded from analysis (below lower detection limit) or diluted accordingly (over upper detection limit).

Reference samples of mAbX were denatured thermally or chemically using GdnHCl to determine the signal range at 218 nm between native and completely unfolded antibody and resulting spectra are depicted in Figure 37. Results obtained during denaturation experiments served as basis for calculations of the Fraction Folded of subsequently analyzed mAbX IVR samples. A selection of measuring conditions is shown to enhance clarity, respectively. Peak ellipticity at 218 nm was generally shifted during increasing thermal or chemical stress to less negative values. However, the signal shift resulting from chemical denaturation was larger and further calculations during IVR sample analysis were based on the ellipticity range between -2931 (native) and 322 deg cm² dmol^{-1} (completely unfolded).

Furthermore, influence of the dialysis procedure on mAbX secondary structure integrity was determined. No influences were found, and hence no results thereof are presented herein.

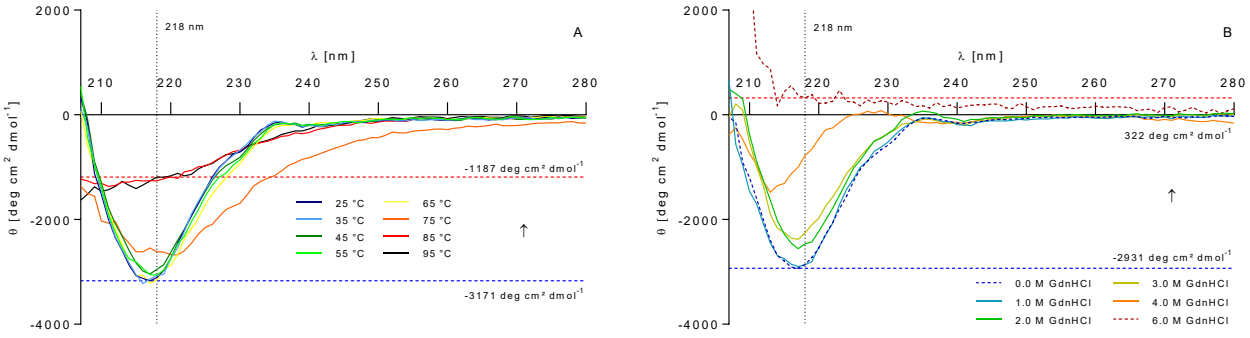

Figure 37: Thermal (A) and chemical (B) denaturation of mAbX observed by CD spectroscopy. Spectra were recorded between 200 and 280 nm. Ellipticity of native (dashed blue lines) and completely unfolded (dashed red lines) mAbX indicate the signal shift at 218 nm. Chemical denaturation resulted in a larger shift and corresponding results were used for calculations of the Fraction Folded after IVR sample analysis. The dotted line shows the characteristic signal of IgG1 β-sheets at 218 nm.

Fluorescence spectroscopy

The tertiary structure integrity of mAbX after *in vitro* release from ICX-2wF SynBiosys®-based microparticles was analyzed with fluorescence spectroscopy. As described earlier, environmental polarity changes of tryptophan residues allowing conclusions about tertiary protein structure were monitored during fluorescence spectroscopy analyses [186].

Detection limits of mAbX were determined by measurement of serially diluted reference solutions. Resulting fluorescence spectra are presented in Figure 38. In Figure 38A, fluorescence intensity values at the peak wavelength measured in mAbX reference solutions of different concentrations are shown. The upper detection limit was determined at a protein concentration of 700 µg/mL resulting in the highest fluorescence intensity. As described in section 2.8.7, the inner filter effect causes complete light absorption prior to illumination of the complete measuring cell resulting in decreased fluorescence intensity of mAbX concentrations exceeding 700 µg/mL [187-189]. Higher concentrated samples were diluted accordingly. Furthermore, normalized fluorescence spectra of serially diluted mAbX reference solution in a low concentration range were compared to determine the lower detection limit (Figure 38B). Antibody concentrations between 0.8 and 3.1 µg/mL resulted in spectral shifts, and consequently, the lower detection limit was determined at 6.3 µg/mL. IVR samples with concentrations below that limit were excluded from analysis.

The wavelength shifts of fluorescence spectra between native and unfolded mAbX after thermal and GdnHCl-induced chemical denaturation was determined as illustrated in Figure 39. A selection of denaturation conditions is shown to enhance clarity in plots, respectively. Thermal denaturation led to a 10 nm peak shift of fluorescence maxima (Figure 39A, B) while

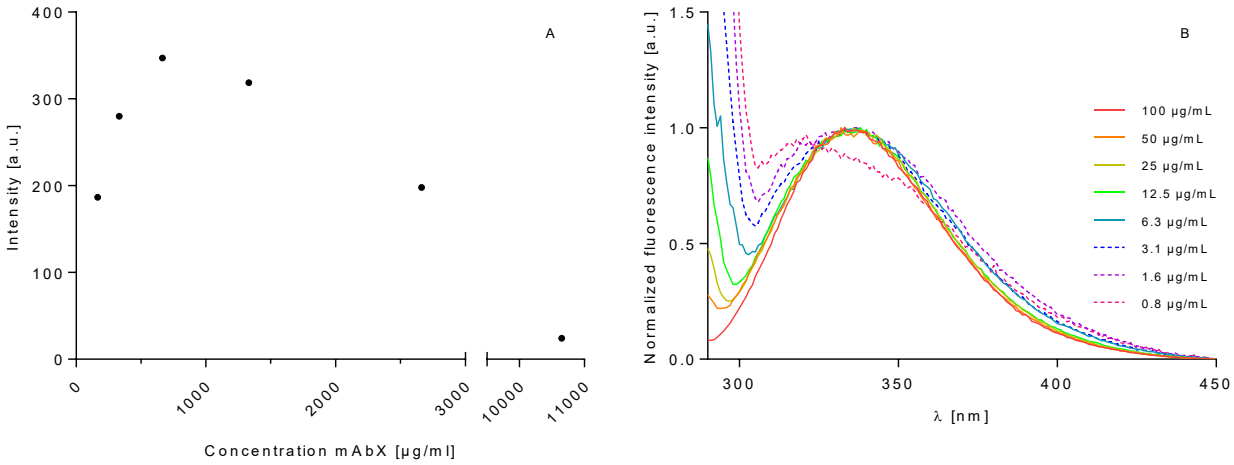

Figure 38: Determination of upper and lower detection limits of mAbX in fluorescence spectroscopy. Serial dilutions of mAbX were prepared in IVR buffer and fluorescence intensities at the maximum wavelength were compared to determine the upper detection limit at 700 µg/mL (A). Shifts of normalized spectra of low concentrated mAbX reference solutions were compared and the lower detection limit was determined at 6.3 µg/mL (B). Dashed lines represent reference solutions with mAbX concentrations below the detection limit.

fluorescence spectra were shifted from 335 to 354 nm as a result of chemical denaturation (Figure 39C, D). Consequently, calculation of the Fraction Folded after IVR sample analysis was based on results obtained by chemical denaturation.

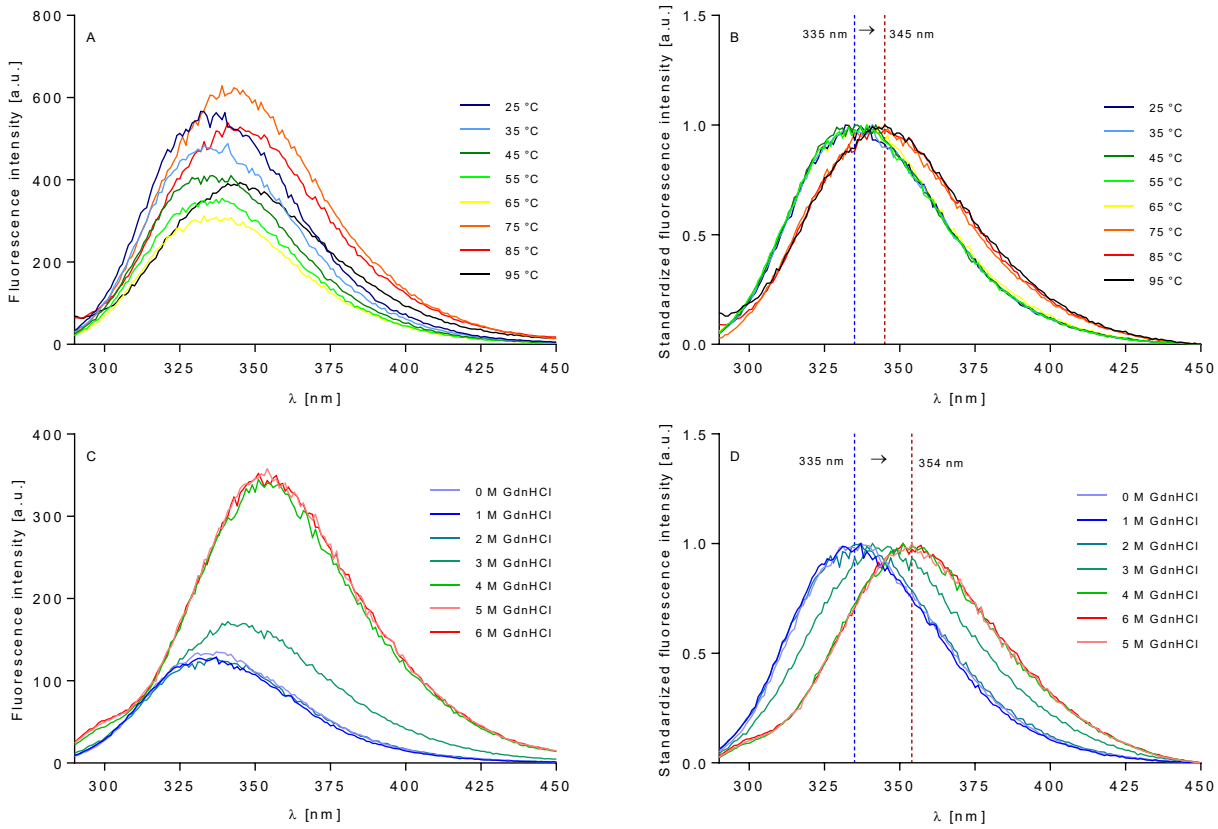

Figure 39: Thermal and chemical denaturation of mAbX reference solutions monitored by fluorescence spectroscopy. Fluorescence spectra obtained after thermal (A) and chemical (C) denaturation were normalized and corresponding spectra are shown in B (thermal denaturation) and D (chemical denaturation). Wavelength shifts of fluorescence maxima from native (dashed blue line) and completely unfolded (dashed red line) are marked.

Enzyme-linked immunosorbent functional assay for mAbX

During *in vitro* and *in vivo* studies, mAbX was quantified utilizing a preexisting functional enzyme-linked immunosorbent assay (ELISA). The compatibility of the assay with mAbX IVR buffer as well as NMRI mouse plasma as sample matrices was evaluated in preparative experiments to ensure unaffected assay performance during later analysis. Standard curves prepared in regular assay buffer, mAbX IVR buffer and NMRI plasma as sample matrix were compared. Results are illustrated in Figure 40. Absorption values generally rose with increasing mAbX concentrations. Curve shapes were highly comparable without occurrence of considerable matrix influences. All standard curves fulfilled the quality requirements described in section 2.8.8. Therefore, *in vitro* and *in vivo* studies could be performed without limitations in assay performance. The limit of quantification (LOQ) was determined at

0.17 ng/mL in NMRI plasma matrix according to specifications defined in section 2.8.8. IVR samples were specifically diluted to target concentrations for analysis, and hence determination of LOQ in IVR buffer sample matrix was superfluous.

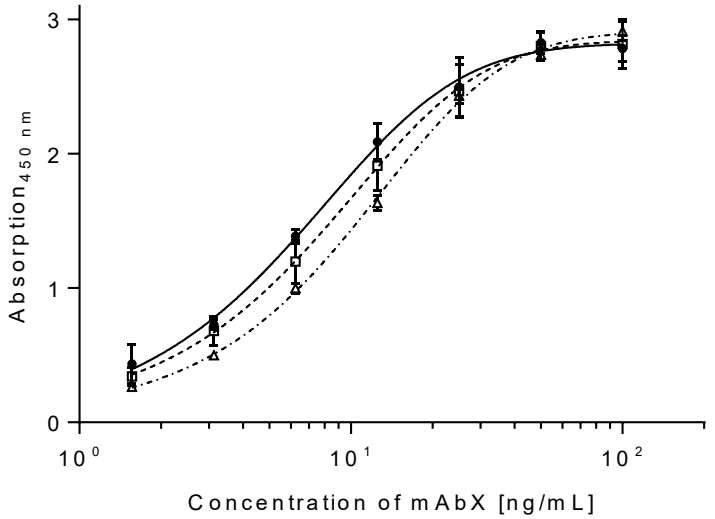

Figure 40: Influence of assay matrices on mAbX standard curves. The model antibody was diluted in assay buffer (●, solid line), mAbX IVR buffer (□, dashed line) or NMRI plasma (△, dashes and dots) and curves were fitted using a 5 parametric logistic fit. Data represents mean values of n = 6 for assay and IVR buffer results, and n = 3 for NMRI plasma results ± SD, respectively.

Cell-based functional assay for mAbX

A cell-based functional assay was established to examine the ability of *in vitro* released mAbX to bind EGFR expressed by human DiFi colorectal cancer cells in comparison with reference samples as explained in section 2.8.10.

Preparative experiments aiming at detection of potential edge effects revealed influences in laterally positioned wells of the plate and the plate scheme shown earlier (see section 2.8.10) was implemented consequently. Furthermore, repeatability as well as influences of sodium azide (NaN_3) originating from residual IVR buffer content in samples were evaluated as part of method implementation experiments. Results thereof are shown in Figure 41. Standard curves of mAbX were examined and predilutions were prepared on basis of cell medium or IVR buffer to detect potential growth inhibition of cells resulting from sodium azide traces. Standard curve shapes were generally comparable even though absolute absorption values varied in parts rather representing inter-plate than intra-plate variances (Figure 41A). To reduce intra-plate variability each sample was compared to a standard reference on the same plate. The mAbX concentration leading to 50% growth inhibition (IC_{50}) was calculated based on standard curve fits and results are depicted in Figure 41B. IC_{50} values of standard curves based on cell

medium or IVR buffer predilutions of mAbX were in a comparable range around 0.7 µg/mL. However, predilution in IVR buffer led to slightly lowered values and mAbX references as well as IVR samples were diluted with identical buffer or media compositions to exclude any potential interference.

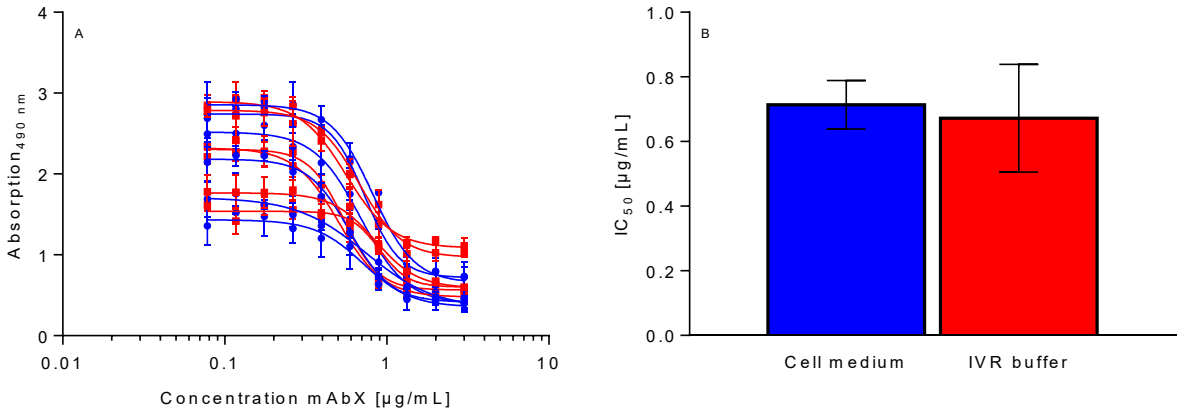

Figure 41: Repeatability of mAbX cell-based functional assay and sodium azide influence. Viable cells were quantified after incubation with different concentrations of mAbX based on predilution with cell medium (●, —) or IVR buffer (■, —) and 4 parametric fits were used to calculate IC_{50} values (A). Average IC_{50} values were calculated and results of differently prepared mAbX dilution rows were in a comparable range (B). IC_{50} results represent mean values ± SD (n = 6).

Reference samples of mAbX were thermally stressed with temperatures between 40 to 95°C to demonstrate accuracy and potential signal range between native and denatured antibody (Figure 42). Increasing temperatures resulted in decreased mAbX potency for cell growth inhibition indicated by a missing drop of adsorption values at certain mAbX concentrations after quantification of viable cells (Figure 42A). Boltzmann sigmoidal fitting of IC_{50} values compared to the respective untreated mAbX sample on each plate led to the curve shown in Figure 42B. The melting temperature (T_m) of mAbX was determined at 72.6°C which was comparable to results of fluorescence spectroscopy (75.3 ± 2.4°C, data not shown herein) confirming precision and reliability of the cell-based assay.

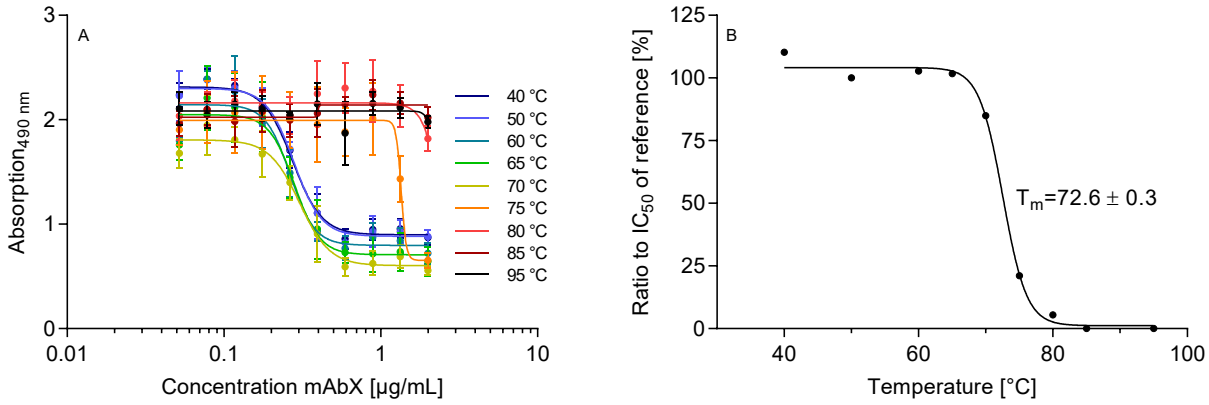

Figure 42: Thermal denaturation of mAbX observed by cell-based functional assay. Viable cells were quantified after incubation with thermally stressed mAbX samples and 4 parametric fitting was used to calculate IC_{50} values (A). Percentages of IC_{50} values compared to the respective reference value on the same plate were calculated and the T_m was determined at 72.6°C using a Boltzmann fit (B).

5.3.2. Stability study of mAbX

Prior to *in vitro* performance analysis of ICX-2wF, the stability of mAbX under *in vitro* release conditions was determined to facilitate identification and interpretation of potential stability loss of the antibody during IVR from SynBiosys® microparticles. Stability was tested in mAbX IVR buffer in comparison to PBS supplemented with Tween® 20 as PBS, pH 7.4 represents the most commonly used release medium [217]. Stability of mAbX was monitored by SE-HPLC as well as circular dichroism and fluorescence spectroscopy. Furthermore, functionality of the antibody was examined utilizing an ELISA as well as a cell-based assay. Results are illustrated in Figure 43. Findings obtained by SE-HPLC revealed a reduction in monomer content over time that was expressed more strongly using IVR buffer compared to PBS (Figure 43A). Approximately 1-2% of total monomer was lost over time for both release media tested while amounts of low (LMWC) and high (HMWC) molecular weight compounds increased, logically. Secondary and tertiary structure stabilities were analyzed disclosing unaffected tertiary structure in both buffer systems (Figure 43B). Secondary structure integrity decreased slightly with values around 90% (PBS) and 80% (IVR buffer) after 29 days under IVR conditions. Comparable trends were observed after determination of the functionality of mAbX (Figure 43C). In ELISA functionality testing as well as cell-based assay, generally slight reductions of functionality were found over time with minor advantages after incubation in IVR buffer. Both assays resulted in values over 85% for mAbX samples based on IVR buffer while PBS-based samples were partly reduced to functionality values between 75-80%.

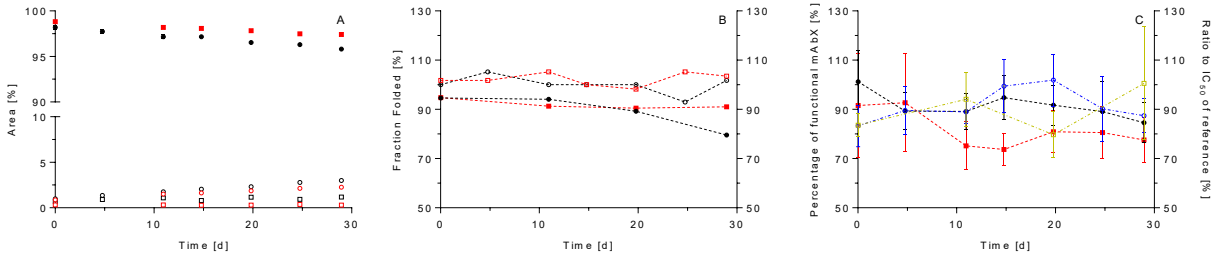

*Figure 43: Stability of mAbX under different IVR conditions over 29 days. **A**: Monomer (filled symbols), high molecular weight compound (HMWC, blank squares) and low molecular weight compound (LMWC, blank circles) content was quantified after incubation in IVR buffer (●, □, ○) or PBS supplemented with Tween® 20 (■, □, ○), respectively. **B**: Fraction Folded of mAbX secondary and tertiary structure in IVR buffer (●, ○) and PBS (■, □) over time. **C**: Percentage of mAbX functionality after incubation in IVR buffer (●, dashed line) as well as PBS (■, dashed line) determined by ELISA. Furthermore, the ratio of IC_{50} to reference values of mAbX incubated in IVR buffer (○, dashes and dots) or PBS (□, dashes and dots) over time determined with cell-based functionality assay is shown. Data represent mean values ± SD (n = 3).*

5.3.3. *In vitro* release

The *in vitro* release behavior of ICX-2wF was analyzed by SE-HPLC according to sections 2.8.2 and 2.8.5. IVR results are shown in Figure 44 and mAbX was linearly released over approximately 10-14 days without remarkable burst during the initial liberation period. Moreover, total and intact amounts of released antibody were found in a comparable range as determined by SE-HPLC. The integrity of released mAbX was further evaluated as described in the subsequent section.

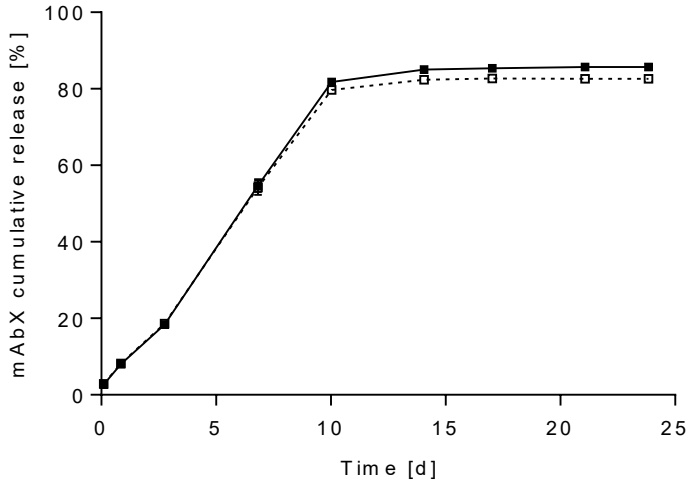

Figure 44: Cumulative in vitro *release of mAbX from ICX-2wF over 24 days. Intact (□) as well as total mAbX (■) released is shown. Data represents mean values ± SD (n = 2).*

5.3.4. Integrity of *in vitro* released mAbX

In vitro released mAbX was analyzed extensively by various methods. Secondary and tertiary structure integrity was examined using circular dichroism and fluorescence spectroscopy. The fundamental functionality of the antibody was determined by a cell-based assay and by ELISA.

Figure 45A shows the IVR of mAbX from SynBiosys® microspheres analyzed by SE-HPLC and functional ELISA. Concentrations of mAbX increased continuously during days 1-6 until a peak around 600 µg/mL was reached. Values decreased thereafter to 400-500 µg/mL at day 10 and concentrations around 100 µg/mL and below after 14-17 days. Results of SE-HPLC and ELISA show comparability with only slightly lower values found by ELISA.

Secondary structure integrity of mAbX released from ICX-2wF was evaluated by circular dichroism spectroscopy. Figure 45B presents spectra of IVR samples of time points 2-6. Ellipticity values ranged from more negative (time points 2-4) to less negative (time points 5 and 6). Tertiary structure integrity of mAbX released from ICX-2wF was examined by fluorescence spectroscopy. In Figure 45D, fluorescence spectra of IVR samples of time points

1-7 are depicted. No clear shift of signal peak wavelengths was observed. The Fraction Folded based on circular dichroism as well as fluorescence spectroscopy measurements was calculated and plotted in comparison with results of the cell-based assay (Figure 45C).

Tertiary structure integrity remained unaffected with values of 84% or higher at all time points. These results were confirmed by circular dichroism spectroscopy with high secondary structure integrity over 83% during the first 10 days of the release. Fraction Folded of secondary structure was decreased to 64% after 14 days. Functionality of mAbX reached values around 80% or higher based on the functional cell-based assay apart from a lower functionality at day 3 (approximately 70%).

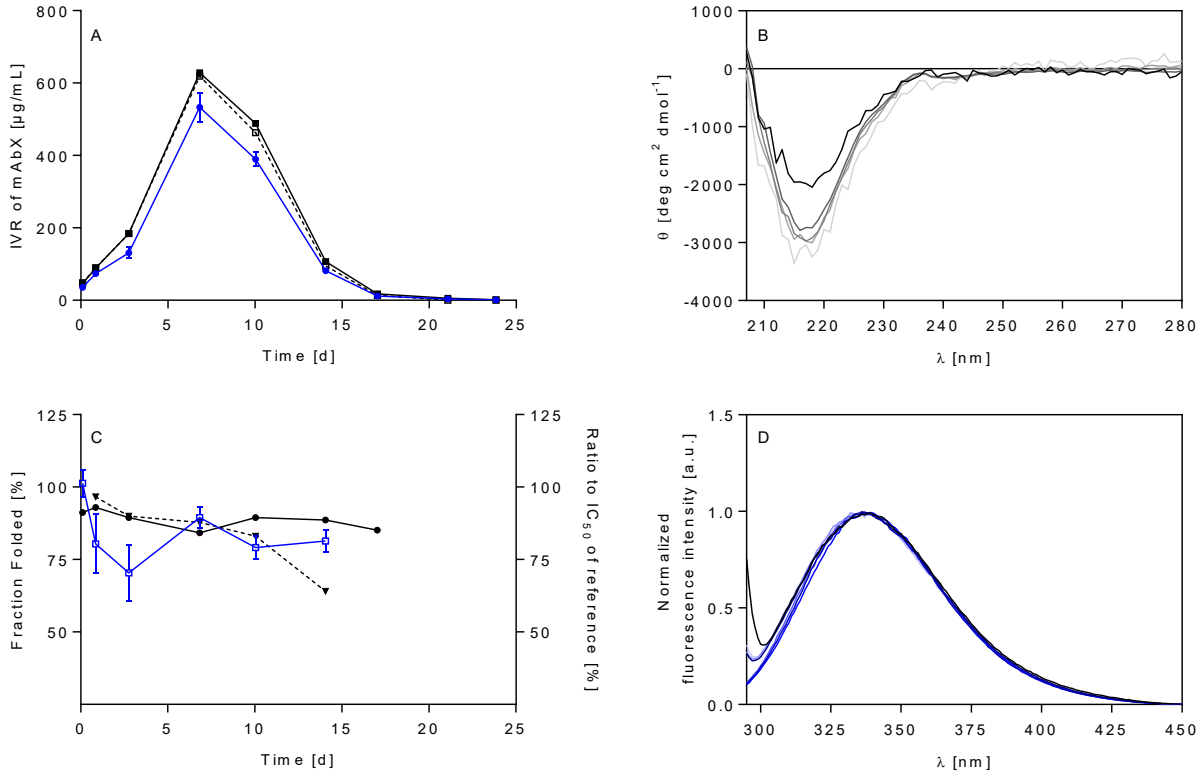

Figure 45: Detailed analysis of in vitro *released mAbX by ELISA (A), spectra obtained by circular dichroism (B) as well as fluorescence spectroscopy measurements (D), and Fraction Folded of circular dichroism and fluorescence spectroscopy combined with cell-based functional assay results (C). **A**: Total (■) and intact (□) IVR data of mAbX determined by SE-HPLC (n = 2) in combination with results of functional ELISA analysis (●, n = 3). **B**: Circular dichroism spectra of mAbX IVR samples ranging from time point 2 (—) to time point 6 (—) with increasingly darker coloration and 10 accumulations per sample. **C**: Fraction Folded based on spectra from circular dichroism (▼, Figure 45B) and fluorescence spectroscopy (●, Figure 45D), calculated according to sections 2.8.6 and 2.8.7. Additionally, cell-based functional assay results for mAbX IVR samples (□) are presented as percentage of IC_{50} of mAbX reference (n = 3). **D**: Fluorescence spectra of mAbX IVR samples ranging from time point 1 (—) to time point 7 (—) with a coloration from light blue to black and 3 repetitive measurements per sample. Data of ELISA (●) and cell-based functional assay (□) represents mean values ± SD (n = 3).*

5.4. *In vivo* results

Results of method implementation and *in vivo* studies are shown in the following section. Solely methods that were established or adapted as part of this work are presented. *In vivo* trials consisted of a first pharmacokinetic study in healthy NMRI mice followed by a second experiment in tumor-bearing NMRI nude mice monitoring pharmacokinetics as well as pharmacodynamic efficacy. The immunogenic potential of ICX-2wF was determined in a further study. Table 11 shows an overview of *in vivo* experiment study design.

5.4.1. Method implementation

Determination of cytokine plasma levels

A 32-plex cytokine/chemokine magnetic bead panel for the simultaneous quantification of 32 different cytokines in plasma samples was utilized and experimental requirements for *in vivo* plasma sample analysis were determined. Blank, pooled and commercially available NMRI mouse plasma was used as assay matrix to reduce potential matrix effects of *in vivo* samples. As part of method implementation experiments, dilution ratios of 1:2, 1:10 and 1:20 of blank NMRI plasma in assay buffer were compared to the serum matrix which was provided with the assay kit. Results for granulocyte-colony stimulating factor (G-CSF) as representative example are shown in Figure 46. Curve shapes of G-CSF standards diluted in different matrices were generally comparable. However, maximum median fluorescent intensities were slightly (1:10 NMRI plasma matrix) or clearly (1:2 NMRI plasma matrix and serum matrix) reduced compared to 1:20 NMRI plasma matrix indicating a negative influence on assay performance. A compromise between sensitivity and negative assay influence was represented by the 1:10

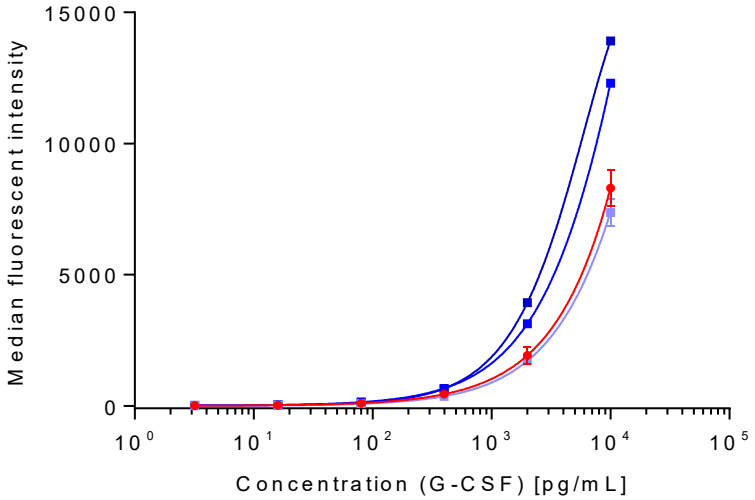

Figure 46: Median fluorescent intensity of G-CSF standard curves in different assay matrices. G-CSF was diluted in serum matrix (●) or NMRI plasma diluted 1:2 (■), 1:10 (■) or 1:20 (■) in assay buffer and curves were fitted with a 5 parametric logistic fit. Data represent mean values ± SD (n = 3).

diluted NMRI plasma matrix. Assay quality requirements were fulfilled with all matrices used. Dilution of plasma samples with a ratio of 1:10 in assay buffer and usage of 1:10 NMRI plasma matrix was found to be suitable for *in vivo* sample analysis.

5.4.2. Immunogenicity

Immunogenic potential of the SynBiosys®-based microparticle formulation of mAbX was evaluated and results are presented in the subsequent section. Systemic cytokine response as well as local inflammatory responses were examined. As illustrated in Table 11, animals were treated subcutaneously with ICX-2wF SynBiosys® formulation (1 and 8 mg mAbX per mouse), polymer-only microparticles (particle amount equivalent to 8 mg/mouse ICX-2wF) and intravenously with reference solution of mAbX (8 mg mAbX per mouse). A further group remained untreated serving as reference.

Cytokine release after administration of microparticles

A number of 32 different cytokines was quantified in plasma samples of animals over 24 hours after single subcutaneous administration of ICX-2wF SynBiosys® formulation (1 and 8 mg mAbX per mouse) or polymer-only microparticles (particle amount equivalent to 8 mg/mouse ICX-2wF). Further groups received a single intravenous injection with reference solution of mAbX (8 mg mAbX per mouse) or remained untreated serving as control. The vast majority of cytokines remained below the detection limit at all time points and is not presented herein.

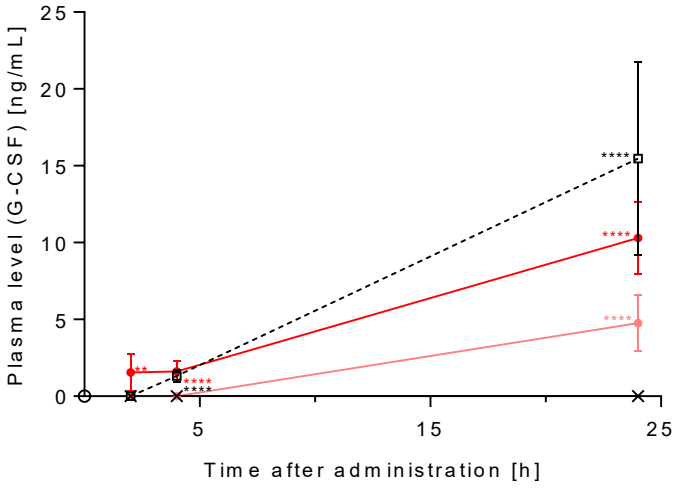

*Figure 47: Plasma levels of G-CSF after treatment with SynBiosys® microparticles and reference groups. ICX-2wF was administered once subcutaneously with mAbX doses of 1 mg/mouse (●) and 8 mg/mouse (●) while polymer-only microparticles (□) were injected similarly with a particle amount equivalent to ICX-2wF 8 mg/mouse. Single intravenous treatment with 8 mg/mouse of mAbX reference solution (x) served as control. Data represent mean values ± SD (n = 3). Significant differences in G-CSF plasma levels between treated groups and untreated animals (○, 0h) are illustrated by ** (p<0.01) and **** (p<0.0001), colored accordingly.*

However, granulocyte-colony stimulating factor (G-CSF) levels were found elevated dose-dependently after administration of mAbX-loaded SynBiosys® microspheres as well as polymer-only microparticles (Figure 47). Injection of ICX-2wF (1 mg/mouse) resulted in G-CSF levels around 5 ng/mL after 24 hours while treatments with ICX-2wF (8 mg/mouse) or polymer-only formulations led to higher values between 10-20 ng/mL. This immune response was significant when compared to untreated or mAbX reference solution groups. Concerning G-CSF, all assay specific quality requirements were fulfilled, and quality controls were recovered in the target ranges.

Histochemical staining of injection area

In addition to systemic cytokine release analysis, the local immune response at the injection sites was evaluated with hematoxylin & eosin staining which was performed by RD-XND-PA (Merck KGaA). A representative image of immune reactions after 4 hours following administration of SynBiosys® polymer-only microparticles to healthy NMRI mice in comparison to an untreated reference biopsy is shown in Figure 48. The inflammatory infiltrate at the injection site of microparticles mainly featured granulocytes and mild numbers of macrophages. The immune response was locally limited to the microparticle-containing area of injection and neighboring regions remained unaffected. No immune response was detected in the untreated reference sample. Reactions in other microparticle-containing groups were comparable also at later time points and are not shown herein.

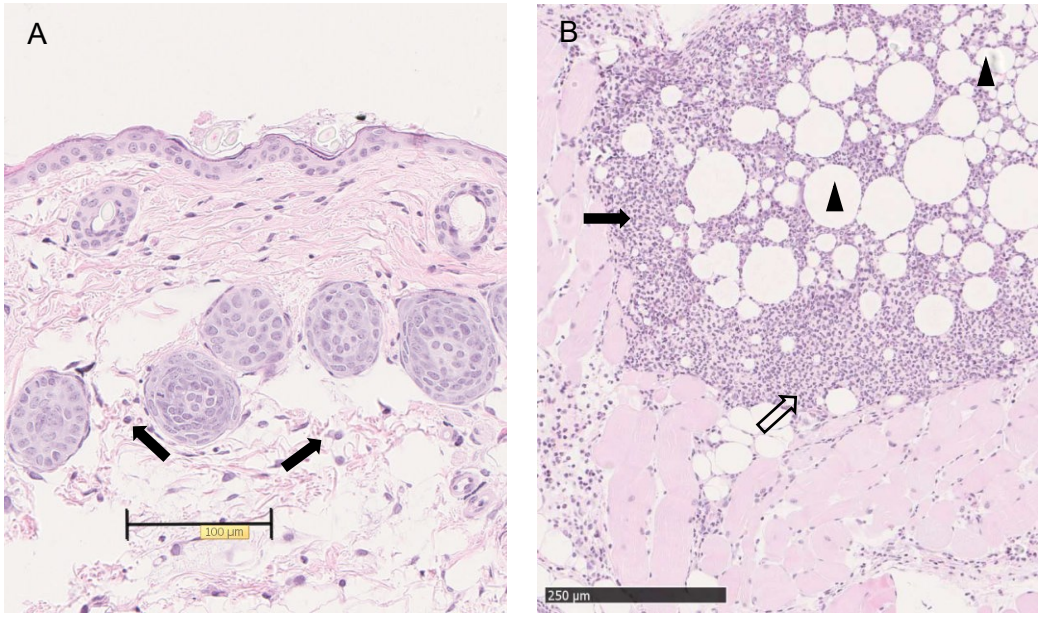

Figure 48: Hematoxylin & eosin staining of SynBiosys® microparticle injection site (B) and untreated reference biopsy (A) 4 hours after s.c. injection. Microparticles (▲) are shown as well as granulocytes (black arrow) and macrophages (blank arrow). The biopsy of the treated animal was collected 4 hours after single subcutaneous injection of polymer-only microparticles of ICX-2wF (amount of particles equivalent to 8 mg mAbX per mouse) and is representative for other microparticle-containing formulations and time points.

5.4.3. Pharmacokinetic study I

Plasma levels of mAbX were determined as described in section 2.9.7 and results are illustrated in Figure 49. Pharmacokinetic parameters were calculated and are listed in Table 19. Reference solutions of mAbX were administered once at a dose of 1 mg per animal intravenously or subcutaneously (Figure 49A). Peak plasma concentrations of 280 µg/mL (i.v.) or 108 µg/mL (s.c.) were observed after 3 hours or 1 day, respectively. Plasma levels of mAbX continuously decreased thereafter at comparable rates with a half-life of 13.7-14.4 days. Subcutaneously administered mAbX reference solution exhibited an absolute bioavailability (F_{abs}) of 65.1%.

ICX-2wF doses of 1, 4 and 8 mg/animal of mAbX were injected once and resulting plasma concentrations are depicted in Figure 49B. Peak plasma levels of 24.9, 223.9 or 325.6 µg/mL were reached after three days, respectively. This was clearly delayed compared to the reference solutions of mAbX. Further on, values decreased partly rapidly with a half-life between 3.4 and 8.9 days until low amounts of mAbX remained after 23 days.

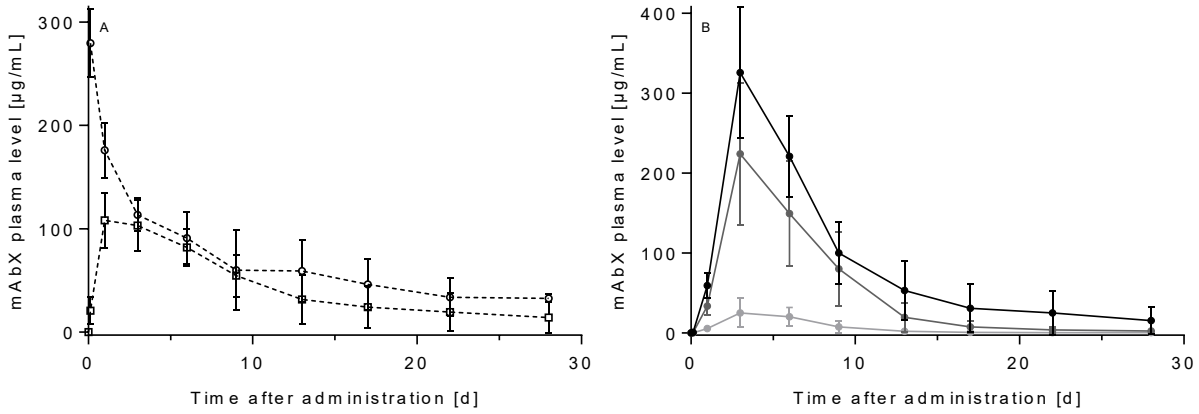

Figure 49: Plasma levels of mAbX over 28 days during PK I. A reference solution of mAbX (A) and different doses of ICX-2wF (B) were administered once to healthy NMRI mice. The mAbX reference solution with a dose of 1 mg/mouse was administered i.v. (○) or s.c. (□). ICX-2wF at mAbX doses of 1 (●), 4 (●) and 8 mg/mouse (●) was injected subcutaneously. Data represent mean values ± SD (n = 6).

Table 19: Pharmacokinetic parameters PK I. After administration of mAbX reference solution and ICX-2wF at different doses, the maximum plasma concentration (C_{max}), time point of C_{max} (t_{max}), half-life ($t_{1/2}$), area under the curve (AUC_{0-28d}) as well as absolute (F_{abs}) and relative bioavailability (F_{rel}) was calculated.

	C_{max} [µg/mL]	t_{max} [h or d]	$t_{1/2}$ [d]	AUC_{0-28d} [µg/mL*h]	F_{abs} [%]	F_{rel} [%]
Reference mAbX i.v. (1.0 mg/animal)	280.0	3 h	13.7	1906.0	100.0	-
Reference mAbX s.c. (1.0 mg/animal)	108.0	1 d	14.4	1240.2	65.1	100.0
ICX-2wF s.c. (1.0 mg/animal)	24.9	3 d	4.6	167.5	8.8	13.5
ICX-2wF s.c. (4.0 mg/animal)	223.9	3 d	3.4	1473.2	19.3	29.7
ICX-2wF s.c. (8.0 mg/animal)	325.6	3 d	8.9	2444.2	16.0	24.6

Absolute (8.8-19.3%) and relative bioavailabilities of mAbX (13.5-29.7%) liberated from microparticles were lower as values of the subcutaneously administered reference solution.

5.4.4. Pharmacokinetic study II

Further studies were performed in tumor-bearing nude NMRI mice to gain deeper insights in pharmacokinetic behavior of ICX-2wF as well as pharmacodynamic efficacy of mAbX released from microparticles. Additionally, the time frame observed was extended from 28 days to 41 days. Plasma concentrations of mAbX were determined according to the description in section 2.9.7 and results are presented in Figure 50. Reference solution of mAbX was administered intravenously as well as subcutaneously and resulting plasma levels were comparable to the findings described in the previous section 5.4.3 (Figure 50A). Briefly, peak plasma concentrations of 244.5 (i.v.) and 108.1 µg/mL (s.c.) were observed 3 hours or 1 day after administration and the relative bioavailability of subcutaneously injected mAbX was 65.6%. Low amounts of mAbX were still found after 27 days. The half-life of mAbX administered as reference solution decreased to 7.7-8.9 days compared to results of PK I.

SynBiosys® formulation ICX-2wF was injected at mAbX doses of 1, 2, 4 and 8 mg/mouse and results are depicted in Figure 50B. Peak plasma levels of 51.6, 95.9, 177.9 and 418.5 µg mAbX per mL were shifted to day 2 to 4 after administration and low amounts of antibody were detected until day 27. Plasma concentrations dropped rapidly after the peak was reached. Values for absolute (25.7-28.8%) and relative bioavailability (39.1-43.9) increased compared to findings of PK I.

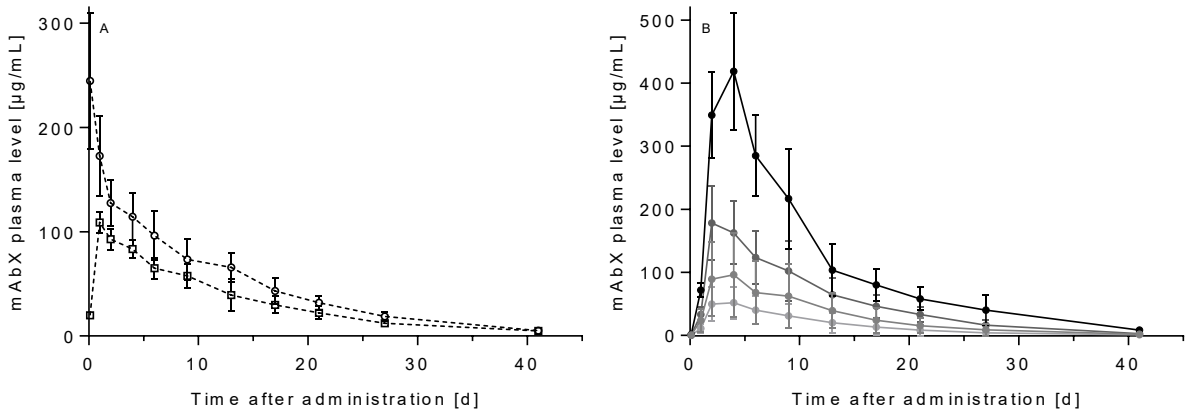

Figure 50: Plasma levels of mAbX over 41 days during PK II. A reference solution of mAbX (A) and different doses of ICX-2wF (B) were administered once to tumor-bearing nude NMRI mice. The mAbX reference solution with a dose of 1 mg/mouse was administered i.v. (○) or s.c. (□). ICX-2wF at mAbX doses of 1 (●), 2 (●), 4 (●) and 8 mg/mouse (●) was injected subcutaneously. Data represent mean values ± SD (n = 7).

Table 20: Pharmacokinetic parameters PK II. After administration of mAbX reference solution and ICX-2wF at different doses, the maximum plasma concentration (C_{max}), time point of C_{max} (t_{max}), half-life ($t_{1/2}$), area under the curve (AUC_{0-28d}) as well as absolute (F_{abs}) and relative bioavailability (F_{rel}) was calculated.

	C_{max} [µg/mL]	t_{max} [h or d]	$t_{1/2}$ [d]	AUC_{0-41d} [µg/mL*h]	F_{abs} [%]	F_{rel} [%]
Reference mAbX i.v. (1.0 mg/animal)	244.5	3 h	7.7	2019.9	100.0	-
Reference mAbX s.c. (1.0 mg/animal)	108.1	1 d	8.9	1325.6	65.6	100.0
ICX-2wF s.c. (1.0 mg/animal)	51.6	4 d	6.0	618.1	30.6	46.6
ICX-2wF s.c. (2.0 mg/animal)	95.9	4 d	6.5	1164.5	28.8	43.9
ICX-2wF s.c. (4.0 mg/animal)	177.9	2 d	5.7	2075.1	25.7	39.1
ICX-2wF s.c. (8.0 mg/animal)	418.5	4 d	7.1	4379.7	27.1	41.3

5.4.5. Dose linearity of ICX-2wF during pharmacokinetic studies I & II

Dose linearity of formulation approaches is a desirable characteristic allowing simplified dosing and dose adjustments [221]. As presented in Table 19 and Table 20, the area under the curve was calculated based on pharmacokinetic behavior of ICX-2wF during PK studies I and II. A linear relationship between mAbX plasma concentrations was found after administration of different doses of ICX-2wF during both pharmacokinetic studies (Figure 51). The dose-dependency of plasma concentrations was demonstrated by determination coefficients of the regression lines of 0.97 and 0.99. While mAbX plasma concentrations in tumor-bearing animals were dose dependent (R^2=0.99), the linear relationship was slightly less pronounced in PK I (0.97).

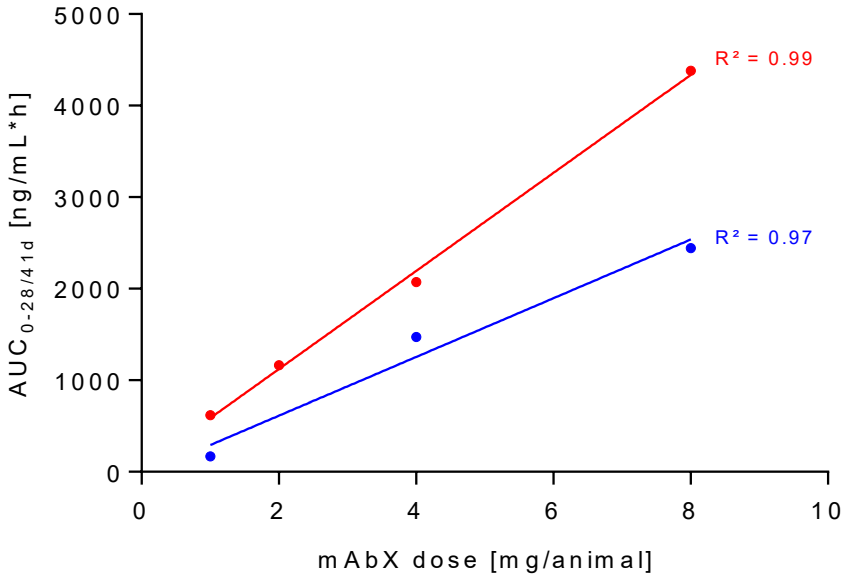

Figure 51: Area under the curve from day 0 to 28 or 41 after single s.c. administration of different doses of ICX-2wF to healthy animals in PK I (●) and tumor-bearing nude mice in PK II (●). Corresponding regression lines of PK I (—) and PK II data (—) are shown together with the determination coefficients of the regression lines (R^2).

5.4.6. Pharmacodynamic study

The relative tumor growth of A-431 xenografts in immunodeficient NMRI nu/nu mice was observed over 42 days after single treatment with different doses of ICX-2wF and mAbX reference solution. An additional control group was treated with mAbX-free polymer-only (P-O) microparticles. The results of the pharmacodynamic study are depicted in Figure 52. The strongest effect and complete tumor growth inhibition was observed in animals treated with mAbX reference solution (1 mg mAbX/mouse) and ICX-2wF (4 and 8 mg mAbX/mouse). In these groups, tumor volumes increased slightly until day 10 and were shrinking subsequently until the end of the study at day 42 with significantly lower tumor volumes compared to the P-O group from day 7 on.

Lower doses of ICX-2wF (1 and 2 mg mAbX/mouse) also led to reduced tumor growth compared to the P-O group. However, tumors regained volume from day 17 on after a phase of slight volume reduction. Significant differences between P-O group and ICX-2wF were found between days 10-17 (1 mg mAbX/mouse) or days 7-31 (2 mg mAbX/mouse). In contrast to that, tumors of the untreated P-O group increased constantly and about 10-fold in volume over 42 days.

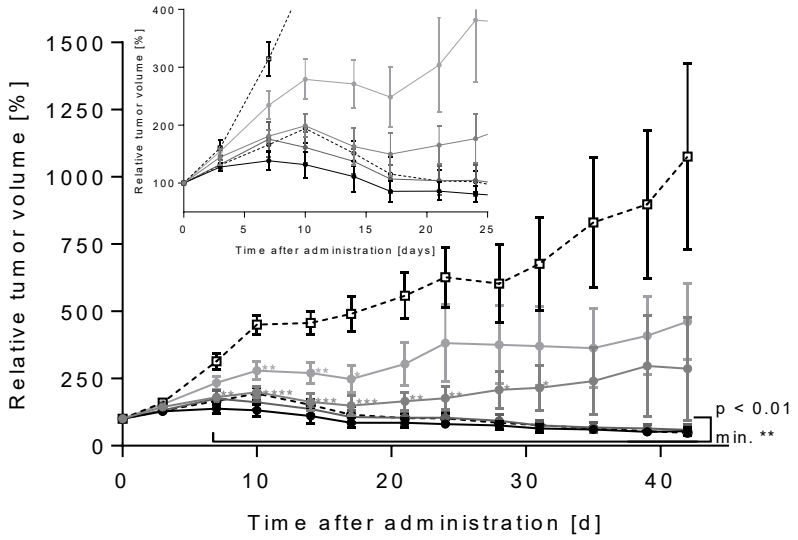

*Figure 52: Relative growth of A-431 tumor xenografts in NMRI nu/nu mice over 42 days after single injection of mAbX and polymer-only reference solutions as well as different doses of ICX-2wF. A mAbX dose of 1 mg/mouse was administered with the reference solution intravenously (○) while ICX-2wF was administered subcutaneously with doses of 1 (●), 2 (●), 4 (●) and 8 mg mAbX/mouse (●). The polymer-only reference (□) was administered subcutaneously while the amount of particles corresponded to the highest dose of mAbX-containing ICX-2wF microparticles. Calculations of the relative tumor volume were related to the initial tumor volume at day 0, respectively. Mean values of n = 7 animals/group are shown ± SE. The inlay shows zoomed results of the first 24 days. Significant differences between the P-O group and groups treated with mAbX-containing formulations are illustrated by * (p < 0.05), ** (p < 0.01), *** (p < 0.001) and **** (p < 0.0001) in the respective coloration. The bracket indicates a minimum significant difference of ** (p < 0.01) between the P-O group and ICX-2wF (4 and 8 mg/mouse) as well as reference solution from day 7 to 42.*

5.5. Summary and discussion

Microspheres loaded with mAbX were manufactured based on the SynBiosys® platform and the findings determined within chapter 4 to evaluate the suitability of these polymers to formulate a monoclonal antibody in a controlled release approach as representative model for a large biological.

The high versatility of the SynBiosys® platform was already demonstrated previously. After determination of a suitable polymer composition as well as manufacturing process on the basis of mAbB, a controlled release formulation (ICX-2wF) of mAbX was developed to analyze *in vitro* and *in vivo* performances of the material more in detail. A high antibody loading of 14.9 wt.% was achieved with a solid encapsulation efficiency of 80% while the particle size distribution was broad potentially resulting from low coacervate droplet stability during W/O/O manufacturing [258]. Likewise, Vidmar *et al.* (1984) observed agglomerated microparticles [259] while Ciombor *et al.* also achieved polydisperse PLGA microparticles manufactured by a similar production process [260]. Nevertheless, ICX-2wF microspheres exhibited a highly continuous and especially reproducible IVR behavior. A uniform liberation of mAbX was observed over 10-14 days *in vitro* with a remarkably low initial release of 8.2% during the first 20h. Polymer-only microparticles were clearly smaller (40.0 µm) compared to mAbX-loaded microspheres (84.0 µm) as no API was encapsulated.

In accordance with the analytical approach for mAbB, *in vitro* released mAbX was examined structurally. Thus, circular dichroism and fluorescence spectroscopy methods for analysis of secondary and tertiary structure modifications of mAbX were established. As described earlier, intrinsic tryptophan fluorescence was used to gain insights in tertiary structure while specific absorption of circularly polarized light by peptide bonds allows conclusions about the secondary structure integrity [184, 186, 240].

Prior to circular dichroism analysis, mAbX samples were dialyzed to exclude IVR buffer-induced measurement interferences or signal overlaps [241], as previously mentioned. No influence of the dialysis procedure on mAbX secondary structure integrity was observed within preparative experiments. Furthermore, detection limits were determined between 82.5-600 µg/mL (circular dichroism spectroscopy) as well as 6.3-700 µg/mL (fluorescence spectroscopy) representing thresholds ensuring exclusion of artefacts in analyses of mAbX IVR samples.

Moreover, reference samples of mAbX were denatured thermally and chemically to determine the signal range between native and completely unfolded protein states in circular dichroism as well as fluorescence spectroscopy measurements. The motivation for that experimental strategy was outlined in detail in section 4.4. The largest possible signal shift without further

artifacts was observed after chemical denaturation in both circular dichroism as well as fluorescence spectroscopy. Therefore, the calculation of the Fraction Folded of mAbX secondary and tertiary structures was based on GdnHCl-based denaturation results.

An enzyme-linked immunosorbent assay was utilized for *in vitro* as well as *in vivo* quantification of mAbX that retained the ability to functionally bind EGFR. Matrix influences on assay performance were found to be small and samples were analyzed in the respective original matrix while standard matrices were adapted accordingly.

Rounding off the *in vitro* analytical spectrum, a cell-based functional assay for mAbX was established using human DiFi colorectal cancer cells overexpressing EGFR [193]. Besides detection of edge effects and adaption of plate schemes according to findings in preparative experiments, the repeatability of the assay as well as influences of sodium azide originating from residual IVR buffer content in samples were evaluated. Sodium azide acts cytostatically and cytotoxically on mammalian cell lines [261], and hence influences on assay results were conceivable. Repeatability was in an acceptable range and the influence of sodium azide on IC_{50} values was relatively low. However, clear sodium azide-induced effects were observed in preliminary experiments with lower dilution of IVR buffer-based samples (data not shown), and hence preparations as well as dilutions of standards and samples for analysis were performed uniformly resulting in identical sodium azide content throughout assay plates. Furthermore, precise functionality of the assay was confirmed by analysis of thermally denatured mAbX reference samples and subsequent determination of the melting temperature at 72.6°C which was highly comparable to fluorescence spectroscopy results (75.3 ± 2.4°C, data not shown).

Prior to analysis of *in vitro* released mAbX, a stability study of the antibody under IVR conditions over 29 days was performed to facilitate differentiation between release or manufacturing related and experimental setup-induced stability loss. SE-HPLC measurements showed a general reduction in monomer content of 1-2% over time while the tertiary structure determined by fluorescence spectroscopy remained unaffected. Secondary structure studies using circular dichroism spectroscopy revealed slightly decreasing structure stability over time. However, mAbX was additionally analyzed by ELISA as well as cell-based assay and functionality of the antibody was only negligibly impaired remaining above 85% until the end of the experiment. In total, mAbX integrity was maintained throughout the stability study apart from minor variations. Additionally, the suitability of IVR buffer as release medium was confirmed by comparison of the results to mAbX stability in PBS supplemented with Tween® 20 (pH 7.4) representing the most commonly used buffer for IVR approaches [217]. Nevertheless, experimental setup of the IVR could not be replicated completely during preliminary stability studies of mAbX. Medium was exchanged regularly after each sample collection during IVR while no exchange could be performed during stability studies.

Following method implementation, the integrity of *in vitro* released antibody was examined intensively.

Aggregation and fragmentation were examined by SE-HPLC. Only a negligible amount of antibody was degraded as indicated by highly comparable values of total and intact mAbX during IVR. Moreover, the functionality of *in vitro* released mAbX was confirmed by ELISA. Additionally, the integrity of secondary and tertiary protein structures of mAbX was determined by circular dichroism and fluorescence spectroscopy. Results thereof were compared as Fraction Folded indicating highly intact protein structures apart from a slight variation in secondary structure integrity after 14 days. A potential explanation is variability of circular dichroism spectroscopy up to 10% due to accumulation of experimental errors [262, 263]. Furthermore, results of the residual methods confirmed the liberation of intact mAbX over the entire release duration. The findings of the Fraction Folded were complemented with results from the cell-based functional assay confirming that the ability of mAbX to effectively inhibit growth of human colorectal cancer cells was maintained throughout particle manufacturing and *in vitro* release. A decreased proportion of functionally intact mAbX was observed around day 3 of IVR by cell-based assay analysis. However, structural analyses and especially ELISA results disproved a reduction in the amount of intact antibody. At days 7-10, mAbX was released with high integrity representing the period with the highest amount of antibody released from ICX-2wF microparticles.

Typically, peptide or protein stability examination in studies on polymer-based controlled release is restricted to two or three analytical methods while HPLC, circular dichroism and fluorescence spectroscopy as well as different functional assays are used in different combinations [135, 136, 260, 264-266]. The composition of five analytical methods to evaluate the condition of *in vitro* released mAbX herein formed a powerful tool to examine the influence of microparticle manufacturing process as well as SynBiosys®-based release from multiple angles allowing a highly diversified assessment.

Conventional PLGA-based protein delivery approaches are often limited due to instabilities of the sensitive biological cargo caused by PLGA hydrolysis and resulting accumulation of acidic degradation products inside microparticles [126, 248, 250, 267-269]. The release of functionally intact mAbX from SynBiosys® microspheres is especially remarkable against this background.

As discussed previously, the integration of polyethylene glycol as hydrophilic component in PLGA-based sustained release approaches leads to a higher degree of water influx compared to conventional, rather hydrophobic PLGA, and thus to a more continuous diffusion-controlled release and a less pronounced pH drop inside microparticles [135, 217, 268]. As a result, the microenvironment in particles becomes more protein-friendly leading to a higher amount of intact protein released [136, 217, 218]. However, so far the beneficial effect of the addition of

polyethylene glycol to microparticle formulations on protein stability has often been limited as release duration was simultaneously accelerated dramatically and burst release increased [268]. As outlined in chapter 4, integration of polyethylene glycol not only leads to improved long-term stability of encapsulated proteins but also protects the antibody during encapsulation and manufacturing. Alternative approaches to enhance the stability of proteins released from PLGA-based microparticles were successful to a certain extent although also drawbacks were exposed as discussed earlier herein (see section 4.4).

In vitro release sample analysis presented herein demonstrates the successful combination of the advantageous effect of including polyethylene glycol in microparticles with a highly continuous release of intact mAbX over 10-14 days by the SynBiosys®-based microparticle formulation ICX-2wF.

The immunogenic potential of the ICX-2wF microparticle formulation of mAbX was examined *in vivo*. Cytokine levels were monitored over 24 hours after single s.c. administration of ICX-2wF SynBiosys® formulation (1 and 8 mg mAbX per mouse) or polymer-only microparticles (particle amount equivalent to 8 mg/mouse ICX-2wF). Additional animals were treated with single intravenous injection of a mAbX reference solution (8 mg mAbX per mouse) or remained untreated. Granulocyte-colony stimulating factor (G-CSF) plasma concentrations were significantly elevated dose-dependently after 4 and 24 hours in response to SynBiosys® microparticle containing injections while no immune response was observed in animals after administration of mAbX reference solution. Murine G-CSF was first isolated in 1983 and induces the formation of neutrophilic granulocyte colonies by binding to the G-CSF receptor [270-272]. Typically, levels of G-CSF rapidly increase after activation of the immune system by external stimuli and the cytokine is secreted by a variety of different cell types [273-277]. These findings were consistent with results of hematoxylin and eosin staining of the injection areas after administration of SynBiosys® microparticle containing formulations. Mainly neutrophilic granulocytes were present in a locally limited sector around the microsphere injection site. In total, these results represent an expectable mild foreign body reaction to ICX-2wF as well as polymer-only microparticles and immunogenic potential of the polymers is assessed as low.

In two consecutive pharmacokinetic studies (PK I and II), mAbX doses of 1, 2, 4 and 8 mg/mouse were administered in comparison with intravenously as well as subcutaneously injected reference solutions of the antibody (1 mg/mouse, respectively). Plasma levels of mAbX and corresponding pharmacokinetic parameters were determined. Peak plasma levels after intravenous injection were higher compared to subcutaneous reference as well as microparticle groups with respect to the dose applied during both studies. Furthermore, C_{max} and t_{max} values were generally in similar ranges for equal doses and formulations comparing PK I and II, respectively. The half-life of mAbX was stable in both pharmacokinetic experiments

after administration of SynBiosys® microparticle containing formulations while decreased values were found after injection of reference solutions in PK II ($t_{1/2}$ = 7.7-8.9 days) compared to PK I ($t_{1/2}$ = 13.7-14.4 days). However, the reason for shortened half-life of mAbX originating from reference solution injections remained unclear as pharmacokinetic profiles were highly comparable. In contrast to that, the bioavailability of mAbX was constant between PK I and II in reference solution groups (65% F_{rel}, approximately) while values in the first study were lower (F_{abs}: 8.8-19.3%, F_{rel}: 13.5-29.7%) compared to results in the second pharmacokinetic trial (F_{abs}: 25.7-30.6%, F_{rel}: 39.1-46.6%) after administration of SynBiosys® microparticle formulations. Bioavailability of subcutaneously administered biotherapeutics is highly variable and strongly depends on the species examined as well as various other factors like injection site and depth or the applied dose [223, 278-280]. In some cases, only low levels clearly below 20% of protein injected were found in the plasma after subcutaneous administration [223, 281, 282]. In this light, the absolute bioavailability of ICX-2wF between 25.7 and 30.6% during PK II was encouraging representing solid values with low variability while results in PK I were less promising.

Plasma levels of mAbX were dose-dependent as demonstrated by pharmacokinetic results and corresponding AUC values. Linear pharmacokinetics facilitate dosing and dose adjustments of formulation candidates [221]. Consequently, results on dose-dependency of mAbX plasma levels are promising.

Interestingly, mAbX plasma concentrations were more (PK I) or less variable (PK II) within animals of the same group, respectively. A potential explanation is the formation of anti-drug antibodies (ADAs) in certain animals leading to reduced antibody plasma levels by neutralization of or complex-building with mAbX resulting in enhanced clearance [283, 284]. The first ADA detection was described in 1970 by Hurter et al. who examined the immunogenicity of porcine and bovine insulins [285] and the topic gained importance with growing presence of biotherapeutic proteins in the last decades. The probability for activated ADA production in response to potentially immunogenic proteins is increased in healthy individuals with intact immune system while ADA formation is less likely in case of immune deficiency [286, 287]. Immune competent NMRI mice were used during PK I while PK II studies were performed with immune-deficient NMRI nude mice. Therefore, increased intra-group variability of mAbX plasma concentrations during PK I is most likely the result of anti-mAbX ADA formation. In contrast to that, ADA production was potentially minimized in PK II leading to more stable results. As stated earlier, bioavailability of mAbX was reduced in immune-competent animals after release from microparticles compared to PK II which could indicate ADA-induced clearance of mAbX. Inter-study bioavailability of the subcutaneously administered mAbX reference solution was stable implying an immunogenic enhancing effect induced by mAbX in combination with microparticles for SynBiosys® formulations.

The controlled release effect of ICX-2wF could be demonstrated as the main peak was shifted to 2-4 days after treatment in contrast to the immediate release reference solution (maximum peak plasma level after 3 or 24 hours). However, also mAbX plasma levels of the reference formulation remained relatively high until day 27 outshining the controlled release ability of ICX-2wF. A potential explanation for the long circulation of mAbX administered in form of reference solution is the recycling by neonatal Fc receptors (FcRn) overlapping the controlled release effect of the SynBiosys® formulation. FcRn was first found in neonatal rats [288] and redirects antibodies of the IgG type to the blood stream by a pH dependent binding and release mechanism [54, 289]. Especially murine FcRn can effectively bind to the Fc region of foreign-species antibodies prolonging their plasma half-life [290]. Thus, further pharmacokinetic analyses utilizing FcRn-knockout mice would represent a reasonable future step to demonstrate the ability of ICX-2wF to release mAbX in a controlled manner over a prolonged period more clearly.

The pharmacodynamic efficacy of ICX-2wF was examined in parallel to the second pharmacokinetic study. The tumor volume was determined over 42 days after single subcutaneous administration of IXC-2wF doses of 1, 2, 4 and 8 mg mAbX per mouse. Doses of 1 mg mAbX per mouse of the reference solution were injected intravenously as well as subcutaneously. Additionally, a polymer-only formulation of SynBiosys®-based microparticles was administered subcutaneously as benchmark. Tumors of animals treated with polymer-only microparticles grew constantly until a 10-fold volume increase was observed after 42 days. In contrast to that, all mAbX-containing formulations significantly inhibited tumor growth. After mAbX treatment, tumors slightly increased in volume for 7-10 days and subsequently remained significantly smaller compared to tumors in the polymer-only group for at least one week. Thereafter, tumors of animals treated with reference solution and ICX-2wF (4 and 8 mg/mouse) constantly shrank while tumors of animals treated with lower doses of ICX-2wF (1 and 2 mg/mouse) restarted growing. These results were expectable taking findings of bioavailability calculations into account. Nevertheless, mAbX released from SynBiosys® microspheres was functionally intact and able to reduce tumor growth effectively indicating a fundamental compatibility of SynBiosys® polymers with a monoclonal antibody.

6. Conclusion and outlook

Biological APIs were on the rise during the past decades and long-term prospects are bright as the biotherapeutics market is anticipated to continue with strong growth over the next years [21]. Nevertheless, peptides often exhibit short circulation times *in vivo* introducing a need for frequent injections and monoclonal antibodies as representatives for large proteins typically require intravenous administration which lowers patients' compliance [23, 25]. Hence, long acting injectable formulations of biologicals offer the possibility of overcoming these drawbacks by changing the dose regimen to less frequent injections and allowing subcutaneous instead of intravenous administration. Additionally, more general potential benefits of controlled release systems are reductions in total dose required as well as lowered peak plasma levels leading to less pronounced side effects. As described previously, conventional PLGA is one of the most commonly used copolymers for controlled release approaches. Despite its use in various approved medicinal products, drawbacks like multiphasic, inconsistent as well as incomplete release behavior and accumulation of acidic polymer degradation products within particles limit the application in controlled release of sensitive biologicals [111, 113, 124].

The aim of this work was the suitability evaluation of the innovative polymer platform SynBiosys® for controlled release of sensitive peptide and large protein therapeutics as an alternative to conventional PLGA. SynBiosys® polymers are biodegradable poly (ether ester) multi-block copolymers composed of variable amounts of clinically proven safe monomers like DL-lactide, glycolide, ε-caprolactone, dioxanone and/or polyethylene glycol. A phase-separated polymer matrix is formed with a combination of hydrophilic, amorphous and hydrophobic crystalline areas. Therefore, protein-friendly, hydrophilic domains are accompanied by hydrophobic sectors introducing stability to microparticles. However, SynBiosys®-based microparticle formulations with different, representative model APIs were examined *in vitro* as well as *in vivo* herein to prove the beneficial properties of the platform.

In a first case study, the 4.1 kDa peptide exenatide which is used in T2DM therapy was encapsulated in SynBiosys®-based microparticle formulations with different target release durations of two and four weeks, respectively. Bydureon®, the marketed and PLGA-based one-week controlled release formulation of exenatide served as benchmark. The typical weaknesses of PLGA as drug delivery vehicle for biologicals were reproduced showing inconsistent release behavior *in vitro* as well as incomplete release with only 65% intact peptide liberation. In contrast to that, exenatide release from SynBiosys® microspheres was highly continuous while burst release was acceptably low for both formulations examined. Furthermore, a cell-based functional assay was implemented indicating a higher integrity of exenatide released from SynBiosys® compared to peptide released from PLGA of Bydureon®.

However, these results require confirmation in future experiments although HPLC findings substantiated the results obtained with the cell assay. Differences in the amounts of intact peptide released as well as the release behavior were attributed to the absence (Bydureon®) or presence (SynBiosys®) of polyethylene glycol leading to a pronounced or diminished pH drop inside of microparticles, respectively [120, 126, 217]. Additionally, the water influx induced by the integration of polyethylene glycol in the polymer matrix allows a more continuous release when compared to conventional degradation-based release of PLGA microspheres [135, 217].

During *in vivo* studies, exenatide-loaded SynBiosys® microparticles exhibited low immunogenic potential as demonstrated by control of systemic cytokine release after administration as well as histochemical staining of skin samples from injection sites, and both parameters were limited to the expectable degree of a mild foreign body reaction. The *in vivo* experimental design of pharmacokinetic experiments was confirmed by the successful reproduction of the inconsistent release behavior of Bydureon® which was comparable to patent data and literature [160, 211]. In contrast to the marketed benchmark, benefits of SynBiosys®-based exenatide formulations were found in absence of an initial lag phase as well as dose-dependent exenatide plasma levels while the relative bioavailability of the peptide was minimally higher after release from Bydureon®. Linear pharmacokinetics were consistent with the *in vitro* findings demonstrating a solid comparability between *in vitro* and *in vivo* performances.

The successful implementation of a T2DM rodent model allowed further investigation of the *in vivo* performance of SynBiosys®-based exenatide microspheres during pharmacodynamic experiments. Pharmacodynamic studies were affected by unforeseeably high morbidity of animals treated with exenatide-containing formulations which was probably caused by unexpected secondary interactions of the drug with GLP-1 receptors of the central nervous system [226-229] without contribution of the drug delivery system. Nevertheless, results of pharmacodynamic studies were remarkable. Whereas the therapeutic benefit of the 2-weeks formulation was less pronounced, single subcutaneous administration of the 4-weeks formulation significantly reduced the non-fasting blood glucose levels in diabetic animals in a comparable range to Bydureon® while the onset of effect was observed immediately in contrast to a delayed effect of the marketed formulation. Additionally, the dosing frequency was lowered from four (Bydureon®) to one (SynBiosys®) and, remarkably, the required exenatide dose was reduced by a factor of 10 while comparable hypoglycemic efficacy was observed. The determination of the proportion of glycated hemoglobin (HbA_{1c}) in total hemoglobin is an indicator for the average blood glucose levels over the preceding weeks to months and is less error prone than daily measurements of the blood glucose level. The promising pharmacodynamic results were confirmed by determination of the HbA_{1c} levels which allowed

the classification of the SynBiosys® polymer platform as suitable and beneficial technology for the controlled release of sensitive peptide therapeutics. With regard to these findings, progression to the examination of SynBiosys®-based microparticles for the sustained liberation of larger proteins was a logical next step.

Therefore, mAbB-loaded microparticles with different polymer compositions were investigated *in vitro* to determine a suitable polymer matrix for the controlled release of large protein therapeutics in a second case study. The monoclonal antibody B belongs to the family of IgG1 antibodies and is directed against cellular Sin1. Dysregulation of this factor is a common feature of various diseases like cancer, obesity or T2DM [168-170]. Six different polymer compositions were utilized for production of microparticles while the manufacturing process as well as antibody target loading were kept constant. The polyethylene glycol content of polymers was varied from 37.5 to 28.1 wt.% influencing the hydrophilicity of the resulting polymer matrices, and thereby the release duration was tuned from days to weeks illustrating the versatility of the SynBiosys® platform. Modification of the polyethylene glycol content is a commonly known way to achieve tunable release rates which is most likely a consequence of more or less pronounced water influx due to varying hydrophilicity [234-236].

Additional to HPLC-based analysis of the *in vitro* release behavior, the structural integrity of the liberated antibody was determined. For that purpose, circular dichroism and fluorescence spectroscopy methods were implemented as part of this work to evaluate the secondary as well as tertiary structure integrity of released mAbB. Method implementation included determination of detection limits as well as signal limits of native and completely denatured reference protein to allow classification of antibody integrity in *in vitro* release samples.

Interestingly, the protein secondary structure integrity was closely related to the hydrophilicity of the polymer matrix and secondary structure stability was increasingly impaired with decreasing hydrophilicity. Obviously, polyethylene glycol protected mAbB against organic solvent interfaces during manufacturing processes and further against accumulating acidic degradation products of the polymer matrix during *in vitro* release. The integration of polyethylene glycol as hydrophilic element in SynBiosys® polymer matrices proved to represent a crucial factor affecting stability and integrity of the encapsulated protein. A reasonable release duration over approximately two weeks with continuous release of structurally highly intact mAbB was achieved using a polymer composition of 90% phase-separated block 50CP30C40-LL40 and 10% phase-separated block 50CP10C20-LL40 accounting for 36.25 wt.% of polyethylene glycol.

Hence, this polymer composition was assessed as suitable for the controlled release of large proteins and the monoclonal antibody mAbX was encapsulated within similarly composed microparticles to further demonstrate the broad applicability of the SynBiosys® polymer platform in a third case study with a more detailed view on *in vitro* and *in vivo* performances of the material. With its direction against the epidermal growth factor receptor (EGFR), the IgG1 antibody mAbX plays a relevant role in the treatment of EGFR-expressing forms of cancer as it inhibits growth of tumor cells and recruits anti-tumoral immune responses.

Microspheres with a high mAbX loading of approximately 15 wt.% were obtained with a profoundly linear release behavior over 10-14 days *in vitro*. Additional to conventional HPLC-based quantification of aggregation and fragmentation, a powerful set of *in vitro* analysis methods for mAbX was implemented as part of this work. Similar to the mAbB studies, circular dichroism and fluorescence spectroscopy methods for mAbX were developed to examine the integrity of secondary and tertiary structures of *in vitro* released mAbX. Again, determination of the detection limits as well as reference signal limits of native and completely denatured antibody were part of the method implementation to allow the classification of protein integrity in *in vitro* release samples. Furthermore, an enzyme-linked immunosorbent assay (ELISA) as well as a cell-based mAbX assay were established to determine the functionality of released protein for binding its target receptor EGFR (ELISA) or for successfully inhibiting growth of colorectal cancer cells (cell-based assay). By extensively analyzing *in vitro* released mAbX by HPLC, ELISA, circular dichroism, fluorescence spectroscopy and cell-based functional assay the high integrity of the antibody over the complete release duration was confirmed. The integrity of mAbX was particularly high between days 7 to 10 of the *in vitro* release representing the period during which the highest amount of antibody was released. Similar to findings of mAbB studies, these results again confirmed the beneficial effects of integrating polyethylene glycol in the polymer matrix of SynBiosys® microparticles on protein stability.

In vivo studies were commenced with investigations on the immunogenic potential of mAbX-loaded microparticles. An assay for the simultaneous quantification of 32 systemic cytokines was established and results of an immunogenicity study confirmed a mild foreign body reaction to mAbX microparticles. Moreover, histochemical stains of the injection site were prepared showing a similar picture.

Two consecutive pharmacokinetic studies in healthy as well as in tumor-bearing immunodeficient mice were performed with mAbX-loaded SynBiosys® microspheres and dose-dependent plasma levels of mAbX were measured in both studies which is an aspirational property of formulation candidates [221]. The relative bioavailability of mAbX was in a promising range (approx. 40-50%) after subcutaneous administration of microparticle formulations to immunodeficient mice. However, results in healthy animals were more variable and the

bioavailability of mAbX was lower which indicated the formation of anti-drug antibodies (ADAs). Although the formation of ADAs was not measured explicitly, it is a logical explanation for the findings presented herein as their secretion is lowered in immunodeficient animals compared to healthy animals [286, 287]. Furthermore, the controlled release ability of the mAbX microparticle formulation was illustrated by a shift of the maximum plasma concentration to days 2 to 4 after administration which was clearly later compared to mAbX reference solution. Nevertheless, also antibody originating from reference solution exhibited a relatively long plasma circulation. A potential explanation was the recycling of mAbX by neonatal Fc receptors (FcRn). Especially murine FcRn can effectively bind to the Fc region of foreign-species antibodies prolonging their plasma half-life [290] which could have led to a reduced pronunciation of the controlled release ability of SynBiosys®-based mAbX microparticles. Further pharmacokinetic studies using FcRn-knockout mice would represent a reasonable starting point to highlight the controlled release ability of mAbX microspheres more effectively. Pharmacodynamic examination of SynBiosys® microparticles demonstrated the therapeutic efficacy of released mAbX which reduced tumor growth effectively and dose-dependently.

Interestingly, Schwendeman et al. as key opinion leader in the field of polymer-based controlled release stated in 2014 that one of the most challenging hurdles in protein release is the stability of the API during liberation while for peptides improvements of cost efficiency during manufacturing are of increasing relevance [225]. Remarkably, these obstacles of polymer-based release of peptide as well as protein therapeutics were successfully addressed herein by allowing significant dose reductions of exenatide and maintaining high stability of mAbB and mAbX after *in vitro* and *in vivo* release from SynBiosys® microspheres.

A majority of studies working on PLGA-based release of protein therapeutics use conventional model proteins like ovalbumin, bovine serum albumin, lysozyme or fluorescently labelled exemplary proteins [112, 120, 135, 136, 234, 235, 260, 291, 292]. Although these approaches allow conclusions on the influence of PLGA on protein stability and certainly offer specific advantages like cost benefits, the application of commonly not therapeutically used models lacks practical relevance. Therefore, the use of the marketed model APIs exenatide and mAbX or of the developmental candidate mAbB attach additional value to the findings of this work.

In conclusion, the SynBiosys® polymer platform proved to be a suitable technology for the controlled release of sensitive peptide and protein therapeutics. Advantages over conventional PLGA-based controlled release approaches were found in an accelerated onset of effect in combination with substantial reductions of the required dose as well as number of treatments in the case of the peptide therapeutic exenatide while also large proteins like monoclonal antibodies were released structurally and functionally intact as well as therapeutically active over 14 days.

Nevertheless, certain questions remained unclear and require further research. Conventionally, the injection volume for subcutaneous administration is limited to 1-3 mL as higher volumes lead to increased pain and lowered patient acceptance [293, 294]. Although occasionally higher subcutaneous injection volumes are observed (e.g. 5 mL for trastuzumab), the limited volume for subcutaneous administration poses challenges for achieving adequate doses of biologicals with controlled release formulations. Therefore, an examination of the maximum feasible loading of large proteins in SynBiosys® microparticles represents a reasonable future step. Furthermore, with respect to long half-lives and circulation periods of large protein therapeutics extended SynBiosys® release periods are required to ensure therapeutic benefits. Adapted polymer compositions with slower release rates would represent an option to achieve extended release over weeks to months. However, release behavior and integrity of the released protein still requires detailed investigation in future experiments.

SynBiosys® microparticles loaded with mAbX exhibited maximum cumulative release percentages of 80 to 90%. The root cause analysis and the characterization of residual protein potentially remaining in microparticles represent interesting topics for closer characterization of the polymer platform.

Finally, chemical modification analysis of released APIs was not part of this work. Nevertheless, as described earlier herein, chemical modifications like acylation and deamidation or maintenance of the initial glycosylation pattern are of relevance during polymer-based release. Therefore, analysis of these parameters in released model drugs would represent a useful addition to the results presented in this work.

Publications

Original research articles

Frank S, Ott M, Fricker G, Araujo J, Duarte A, Kordalivand N, Zuidema J, Visscher J, Hendriks G, Steendam R, Joehnck M, Krog A, and Henzler T: *Exenatide-loaded SynBiosys® microparticles with improved release kinetics and enhanced glycemic efficacy after subcutaneous administration to type II diabetic SD rats*. Journal of Controlled Release [submitted 08/2020]

References

1. Rader, R.A. (Re)defining biopharmaceutical. *Nat. Biotechnol.* **26**, 743-751 (2008).
2. Katz, K.A. 'Biologics': a clinically meaningless term. *Br. J. Dermatol.* **154**, 809-812 (2006).
3. Walsh, G. Biopharmaceuticals and biotechnology medicines: an issue of nomenclature. *Eur. J. Pharm. Sci.* **15**, 135-138 (2002).
4. Walsh, G. Biopharmaceutical benchmarks 2018. *Nat. Biotechnol.* **36**, 1136-1145 (2018).
5. Office of The Federal Register, E.I.L.L.C. Title 21 Food and Drugs Parts 600 to 799 (Revised as of January 3, 2020): 21-CFR. (U.S. Government Printing Office, 2020).
6. Walsh, G. & Murphy, B. Biopharmaceuticals, an Industrial Perspective. (Springer Science & Business Media, 1999).
7. Miller, W.L. & Baxter, J.D. Recombinant DNA--a new source of insulin. *Diabetologia* **18**, 431-436 (1980).
8. Galloway, J.A. et al. Clinical pharmacologic studies with human insulin (recombinant DNA). *Diabetes Care* **5 Suppl 2**, 13-22 (1982).
9. Chance, R.E. & Frank, B.H. Research, development, production, and safety of biosynthetic human insulin. *Diabetes Care* **16 Suppl 3**, 133-142 (1993).
10. Cosimi, A.B. Clinical development of Orthoclone OKT3. *Transplant. Proc.* **19**, 7-16 (1987).
11. Flodh, H. Human growth hormone produced with recombinant DNA technology: development and production. *Acta Paediatr. Scand. Suppl.* **325**, 1-9 (1986).
12. Cronin, M.J. Pioneering recombinant growth hormone manufacturing: pounds produced per mile of height. *J. Pediatr.* **131**, S5-7 (1997).
13. Nagata, S. et al. Synthesis in E. coli of a polypeptide with human leukocyte interferon activity. *Nature* **284**, 316 (1980).
14. Streuli, M., Nagata, S. & Weissmann, C. At least three human type alpha interferons: structure of alpha 2. *Science* **209**, 1343-1347 (1980).
15. Lin, F.-k.T.O., CA) (Kiren-Amgen, Inc. (Thousand Oaks, CA), United States; 1987).
16. Jacobs, K. et al. Isolation and characterization of genomic and cDNA clones of human erythropoietin. *Nature* **313**, 806-810 (1985).
17. Nagata, S. et al. Molecular cloning and expression of cDNA for human granulocyte colony-stimulating factor. *Nature* **319**, 415-418 (1986).
18. Souza, L.M. et al. Recombinant human granulocyte colony-stimulating factor: effects on normal and leukemic myeloid cells. *Science* **232**, 61 (1986).
19. Anderson, D. et al. A PrimatizedMAb to Human CD4 Causes Receptor Modulation, without Marked Reduction in CD4+T Cells in Chimpanzees:In Vitroandin VivoCharacterization of a MAb (IDEC-CE9.1) to Human CD4. *Clin. Immunol. Immnopathol.* **84**, 73-84 (1997).
20. Coelho, T. et al. Safety and efficacy of RNAi therapy for transthyretin amyloidosis. *N. Engl. J. Med.* **369**, 819-829 (2013).
21. Grilo, A.L. & Mantalaris, A. The Increasingly Human and Profitable Monoclonal Antibody Market. *Trends Biotechnol.* **37**, 9-16 (2019).
22. Leader, B., Baca, Q.J. & Golan, D.E. Protein therapeutics: a summary and pharmacological classification. *Nature Reviews Drug Discovery* **7**, 21 (2008).
23. Fosgerau, K. & Hoffmann, T. Peptide therapeutics: current status and future directions. *Drug Discov. Today* **20**, 122-128 (2015).
24. Van Der Walle, C. Peptide and Protein Delivery. (Elsevier Science, 2011).
25. Wright, J.C. & Burgess, D.J. Long Acting Injections and Implants. (Springer New York, 2012).
26. Jorgensen, L. & Nielson, H.M. Delivery Technologies for Biopharmaceuticals: Peptides, Proteins, Nucleic Acids and Vaccines. (Wiley, 2009).
27. Peters, T. in Advances in Protein Chemistry, Vol. 37. (eds. C.B. Anfinsen, J.T. Edsall & F.M. Richards) 161-245 (Academic Press, 1985).

28. Jiunn, H.L. Pharmacokinetics of Biotech Drugs: Peptides, Proteins and Monoclonal Antibodies. *Curr. Drug Metab.* **10**, 661-691 (2009).
29. Abuchowski, A., McCoy, J.R., Palczuk, N.C., van Es, T. & Davis, F.F. Effect of covalent attachment of polyethylene glycol on immunogenicity and circulating life of bovine liver catalase. *J. Biol. Chem.* **252**, 3582-3586 (1977).
30. Abuchowski, A., van Es, T., Palczuk, N.C. & Davis, F.F. Alteration of immunological properties of bovine serum albumin by covalent attachment of polyethylene glycol. *J. Biol. Chem.* **252**, 3578-3581 (1977).
31. Hershfield, M.S. et al. Treatment of Adenosine Deaminase Deficiency with Polyethylene Glycol–Modified Adenosine Deaminase. *New Engl. J. Med.* **316**, 589-596 (1987).
32. Ho, D.H. et al. Clinical pharmacology of polyethylene glycol-L-asparaginase. *Drug Metab. Dispos.* **14**, 349-352 (1986).
33. Molineux, G. The design and development of pegfilgrastim (PEG-rmetHuG-CSF, Neulasta). *Curr. Pharm. Des.* **10**, 1235-1244 (2004).
34. Kearns, C.M., Wang, W.C., Stute, N., Ihle, J.N. & Evans, W.E. Disposition of recombinant human granulocyte colony-stimulating factor in children with severe chronic neutropenia. *The Journal of Pediatrics* **123**, 471-479 (1993).
35. Muller, A.F., Kopchick, J.J., Flyvbjerg, A. & van der Lely, A.J. Clinical review 166: Growth hormone receptor antagonists. *J. Clin. Endocrinol. Metab.* **89**, 1503-1511 (2004).
36. Choy, E.H. et al. Efficacy of a novel PEGylated humanized anti-TNF fragment (CDP870) in patients with rheumatoid arthritis: a phase II double-blinded, randomized, dose-escalating trial. *Rheumatology (Oxford)* **41**, 1133-1137 (2002).
37. da Silva Freitas, D., Mero, A. & Pasut, G. Chemical and enzymatic site specific PEGylation of hGH. *Bioconjug. Chem.* **24**, 456-463 (2013).
38. Qiu, H. et al. Site-specific PEGylation of human thyroid stimulating hormone to prolong duration of action. *Bioconjug. Chem.* **24**, 408-418 (2013).
39. Na, D.H. & DeLuca, P.P. PEGylation of octreotide: I. Separation of positional isomers and stability against acylation by poly(D,L-lactide-co-glycolide). *Pharm. Res.* **22**, 736-742 (2005).
40. Torchilinl, V.P. & Papisov, M.I. Why do Polyethylene Glycol-Coated Liposomes Circulate So Long?: Molecular Mechanism of Liposome Steric Protection with Polyethylene Glycol: Role of Polymer Chain Flexibility. *J. Liposome Res.* **4**, 725-739 (1994).
41. Patel, A., Cholkar, K. & Mitra, A.K. Recent developments in protein and peptide parenteral delivery approaches. *Ther. Deliv.* **5**, 337-365 (2014).
42. Yamaoka, T., Tabata, Y. & Ikada, Y. Distribution and tissue uptake of poly (ethylene glycol) with different molecular weights after intravenous administration to mice. *J. Pharm. Sci.* **83**, 601-606 (1994).
43. Elliott, S. et al. Enhancement of therapeutic protein in vivo activities through glycoengineering. *Nat. Biotechnol.* **21**, 414-421 (2003).
44. Runkel, L. et al. Structural and Functional Differences between Glycosylated and Non-Glycosylated Forms of Human Interferon-Beta (IFN-beta). *Pharm. Res.* **15**, 641-649 (1998).
45. Langer, B.G., Weisel, J.W., Dinauer, P.A., Nagaswami, C. & Bell, W.R. Deglycosylation of fibrinogen accelerates polymerization and increases lateral aggregation of fibrin fibers. *J. Biol. Chem.* **263**, 15056-15063 (1988).
46. Stowers, A.W. et al. A recombinant vaccine expressed in the milk of transgenic mice protects Aotus monkeys from a lethal challenge with Plasmodium falciparum. *Proc. Natl. Acad. Sci. U. S. A.* **99**, 339-344 (2002).
47. Locatelli, F. & Vecchio, L.D. Darbepoetin alfa. Amgen. *Current opinion in investigational drugs (London, England : 2000)* **2**, 1097-1104 (2001).
48. Seipke, G., Berchthold, H., Geisen, K., Hilgenfeld, R. & Rosskamp, R. HOE 901: a new insulin with prolonged action. *Eur. J. Endocrinol.* **132**, 25 (1995).

49. Howey, D.C., Bowsher, R.R., Brunelle, R.L. & Woodworth, J.R. [Lys(B28), Pro(B29)]-human insulin. A rapidly absorbed analogue of human insulin. *Diabetes* **43**, 396-402 (1994).
50. Peppel, K., Crawford, D. & Beutler, B. A tumor necrosis factor (TNF) receptor-IgG heavy chain chimeric protein as a bivalent antagonist of TNF activity. *The Journal of experimental medicine* **174**, 1483-1489 (1991).
51. Iuga, A.O. & McGuire, M.J. Adherence and health care costs. *Risk Manag Healthc Policy* **7**, 35-44 (2014).
52. Grumezescu, A.M. Drug Targeting and Stimuli Sensitive Drug Delivery Systems. (Elsevier Science, 2018).
53. Shire, S.J., Gombotz, W., Bechtold-Peters, K. & Andya, J. Current Trends in Monoclonal Antibody Development and Manufacturing. (Springer New York, 2009).
54. Rodewald, R. & Kraehenbuhl, J.P. Receptor-mediated transport of IgG. *J. Cell Biol.* **99**, 159s-164s (1984).
55. Pivot, X. et al. Patients' preferences for subcutaneous trastuzumab versus conventional intravenous infusion for the adjuvant treatment of HER2-positive early breast cancer: final analysis of 488 patients in the international, randomized, two-cohort PrefHer study. *Ann. Oncol.* **25**, 1979-1987 (2014).
56. De Cock, E. et al. Time Savings with Rituximab Subcutaneous Injection versus Rituximab Intravenous Infusion: A Time and Motion Study in Eight Countries. *PLoS One* **11**, e0157957 (2016).
57. Yewey, G.L., Duysen, E.G., Cox, S.M. & Dunn, R.L. Delivery of proteins from a controlled release injectable implant. *Pharm. Biotechnol.* **10**, 93-117 (1997).
58. Zentner, G.M. et al. Biodegradable block copolymers for delivery of proteins and water-insoluble drugs. *J. Controlled Release* **72**, 203-215 (2001).
59. Cleland, J.L., Daugherty, A. & Mrsny, R. Emerging protein delivery methods. *Curr. Opin. Biotechnol.* **12**, 212-219 (2001).
60. Nicholson, R.I. et al. Therapeutic significance and the mechanism of action of the LH-RH agonist ICI 118630 in breast and prostate cancer. *J. Steroid Biochem.* **20**, 129-135 (1984).
61. Moul, J.W. & Civitelli, K. Managing advanced prostate cancer with Viadur (leuprolide acetate implant). *Urol. Nurs.* **21**, 385-388, 393-384; quiz 395-386 (2001).
62. Chertin, B. et al. An implant releasing the gonadotropin hormone-releasing hormone agonist histrelin maintains medical castration for up to 30 months in metastatic prostate cancer. *J. Urol.* **163**, 838-844 (2000).
63. Ju, X.-J. & Chu, L.-Y. in Microfluidics for Pharmaceutical Applications. (eds. H.A. Santos, D. Liu & H. Zhang) 217-280 (William Andrew Publishing, 2019).
64. Thakkar, H., Sharma, R.K., Mishra, A.K., Chuttani, K. & Murthy, R.R. Albumin microspheres as carriers for the antiarthritic drug celecoxib. *AAPS PharmSciTech* **6**, E65-E73 (2005).
65. Burgess, D.J. & Davis, S.S. Potential use of albumin microspheres as a drug delivery system: II. In vivo deposition and release of steroids. *Int. J. Pharm.* **46**, 69-76 (1988).
66. Nagai, N. et al. Preparation and characterization of collagen microspheres for sustained release of VEGF. *J. Mater. Sci. Mater. Med.* **21**, 1891-1898 (2010).
67. Dinarvand, R., Mahmoodi, S., Farboud, E., Salehi, M. & Atyabi, F. Preparation of gelatin microspheres containing lactic acid--effect of cross-linking on drug release. *Acta. Pharm.* **55**, 57-67 (2005).
68. Solorio, L., Zwolinski, C., Lund, A.W., Farrell, M.J. & Stegemann, J.P. Gelatin microspheres crosslinked with genipin for local delivery of growth factors. *J. Tissue Eng. Regen. Med.* **4**, 514-523 (2010).
69. Sun, Y., Tang, Y., Chu, M., Song, S. & Xin, Y. A convenient and adjustable surface-modified complex containing poly-L-glutamic acid conjugates as a vector for gene delivery. *International journal of nanomedicine* **3**, 249-256 (2008).
70. Portilla-Arias, J.A., Camargo, B., Garcia-Alvarez, M., de Ilarduya, A.M. & Munoz-Guerra, S. Nanoparticles made of microbial poly(gamma-glutamate)s for encapsulation and delivery of drugs and proteins. *J. Biomater. Sci. Polym. Ed.* **20**, 1065-1079 (2009).

71. Niu, X., Feng, Q., Wang, M., Guo, X. & Zheng, Q. Porous nano-HA/collagen/PLLA scaffold containing chitosan microspheres for controlled delivery of synthetic peptide derived from BMP-2. *J. Controlled Release* **134**, 111-117 (2009).
72. Guliyeva, Ü., Öner, F., Özsoy, Ş. & Haziroğlu, R. Chitosan microparticles containing plasmid DNA as potential oral gene delivery system. *Eur. J. Pharm. Biopharm.* **62**, 17-25 (2006).
73. Amidi, M. et al. Preparation and physicochemical characterization of supercritically dried insulin-loaded microparticles for pulmonary delivery. *Eur. J. Pharm. Biopharm.* **68**, 191-200 (2008).
74. Suarez, S., Grover, G.N., Braden, R.L., Christman, K.L. & Almutairi, A. Tunable protein release from acetalated dextran microparticles: a platform for delivery of protein therapeutics to the heart post-MI. *Biomacromolecules* **14**, 3927-3935 (2013).
75. Yuan, W., Wu, F., Guo, M. & Jin, T. Development of protein delivery microsphere system by a novel S/O/O/W multi-emulsion. *Eur. J. Pharm. Sci.* **36**, 212-218 (2009).
76. Coulembier, O., Degee, P., Hedrick, J. & Dubois, P. From controlled ring-opening polymerization to biodegradable aliphatic polyester: Especially poly(β-malic acid) derivatives. *Prog. Polym. Sci.* **31**, 723-747 (2006).
77. Boswell, G. & Scribner, R. (Google Patents, 1973).
78. Wu, X.S. & Wang, N. Synthesis, characterization, biodegradation, and drug delivery application of biodegradable lactic/glycolic acid polymers. Part II: biodegradation. *J. Biomater. Sci. Polym. Ed.* **12**, 21-34 (2001).
79. Okada, H. One- and three-month release injectable microspheres of the LH-RH superagonist leuprorelin acetate. *Adv. Drug Del. Rev.* **28**, 43-70 (1997).
80. Wang, N. & Wu, X.S. Synthesis, characterization, biodegradation, and drug delivery application of biodegradable lactic/glycolic acid oligomers: Part II. Biodegradation and drug delivery application. *J. Biomater. Sci. Polym. Ed.* **9**, 75-87 (1997).
81. Miller, R.A., Brady, J.M. & Cutright, D.E. Degradation rates of oral resorbable implants (polylactates and polyglycolates): rate modification with changes in PLA/PGA copolymer ratios. *J. Biomed. Mater. Res.* **11**, 711-719 (1977).
82. Okada, H., Ogawa, Y. & Yashiki, T. (Google Patents, 1987).
83. Avgoustakis, K. Polylactic-co-glycolic acid (PLGA). *Encyclopedia of biomaterials and biomedical engineering* **1**, 1-11 (2005).
84. Patlolla, A., Collins, G. & Livingston Arinzeh, T. Solvent-dependent properties of electrospun fibrous composites for bone tissue regeneration. *Acta Biomater.* **6**, 90-101 (2010).
85. Höglund, A., Hakkarainen, M. & Albertsson, A.C. Degradation Profile of Poly(ϵ-caprolactone)–the Influence of Macroscopic and Macromolecular Biomaterial Design. *Journal of Macromolecular Science, Part A* **44**, 1041-1046 (2007).
86. Darney, P.D., Monroe, S.E., Klaisle, C.M. & Alvarado, A. Clinical evaluation of the Capronor contraceptive implant: Preliminary report. *Am. J. Obstet. Gynecol.* **160**, 1292-1295 (1989).
87. Singh, J., Pandit, S., Bramwell, V.W. & Alpar, H.O. Diphtheria toxoid loaded poly-(epsilon-caprolactone) nanoparticles as mucosal vaccine delivery systems. *Methods* **38**, 96-105 (2006).
88. Huang, M.J. et al. One-step preparation of poly(epsilon-caprolactone)-poly(ethylene glycol)-poly(epsilon-caprolactone) nanoparticles for plasmid DNA delivery. *J. Biomed. Mater. Res. A* **86**, 979-986 (2008).
89. Pietrzak, W.S., Sarver, D.R. & Verstynen, M.L. Bioabsorbable polymer science for the practicing surgeon. *J. Craniofac. Surg.* **8**, 87-91 (1997).
90. Ray, J.A., Doddi, N., Regula, D., Williams, J.A. & Melveger, A. Polydioxanone (PDS), a novel monofilament synthetic absorbable suture. *Surg. Gynecol. Obstet.* **153**, 497-507 (1981).
91. Alavattem, S. & Brody, R.S. (Batelle Memorial Institute, Columbus, OH (US), United States; 2006).
92. Ghasemi, R. et al. mPEG-PLA and PLA-PEG-PLA nanoparticles as new carriers for delivery of recombinant human Growth Hormone (rhGH). *Sci. Rep.* **8**, 9854 (2018).

93. Buske, J. et al. Influence of PEG in PEG-PLGA microspheres on particle properties and protein release. *Eur. J. Pharm. Biopharm.* **81**, 57-63 (2012).
94. Yamaoka, T., Tabata, Y. & Ikada, Y. Distribution and Tissue Uptake of Poly(ethylene glycol) with Different Molecular Weights after Intravenous Administration to Mice. *J. Pharm. Sci.* **83**, 601-606 (1994).
95. Murty, S.B., Wei, Q., Thanoo, B.C. & DeLuca, P.P. In vivo release kinetics of octreotide acetate from experimental polymeric microsphere formulations using oil/water and oil/oil processes. *AAPS PharmSciTech* **5**, e49 (2004).
96. Cohen, S., Yoshioka, T., Lucarelli, M., Hwang, L.H. & Langer, R. Controlled delivery systems for proteins based on poly(lactic/glycolic acid) microspheres. *Pharm. Res.* **8**, 713-720 (1991).
97. Alex, R. & Bodmeier, R. Encapsulation of water-soluble drugs by a modified solvent evaporation method. I. Effect of process and formulation variables on drug entrapment. *J. Microencapsul.* **7**, 347-355 (1990).
98. Lee, P.W. & Pokorski, J.K. Poly(lactic-co-glycolic acid) devices: Production and applications for sustained protein delivery. *Wiley interdisciplinary reviews. Nanomedicine and nanobiotechnology* (2018).
99. Shi, M. et al. Double walled POE/PLGA microspheres: encapsulation of water-soluble and water-insoluble proteins and their release properties. *J. Controlled Release* **89**, 167-177 (2003).
100. Blanco-Príeto, M.a.J. et al. Characterization and morphological analysis of a cholecystokinin derivative peptide-loaded poly(lactide-co-glycolide) microspheres prepared by a water-in-oil-in-water emulsion solvent evaporation method. *J. Controlled Release* **43**, 81-87 (1997).
101. Silva, A.L. et al. Optimization of encapsulation of a synthetic long peptide in PLGA nanoparticles: Low-burst release is crucial for efficient CD8+ T cell activation. *Eur. J. Pharm. Biopharm.* **83**, 338-345 (2013).
102. Okochi, H. & Nakano, M. Comparative Study of Two Preparation Methods of w/o/w Emulsions : Stirring and Membrane Emulsification. *Chem. Pharm. Bull. (Tokyo)* **45**, 1323-1326 (1997).
103. Ma, G.-H., Sone, H. & Omi, S. Preparation of Uniform-Sized Polystyrene−Polyacrylamide Composite Microspheres from a W/O/W Emulsion by Membrane Emulsification Technique and Subsequent Suspension Polymerization. *Macromolecules* **37**, 2954-2964 (2004).
104. Joscelyne, S.M. & Trägårdh, G. Membrane emulsification — a literature review. *J. Membr. Sci.* **169**, 107-117 (2000).
105. Nihant, N., Grandfils, C., Jérôme, R. & Teyssié, P. Microencapsulation by coacervation of poly(lactide-co-glycolide) IV. Effect of the processing parameters on coacervation and encapsulation. *J. Controlled Release* **35**, 117-125 (1995).
106. Thomasin, C., Ho, N.T., Merkle, H.P. & Gander, B. Drug microencapsulation by PLA/PLGA coacervation in the light of thermodynamics. 1. Overview and theoretical considerations. *J. Pharm. Sci.* **87**, 259-268 (1998).
107. Nihant, N. et al. Microencapsulation by coacervation of poly(lactide-co-glycolide). III. Characterization of the final microspheres. *Polym. Int.* **34**, 289-299 (1994).
108. Sanders, L.M., McRae, G.I., Vitale, K.M. & Kell, B.A. Controlled delivery of an LHRH analogue from biodegradable injectable microspheres. *J. Controlled Release* **2**, 187-195 (1985).
109. Stassen, S. et al. Microencapsulation by coacervation of poly(lactide-co-glycolide): 1. Physicochemical characteristics of the phase separation process. *Polymer* **35**, 777-785 (1994).
110. Wu, X.S. Synthesis, Characterization, Biodegradation, and Drug Delivery Application of Biodegradable Lactic/Glycolic Acid Polymers: Part III. Drug Delivery Application. *Artificial Cells, Blood Substitutes, and Biotechnology* **32**, 575-591 (2004).
111. Chen, L., Apte, R.N. & Cohen, S. Characterization of PLGA microspheres for the controlled delivery of IL-1α for tumor immunotherapy. *J. Controlled Release* **43**, 261-272 (1997).

112. Igartua, M. et al. Stability of BSA encapsulated into PLGA microspheres using PAGE and capillary electrophoresis. *Int. J. Pharm.* **169**, 45-54 (1998).
113. Xing, D.K.L. et al. Physicochemical and immunological studies on the stability of free and microsphere-encapsulated tetanus toxoid in vitro. *Vaccine* **14**, 1205-1213 (1996).
114. Fu, K., Pack, D.W., Klibanov, A.M. & Langer, R. Visual Evidence of Acidic Environment Within Degrading Poly(lactic-co-glycolic acid) (PLGA) Microspheres. *Pharm. Res.* **17**, 100-106 (2000).
115. Shao, P.G. & Bailey, L.C. Porcine insulin biodegradable polyester microspheres: stability and in vitro release characteristics. *Pharm. Dev. Technol.* **5**, 1-9 (2000).
116. Ding, A.G. & Schwendeman, S.P. Acidic microclimate pH distribution in PLGA microspheres monitored by confocal laser scanning microscopy. *Pharm. Res.* **25**, 2041-2052 (2008).
117. Lu, W. & Park, T.G. Protein release from poly(lactic-co-glycolic acid) microspheres: protein stability problems. *PDA J. Pharm. Sci. Technol.* **49**, 13-19 (1995).
118. Oliyai, C., Patel, J.P., Carr, L. & Borchardt, R.T. Solid state chemical instability of an asparaginyl residue in a model hexapeptide. *J. Pharm. Sci. Technol.* **48**, 167-123 (1994).
119. Sandor, M., Riechel, A., Kaplan, I. & Mathiowitz, E. Effect of lecithin and MgCO3 as additives on the enzymatic activity of carbonic anhydrase encapsulated in poly(lactide-co-glycolide) (PLGA) microspheres. *Biochim. Biophys. Acta* **1570**, 63-74 (2002).
120. Zhu, G., Mallery, S.R. & Schwendeman, S.P. Stabilization of proteins encapsulated in injectable poly (lactide- co-glycolide). *Nat. Biotechnol.* **18**, 52-57 (2000).
121. Zambaux, M.F., Bonneaux, F., Gref, R., Dellacherie, E. & Vigneron, C. Preparation and characterization of protein C-loaded PLA nanoparticles. *J. Controlled Release* **60**, 179-188 (1999).
122. Manuela Gaspar, M., Blanco, D., Cruz, M.E.M. & José Alonso, M.a. Formulation of l-asparaginase-loaded poly(lactide-co-glycolide) nanoparticles: influence of polymer properties on enzyme loading, activity and in vitro release. *J. Controlled Release* **52**, 53-62 (1998).
123. Blanco, M.D. & Alonso, M.J. Development and characterization of protein-loaded poly(lactide-co-glycolide) nanospheres. *Eur. J. Pharm. Biopharm.* **43**, 287-294 (1997).
124. Park, T.G., Lee, H.Y. & Nam, Y.S. A new preparation method for protein loaded poly (D, L-lactic-co-glycolic acid) microspheres and protein release mechanism study. *J. Controlled Release* **55**, 181-191 (1998).
125. Ibrahim, M.A., Ismail, A., Fetouh, M.I. & Göpferich, A. Stability of insulin during the erosion of poly(lactic acid) and poly(lactic-co-glycolic acid) microspheres. *J. Controlled Release* **106**, 241-252 (2005).
126. Uchida, T., Yagi, A., Oda, Y., Nakada, Y. & Goto, S. Instability of bovine insulin in poly(lactide-co-glycolide) (PLGA) microspheres. *Chem. Pharm. Bull. (Tokyo)* **44**, 235-236 (1996).
127. Houchin, M.L., Heppert, K. & Topp, E.M. Deamidation, acylation and proteolysis of a model peptide in PLGA films. *J. Controlled Release* **112**, 111-119 (2006).
128. Lucke, A., Kiermaier, J. & Gopferich, A. Peptide acylation by poly(alpha-hydroxy esters). *Pharm. Res.* **19**, 175-181 (2002).
129. Murty, S.B., Na, D.H., Thanoo, B.C. & DeLuca, P.P. Impurity formation studies with peptide-loaded polymeric microspheres Part II. In vitro evaluation. *Int. J. Pharm.* **297**, 62-72 (2005).
130. Murty, S.B., Goodman, J., Thanoo, B.C. & DeLuca, P.P. Identification of chemically modified peptide from poly(D,L-lactide-co-glycolide) microspheres under in vitro release conditions. *AAPS PharmSciTech* **4**, E50 (2003).
131. Ara, M., Watanabe, M. & Imai, Y. Effect of blending calcium compounds on hydrolytic degradation of poly(dl-lactic acid-co-glycolic acid). *Biomaterials* **23**, 2479-2483 (2002).
132. Marinina, J., Shenderova, A., Mallery, S.R. & Schwendeman, S.P. Stabilization of vinca alkaloids encapsulated in poly(lactide-co-glycolide) microspheres. *Pharm. Res.* **17**, 677-683 (2000).

133. Na, D.H., Lee, K.C. & DeLuca, P.P. PEGylation of octreotide: II. Effect of N-terminal mono-PEGylation on biological activity and pharmacokinetics. *Pharm. Res.* **22**, 743-749 (2005).
134. Hissink, C.E., Steendam, R., Meyboom, R. & Flipsen, T.A.C. WO2005068533: Biodegradable multi-block co-polymers. (2005).
135. Tran, V.T. et al. Protein-loaded PLGA-PEG-PLGA microspheres: a tool for cell therapy. *Eur. J. Pharm. Sci.* **45**, 128-137 (2012).
136. Kim, J.H., Taluja, A., Knutson, K. & Han Bae, Y. Stability of bovine serum albumin complexed with PEG-poly(L-histidine) diblock copolymer in PLGA microspheres. *J. Control. Release* **109**, 86-100 (2005).
137. Kissel, T., Li, Y. & Unger, F. ABA-triblock copolymers from biodegradable polyester A-blocks and hydrophilic poly(ethylene oxide) B-blocks as a candidate for in situ forming hydrogel delivery systems for proteins. *Adv Drug Deliv Rev* **54**, 99-134 (2002).
138. Teekamp, N. et al. Polymeric microspheres for the sustained release of a protein-based drug carrier targeting the PDGFbeta-receptor in the fibrotic kidney. *Int. J. Pharm.* **534**, 229-236 (2017).
139. van Dijk, F. et al. Pharmacokinetics of a sustained release formulation of PDGFbeta-receptor directed carrier proteins to target the fibrotic liver. *J. Control. Release* **269**, 258-265 (2018).
140. Stankovic, M. et al. Tailored protein release from biodegradable poly(epsilon-caprolactone-PEG)-b-poly(epsilon-caprolactone) multiblock-copolymer implants. *Eur. J. Pharm. Biopharm.* **87**, 329-337 (2014).
141. Zandstra, J. et al. Microsphere-Based Rapamycin Delivery, Systemic Versus Local Administration in a Rat Model of Renal Ischemia/Reperfusion Injury. *Pharm. Res.* **32**, 3238-3247 (2015).
142. Sandker, M.J. et al. Degradation, Intra-Articular Biocompatibility, Drug Release, and Bioactivity of Tacrolimus-Loaded Poly(d-l-lactide-PEG)-b-poly(l-lactide) Multiblock Copolymer-Based Monospheres. *ACS Biomaterials Science & Engineering* **4**, 2390-2403 (2018).
143. Ramazani, F. et al. Sunitinib microspheres based on [PDLLA-PEG-PDLLA]-b-PLLA multi-block copolymers for ocular drug delivery. *Eur. J. Pharm. Biopharm.* **95**, 368-377 (2015).
144. Lockwood, N.A. et al. In vitro and in vivo characterization of novel biodegradable polymers for application as drug-eluting stent coatings. *J. Biomater. Sci. Polym. Ed.* **21**, 529-552 (2010).
145. Saeedi, P. et al. Global and regional diabetes prevalence estimates for 2019 and projections for 2030 and 2045: Results from the International Diabetes Federation Diabetes Atlas, 9(th) edition. *Diabetes Res. Clin. Pract.* **157**, 107843 (2019).
146. IDF in 9th edn. Brussels, Vol. 2020 (International Diabetes Federation, Belgium; 2019).
147. DeFronzo, R.A. Banting Lecture. From the triumvirate to the ominous octet: a new paradigm for the treatment of type 2 diabetes mellitus. *Diabetes* **58**, 773-795 (2009).
148. DeFronzo, R.A. et al. Type 2 diabetes mellitus. *Nat Rev Dis Primers* **1**, 15019 (2015).
149. Davidson, M.B., Bate, G. & Kirkpatrick, P. Exenatide. *Nat. Rev. Drug Discov.* **4**, 713-714 (2005).
150. Eng, J., Kleinman, W.A., Singh, L., Singh, G. & Raufman, J.P. Isolation and characterization of exendin-4, an exendin-3 analogue, from Heloderma suspectum venom. Further evidence for an exendin receptor on dispersed acini from guinea pig pancreas. *J. Biol. Chem.* **267**, 7402-7405 (1992).
151. Mack, C.M. et al. Antiobesity action of peripheral exenatide (exendin-4) in rodents: effects on food intake, body weight, metabolic status and side-effect measures. *Int. J. Obesity* **30**, 1332-1340 (2006).
152. Wishart, D.S. et al. DrugBank: a comprehensive resource for in silico drug discovery and exploration. *Nucleic Acids Res.* **34**, D668-672 (2006).
153. Park, H. et al. Effect of Stabilizers on Encapsulation Efficiency and Release Behavior of Exenatide-Loaded PLGA Microsphere Prepared by the W/O/W Solvent Evaporation Method. *Pharmaceutics* **11** (2019).

154. Eng, J., Gutterman, V. & Nicolis, C. Exendin (9-39) amide inhibits the insulin secretagogue activity of exendin 4 and GLP-1 but enhances that of glucagon in dogs. *Digestion* **54** (1993).
155. Mojsov, S., Weir, G. & Habener, J. Insulinotropin: glucagon-like peptide I (7-37) co-encoded in the glucagon gene is a potent stimulator of insulin release in the perfused rat pancreas. *The Journal of clinical investigation* **79**, 616-619 (1987).
156. Kolterman, O.G. et al. Synthetic exendin-4 (exenatide) significantly reduces postprandial and fasting plasma glucose in subjects with type 2 diabetes. *The Journal of Clinical Endocrinology & Metabolism* **88**, 3082-3089 (2003).
157. Kolterman, O.G. et al. Pharmacokinetics, pharmacodynamics, and safety of exenatide in patients with type 2 diabetes mellitus. *Am. J. Health Syst. Pharm.* **62**, 173-181 (2005).
158. Gedulin, B.R. et al. Exenatide (exendin-4) improves insulin sensitivity and β-cell mass in insulin-resistant obese fa/fa Zucker rats independent of glycemia and body weight. *Endocrinology* **146**, 2069-2076 (2005).
159. Szayna, M. et al. Exendin-4 decelerates food intake, weight gain, and fat deposition in Zucker rats. *Endocrinology* **141**, 1936-1941 (2000).
160. Wright, S.G. et al. US 2005/0271702 A1: Polymer-based sustained release device. (2005).
161. Gilroy, C.A., Luginbuhl, K.M. & Chilkoti, A. Controlled release of biologics for the treatment of type 2 diabetes. *J. Control. Release* **240**, 151-164 (2016).
162. Köhler, G. & Milstein, C. Continuous cultures of fused cells secreting antibody of predefined specificity. *Nature* **256**, 495-497 (1975).
163. Morrison, S.L., Johnson, M.J., Herzenberg, L.A. & Oi, V.T. Chimeric human antibody molecules: mouse antigen-binding domains with human constant region domains. *Proc. Natl. Acad. Sci. U. S. A.* **81**, 6851-6855 (1984).
164. Jones, P.T., Dear, P.H., Foote, J., Neuberger, M.S. & Winter, G. Replacing the complementarity-determining regions in a human antibody with those from a mouse. *Nature* **321**, 522-525 (1986).
165. Salfeld, J., Kaymakcalan, Z., Tracey, D., Roberts, A. & Kamen, R. Generation of fully human anti-TNF antibody D2E7. *Arthritis Rheum.* **41** (1998).
166. Vidarsson, G., Dekkers, G. & Rispens, T. IgG Subclasses and Allotypes: From Structure to Effector Functions. *Front. Immunol.* **5** (2014).
167. Le Basle, Y., Chennell, P., Tokhadze, N., Astier, A. & Sautou, V. Physicochemical Stability of Monoclonal Antibodies: A Review. *J. Pharm. Sci.* **109**, 169-190 (2020).
168. Yang, G., Murashige, D.S., Humphrey, S.J. & James, D.E. A Positive Feedback Loop between Akt and mTORC2 via SIN1 Phosphorylation. *Cell Rep* **12**, 937-943 (2015).
169. Laplante, M. & Sabatini, D.M. mTOR signaling in growth control and disease. *Cell* **149**, 274-293 (2012).
170. Humphrey, S.J. et al. Dynamic adipocyte phosphoproteome reveals that Akt directly regulates mTORC2. *Cell Metab.* **17**, 1009-1020 (2013).
171. Cohen, S., Carpenter, G. & King, L., Jr. Epidermal growth factor-receptor-protein kinase interactions. Co-purification of receptor and epidermal growth factor-enhanced phosphorylation activity. *J. Biol. Chem.* **255**, 4834-4842 (1980).
172. Hynes, N.E. & MacDonald, G. ErbB receptors and signaling pathways in cancer. *Curr. Opin. Cell Biol.* **21**, 177-184 (2009).
173. Sheng, Q. & Liu, J. The therapeutic potential of targeting the EGFR family in epithelial ovarian cancer. *Br. J. Cancer* **104**, 1241-1245 (2011).
174. Wee, P. & Wang, Z. Epidermal Growth Factor Receptor Cell Proliferation Signaling Pathways. *Cancers (Basel)* **9** (2017).
175. Sharma, S.V., Bell, D.W., Settleman, J. & Haber, D.A. Epidermal growth factor receptor mutations in lung cancer. *Nat. Rev. Cancer* **7**, 169-181 (2007).
176. Hilario, E.C. et al. An Improved Method of Predicting Extinction Coefficients for the Determination of Protein Concentration. *PDA J. Pharm. Sci. Technol.* **71**, 127-135 (2017).

177. Harn, N. et al. in Current Trends in Monoclonal Antibody Development and Manufacturing. (eds. S.J. Shire, W. Gombotz, K. Bechtold-Peters & J. Andya) 229-246 (Springer New York, New York, NY; 2010).
178. Mehta, S.B., Bee, J.S., Randolph, T.W. & Carpenter, J.F. Partial unfolding of a monoclonal antibody: role of a single domain in driving protein aggregation. *Biochemistry* **53**, 3367-3377 (2014).
179. Buijs, J., Norde, W. & Lichtenbelt, J.W.T. Changes in the Secondary Structure of Adsorbed IgG and F(ab')2 Studied by FTIR Spectroscopy. *Langmuir* **12**, 1605-1613 (1996).
180. Vermeer, A.W., Bremer, M.G. & Norde, W. Structural changes of IgG induced by heat treatment and by adsorption onto a hydrophobic Teflon surface studied by circular dichroism spectroscopy. *Biochim. Biophys. Acta* **1425**, 1-12 (1998).
181. Joshi, V., Shivach, T., Yadav, N. & Rathore, A.S. Circular dichroism spectroscopy as a tool for monitoring aggregation in monoclonal antibody therapeutics. *Anal. Chem.* **86**, 11606-11613 (2014).
182. Bork, P., Holm, L. & Sander, C. The immunoglobulin fold. Structural classification, sequence patterns and common core. *J. Mol. Biol.* **242**, 309-320 (1994).
183. Padlan, E.A. Anatomy of the antibody molecule. *Mol. Immunol.* **31**, 169-217 (1994).
184. Kelly, S.M., Jess, T.J. & Price, N.C. How to study proteins by circular dichroism. *Biochim. Biophys. Acta* **1751**, 119-139 (2005).
185. Tanford, C., Kawahara, K. & Lapanje, S. Proteins as Random Coils. I. Intrinsic Viscosities and Sedimentation Coefficients in Concentrated Guanidine Hydrochloride. *J. Am. Chem. Soc.* **89**, 729-736 (1967).
186. Lakowicz, J. Principles of Fluorescence Spectroscopy, Vol. 1. (2006).
187. Fonin, A.V., Sulatskaya, A.I., Kuznetsova, I.M. & Turoverov, K.K. Fluorescence of dyes in solutions with high absorbance. Inner filter effect correction. *PLoS One* **9**, e103878 (2014).
188. Parker, C.A. & Rees, W.T. Fluorescence spectrometry. A review. *Analyst* **87**, 83-111 (1962).
189. Stokes, G.G. On the Change of Refrangibility of Light. *Philosophical Transactions of the Royal Society of London* **142**, 463-562 (1852).
190. Aydin, S. A short history, principles, and types of ELISA, and our laboratory experience with peptide/protein analyses using ELISA. *Peptides* **72**, 4-15 (2015).
191. Shrivastava, A. & Gupta, V. Methods for the determination of limit of detection and limit of quantitation of the analytical methods. *Chronicles of Young Scientists* **2**, 21 (2011).
192. Furman, B.L. The development of Byetta (exenatide) from the venom of the Gila monster as an anti-diabetic agent. *Toxicon* **59**, 464-471 (2012).
193. Boman, B.M. et al. 541-548 (Springer Japan, Tokyo; 1990).
194. Skovso, S. Modeling type 2 diabetes in rats using high fat diet and streptozotocin. *J Diabetes Investig* **5**, 349-358 (2014).
195. Reed, M.J. et al. A new rat model of type 2 diabetes: the fat-fed, streptozotocin-treated rat. *Metabolism* **49**, 1390-1394 (2000).
196. Junod, A., Lambert, A.E., Stauffacher, W. & Renold, A.E. Diabetogenic action of streptozotocin: relationship of dose to metabolic response. *The Journal of clinical investigation* **48**, 2129-2139 (1969).
197. Furman, B.L. Streptozotocin-Induced Diabetic Models in Mice and Rats. *Curr. Protoc. Pharmacol.* **70**, 5.47.41-20 (2015).
198. Barnes, D.W. Epidermal growth factor inhibits growth of A431 human epidermoid carcinoma in serum-free cell culture. *The Journal of Cell Biology* **93**, 1 (1982).
199. Haigler, H., Ash, J.F., Singer, S.J. & Cohen, S. Visualization by fluorescence of the binding and internalization of epidermal growth factor in human carcinoma cells A-431. *Proceedings of the National Academy of Sciences* **75**, 3317 (1978).
200. John, W.G. Glycated Haemoglobin Analysis. *Ann. Clin. Biochem.* **34**, 17-31 (1997).
201. Little, R.R., Rohlfing, C.L., Sacks, D.B. & National Glycohemoglobin Standardization Program Steering, C. Status of hemoglobin A1c measurement and goals for

improvement: from chaos to order for improving diabetes care. *Clin. Chem.* **57**, 205-214 (2011).
202. Jaisson, S. et al. Interference of the most frequent haemoglobin variants on quantification of HbA1c: comparison between the LC-MS (IFCC reference method) and three routinely used methods. *Diabetes Metab.* **39**, 363-369 (2013).
203. Al-Abed, Y. et al. Inhibition of advanced glycation endproduct formation by acetaldehyde: Role in the cardioprotective effect of ethanol. *Proc. Natl. Acad. Sci. U. S. A.* **96**, 2385-2390 (1999).
204. Djoba Siawaya, J.F. et al. An evaluation of commercial fluorescent bead-based luminex cytokine assays. *PLoS One* **3**, e2535 (2008).
205. Khan, S.S., Smith, M.S., Reda, D., Suffredini, A.F. & McCoy, J.P., Jr. Multiplex bead array assays for detection of soluble cytokines: comparisons of sensitivity and quantitative values among kits from multiple manufacturers. *Cytometry B Clin. Cytom.* **61**, 35-39 (2004).
206. Fischer, A.H., Jacobson, K.A., Rose, J. & Zeller, R. Hematoxylin and eosin staining of tissue and cell sections. *CSH protocols* **2008**, pdb.prot4986 (2008).
207. Elahi, D. et al. GLP-1 (9-36) amide, cleavage product of GLP-1 (7-36) amide, is a glucoregulatory peptide. *Obesity (Silver Spring)* **16**, 1501-1509 (2008).
208. Knudsen, L.B. & Pridal, L. Glucagon-like peptide-1-(9-36) amide is a major metabolite of glucagon-like peptide-1-(7-36) amide after in vivo administration to dogs, and it acts as an antagonist on the pancreatic receptor. *Eur. J. Pharmacol.* **318**, 429-435 (1996).
209. DeYoung, M.B., MacConell, L., Sarin, V., Trautmann, M. & Herbert, P. Encapsulation of exenatide in poly-(D,L-lactide-co-glycolide) microspheres produced an investigational long-acting once-weekly formulation for type 2 diabetes. *Diabetes Technol. Ther.* **13**, 1145-1154 (2011).
210. Scott, L.J. Exenatide Extended-Release. *Drugs* **72**, 1679-1707 (2012).
211. Fineman, M. et al. Pharmacokinetics and Pharmacodynamics of Exenatide Extended-Release After Single and Multiple Dosing. *Clin. Pharmacokinet.* **50**, 65-74 (2011).
212. Shi, L. et al. Effect of molecular weight of poly (Lacticco-Glycolide) on properties of exenatide-loaded microspheres. *China Modern Medicine* **7**, 117-118 (2009).
213. Liu, B. et al. Preparation, characterization, and pharmacodynamics of exenatide-loaded poly(DL-lactic-co-glycolic acid) microspheres. *Chem. Pharm. Bull. (Tokyo)* **58**, 1474-1479 (2010).
214. Gong, N. et al. Site-specific PEGylation of exenatide analogues markedly improved their glucoregulatory activity. *Br. J. Pharmacol.* **163**, 399-412 (2011).
215. Lau, J. & Hansen, T.K. (Google Patents, 2011).
216. Golla, R. & Seethala, R. A homogeneous enzyme fragment complementation cyclic AMP screen for GPCR agonists. *J. Biomol. Screen.* **7**, 515-525 (2002).
217. Giteau, A., Venier-Julienne, M.C., Aubert-Pouessel, A. & Benoit, J.P. How to achieve sustained and complete protein release from PLGA-based microparticles? *Int. J. Pharm.* **350**, 14-26 (2008).
218. Péan, J.-M. et al. Why Does PEG 400 Co-Encapsulation Improve NGF Stability and Release from PLGA Biodegradable Microspheres? *Pharm. Res.* **16**, 1294-1299 (1999).
219. Tsirogianni, A.K., Moutsopoulos, N.M. & Moutsopoulos, H.M. Wound healing: immunological aspects. *Injury* **37 Suppl 1**, S5-12 (2006).
220. Sakallioglu, A.E. et al. Sustained local application of low-dose epidermal growth factor on steroid-inhibited colonic wound healing. *J. Pediatr. Surg.* **39**, 591-595 (2004).
221. Eisenblaetter, T. & Teichert, L. in Drug Discovery and Evaluation: Methods in Clinical Pharmacology. (eds. H.G. Vogel, J. Maas & A. Gebauer) 23-40 (Springer Berlin Heidelberg, Berlin, Heidelberg; 2011).
222. Collins, D.S. et al. Optimizing the Bioavailability of Subcutaneously Administered Biotherapeutics Through Mechanochemical Drivers. *Pharm. Res.* **34**, 2000-2011 (2017).
223. Richter, W.F., Bhansali, S.G. & Morris, M.E. Mechanistic determinants of biotherapeutics absorption following SC administration. *AAPS J* **14**, 559-570 (2012).

224. Kinnunen, H.M. & Mrsny, R.J. Improving the outcomes of biopharmaceutical delivery via the subcutaneous route by understanding the chemical, physical and physiological properties of the subcutaneous injection site. *J. Controlled Release* **182**, 22-32 (2014).
225. Schwendeman, S.P., Shah, R.B., Bailey, B.A. & Schwendeman, A.S. Injectable controlled release depots for large molecules. *J. Control. Release* **190**, 240-253 (2014).
226. Pérez-Tilve, D. et al. Exendin-4 increases blood glucose levels acutely in rats by activation of the sympathetic nervous system. *American journal of physiology. Endocrinology and metabolism* **298**, E1088-E1096 (2010).
227. Aziz, A., Anderson, G.H., Giacca, A. & Cho, F. Hyperglycemia after protein ingestion concurrent with injection of a GLP-1 receptor agonist in rats: a possible role for dietary peptides. *Am. J. Physiol. Regul. Integr. Comp. Physiol.* **289**, R688-694 (2005).
228. Jessen, L. et al. Central Nervous System GLP-1 Receptors Regulate Islet Hormone Secretion and Glucose Homeostasis in Male Rats. *Endocrinology* **158**, 2124-2133 (2017).
229. Vahl, T.P. et al. Glucagon-like peptide-1 (GLP-1) receptors expressed on nerve terminals in the portal vein mediate the effects of endogenous GLP-1 on glucose tolerance in rats. *Endocrinology* **148**, 4965-4973 (2007).
230. Sandoval, D. & Sisley, S.R. Brain GLP-1 and insulin sensitivity. *Mol. Cell. Endocrinol.* **418 Pt 1**, 27-32 (2015).
231. Li, X.G. et al. Pharmacokinetic/pharmacodynamic studies on exenatide in diabetic rats. *Acta Pharmacol. Sin.* **33**, 1379-1386 (2012).
232. Sherwani, S.I., Khan, H.A., Ekhzaimy, A., Masood, A. & Sakharkar, M.K. Significance of HbA1c Test in Diagnosis and Prognosis of Diabetic Patients. *Biomark Insights* **11**, 95-104 (2016).
233. Campbell, L., Pepper, T. & Shipman, K. HbA1c: a review of non-glycaemic variables. *J. Clin. Pathol.* **72**, 12-19 (2019).
234. Yeh, M.-K., Jenkins, P.G., Davis, S.S. & Coombes, A.G.A. Improving the delivery capacity of microparticle systems using blends of poly(DL-lactide co-glycolide) and poly(ethylene glycol). *J. Controlled Release* **37**, 1-9 (1995).
235. Cleek, R.L., Ting, K.C., G. Eskin, S. & Mikos, A.G. Microparticles of poly(dl-lactic-co-glycolic acid)/poly(ethylene glycol) blends for controlled drug delivery. *J. Controlled Release* **48**, 259-268 (1997).
236. Hedberg, E.L., Shih, C.K., Solchaga, L.A., Caplan, A.I. & Mikos, A.G. Controlled release of hyaluronan oligomers from biodegradable polymeric microparticle carriers. *J. Control. Release* **100**, 257-266 (2004).
237. Lowe, D. et al. Aggregation, stability, and formulation of human antibody therapeutics. *Adv. Protein Chem. Struct. Biol.* **84**, 41-61 (2011).
238. Arakawa, T., Ejima, D., Li, T. & Philo, J.S. The critical role of mobile phase composition in size exclusion chromatography of protein pharmaceuticals. *J. Pharm. Sci.* **99**, 1674-1692 (2010).
239. Wang, W. & Roberts, C.J. Protein aggregation - Mechanisms, detection, and control. *Int. J. Pharm.* **550**, 251-268 (2018).
240. Kelly, S.M. & Price, N.C. The application of circular dichroism to studies of protein folding and unfolding. *Biochim. Biophys. Acta* **1338**, 161-185 (1997).
241. Greenfield, N.J. Using circular dichroism spectra to estimate protein secondary structure. *Nat. Protoc.* **1**, 2876-2890 (2007).
242. Matsuo, K., Sakurada, Y., Yonehara, R., Kataoka, M. & Gekko, K. Secondary-structure analysis of denatured proteins by vacuum-ultraviolet circular dichroism spectroscopy. *Biophys. J.* **92**, 4088-4096 (2007).
243. Robinson, D.R. & Jencks, W.P. THE EFFECT OF COMPOUNDS OF THE UREA-GUANIDINIUM CLASS ON THE ACTIVITY COEFFICIENT OF ACETYLTETRAGLYCINE ETHYL ESTER AND RELATED COMPOUNDS. *J. Am. Chem. Soc.* **87**, 2462-2470 (1965).
244. O'Brien, E.P., Dima, R.I., Brooks, B. & Thirumalai, D. Interactions between Hydrophobic and Ionic Solutes in Aqueous Guanidinium Chloride and Urea Solutions:

Lessons for Protein Denaturation Mechanism. *J. Am. Chem. Soc.* **129**, 7346-7353 (2007).
245. Singh, R., Hassan, M.I., Islam, A. & Ahmad, F. Cooperative Unfolding of Residual Structure in Heat Denatured Proteins by Urea and Guanidinium Chloride. *PLoS One* **10**, e0128740 (2015).
246. van de Weert, M., Hoechstetter, J., Hennink, W.E. & Crommelin, D.J. The effect of a water/organic solvent interface on the structural stability of lysozyme. *J. Control. Release* **68**, 351-359 (2000).
247. Kwon, Y.M., Baudys, M., Knutson, K. & Kim, S.W. In Situ Study of Insulin Aggregation Induced by Water-Organic Solvent Interface. *Pharm. Res.* **18**, 1754-1759 (2001).
248. van de Weert, M., Hennink, W.E. & Jiskoot, W. Protein Instability in Poly(Lactic-co-Glycolic Acid) Microparticles. *Pharm. Res.* **17**, 1159-1167 (2000).
249. Makadia, H.K. & Siegel, S.J. Poly Lactic-co-Glycolic Acid (PLGA) as Biodegradable Controlled Drug Delivery Carrier. *Polymers* **3**, 1377-1397 (2011).
250. Pisal, D.S., Kosloski, M.P. & Balu-Iyer, S.V. Delivery of therapeutic proteins. *J. Pharm. Sci.* **99**, 2557-2575 (2010).
251. Kang, J. & Schwendeman, S.P. Comparison of the effects of Mg(OH)2 and sucrose on the stability of bovine serum albumin encapsulated in injectable poly(d,l-lactide-co-glycolide) implants. *Biomaterials* **23**, 239-245 (2002).
252. Jiang, W. & Schwendeman, S.P. Stabilization of tetanus toxoid encapsulated in PLGA microspheres. *Mol. Pharm.* **5**, 808-817 (2008).
253. Na, D.H., Murty, S.B., Lee, K.C., Thanoo, B.C. & DeLuca, P.P. Preparation and stability of poly(ethylene glycol) (PEG)ylated octreotide for application to microsphere delivery. *AAPS PharmSciTech* **4**, 574-580 (2003).
254. Johnson, O.L. et al. A month–long effect from a single injection of microencapsulated human growth hormone. *Nat. Med.* **2**, 795-799 (1996).
255. Cleland, J.L. & Jones, A.J.S. Stable Formulations of Recombinant Human Growth Hormone and Interferon-γ for Microencapsulation in Biodegradable Mircospheres. *Pharm. Res.* **13**, 1464-1475 (1996).
256. Shirangi, M. et al. Inhibition of Octreotide Acylation Inside PLGA Microspheres by Derivatization of the Amines of the Peptide with a Self-Immolative Protecting Group. *Bioconjug. Chem.* **27**, 576-585 (2016).
257. Zhu, G. & Schwendeman, S. in Proceed. Int'l. Symp. Control. Rel. Bioact. Mater, Vol. 26 6446 (1999).
258. Wu, X.S. (ed.) Preparation, characterization, and drug delivery applications of microspheres based on biodegradable lactic/glycolic acid polymers. (Marcel Dekker, New York; 1995).
259. Vidmar, V. & Jalšenjak, I. Poly(lactic acid) microencapsulated oxytetracycline: in vitro and in vivo evaluation. *J. Microencapsulation* **1**, 131-136 (1984).
260. Ciombor, D.M. et al. Encapsulation of BSA using a modified W/O/O emulsion solvent removal method. *J. Microencapsul.* **23**, 183-194 (2006).
261. Slameňová, D. & Gabelová, A. The effects of sodium azide on mammalian cells cultivated in vitro. *Mutation Research/Fundamental and Molecular Mechanisms of Mutagenesis* **71**, 253-261 (1980).
262. Hennessey, J.P. & Johnson, W.C., Jr. Experimental errors and their effect on analyzing circular dichroism spectra of proteins. *Anal. Biochem.* **125**, 177-188 (1982).
263. Miles, A.J., Wien, F., Lees, J.G. & Wallace, B.A. Calibration and standardisation of synchrotron radiation and conventional circular dichroism spectrometers. Part 2: Factors affecting magnitude and wavelength. *Spectroscopy* **19** (2005).
264. Xing, D.K. et al. Physicochemical and immunological studies on the stability of free and microsphere-encapsulated tetanus toxoid in vitro. *Vaccine* **14**, 1205-1213 (1996).
265. Johansen, P., Merkle, H.P. & Gander, B. Physico-chemical and antigenic properties of tetanus and diphtheria toxoids and steps towards improved stability. *Biochim. Biophys. Acta* **1425**, 425-436 (1998).

266. Liang, R. et al. Stability of exenatide in poly(D,L-lactide-co-glycolide) solutions: a simplified investigation on the peptide degradation by the polymer. *Eur. J. Pharm. Sci.* **50**, 502-510 (2013).
267. Awwad, S. & Angkawinitwong, U. Overview of Antibody Drug Delivery. *Pharmaceutics* **10** (2018).
268. Schwendeman, S.P. Recent advances in the stabilization of proteins encapsulated in injectable PLGA delivery systems. *Crit. Rev. Ther. Drug Carrier Syst.* **19**, 73-98 (2002).
269. Estey, T., Kang, J., Schwendeman, S.P. & Carpenter, J.F. BSA degradation under acidic conditions: a model for protein instability during release from PLGA delivery systems. *J. Pharm. Sci.* **95**, 1626-1639 (2006).
270. Nicola, N.A., Metcalf, D., Matsumoto, M. & Johnson, G.R. Purification of a factor inducing differentiation in murine myelomonocytic leukemia cells. Identification as granulocyte colony-stimulating factor. *J. Biol. Chem.* **258**, 9017-9023 (1983).
271. Metcalf, D. The colony-stimulating factors and cancer. *Nat. Rev. Cancer* **10**, 425-434 (2010).
272. Fukunaga, R., Ishizaka-Ikeda, E. & Nagata, S. Purification and characterization of the receptor for murine granulocyte colony-stimulating factor. *J. Biol. Chem.* **265**, 14008-14015 (1990).
273. Kawakami, M. et al. Levels of serum granulocyte colony-stimulating factor in patients with infections. *Blood* **76**, 1962-1964 (1990).
274. Koeffler, H.P. et al. Recombinant human TNF alpha stimulates production of granulocyte colony-stimulating factor. *Blood* **70**, 55-59 (1987).
275. Kaushansky, K., Lin, N. & Adamson, J.W. Interleukin 1 stimulates fibroblasts to synthesize granulocyte-macrophage and granulocyte colony-stimulating factors. Mechanism for the hematopoietic response to inflammation. *J. Clin. Invest.* **81**, 92-97 (1988).
276. Zsebo, K.M. et al. Vascular endothelial cells and granulopoiesis: interleukin-1 stimulates release of G-CSF and GM-CSF. *Blood* **71**, 99-103 (1988).
277. Vellenga, E., Rambaldi, A., Ernst, T.J., Ostapovicz, D. & Griffin, J.D. Independent regulation of M-CSF and G-CSF gene expression in human monocytes. *Blood* **71**, 1529-1532 (1988).
278. Lancerotto, L. et al. Layers of the abdominal wall: anatomical investigation of subcutaneous tissue and superficial fascia. *Surg. Radiol. Anat.* **33**, 835-842 (2011).
279. Martinez, M.N. Factors influencing the use and interpretation of animal models in the development of parenteral drug delivery systems. *AAPS J* **13**, 632-649 (2011).
280. Jin, J.F. et al. The optimal choice of medication administration route regarding intravenous, intramuscular, and subcutaneous injection. *Patient Prefer Adherence* **9**, 923-942 (2015).
281. Porter, C. & Edwards, G. Lymphatic transport of proteins after s.c. injection: Implications of animal model selection. *Adv. Drug Del. Rev.* **50**, 157-171 (2001).
282. Kagan, L., Turner, M.R., Balu-Iyer, S.V. & Mager, D.E. Subcutaneous absorption of monoclonal antibodies: role of dose, site of injection, and injection volume on rituximab pharmacokinetics in rats. *Pharm. Res.* **29**, 490-499 (2012).
283. van Schie, K.A. et al. The antibody response against human and chimeric anti-TNF therapeutic antibodies primarily targets the TNF binding region. *Ann. Rheum. Dis.* **74**, 311-314 (2015).
284. van Schouwenburg, P.A. et al. Adalimumab elicits a restricted anti-idiotypic antibody response in autoimmune patients resulting in functional neutralisation. *Ann. Rheum. Dis.* **72**, 104-109 (2013).
285. Hurter, P. & Kuhnau, J. [Avidity and binding capacity of bovine and porcine insulin binding antibodies in childhood diabetes]. *Monatsschr. Kinderheilkd.* **118**, 250-252 (1970).
286. The European Agency for the Evaluation of Medicinal Products (EMEA) Committee for Proprietary Medicinal Products (CPMP 3097/02) (2002).
287. Schellekens, H. Bioequivalence and the immunogenicity of biopharmaceuticals. *Nat. Rev. Drug Discov.* **1**, 457-462 (2002).

288. Jones, E.A. & Waldmann, T.A. The mechanism of intestinal uptake and transcellular transport of IgG in the neonatal rat. *The Journal of clinical investigation* **51**, 2916-2927 (1972).
289. Mostov, K.E. & Simister, N.E. Transcytosis. *Cell* **43**, 389-390 (1985).
290. Proetzel, G. & Roopenian, D.C. Humanized FcRn mouse models for evaluating pharmacokinetics of human IgG antibodies. *Methods* **65**, 148-153 (2014).
291. Igartua, M. et al. Influence of formulation variables on the in-vitro release of albumin from biodegradable microparticulate systems. *J. Microencapsul.* **14**, 349-356 (1997).
292. Park, T.G., Lu, W. & Crotts, G. Importance of in vitro experimental conditions on protein release kinetics, stability and polymer degradation in protein encapsulated poly (D, L-lactic acid-co-glycolic acid) microspheres. *J. Controlled Release* **33**, 211-222 (1995).
293. Berteau, C. et al. Evaluation of the impact of viscosity, injection volume, and injection flow rate on subcutaneous injection tolerance. *Med Devices (Auckl)* **8**, 473-484 (2015).
294. Jorgensen, J.T. et al. Pain assessment of subcutaneous injections. *Ann. Pharmacother.* **30**, 729-732 (1996).